The Network Properties and Solvent Uptake Characteristics of Epoxy-Amine Polymer Networks

Francis Gurman

A thesis submitted in partial fulfilment of the requirements for the degree of

Doctor of Philosophy

University of Sheffield

May 12, 2025

Abstract

Epoxy-amine resins are widely used as anti-corrosive coatings. However, water pathways eventually form throughout these coatings, resulting in corrosion. Given that the massive global costs of corrosion, it is imperative to understand the failure mechanisms of these coatings.

Epoxy-amine systems composing of the epoxy monomer DER331 (bisphenol-A) and the amine crosslinking agent m-Xylylenediamine (MXDA) were created to investigate the potential causes of this failure mechanism. In order to more closely mimic industrially-made coatings, samples of these epoxy-amine systems were made with varying levels of epoxy, with solvents (3:1 ratio mix of xylene and butanol) and with the homopolymerizing agent 2,4,6-Tris(dimethylaminomethyl)phenol (DMP-30).

Cure kinetics, final conversion and final glass-transition temperature (T_g) measurements were measured via differential scanning calorimetry (DSC). Network properties of the cured systems were measured vis small-angle neutron scattering (SANS) and positron-annihilation lifetime spectroscopy (PALS). Solvent uptake measurements were then taken, the results from which were related to those from the previous two investigations to determine how different networks affected uptake and why.

DSC measurements showed DMP-30 to raise the conversion of epoxy to a maximum and the homopolymerized network to have a slightly higher crosslink density than the epoxy-amine network. DMP-30 also raised the rate of conversion in epoxy-amine formulations. SANS measurements showed samples cured with solvents displayed a heterogeneous network. Solvent uptake was also shown to be greater than samples cured without solvents. It was deduced that solvents separated from epoxy-amine during cure before evaporating, resulting in 'voids,' areas of low crosslink density into which solvents can easily enter. A greater conversion rate leads to greater uptake, believed to be due to greater void sizes in the network. For non-solvent formulations, solvents must probe the polymer network. Uptake for these formulations is therefore dependent on crosslink density and the density of hydrogen-bonding sites.

Acknowledgements

Firstly, I would like to thank the Nobel Committee for when they eventually award me for this thesis. Be the Nobel Prize for physics or chemistry, I do not mind. Maybe even for literature, given the prose on display in this work.

In all sincerity, I would firstly like to thank my parents, Jane and Steven, for their guidance over the years, even if sometimes I was not always receptive to it. Thanks especially go to my mother for how much effort she has put in in helping me through every stage of life. Thanks also to my brother, Joseph, someone who has already managed to achieve great things in his career, and earns a lot more money than I do.

Thank you Dr Andrew Parnell who has been a great supervisor over these past few years. A man of infectious charm and humour who has always been on hand to help me. I do not know how much of my PhD I would have enjoyed without Andy. Thanks also to Professors Tony Ryan, Patrick Fairclough and Richard Jones for help with the more esoteric polymer physics issues. Thanks to Dr Stephanie Burg for her help throughout the years even when she had more important things to do than help a silly PhD student with his experiments. Also thanks to Stephanie for not murdering me after certain occurrences involving a lab oven. Thanks to Dr Melody Obeng for helping me through the early stages of my PhD. Thanks to Grace Fidler for the work she did with me on small-angle neutron scattering.

My PhD would have been a lot lonelier without Joe Orgill and Derick Liew, who both soon will have PhDs of their own. Joe did abandon me for the big bad city of Didcot for a year but the other years made up for that. That day we visited all the hospitals in Sheffield was the best say of my PhD. Shout out to Derick for being my gym and skiing partner. I dread to think what you have written about me in your acknowledgments section.

Finally, I would like to thank all the organisations and persons that have kept me somewhat mentally sane over the past few years. Thanks to the choir of Saint John's Church, Ranmoor, The University of Sheffield Singers Society and to The Sheffield University Bankers Hockey Club for letting me sing and play hockey multiple times each week. Thank you Riot Games because I unfortunately still sink hours into watching and playing League of Legends. Thanks to all the boys from Leicester, wherever you may be now (mainly still in Leicester). And last, thanks to Benediktas Valys, a man of terrible music taste and truly awful podcast taste, for his friendship over the past eight years.

Declaration

The work described in this thesis was undertaken at the University of Sheffield between October 2020 and October 2024 under the supervision of Doctor Andrew Parnell. Unless otherwise stated, it is the work of the author and has not been submitted in whole or in part for any other degree at this or any other insitution.

Francis Gurman, October 2024

Publicly Presented Work

1. University of Sheffield Sustainability Annual Symposium, hosted by the Grantham Centre for Sustainable Futures, 2021. Poster.

2. Macrogroup Young Researcher Meeting at Warwick University, 2024. Poster

3. Royal Society of Chemistry 16th International Conference on Materials Chemistry at University College Dublin, 2023. Poster.

4. Insitute of Physics Physical Aspects of Polymer Science at Edinburgh University, 2024. Talk titled 'Solvent Uptake in Anti-Corrosive Coatings.'

Nomenclature

List of variable symbols only from experimental chapters for now. Cannot get the formatting correct. Taking all the variables from the theory section would make it too much of a mess. May remove the variables from the method section. Think this approach also keeps everything more relevant.

Curing Nomenclature

T_g	Glass transition temperature
EEW	Epoxide equivalent weight
AHEW	Amine hydrogen equivalent weight
r	stoichiometry
p	Extent of reaction
ΔH_0	Enthalpy per mole
ΔH_{epoxy}	Enthalpy of one mole of epoxy rings opening
ΔT	Change in temperature
C_p	Heat capacity of the system at constant pressure
c_p	Specific heat capacity of the system at constant pressure

Scattering Nomenclature

Q	Wavevector transfer
SLD	Scattering length density
I	Intensity
n	Porod exponent
A	Porod scale
ξ	Correlation length
m	Lorentzian exponent
C	Lorentzian scale
$\boldsymbol{P}$	Momentum transfer
$\hbar$	Reduced Plank constant
$\boldsymbol{k_i}$	Initial wavevector
$\boldsymbol{k_f}$	Final wavevector
$\boldsymbol{E}$	Energy transfer
$\boldsymbol{\omega_i}$	Initial frequency
$\boldsymbol{\omega_f}$	Final frequency
m_n	Neutron mass
λ	Wavelength
θ	Angle
ψ	Wavefunction
z	Direction of wave propagation
$\boldsymbol{\Phi}$	Incident flux
b	Scattering length
I_0	incident flux
$\Delta\Omega$	Solid angle
η	Detector efficiency
T	Neutron transmission of the sample
V_s	Volume of the illuminated sample
$\frac{\delta\Sigma}{\delta\Omega}$	Differential scanning cross-sectional area
N	Number concentration of scattering centres
V	Volume of a scattering centre
$\Delta\rho$	Contrast in scattering length
P	Form factor
S	Shape factor
b_i	Coherent neutron scattering length of a nucleus
δ	Bulk density of a molecule
N_A	Avagadro's constant
M	Molecular weight
σ	Scattering cross section
σ_{coh}	Coherent Scattering cross section
σ_{inc}	Scattering cross section
σ_{abs}	Absorption scattering cross section

R_g	Radius of gyration
$g(r)$	Density distribution function
c	Polymer concentration
c^*	Overlap concentration
l	Persistence length
r_i	Distance from the i^{th} bead to the centre of mass
S_p	Surface area of target particle
ν	Volume of a segment
ACF	Autocorrelation function
$\beta(\boldsymbol{r})$	Scattering length density function

Positron Annihilation Lifetime Spectroscopy Nomenclature

T_{oPs}	Ortho-Positronium lifetime
R	free-volume radius
FV	Free volume
FFV	Fractional free volume
I_1	Relative intensity of free positron decay
I_2	Relative intensity of para-positronium decay
I_3	Relative intensity of oPs lifetime

Solvent Uptake Nomenclature

M_t	% mass uptake
M_m	Maximum % mass uptake
L	Sample thickness
t	Immersion time
D	Diffusion coefficient

Abbreviations

DGEBA	bisphenol A diglycidyl ether
MXDA	m-Xylylenediamine
DMP-30	2,4,6-tris(dimethylaminomethyl)phenol
NS	Sample cured without solvents
S	Sample cured with solvents
DSC	Dynamic Scanning Calorimetry
NIR spectroscopy	Near-infrared spectroscopy
SANS	Small-angle neutron scattering
PALS	Positron-annihilation light spectroscopy

Contents

List of Figures

Chapter 1

Introduction

'Gold or glass cannot equal [wisdom]' - Job 28:17 (ASV)

The degredation of metals via corrosion is a wide-ranging, global problem costing an estimated $2.5trillion, or 3.4% of the global GDP, per year [1]. It covers a varieity of industries, mainly the infrastructure (bridges, gas and liquid pipelines and HAZMAT storage), utilities (water and sewage) and transportation (motor vehicles) industries. Corrosion is a naturally-occurring phenomenon in which an anode (usually a metal) loses electrons when in contact with a cathode (usually oxygen or water), which gains them. In practical terms, this results in the degradation of metals when they come into contact with oxygen or water [1]. There are also human and environmental costs of corrosion. Corrosion of apparatus results in injuries and deaths [2]. Environmental impacts can scale from small-scale, common occurrences such as the damage to machinery and vehicles resulting in increased fuel use via reduced efficiency, to larger-scale impacts such as oil spills.

One method for preventing corrosion is via a protective coating, which forms a physical barrier between the environment and the surface that needs protecting. Epoxy-amines, a type of crosslinked polymer network, are a popular choice of material for these coatings. They have good corrosion and chemical resistance, are tough and adhesive [3, 4], and are also inexpensive [5]. Corrosion resistance, chemical toughness and hardness are increased by raising the crosslink density of the epoxy-amine network [4], itself maximized by maximizing the conversion of epoxy, the amount of epoxy that has reacted to form part of the epoxy-amine polymer network, in the epoxy-amine [6]. Conversion can be maximized by having an equal number of epoxy and amine groups. Alternatively, an excess of epoxy can be homopolymerized in the presence of a homopolymerizing agent, such as 2,4,6-tris(dimethylaminomethyl)phenol (DMP-30) [7]. Epoxy-amines are viscous, and so are mixed with solvents so that they can be applied to surfaces via spraying [4, 8]. Solvents subsequently evaporate, leaving behind a crosslinked epoxy-amine network. By curing with solvents the conversion of the coating can be raised for lower cure temperatures [9]. Despite their beneficial properties, over time epoxy-amines fail to prevent corrosion. It is not entirely clear

why this failure occurs [10]. A current hypothesis is that there is local water uptake in low-crosslink density regions. This may come about due to curing with solvents, with solvents phase separating from epoxy-amine during network formation [11, 12]. Water can enter these regions, swelling them, enlarging them so that they eventually create pathways throughout the entire coating, through which water can travel through the coating and reach the protected surface, resulting in corrosion [13, 14].

Given its impact on the properties of the final coating, it is important to understand the conversion of epoxy-amine resins. Differential scanning calorimetry (DSC) is a popular tool for determining the glass transition temperature, T_g, the temperature of a polymer below which, it is a glass and has more brittle characteristrics, and above which it is a rubber and has more elastic characteristics. T_g depends on the extent of monomer conversion and polymer crosslink density and so has been used as a proxy for these two measurements when investigating in cured epoxy resins [15, 16, 17]. T_g has also been measured for epoxy resins when cured with solvents, with solvents lowering T_g of the network by $\sim$10°C [11, 18] compared to identical epoxy resins cured without solvents. DSC can also be used to measure the enthalpy of reaction of uncured epoxy-amines, giving information on the system's reaction kinetics [19, 20]. However, despite the use of DMP-30 in anti-corrosion coatings, little work has been done on the reaction kinetics and T_g of epoxy-amines of varying epoxy levels when cured with DMP-30.

Scattering techniques, such as small- and wide-angle x-ray scattering (SAXS and WAXS), and small-angle neutron scattering (SANS), have seen use investigating polymer structures, from the scale of the network [21] down to the length of monomers [22]. This is of direct importance given that the proposed failure mechanism in epoxy-amine coatings comes from changes in its network. Solvent uptake in epoxy-amines has been used in conjunction with SANS measurements to measure its changes to network structure, and to provide contrast for the SANS signal [23, 24, 25, 26]. Water uptake has been used to measure uptake mechanisms in epoxy-amines. It has been determined that water uptake is dependent on the free volume [11, 27, 28] of the network, its affinity for water [27, 29] and ageing effects (the relaxation of polymer chains in the network, affecing network properties) [30]. However, very few scattering studies or uptake measurements have been carried out on epoxy-amines cured with solvents. Given their use in anti-corrosive coatings and the possibility that they are the cause of the failure in these coatings, this presents a gap in the literature that this work aims to address.

The investigations in this thesis aimed to determine curing kinetics, network properties and solvent uptake characteristics of epoxy-amine resins, to better understand their use as anti-corrosion coatings. The epoxy, the monomer for these polymer networks, used was DER331 (bisphenol-A). The amine, the crosslinking agent, used was m-Xylylenediamine (MXDA). Networks were made of equal amounts of epoxy groups and amine groups (stoichiometric ratio) and excess epoxy to determine how changes in epoxy conversion affected the network properties of the cured resin. These were

made both with and without the homopolymerizing agent DMP-30, and with and without solvent. The solvent used was a 3:1 mixture of xylene and butanol, such that the mixture before curing was 60% epoxy-amine and 40% solvent. A mixture of xylene and butanol provides a solvent into which the polymer network can dissolve [31]. This thesis is split into six sections. Chapter 2 discusses the theoretical background of polymers, the glass transition temperature, the reactions present in the curing of epoxy-amine resins, the solvent uptake mechanisms in polymers and the use of solvents in protective coatings. Chapter 3 states how the different epoxy-amine samples were prepared, and gives details of the methods and equipment used in these investigations. Chapters 4, 5 and 6 discuss the investigations carried out. These are presented in the format of research papers. In chapter 4, the investigation into the reaction kinetics and final glass transition temperatures of epoxy-amines is explained. Chapter 5 discusses the investigation into the structures of epoxy-amines via SANS measurements. Chapter 6 discusses the solvent uptake of epoxy-amine samples when immersed in water or methanol, and relates this back to the conclusions drawn from sections 4 and 5. Finally, chapter 7 re-outlines the aims of the thesis, conclusions drawn from each investigation and possible future work.

Bibliography

[1] Gretchen A Jacobson. *Corrosion Basics*. https://www.nace.org/resources/general-resources/corrosion-basics [Accessed: (18/10/24)].

[2] G. Koch et al. *International Measures of Prevention, Application, and Economics of Corrosion Technologies Study*. http://impact.nace.org/documents/Nace-International-Report.pdf [Accessed: (18/10/24)].

[3] E. Duemichen et al. "Analyzing the network formation and curing kinetics of epoxy resins by in situ near-infrared measurements with variable heating rates". In: *Thermochimica Acta* 616 (2015), 49–60. DOI: 10.1016/j.tca.2015.08.008.

[4] P. A. Sørensen et al. "Anticorrosive coatings: a review". In: *Journal of Coatings Technology and Research* 6.2 (2009), pp. 135–176. DOI: 10.1007/s11998-008-9144-2.

[5] S. B. Lyon, R. Bingham, and D J Mills. "Advances in corrosion protection by organic coatings: What we know and what we would like to know". In: *Progress in Organic Coatings* 102 (2017), 2–7. DOI: 10.1016/j.porgcoat.2016.04.030.

[6] Fred Meyer et al. "The effect of stoichiometry and thermal history during cure on structure and properties of epoxy networks". In: *Polymer* 36.7 (1995), 1407–1414. DOI: 10.1016/0032-3861(95)95918-q.

[7] John D. McCoy et al. "Cure mechanisms of diglycidyl ether of bisphenol A (DGEBA) epoxy with diethanolamine". In: *Polymer* 105 (2016), 243–254. DOI: 10.1016/j.polymer.2016.10.028.

[8] G. Zhang et al. "Permeable epoxy coating with reactive solvent for anticorrosion of concrete". In: *Progress in Organic Coatings* 117 (2018), pp. 29–34. DOI: 10.1016/j.porgcoat.2017.12.018.

[9] A. R. Marrion. *The Chemistry and Physics of Coatings*. 2nd ed. The Royal Society of Chemistry, 2004.

[10] S. Morsch, S. Lyon, and S. R. Gibbon. "The degradation mechanism of an epoxy-phenolic can coating". In: *Progress in Organic Coatings* 102 (2017), 37–43. DOI: 10.1016/j.porgcoat.2016.03.019.

[11] C. Yi et al. "Curing kinetics and mechanical properties of epoxy based coatings: The influence of added solvent". In: *Progress in Organic Coatings* 124 (2018), pp. 165–174. DOI: 10.1016/j.porgcoat.2018.08.009.

[12] M. Dušková-Smrčková, K. Dušek, and P. Vlasák. "Solvent activity changes and phase separation during crosslinking of coating films". In: *Macromolecular Symposia* 198.1 (2003), pp. 259–270. DOI: 10.1002/masy.200350822.

[13] T. Nguyen, J. B. Hubbard, and J. M. Pommersheim. "Unified model for the degradation of organic coatings on steel in a neutral electrolyte". In: *JCT, Journal of Coatings Technology* 68.855 (1996), 45–56.

[14] C. M. Sahagun and S. E. Morgan. "Thermal Control of Nanostructure and Molecular Network Development in Epoxy-Amine Thermosets". In: *ACS Applied Materials and Interfaces* 4.2 (2000), pp. 564–572. DOI: 10.1021/am201515y.

[15] J. Ehlers et al. "Theoretical Study of the Epoxy-Amine Curing Reaction". In: *Macromolecules* 40.12 (2007), pp. 4370–4377. DOI: 10.1021/ma070423m.

[16] K. C. Cole, J. J. Heckler, and D. Noel. "A New Approach to Modeling the Cure Kinetics of Epoxy Amine Thermosetting Resins. 2. Application to a Typical System Based on Bis[4- (diglycidylamino)phenyl]methane and Bis(4-aminophenyl) Sulfone". In: *Macromolecules* 24.11 (1990), pp. 3098–3110. DOI: 10.1021/ma00011a012.

[17] V. L. Zvetkov. "A Modified Kinetic Model of the Epoxy-Amine Reaction". In: *Macromolecular Chemistry and Physics* 203.3 (2002), pp. 467–476. DOI: 10.1002/1521-3935(20020201)203:3<467::AID-MACP467>3.0.CO;2-Q.

[18] H. Shing-Gwo and W. Chung-Sheng. "DSC and FTIR analysis of the curing behaviors of epoxy/DICY/solvent open systems". In: *Thermochimica Acta* 316.2 (1998), pp. 167–175. DOI: 10.1016/S0040-6031(98)00356-6.

[19] J. Galy, A. Sabra, and J-P. Pascault. "Characterization of epoxy thermosetting systems by differential scanning calorimetry". In: *Polymer Engineering and Science* 26.21 (1986), 1514–1523. DOI: 10.1002/pen.760262108.

[20] B. Ekbrant and A. Skov A. Daugaard. "Epoxy-rich systems with preference for etherification over amine-epoxy reactions for tertiary amine accelerators". In: *Macromolecules* 54.9 (2021), 4280–4287. DOI: 10.1021/acs.macromol.0c02630.

[21] J. Witte et al. "A comparison of the network structure and inner dynamics of homogeneously and heterogeneously crosslinked PNIPAM microgels with high crosslinker content". In: *Soft Matter* 15 (2000), 792–802. DOI: 10.1039/c8sm02141d.

[22] R. Lovell and A. H. Windle. "WAXS investigation of local structure in epoxy networks". In: *Polymer* 31.4 (1990), pp. 593–601. DOI: 10.1016/0032-3861(90)90274-3.

[23] W.L. Wu and B. J. Bauer. "Network structure of epoxies - a neutron scattering study: 2". In: *Polymer* 27.2 (1986), pp. 169–180. DOI: 10.1016/0032-3861(86)90322-8.

[24] W.L. Wu et al. "Epoxy Network Structure. 4. A Neutron Scattering Study of Epoxies Swollen in a Deuteriated Solvent". In: *Macromolecules* 21.3 (1988), 756–764.

[25] A. Izumi et al. "Cross-link inhomogeneity in phenolic resins at the initial stage of curing studied by 1 H-pulse NMR spectroscopy and complementary SAXS/WAXS and SANS/WANS with a solvent-swelling technique". In: *Polymer* 103 (2016), 152–162. DOI: 10.1016/j.polymer.2016.09.067.

[26] M. Aoki et al. "Mesoscopic Heterogeneity in the Curing Process of an EpoxyAmine System". In: *Macromolecules* 52.5 (2019), pp. 2075–2082. DOI: 10.1021/acs.macromol.8b02416.

[27] J. Wang et al. "Effect of curing agent polarity on water absorption and free volume in epoxy resin studied by PALS". In: *Nuclear Instruments and Methods in Physics Research Section B: Beam Interactions with Materials and Atoms* 268.14 (2010), pp. 2355–2361. DOI: 10.1016/j.nimb.2010.04.010.

[28] M. R. VanLandingham, R. F. Eduljee, and J. W. Gillespie. "Moisture diffusion in epoxy systems". In: *Applied Polymer Science* 71.5 (1999), pp. 787–798. DOI: 10.1002/(SICI)1097-4628(19990131)71:5<787::AID-APP12>3.0.CO;2-A.

[29] L. C. Soles et al. "Contributions of the nanovoid structure to the moisture absorption properties of epoxy resins". In: *Journal of Polymer Science Part B: Polymer Physics* 36.17 (1998), pp. 3007–3154. DOI: 10.1002/(SICI)1099-0488(199812)36:17<3035::AID-POLB4>3.0.CO;2-Y.

[30] G. Pitarresi et al. "Absorption kinetics and swelling stresses in hydrothermally aged epoxies investigated by photoelastic image analysis". In: *Polymer Degradation and Stability* 111 (2015), pp. 55–63. DOI: 10.1016/j.polymdegradstab.2014.10.019.

[31] R. Lambourne and T. A. Strivens, eds. *Paint and Surface Coatings: Theory and Practice*. 2nd ed. Woodhead Publishing Ltd, 1999. ISBN: 85573 348 X.

Chapter 2

Theory

2.1 Crosslinked Polymer Networks

2.1.1 Polymers

Polymers are large molecules built up of repeating units, known as monomers, covalently bonded together [1]. Monomers can form polymers via one of two processes: step polymerization or chain polymerization. In step polymerization, groups of monomers react with other groups of monomers to form larger molecules (the polymer). Epoxy-amines are polymers formed via step-polymerization. If there are still reactive sites on these larger molecules, they can react again. In this way, step-growth polymerization produces polymers that double in size during each reaction step, as polymers get larger and react with other larger polymers [2]. Chain growth polymerization starts with the formation of a reactive centre that reacts only with monomers. After reacting with a monomer, this reactive centre shifts to the end of the polymer forming a linear chain of monomers forms with a reactive end. This chain then extends via a large number of successive reactions with each individual monomer. Epoxy homopolymerization proceeds via chain-growth polymerization [3]. In chain growth, the size of polymers therefore increases by one unit during each reaction step. In step polymerization, polymers are produced with a wide range of degrees of polymerization, N, the total number of monomers that make up the polymer. Chain growth polymerization produces a much narrower range of N values. The distribution of these degrees of polymerization affects the properties of the polymer systems [1].

2.1.2 The sol-gel transition

The properties of a polymer changes when monomers can form crosslinks, producing a three-dimensional polymer network, eventually forming a single, macroscopic polymer known as a rubber or a gel [1]. As a gel, the polymer has mechanical properties similar to a solid, despite being structurally disordered [4]. A rubber's properties depend on its cross-link density, and the molecular weight between cross-links. A chemical gel can be constructed if its monomers (and crosslinking agents) have enough reactive, or functional, groups to form the required three-dimensional network [4]. With only two functional groups, only a linear chain can be formed. With an average of more

than two functional groups between the monomer and crosslinking agent, branching can occur, enabling gelation to occur.

The transition from a liquid to a gel in a 3-D polymer network is a discontinuous change, known as the sol-gel transition [4]. This occurs when the largest polymer in the system becomes big enough so that it spans the entirety of the reaction vessel [5]. This is the percolation model, shown in figure 2.1 [4].

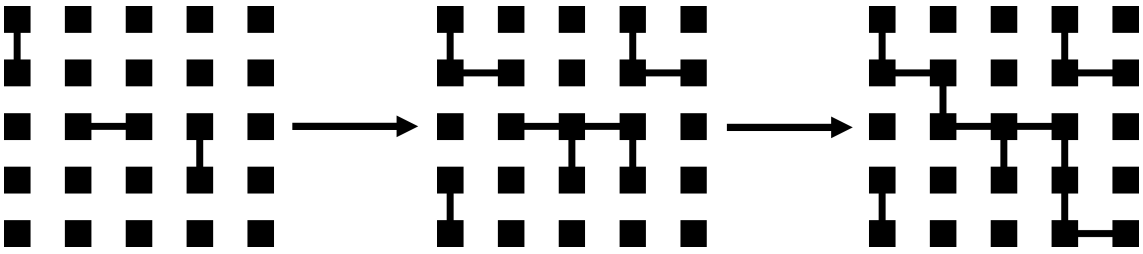

Figure 2.1: Schematic of the percolation model of gelation. Initially, there is a mixture of monomers, as represented by an array of points. Bonds form between them, represented by lines, eventually forming clusters of points. Eventually, this cluster spans the entire array, signalling the onset of gelation.

Epoxy-amines, the class of molecules studied in this work, can form gels. Where epoxy-amine resins are formed from DGEBA monomers, the epoxy group reacts with the crosslinking agent, the diamine to build the polymer network. For systems such as these, comprising of two components, the gel point depends on the ratio of the two types of functional group (often called the stoichiometry), and the degree of functionality of the two different functional groups:

$$P_{gel} = \frac{1}{\sqrt{r(F_{sA}-1)(F_{sB}-1)}} \tag{2.1}$$

where F_{sA} and F_{sB} refer to the average functionalities of the two components A, the monomer, and B, the crosslinking agent, respectively. In this equation r is the stoichiometry, the initial ratio of the number of functional groups in A to those in B [5].

2.1.3 The kinetics of crosslinking

For the two components, A and B, as mentioned in equation 2.1, the A and B molecules will diffuse close to one another and either react or diffuse apart. For the reaction between monomer and crosslinking agent, the overall reaction rate constant, k_{obs} is given as:

$$\frac{1}{k_{obs}} = \frac{k_{-D}}{k_D}\frac{1}{k_r} + \frac{1}{k_D} \tag{2.2}$$

where k_r is the rate of reaction. k_D and k_{-D} are the rate constants of A and B diffusing together and apart [5]. For high molecular mobility and a high concentration

of functional groups ($k_D >> k_r$), the reaction rate constant is simplified to:

$$k_{obs} = \frac{k_D}{k_{-D}} k_r \tag{2.3}$$

For low-levels of crosslinking, the reaction rate can be described by the Arrhenius equation:

$$\ln(k_r) = A\exp\left(\frac{E_A}{RT}\right) \tag{2.4}$$

where A is the pre-exponential factor, E_A is the activation energy (usually negative) of the reaction, R is the gas constant and T is the temperature. Before vitrification, the reaction rate constant is found to be independent of conversion. It is conversion, not rate of conversion. As conversion increases, viscosity increases, so it may be thought that rate depends on conversion due to reduced diffusion of reacting species. This is not the case prior to vitrification. As conversion increases, the glass transition temperature, T_g, of the network rises so that it is similar to the cure temperature. This is because as polymerization reactions occur, polymer molecules form crosslinks and increase in size. Crosslinks reduce the flexibility of polymer chains, reducing their mobility. The increase in size of łpolymer chains reduces the number of chain ends in the polymer. Chain ends occupy a greater free volume than the rest of the polymer chain, due to increased flexibility. A reduction in the number of chain ends reduces the polymer's overall mobility, raising its T_g. As T_g approaches the cure temperature, the mobility of the polymer is therefore reduced such that $k_r >> k_D$. At this point, the rate of reaction is not chemically controlled, as described in equation 2.4, but diffusion controlled [5]. This change in the rate of reaction as conversion increases shown in figure 2.2 for a series of epoxy-amines [6]. From equation 2.2, it can be shown that under these conditions $k_{obs} = k_D$ [5]. This switch occurs at a critical conversion, a_c. A 'diffusion factor,' $f(\alpha)$ is given as:

$$f(\alpha) = \frac{k_{obs}}{k_c} = \frac{1}{1 - \exp[C(\alpha - \alpha_c)]} \tag{2.5}$$

$$\text{where } \frac{1}{k_{obs}} = \frac{1}{k_d} + \frac{1}{k_c} \tag{2.6}$$

where C is a constant and k_d and k_c are the overall diffusion rate constant and non-diffusion rate constant, respectively. $f(\alpha) = 1$ for α significantly lower than α_c, decreases to 0.5 when $\alpha = \alpha_c$, and then decreases to 0 beyond that. α_c was found to be linear with temperature [7]. According to free volume theory, the diffusion rate constant of the reaction falls to zero once the T_g exceeds the curing temperature by 51°C. However, in practice, further conversion effectively falls to 0 when T_g is 25-35°C above the cure temperature [5].

2.2 The Glass Transition, T_g

As viscoelastic materials, the state and therefore the mechanical properties of an amorphous polymer depend on the temperature and time over which measurements take place. For low temperatures and short time intervals, these polymers are in the glassy state. Specifically, this glassy state is taken as the state in which molecular motions

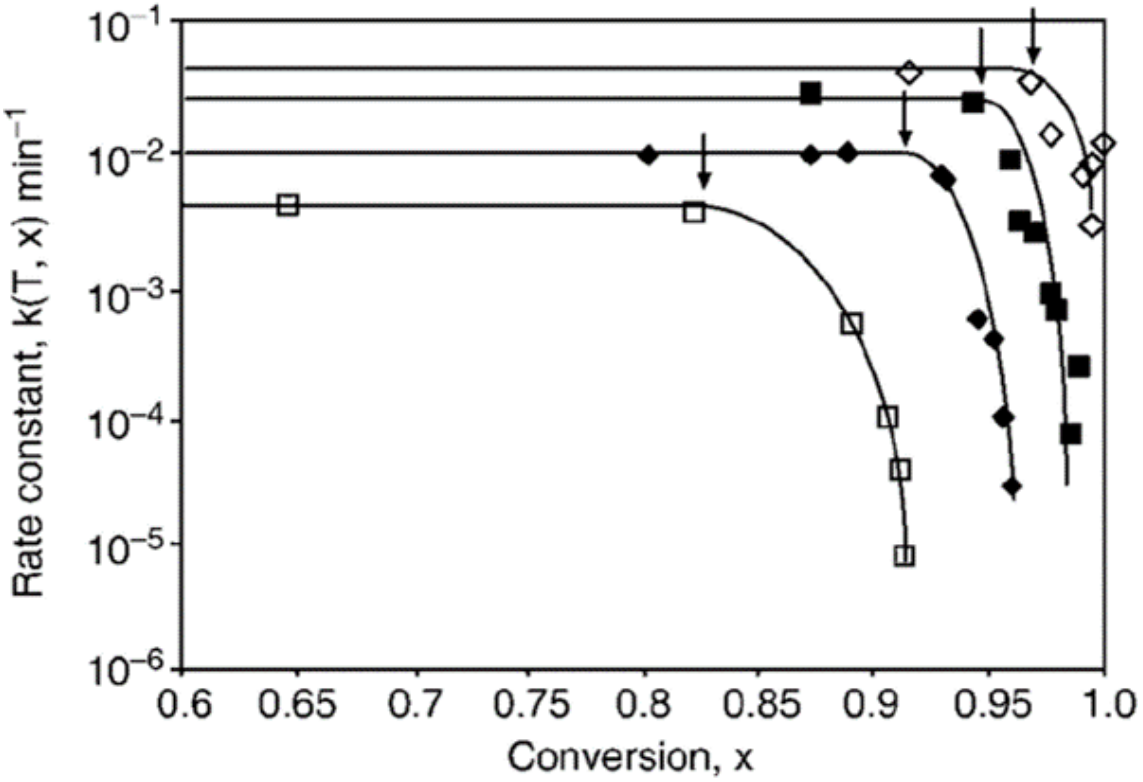

Figure 2.2: Change in rate constant, k, as epoxy conversion, x, changes for reactions of an epoxy-amine reaction at different temperatures. The epoxy was a diglycidyl ether of bisphenol A and the amine trimethylene glycol di-p-aminobenzoate. The hollow squares show the reaction at 100°C, the black diamonds the reaction at 120°C, the black squares the reaction at 140°C and the hollow diamonds the reaction at 150°C [6].

occur over such a long time scale that equilibrium cannot be established by experiment [8]. Upon heating, the polymers soften and go above the 'glass transition temperature,' T_g. Above this temperature, they are rubbery [9]. In a crosslinked network, T_g increases as the crosslinking reactions proceed and molecular weight builds. At a certain value of conversion, T_g is equal to the cure temperature, and the system vitrifies [5].

In the glassy state, the polymer is brittle with a typical Young's modulus ($E = \sigma/\epsilon$ where σ and ϵ are the tensile stresses and strains, respectively) being 3×10^9Pa. Molecular motion is confined to vibrations and short-ranged rotations. In the glass transition region, the polymer behaviour is 'leathery.' Molecular motion can now be more coordinated between chain atoms over longer ranges. Below the glass transition temperature, coordinated motion is limited such that only 1-4 chain atoms can move in a coordinated manner. In the T_g region, this increases such that 10-50 can [9]. The Young's modulus value subsequently drops by a factor of 1000 over a 20-30°C temperature range. Above T_g, the polymer enters the 'rubbery plateau' region. In this region, the polymer exhibits long-ranged elasticity. The modulus, E, for a crosslinked polymer, follows the relationship $E = 3nRT$ where n is the number of active chain segments, R is the gas constant and T is the temperature. A typical modulus in this region would be 2×10^6Pa [9].

The glass transition, in terms of volume and entropy, is a second-order phase transition in that there is a change in slope when plotted against temperature and pressure, and a discontinuity in the derivative of these relationships. For volume, this is shown as an increase in the volumetric coefficient of expansion, α in a 10-30°C range across T_g:

$$\alpha = \frac{1}{V}\left(\frac{\delta V}{\delta T}\right)_P \tag{2.7}$$

where V is the volume of the material and P is the pressure. This relationship between the change in V and α at the glass transition temperature is also true for the enthalpy and heat capacity at constant temperature [9]. These relationships are shown in figure 2.3.

The freezing of α relaxations, associated with the segmental motion of polymer chains, is responsible for the glass transition. At T_g, $\tau_\alpha \approx 10^3$s [10]. These relaxations require both an activation energy and an activation volume (the empty volume needed for local motion), as well as a dependence upon pressure [10, 11].

2.2.1 Theories of the Glass Transition

The glass transition has been historically difficult to define, with many models arising to explain it [11]. There are two main groups of theories used to describe the glass transition temperature: the free-volume theory and the thermodynamic theory. Free-volume theory defines T_g based on free-volumes that exist as voids in the polymer network. It relates viscoelastic motion to time and temperature and provides relationships between coefficients of expansion above and below T_g. The thermodynamic model relates relaxations of chain motions to an actual equilibrium point, denoting

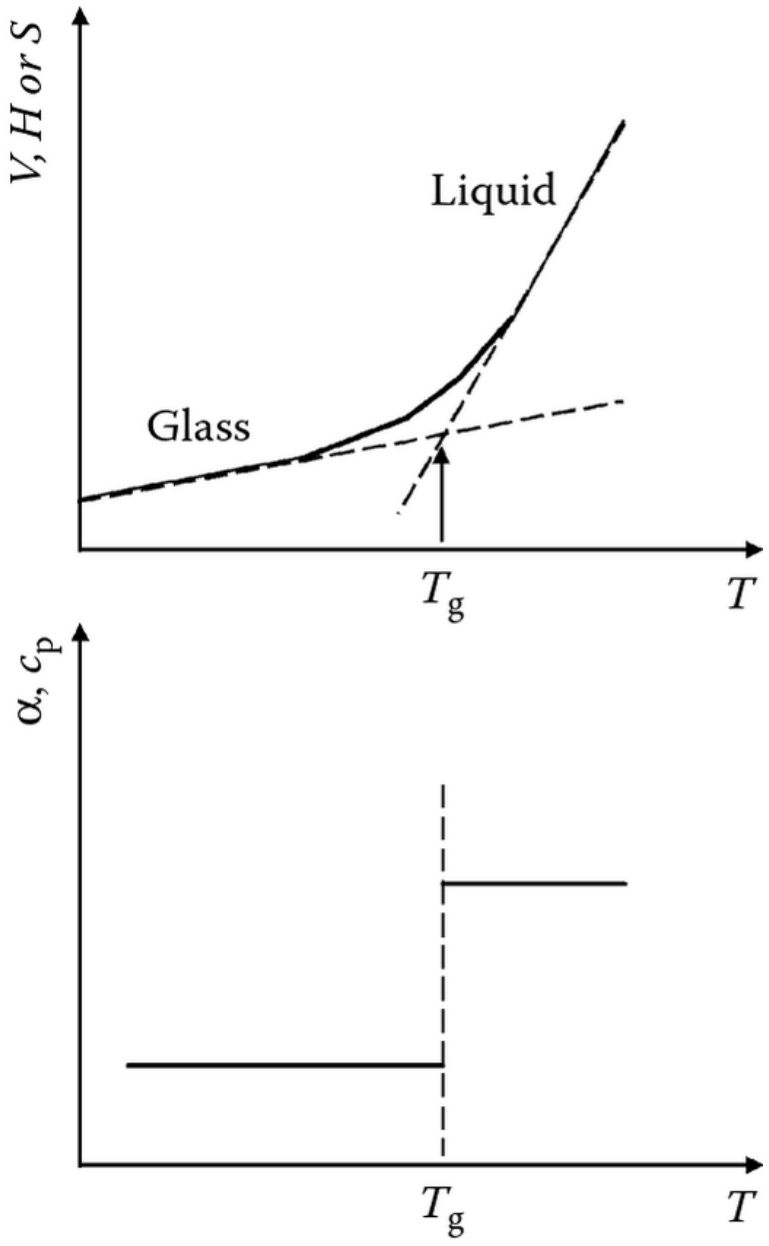

Figure 2.3: Plots showing the glass transition temperature in the relationship between temperature and volume (V), enthalpy (H) and entropy (S); and for the derivative of V and H [2].

the glass transition as a true second-order phase transition. It relates T_g variations to molecular weight and crosslink density [9]. These theories have been criticized for not explaining accurately how free volumes changes when pressure and temperature are not fixed [11, 12]. Although they may not fully explain the glass transition, these models are still of some use as they help explain experimental results [11].

The Free-Volume Theory

Free volume theory models a polymer network as areas of polymer chains and areas devoid of these chains, known as 'holes' [9]. These holes make up a 'free-volume' in the network. The total volume, V, is therefore composed of the polymer molecules, V_0 and the free volume, V_f:

$$V = V_0 + V_f \tag{2.8}$$

The fractional free volume, f, is defined as:

$$f = \frac{V_f}{V_0 + V_f} \approx \frac{V_f}{V_0} \tag{2.9}$$

Each of these terms are temperature dependent. Polymer chains can move in the network, switching places with these holes. It is these movements that allow for the coordinated movements that arise in polymers in the rubbery state. Given the size of polymer chains, a critical free volume must exist before chain motion can occur [9]. In its liquid and rubbery states, the free volume in a polymer will increase with temperature. As temperature decreases, free volume decreases until a critical free volume is reached, and large-scale motion can no longer take place. The temperature at which this occurs is termed the glass transition temperature. Below T_g, the free volume remains constant as chains are held in place. Below T_g, overall volume still decreases as temperature decreases, as there is a decrease in the amplitude of thermal vibrations in the polymer molecules [2]. The difference in expansion coefficients between a polymer in its rubbery and glassy states (α_R and α_G, respectively) was shown to be linked to its T_g. Using Simha and Boyer's model:

$$(\alpha_R - \alpha_G)T_g = K_1 \tag{2.10}$$

where K_1 is a constant, meaning the free volume in the glassy state is the same for all polymers. K_1 was initially determined to be 11.3%, although other estimates have it at 2% [9].

The local conformations of polymer chains are independent of temperature and polymer molecular weight. The occupied volume is thus made up of the system's molecules, known as it's 'hardcore' volume, V_{hc}, and the volume occupied by both the hardcore volume and the vibrations of these molecules, V_{vib}. There are therefore two ways of defining free volume: volume that is not contained by the hardcore volume, V_{free}, and that which is not contained by the vibrational volume, $V_{free:exs}$. These occupied volumes and the subsequent free volumes are shown in figure 2.4 along with their temperature dependence [12].

T_g can also be defined in terms of percent free volume in comparison to changes in

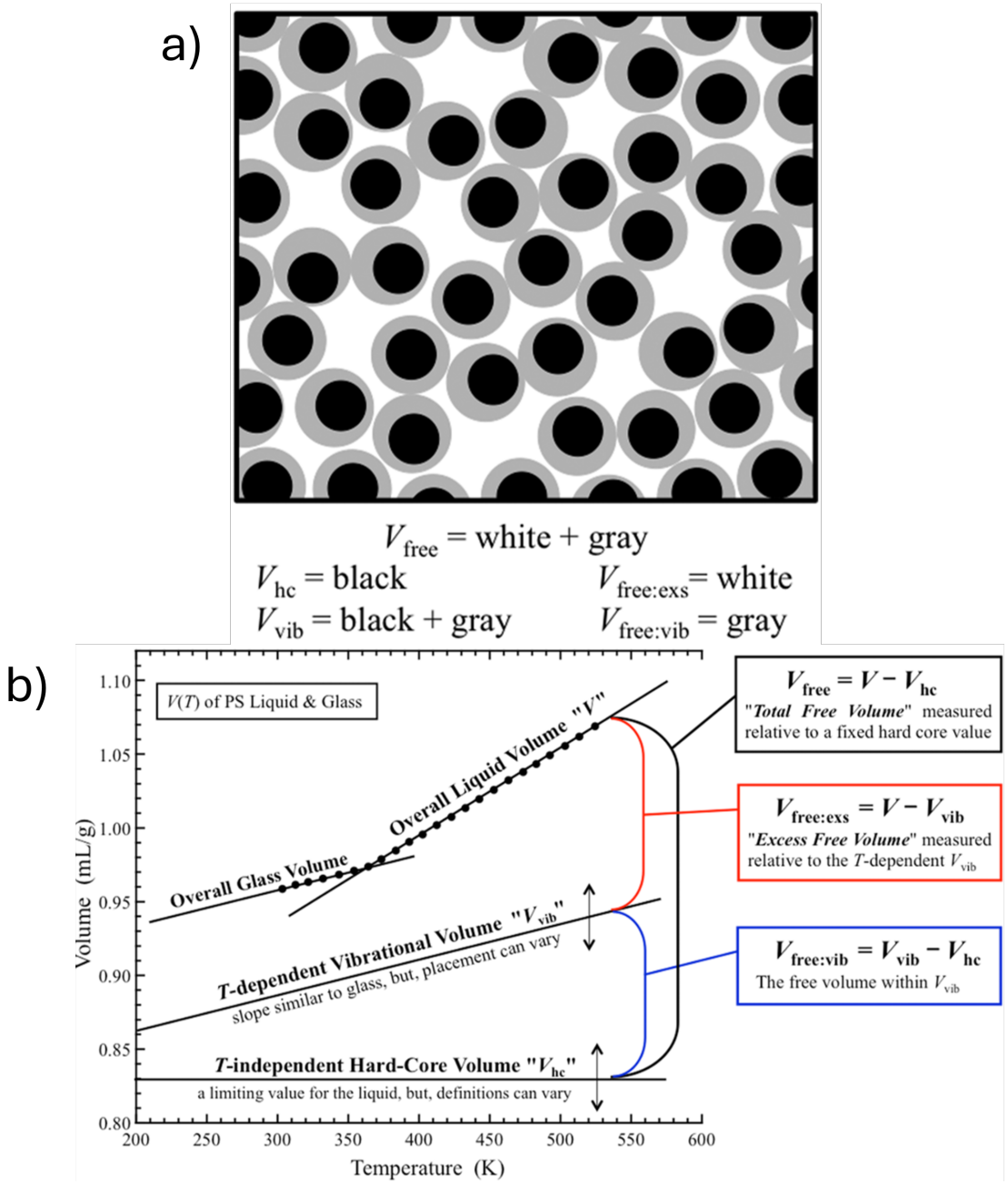

Figure 2.4: a) diagram showing the differing definitions of occupied volume and free volume. The black circle is the 'hardcore' volume, V_{hc} the space taken up by molecules. The grey area shows the extra space occupied by the vibrations of these molecules, $V_{free:vib}$. The black and grey areas together form the vibrational volume, V_{vib}. The respective free-volume definitions are therefore shown: from the hardcore volume , V_{free}, and from the vibrational volume, $V_{free:exs}$ b) shows the temperature dependence of these occupied and free volumes [12].

polymer viscosity. The Williams-Landel-Ferry (WLF) equation defines this % of free volume in terms of viscosity. The WLF equation comes from the Doolittle equation that describes viscous flow:

$$ln(\eta) = ln(A) + B\left(\frac{V - V_f}{V_f}\right) \tag{2.11}$$

where A and B are constants and η is the viscosity. B can be seen as the activation energy and is associated with diffusive motion [12]. The WLF equation used a B value of 1 [9, 12]. Viscous flow is temperature dependent. Treating the ratios of viscosity to be approximately that of relaxation times, $\tau/\tau_{ref} \approx \eta/\eta_{ref}$ [12], the WLF equation can be written as:

$$ln\left(\frac{\tau}{\tau_g}\right) = \frac{-C_1(T - T_g)}{C_2 + T - T_g} \tag{2.12}$$

where C_1 and C_2 are constants, determined experimentally to be 17.44 and 51.6 when T_g is the reference temperature [2]. From viscosity data, the fractional free volume at T_g has been determined to be 0.025 [2, 9], much lower than that given by the results from equation 2.10. This may come from the use of definitions of free-volume as shown in figure 2.4. Simha and Boyer incorporated the vibrations of the molecules, $V_{vib:free}$ to determine the occupied volume at $T = 0$K. The WLF equation on the other hand only considers V_{hc} [12].

There are issues with determining T_g via both Simha and Boyer's model and the WLF equation. As stated in equation 2.10, Simha and Boyer's model states that all polymers should have the same fractional free volume at T_g. White and Lipton's 'locally correlated lattice' (LCL) model determined this not to be the case, but that fractional free volume increased with a polymer's T_g [12]. Furthermore, this fractional free-volume also appeared to be too great [12]. For the WLF equation, results have shown that fractional free volumes did agree with experimental viscosity values, but only if B=1.62, not 1 as used in the WLF equation [13].

The LCL model provides an alternative means of determining free volume. From this, changes in free volume could be observed for different temperatures. Free volumes could thus be determined at T_g using comparisons to experimental T_g values for different polymers [12]. The LCL model presents the polymer as a compressible fluid of chain-like molecules. It is compressible as there are available free volumes it can occupy. Three parameters are given: r, the number of segments per molecule; ν, the temperature-independent hardcore volume of a segment and ϵ, the nonbonded near-neighbour segment-segment interaction energy. The hardcore volume, V_{hc}; free volume, V_{free} and fractional free volume, $\%V_{free}$ are defined as:

$$V_{hc} = Nr\nu \tag{2.13}$$

$$N_{free} = 1 - V_{hc} = 1 - Nr\nu \tag{2.14}$$

$$\%V_{free} = 100 \times \frac{V_{free}}{V_{hc}} = 100 \times \frac{1 - Nr\nu}{V} \tag{2.15}$$

It should be noted that this model takes V_{free} is the $V_{free:exs}$ shown in figure 2.4 [12]. The LCL model presents the polymer as a lattice of occupied and occupied sites. The probability of a site being unoccupied is presented as being temperature dependent. It should be noted that the LCL model does not feature a T_g. Instead, it features separate models for a glass and a melt, with separate parameters $r\nu_{glass}$ and $r\nu_{melt}$. It states that there is a minimum percent free volume that a polymer must be able to access in order to transition from a glass to a melt. This minimum percent free volume is made up of contributions from thermal vibration , V_{vib} and 'frozen-in' packing imperfections [12].

There are yet more free-volume theories that shall be discussed briefly. The Simha and Somcysnky model states monomers are trapped by their surroundings. Empty sites (holes or defects) are needed for motion [11, 14]. A theoretical free volume is determined from volume measurements at different temperatures and pressures, which can be substituted into equation 2.11 to determine T_g. The dynamic lattice model in which molecules are placed in lattice cites with all lattice cites being occupied. Rearrangements are thermally activated, with an activation energy that depends on the local density. These rearrangements can eventually result in larger-scale rearrangements, such as α relaxations. A probability of rearrangement is determined, which is used to determine τ_α [11, 15]. The Cohen and Grest model states that polymers (and liquids) are made up of solid and glass-like cells. Only the liquid-like cells have free volume. Free volume and therefore molecular motion was dependent on the number of these liquid-like cells. The model determines a temperature-dependence of the number of liquid-like cells, from which the temperature-dependence of τ_α can be determined [11, 16]. These models do agree with some experimental results, but they all have limits. Disagreements occur when either temperature or pressure is changed, or high pressures are reached. Furthermore, it appears as though free volume theories do not take into account contributions from thermal energy, which are strong, especially for hydrogen bonded materials [11].

The Thermodynamic Model

The thermodynamic model, the Gibbs and DiMarzio Theory, states that there is a true second-order phase transition after an infinitely long time period, at which point the material reaches an equilibrium state. This theory states changes to T_g with changes in crosslink density and molecular weight [9]. This would produce a glass having entropy similar to that of a crystal and produces a 'true' T_g, T_2, $\sim$50°C below the regular T_g [2]. T_2 has been found to vary with molecular weight, percent of monomer as plasticizer and degree of crosslinking [8]. The entropy, S, of this glass comes from statistical thermodynamics:

$$S = kT\left(\frac{\delta \ln Q}{\delta T}\right)_{V,n} + k\ln Q \tag{2.16}$$

where n is the number of polymer chains and Q is the 'configurational partition function.' Q comes from the different number of ways the molecules of the polymer can be arranged. At the temperature of a second-order transition, the temperature-dependent

conformational entropy, S_c must be 0. For a crosslinked network:

$$S_c = S_0 + \Delta S_R = 0 \tag{2.17}$$

where S_0 is the conformational entropy of an uncrosslinked system and ΔS_R is the change in conformational entropy due to crosslinking [17]. Crosslinking thus lowers the entropy, and thus is concluded to raise this transition temperature.

The Adam and Gibbs model is one of the most popular attempts at explaining the glass transition [11]. In this model, relaxations occur via 'cooperatively rearranging regions' (CRR) which can rearrange into different configurations, given enough energy [8]. Relaxation behaviour is dependent on the size of CRR, which in turn depends on it's configurational entropy, in turn coming from the number of configurations available to the CRR. CRR's of greater sizes have lower configurational entropies [8]. Decreases in temperature and increases in pressure increase the size of the CRR, reducing configurational entropy [11].

Avramov's model is based around the hypothesis that molecular motions are thermally activated. These motions have a range of activation energies. The viscosity of the polymer is taken as inversely proportional to the mean jump frequency of the molecular motions. By determining this mean jump frequency, viscosity can be determined, and related to both temperature and pressure [11, 18, 19].

2.2.2 Factors that Affect T_g

As stated in section 2.2.1, crosslinking raises the T_g of a polymer. An increased monomer molecular weight also increases T_g. The dependence of a polymer's T_g on these two factors is given as:

$$\frac{T(\chi') - T(0)}{T(0)} = \frac{KM\chi'/\gamma}{1 - KM\chi'/\gamma} \tag{2.18}$$

where χ' is the number of crosslinks per gram, M is the monomer molecular weight, γ is the number of flexible bonds per mer, backbone and side chain. K is a constant [17]. The change in T_g due to an increased crosslink density, $\Delta T_{g,c}$ has also been given as:

$$\Delta T_{g,c} = ZD \tag{2.19}$$

where D is the crosslink density and Z is a constant [9].

T_g is also affected by the molecular weight of the polymer chain, M:

$$T_g = T_{g,\infty} - \frac{K}{(\alpha_R - \alpha_G)M} = T_{g,\infty} - \left(\frac{2\rho N_A \theta}{\alpha_f M_n}\right) \tag{2.20}$$

where $T_{g,\infty}$ is the glass transition temperature at infinite molecular weight, K is a constant that depends on the polymer and α_R and α_G are the cubic expansion coefficients of the polymer in its rubbery and glassy states, respectively [2, 9]. θ is the free-volume contribution from one chain end, for a linear polymer this is 2θ; ρ is the polymer density; $\alpha_f = \alpha_R - \alpha_G$, the free volume expansivity and M_n is the polymer molecular weight [2]. A decrease in free volume corresponds to an increase in the

number of connected monomers. This causes a decrease in the number of free ends, increasing the T_g [9].

The specific chemical structure of the polymer affects its T_g. Factors that reduce chain flexibility raise T_g as more energy is required for molecular motion [9]. For instance, increased crosslink density and molecular mass raise T_g by reducing the amount of flexible chain ends. Polar molecules raise T_g due to increased lateral forces that reduce molecular motion. Asymmetric chains, less-flexible bonds and increased functionality raise T_g as molecular rotation is reduced. Chains that include larger groups, such as phenol rings, raise T_g as they can get 'caught' on other chains, or just reduce mobility through their greater masses and intrinsic stiffness [2]. Plasticizers reduce the T_g of polymers. These are (usually small) molecules that can dissolve in the polymer. They get caught in the gaps in a polymer network, increasing the distance between chains and reducing the intermolecular forces, such as those between polar molecules, thus increasing their mobility and lowering T_g [2, 9]. Water can form hydrogen bonds with the O-H groups in polymer networks. When only one hydrogen bond is formed, separation between polymer chains increases, lowering T_g. Multiple hydrogen bonds effectively act as pseudo-crosslinks, raising T_g. This shall be stated in greater detail in section 2.4.1.

2.2.3 Effects of Vitrification on Polymerization

At the start of polymerization, monomers are in a liquid state. These liquid monomers effectively act as plasticizers. During polymerization, the overall number of these plasticizing monomers reduces as they form the network, and the molecular weight of the polymer increases. T_g can therefore increase above the system's temperature, resulting in vitrification. As a glass, the overall molecular motion reduces significantly and thus so too does the rate of any subsequent polymerization. In order to further increase polymerization, the temperature needs to be raised so that it is once again greater than T_g. This is shown in figure 2.5 in the form of a time-temperature-transformation (TTT) diagram, a diagram showing the different states a polymer is at for curing at constant temperature for different time periods. It can be seen from the diagram that a polymer needs to be cured above $T_{g\infty}$ for there to be full cure before vitrification. It can also be seen that at low enough cure temperatures, the network can vitrify before gelation. This means that its conversion will become diffusion-dependent before a full network is formed. This is known as B-staging [5].

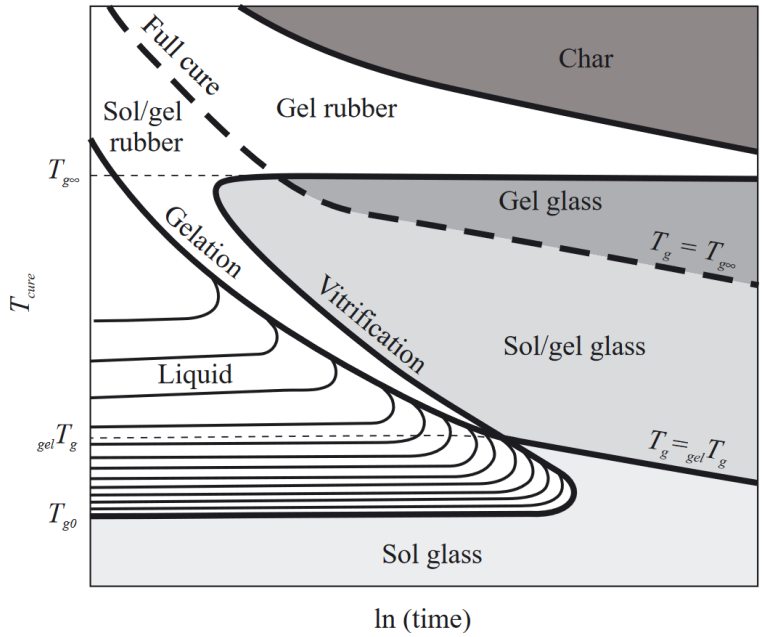

Figure 2.5: Time-temperature-transformation (TTT) diagram showing the different states of a polymer for specific temperatures over different time periods [20].

During conversion, networks can shrink. Epoxy-amine networks will shrink in volume by $\sim 5\%$. Above T_g, there is enough mobility in the system that it can accommodate this shrinkage. However, this is not the case upon vitrification. As conversion continues post-vitrification, if the network is connected to a rigid substrate as would be the case if used as a protective coating, stresses would start to occur as the network cannot move into the required smaller volume, potentially leading to delamination and cracking. Whilst a glass, the network lacks the mobility such that it cannot readjust during temperature changes. This results in increased physical ageing [5].

2.3 Epoxy Reactions

2.3.1 Epoxy-amine

Epoxy-amine polymers form via a step polymerization reaction in which an amine reacts with an epoxide ring. In the epoxide ring, the presence of the oxygen atom results in an electrophilic carbon ring. It therefore attracts the nucleophilic primary amine. In the subsequent reaction, the primary amine becomes a secondary amine which reacts with another epoxide ring via the same mechanism [21]. These mechanisms are shown in figure 2.6. The epoxy shown is DER331, and the amine MXDA, both used in the investigations described in this thesis. Note that DER331 contains two epoxide rings, giving it a functionality of two. MXDA has two primary amines, giving it a functionality of four. A mixture of the two can therefore form a crosslinked network. The reaction starts between the primary amine and epoxide ring, but around a conversion of α=0.4, this reaction becomes insignificant in place of the secondary

amine reaction. The primary amine concentration becomes negligible at α ~0.6, and secondary amine at α ~0.8 [7, 22].

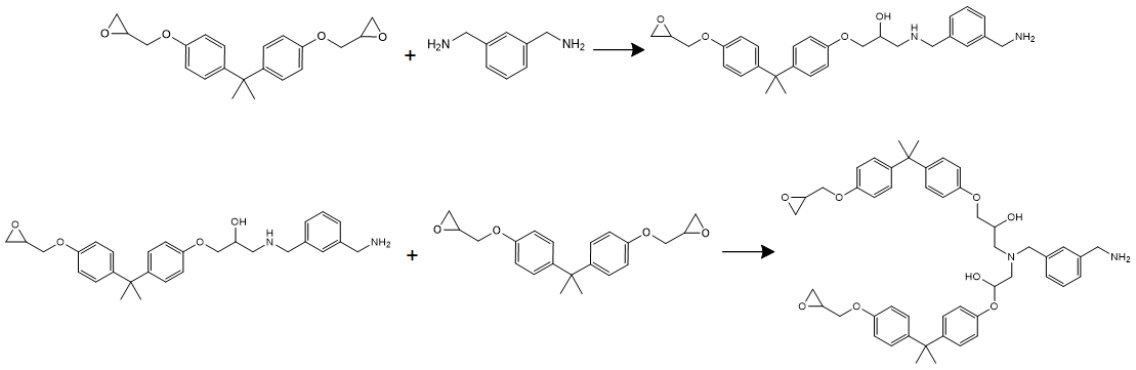

Figure 2.6: Reactions of an amine group from the amine curing agent MXDA with epoxide rings from the molecules of the epoxy DER331. Initially, a primary amine reacts with an epoxide ring to produce a secondary amine. This secondary amine can also react with an epoxide ring, producing a tertiary amine.

During the epoxy-amine reaction, there are three different types of intermediate hydrogen-bonded transition complexes that can form. They are either epoxy-amine, epoxy-hydroxyl or amine hydroxyl. It is these transition complexes that govern the rate of epoxy-amine reactions [23].

2.3.2 Etherification

Etherification can also occur between an epoxide ring and a hydroxyl group, resulting in an ether link [24]. This is shown in figure 2.7. The hydroxyl group remains at the completion of the reaction, keeping the hydroxyl concentration constant.

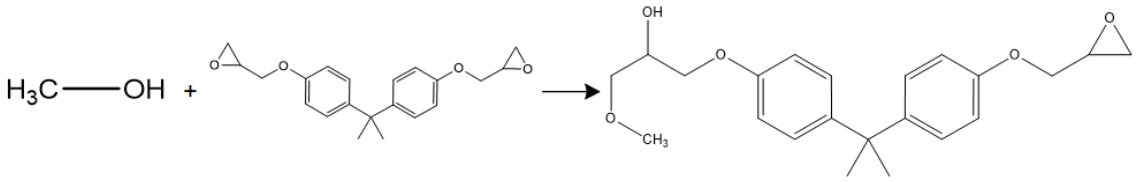

Figure 2.7: The etherification reaction that takes place for an epoxy group, on the epoxy DER331, with a hydroxyl group

Etherification reactions result in changes to the structure of the polymer network, affecting the overall T_g. The activation energy of this reaction is significantly higher than that of the epoxy-amine reaction. This reaction therefore occurs only at higher temperatures, when there is excess epoxy present [25, 26, 27] and when conversion is high. At 180°C, etherification has been shown to have a significant effect above $\alpha = 0.2$ [7].

2.3.3 Homopolymerization

In the presence of an alcohol and a tertiary amine, an epoxy group can undergo chain-growth homopolymerization [3]. This is an etherification reaction, with the tertiary amine having a catalytic effect. The reaction involves initiation, propagation and termination steps. The initiation is shown in figure 2.8. The tertiary amine, with its lone electron pair, is nucleophilic and bonds to a carbon in the epoxide ring. The alcohol meanwhile forms a hydrogen bond with the oxygen in the epoxide ring. The resultant three molecule transition state opens up the epoxide ring. A zwitterion forms along with a negatively charged oxygen atom and a positively charged nitrogen. The oxygen can engage in proton transfer with an alcohol in a reversible reaction to produce an alcoxide. The formation of the zwitterion and alkoxide is slow, resulting in a long induction period [28]. Propagation of the homopolymerization reaction is shown in figure 2.9. The alcoxide produced can react with the carbon in the epoxide ring, opening the ring and transferring its negative charge to the ring's oxygen. This negatively charged oxygen can react with the carbons on other epoxide rings, resulting in chain propagation. The negatively charged oxygen can also undergo proton transfer with an alcohol, keeping alcoxide concentration constant.
The termination step is shown in figure 2.10. The reaction is terminated when the positively charged nitrogen of the zwitterion produced in the initiation step reacts with the alcoxide. An ether bond is formed and the nitrogen neutralised, reforming the tertiary amine.
The relative rates of initiation, propagation and termination reactions determine not just the rate of reaction, but also the chain length and network structure of the polymer [3]. Given the complexity of the homopolymerization reaction, alternate mechanisms have been postulated. These mechanisms still involve an initition of an attack on the epoxide ring to produce a negatively charged oxygen ion and a propogation of chain polymerization involving this oyxgen ion. Adding to this complexity, homopolymerization of an epoxy can also occur via a tertiary amine without hydroxyl groups [28] [29].

2.3.4 Catalysed Reactions

In an epoxy-amine reaction, a transition state forms as the amine attacks the epoxy ring's carbon. The presence of an alcohol can lower the activation energy of this transition state. This is done by forming a hydrogen bond with the oxygen in the ring, stabilizing the transition state. Furthermore, in the presence of solvents, as the solvent becomes more polar, the activation energy of this state is once again lowered for the same reason. During the epoxy-amine reaction, hydroxyl groups form. Thus, autocatalysis takes place as polymerization occurs [30]. This 'self-promoted' route has a lower activation energy than the uncatalyzed pathway, but greater than that of a hyxroxyl-catalyzed reaction [30].

When incorporating solvent into the curing process, increasing the polarity of the solvent has been shown to lead to earlier transition state. Polar solvent 'solvates' (surrounds with a number of solvent molecules) the O- and N+ ions. This increased

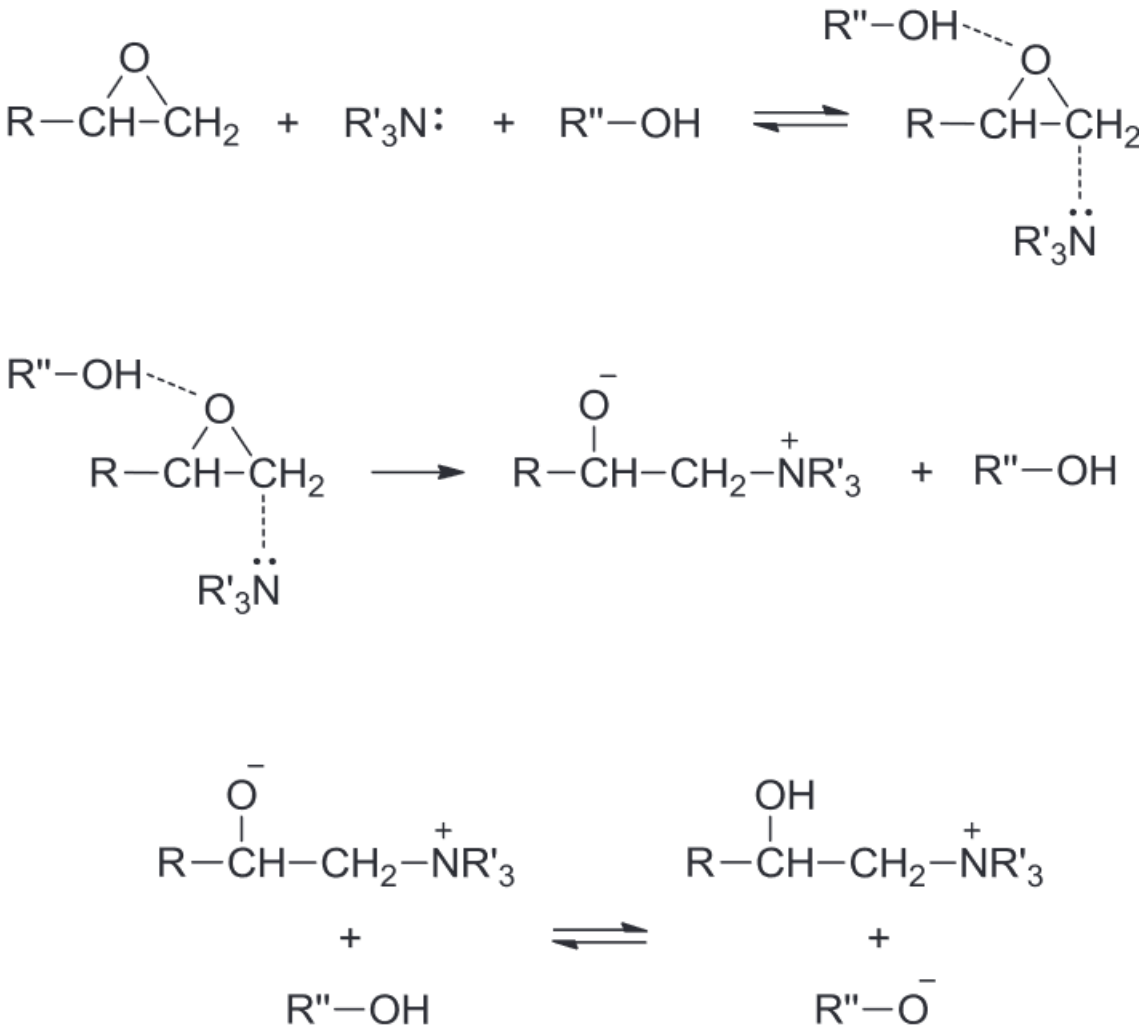

Figure 2.8: Initiation of the homopolymerization of epoxy in the presence of a tertiary amine and alcohol. R refers to the rest of the epoxy molecule, R' to the rest of the tertiary amine and R" to the rest of the alcohol.

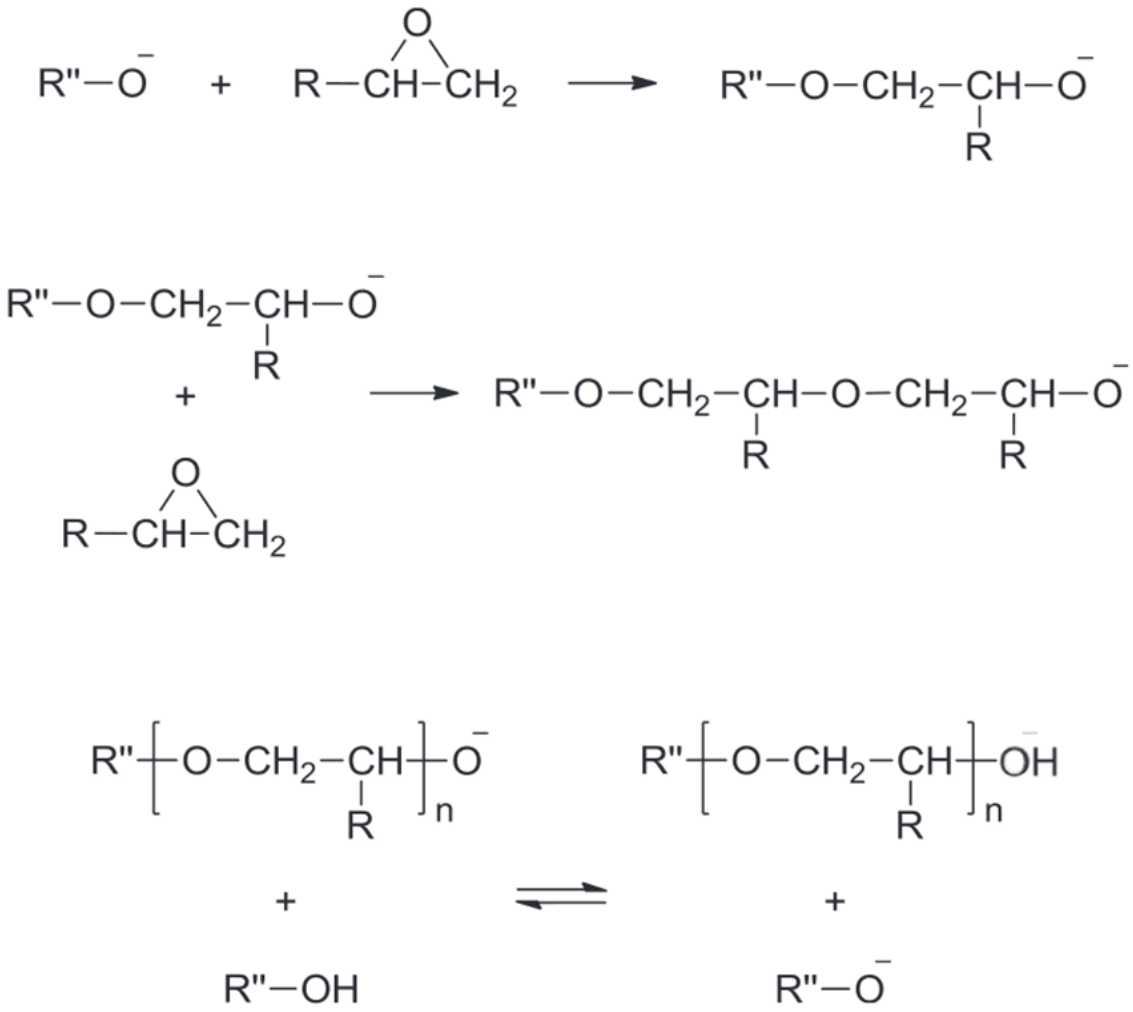

Figure 2.9: The propagation of the epoxy homopolymerization reaction in the presence of a tertiary amine and alcohol. R refers to the rest of the epoxide molecule and R" to the rest of the alcohol.

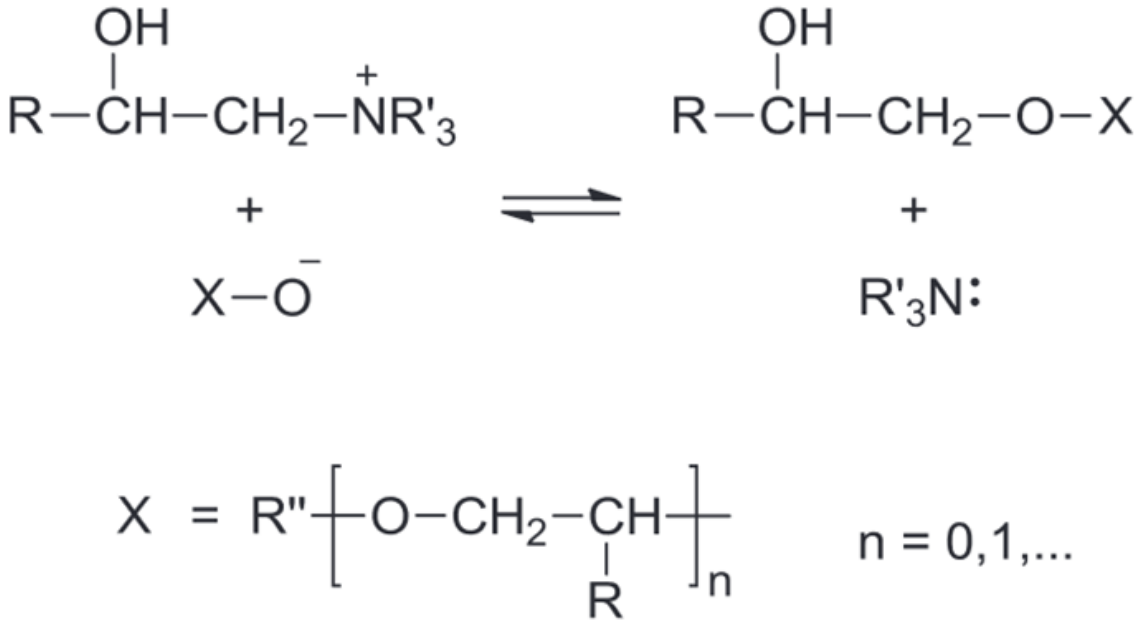

Figure 2.10: Termination of epoxy homopolymerization, in the presence of a tertiary amine and alcohol. R refers to the rest of the epoxide molecule, R' to the rest of the amine and R" to the rest of the alcohol.

separation from the final product has been shown to reduce the activation energy of the epoxy-amine reaction [30].

Tertiary amines such as DMP-30 can also accelerate the epoxy-amine reaction, again by forming a hydrogen bond with the oxygen in the epoxide ring [31]. The presence of a hydroxyl group can further reduce the activation energy by forming this hydrogen bond whilst the nitrogen attacks the carbon in the ring, as explained in section 2.3.3. Besides the presence of hydroxyl groups, the effectiveness of tertiary-amine accelerators in lowering the activation energy of the epoxy-amine reaction increases with its number of nitrogens, its lack of bulkiness and its electron density, in descending order of effectiveness. The number of nitrogen atoms in the accelerator raises the probability of nucleophilic attack on an epoxide ring. A reduced accelerator bulkiness increases its effectiveness by making it more mobile [31].

2.3.5 Carbamation

During the curing process, amines can react with carbon dioxide in air to produce an ammonium carbamate. With water vapour also being present, it can form hydrates of amine carbamate. These reactions are shown in figure 2.11. Carbamation appears as a cloudy or white layer on the surface of the cured resin [32].

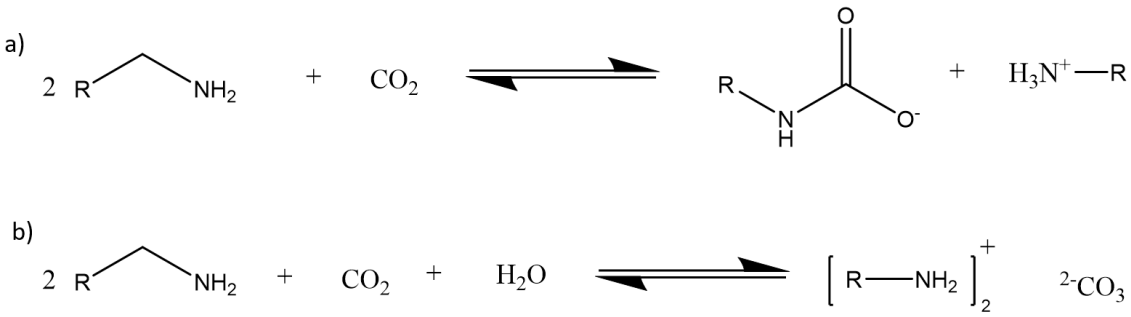

Figure 2.11: Reactions of an amine with a) carbon dioxide and b) carbon dioxide and water.

Carbamation effectively reduces stoichiometry in an epoxy-amine system. Reactive amine groups that would have reacted with epoxy groups instead undergo the carbamation reaction [32]. Carbamation mainly affects surface-level amines, due to the strong gradient in carbon dioxide near the surface, with the surface layer of $<0.1\mu$m thick showing an increased free volume compared to the bulk of the resin [33]. Due to carbamation of the surface, the resin loses the adhesive properties associated with highly cured epoxy-amines [34].

Carbamation can be reduced by changing the environment within which the resin cures. Under a nitrogen environment, the carbon dioxide and water required for amine to undergo carbamation are not present. Increasing the cure rate also reduces carbamation, as amines react with epoxide groups before they can carbamate [32]. Via both of these carbamation mitigation methods, the free volume at the surface of epoxy-amine resins is similar to that of the bulk [33].

2.3.6 Cure Kinetics of Epoxy-Amines

During conversion of epoxy-amines, the conversion of both epoxy, α and primary amines, β can be considered:

$$\alpha = 1 - \frac{E}{E_0} \tag{2.21}$$

$$\beta = 1 - \frac{2A_1 + A_2}{2A_{10}} \tag{2.22}$$

where E and E_0 are the current and initial concentrations of epoxy groups respectively, A_1 and A_{10} are the current and initial concentrations of primary amine groups and A_2 is the concentration of secondary amine groups. Determination of the reaction rate in an epoxy-amine reaction is based on the production of the reacted epoxy, x:

$$\frac{dx}{dt} = \left(k_1' c_0 + k_1 x\right)\left(e_0 - x\right)\left(a_p + R' a_s\right) \tag{2.23}$$

where k_1 and k_1' are the reactivity rates of the uncatalyzed and catalyzed primary amine reactions, respectively, e_0 and c_0 are the initial concentrations of epoxy and hydroxyl groups and a_p and a_s are the current concentration of primary and secondary amine groups. R' is the reactivity ratio; $R' = \frac{k_2}{k_1} = \frac{k_2'}{k_1'}$, where k_2 and k_2' are the

reactivity rates of the uncatalyzed and catalyzed secondary amine reactions. It is an assumption that $\frac{k_2}{k_1} = \frac{k_2'}{k_1'}$ [35]. In secondary amines, the reactivity of the remaining hydrogen is reduced due to steric hindrance reducing its mobility [23] [30]. It has also been suggested that the difference in reactivity is not entirely down to steric effects [30]. The reaction rate of secondary amines is therefore less than that of the primary amine [23]. A large k_1' value will result in a more linear network, whereas similar k_1' and k_2' values will produce a more randomly crosslinked network [23]. This relative reaction is believed to always exist between 0.5 and 1 [30]. The reactivity ratio has been shown to increase with temperature. For an epoxy-amine system, R' increased from 0.16 to 0.33 for a temperature range of 100-160°C [36].

Assuming that $R' = 0.5$ (the reactivity of a hydrogen atom in a primary amine is equal to that of a secondary amine):

$$\frac{d\alpha}{dt} = [k_1(T) + \alpha k_2(T)](1 - \alpha)(r - \alpha) \tag{2.24}$$

where k_1 is the rate constant for the epoxy-amine reaction, catalysed from groups initially present in the mixture and k_2 is the rate constant for catalysis from hydroxyl groups formed during curing. As conversion increases and hydroxyl groups are formed, the activation energy of the epoxy - primary amine reaction drops due to increased catalyzation of the reaction [37]. r is the stoichiometry of the mixture, the ratio of primary amines to epoxide groups) [7]. Equation 2.24 has been found to hold for low conversion rates, up to α <0.2, with an increase in deviation between $0.2 < \alpha < 0.3$. Equation 2.24 does not hold for $\alpha < 0.3$ as the etherification reaction becomes more prominent [7]. The activation energy of the epoxy-primary amine reaction has been found to be 55-60kJmol^{-1}. As conversion increases, this decreases to ∼20kJmol^{-1} This indicates that the rate determining step has switched from a chemically controlled process to a diffusion controlled one [22], as stated in section 2.1.3.

There is a shift in the mechanism of reaction at a critical hydroxyl concentration, P. At the early stages of reaction, with low hydroxyl concetration, hydroxyl groups tend to form complexes with epoxy groups. As conversion reactions progress and epoxy is consumed, more hydroxyl-amine complexes form. At P, the concentration of hydroxyl-amine complexes is great enough to influence the kinetics of the epoxy-amine reactions. At hydroxyl concentrations greater than P, the structure of the polymer network stops depending on the ratio $\frac{k_2'}{k_1'}$. It should be noted that $\sim 90\%$ of primary amines have reacted to form secondary amines by the time P is reached. The reaction rate of secondary amines is also further reduced when hydroxyl-amine complexes are formed due to the amine hydrogen being 'tied' to the hydroxyl group via hydrogen bonding [23].

A more rigorous model gives conversion both in terms of number of epoxy groups

that react, α; and also β, the number of amine bonds (N-H) that have reacted:

$$\frac{d\beta}{dt} = [(k_1 + Bk_2\beta)(1-\beta)](1-\alpha)f(\alpha,T) \tag{2.25}$$

$$\frac{d\alpha}{dt} = [B(k_1 + Bk_2\beta)(1-\beta) + k_3\beta^3](1-\alpha)f(\alpha,T) \tag{2.26}$$

$$\text{where } f(\alpha,T) = [1 + \exp(30.1\alpha + 4.06 - 0.1671T)]^{-1} \tag{2.27}$$

T, the temperature, is once again in Celsius. k_3 refers to the rate constant for the epoxide-hydroxyl reaction (the etherification reaction). This epoxide-hydroxyl reaction dominates from $\alpha = 0.3$ to $\alpha = 0.7$ or 0.8. The reaction rate then sees a sudden drop and falls to 0 before completion [7]. The activation energies of the X-catalysed (catalysed via impurities) and hydroxyl-catalysed epoxy-amine reactions were found to be 61.4 and 72.5kJmol^{-1}, respectively. For the etherification reaction it was found to be 101.4kJmol^{-1} [7].

2.4 Diffusion

2.4.1 Diffusion

The diffusion kinetics of a solvent over time are governed by Fick's 1st Law. Diffusion in one dimension, x, is given by:

$$J = -D\frac{d\phi}{dx} \tag{2.28}$$

where J is the flux of the diffusing solvent, and is a measure of the flow through an area per unit time. D is the diffusion coefficient and ϕ is the concentration [4]. The diffusion coefficient clearly depends on the temperature due to increased solvent mobility, as well as possible changes to the matrix through which the solvent is diffusing. The solvent equilibrium content also depends on temperature [38] [39]. An increase in temperature leads to an increase in bound water, water that forms inetermolecular forces (in this case hydrogen bonds) with the polymer network. At higher temperatures, there is also an increase in the plasticization of the polymer netwok by water [39]. The dependence of the diffusion coefficient on temperature is given as:

$$D = D_0 \exp\left(\frac{-A_0}{RT}\right) \tag{2.29}$$

where D_0 is a constant, A_0 is the activation energy of diffusion, R the universal gas constant and T temperature. The rate of solvent flow is governed by Fick's 2nd Law:

$$\frac{\delta\phi}{\delta t} = D\frac{\delta^2\phi}{\delta x^2} \tag{2.30}$$

where t is the time period. From this, the % mass uptake at time t, M_t can be determined to be:

$$\frac{M_t}{M_m} = 1 - \sum_{n=0}^{\infty} \frac{8}{(2n+1)^2\pi^2} \exp\left[\frac{-D(2n+1)^2\pi^2 t}{4L^2}\right] \tag{2.31}$$

where M_m is the maximum % mass uptake and L is the sample thickness [40]. For a short time period at the onset of diffusion, when $\frac{M_t}{M_m} < 0.5$, mass uptake from solvent

diffusion is proportional to $\sqrt{t}$ [41]:

$$M_t = \frac{4M_m}{L}\sqrt{\frac{tD}{\pi}} \tag{2.32}$$

This assumes the film has two sides. With one side, L is doubled [41]. It also assumes that D is a constant:

$$D = \frac{\pi}{16}\left(\frac{L}{M_m}\right)^2\left(\frac{M_{t2} - M_{t1}}{\sqrt{t_2} - \sqrt{t_1}}\right)^2 \tag{2.33}$$

where M_{t1} and M_{t2} are the % mass uptakes at times t_1 and t_2, respectively [40].

During the initial period of solvent uptake, diffusion in polymers is often Fickian in nature. However, over longer time periods, simulations and experimental results have shown that there is a second diffusion mechanism alongside Fickian diffusion [42] [39]. This appears as an increased mass gain or taking longer to reach equilibrium. Both the mass gain and the time to equilibrium depend on temperature [39]. This second, much slower, diffusion mechanism could either come from water, where 'bound' water is believed to have a delayed effect on diffusion; or from the polymer network as it relaxes during water ingress. With very few parameters, the Berens and Hopfenberg model details diffusion due to network relaxation. This is a model that is relatively easy to use:

$$w_{BH}(t) = w_F(t) + w_R(t) \tag{2.34}$$

$$\text{where } w_R(t) = w_{\infty R}\left[1 - \exp\left(\frac{-t}{\tau_R}\right)\right] \tag{2.35}$$

where w_{BH} is the overall mass gain, w_F is the mass gain from Fickian diffusion and w_R from relaxation of the polymer network. $w_{\infty R}$ is the equilibrium water content due to network relaxation and τ_R is the first-order relaxation time. The uptake from both diffusion and this larger timescale polymer relaxation, as described by the Berens and Hopfenberg model, is shown in figure 2.12. Non-Fickian diffusion is observed when the polymer network relaxation time is much smaller or greater than the Fickian diffusion time [39]. In epoxy-amine resins, greater levels of non-Fickian diffusion are observed in stoichiometric or epoxy-rich formulations than in amine-rich formulations. The activation energy of diffusion is also observed to be lower in epoxy-rich formulations, and the saturation level higher [38].

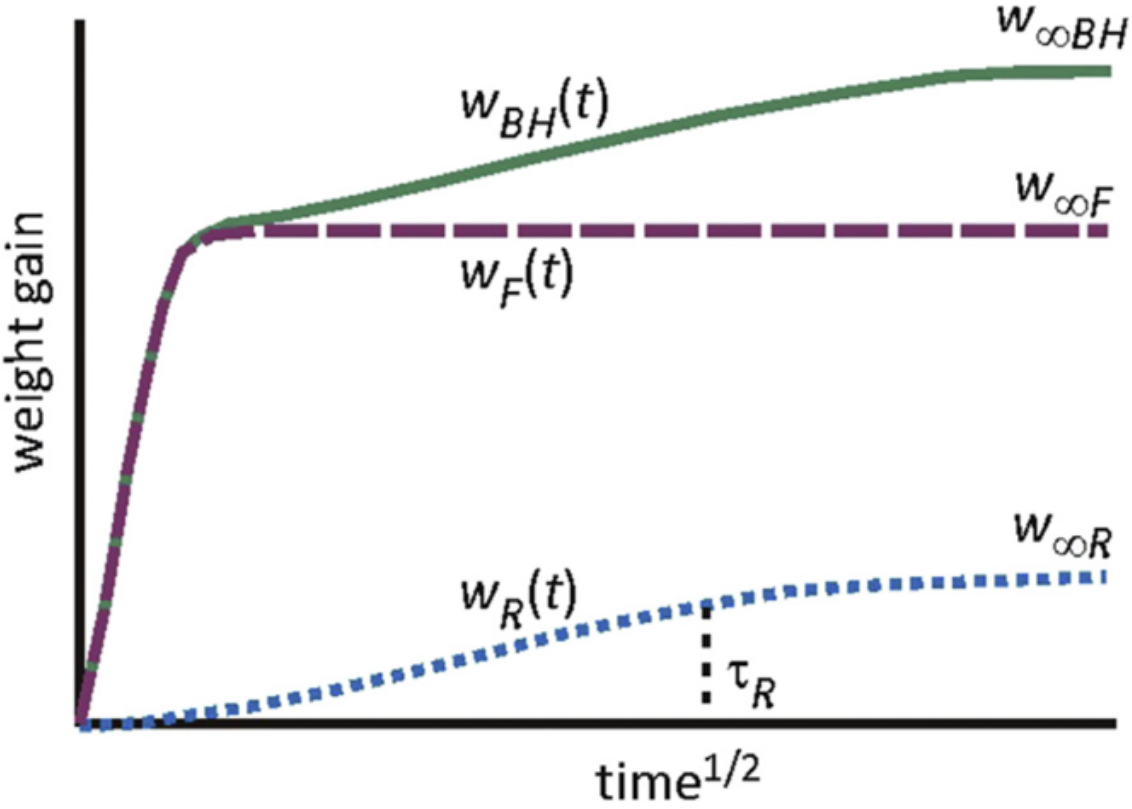

Figure 2.12: Schematic showing the overall mass uptake, mass uptake due to diffusion and mass uptake due to polymer relaxation of a polymer network when immersed in a solvent. w_{BH} represents the total uptake, w_F the contribution to uptake from Fickian diffusion and w_R the contribution to uptake from polymer relaxation as described by the Berens and Hopfenberg model. [39]

2.4.2 Water uptake

Water uptake in polymer networks depends on the number of molecule-sized holes in the network and so is heavily dependent on the free volume [38, 40]. Uptake is also dependent on the network's 'polymer-water affinity' [38]. This relates to hydrogen bonding sites on the polymer with which water can bond to. Hydrogen bonding is important in epoxies due to the presence of hydroxyl groups. However due to the inaccessibility of these H-bonding sites, it is the free volumes in the network that dominate the diffusion. The number and size of these free volumes depends on conversion, stoichiometry, chain flexibility and the 'cohesive energy density' of the polymer. The voids/holes in the network i.e. its free volume form due to incomplete conversion, resulting in areas of low crosslink density. With this decreased crosslink density (and decreased molecular weight), there are more isolated polymer chains that can associate with the solvent. A reduction in crosslink density also raises chain mobility, allowing solvent to more easily penetrate the polymer network [43]. The free volume has been shown to increase with cure temperature in epoxy-amine resins, and so too does the

absorption equilibrium content [44].

In a dry epoxy-amine network, 65% of the hydroxyl group hydrogens do not form hydrogen bonds, they are 'free' [38]. The remaining 35% are hydrogen bonded either to other hydroxyl group oxygens (26%), ether group oxygens (4%) or tertiary amine nitrogens (5%) [45]. Hydroxyl groups can more easily bond to the water molecules as they have greater steric freedom [38]. Water uptake is focused on these polar groups, reducing the number of hydroxyl-hydroxyl hydrogen bonds in the polymer network and also forming hydrogen bonds preferentially with these hydroxyl groups. Some water is free, bonded to other water molecules rather than the polymer network. This free water increases as moisture content increases [45].

The absorption of water into epoxy resins has been shown to have a negative effect on the network. Specifically these effects stem from the bound water. The polymer-water H-bonds displace the polymer-polymer H-bonds, affecting the overall network structure and connectivity, leading to swelling and plasticization [38]. This is more of an issue in lower crosslink density regions, due to greater levels of diffusion. For a 1% mass uptake of water, epoxy resins with different curing agents have had a T_g drop of $\sim$10°C and losses of 10% in storage modulus and 15% in tensile strength [42]. Increased water uptake has been shown to lead to higher T_g drops. Large T_g reductions have been observed in amine-rich epoxy-amines [38]. This diffusion process has been shown to occur at greater levels at higher temperatures [38, 39]. This T_g almost reverts to its original value upon drying [39], believed to be due to plasticization from the water. This non-Fickian diffusion process has been shown to occur to a greater extent at higher temperatures [38, 39]. It is believed to occur due to increased polymer relaxation. Immediately following water uptake, there is an initial instantaneous stress in the polymer network that decreases over time as water plasticizes the network. This stress is also seen in drying and in practical terms can lead to separation debonding/delamination between a coating and its substrate if high enough [46].

The bound water in the network has been postulated to be made up of two types [47, 48]. These are shown in figure 2.13. These types of bound water also apply to other solvents that can form multiple hydrogen bonds, such as methanol [40]. Type one features the solvent forming one hydrogen-bond to the polymer network. For water, these bonds have an activation energy of $\approx 42\text{kJmol}^{-1}$ [47]. It is this type of bonding between solvent and network that swells and plasticizes the network, by disrupting the Van-der-Waals forces between different chains in the polymer. Type one bonding is the dominant form of 'bound' solvent that occurs during swelling. Type two involves the solvent forming multiple hydrogen-bonds with the polymer. This effectively acts as a crosslinking mechanism. Water uptake can therefore raise T_g in lower-crosslink networks. In more densely crosslinked networks, T_g is lowered as type two bonding takes place due to network disruption, leading to microcracks [49]. The T_g change also depends on the bond strength in type two bonding [50]. For water, this has an activation energy of $\approx 63\text{kcalmol}^{-1}$. It should be noted that the difference in activation

energy between type one and type two bonds is of the order of a hydrogen-bond [47]. Given this raised activation energy, it has been seen that temperatures in the range of 100-110°C are needed to remove all bound water from polymer networks [47, 49]. Type two bonding takes extended times and elevated temperature. During swelling, a large drop in T_g is initially seen due to type one bonding, followed by a small, gradual increase as type two bonding increases [47].

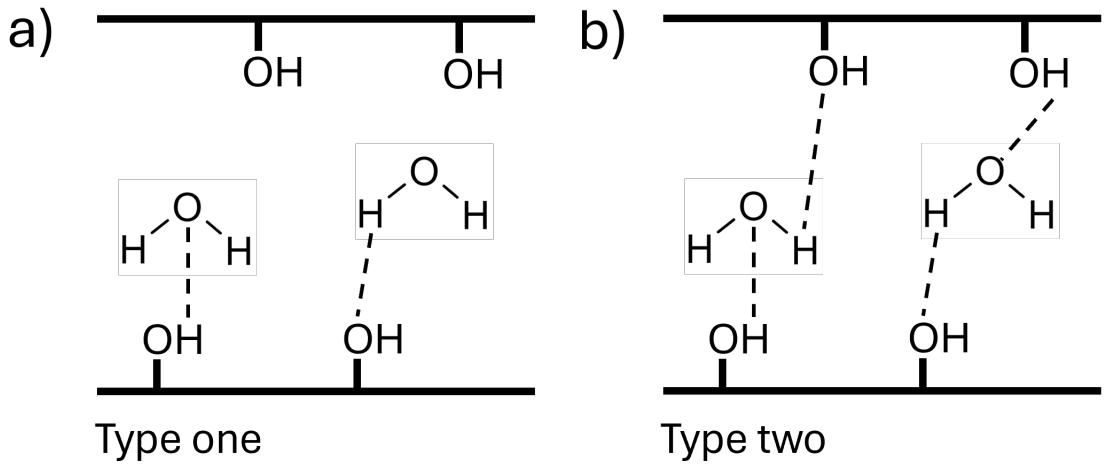

Figure 2.13: The two types of bound water in a polymer network. a) shows type one bound water, in which water forms only one hydrogen-bond with the polymer network. b) shows type two, in which multiple hydrogen bonds are formed between water and the network. The bonds shown are with hydroxyl groups present in the polymer network, such as in epoxy-amines.

2.5 Curing with Solvents

Epoxy-amines can be mixed with solvents so that the polymer mix dissolves in the solvent, reducing the mix viscosity. The coating can therefore be more easily applied to a substrate via spraying [51]. Plasticizing the network via dissolving in solvents also suppresses T_g and raises species mobility [5]. Solvent evaporation occurs mainly during the early stages of network formation. It results in increased functional group concentration and thus increased reactivity. As the solvent evaporates, the T_g is raised (and mobility drops) [5]. By suppressing the T_g in this way, the conversion and subsequent T_g of the network can be raised for lower curing temperatures (as a T_g closer to the cure temp inhibits conversion) [5] [52]. Solvents of different volatility will be able to suppress this T_g for different lengths of time [5]. Generally, multiple solvents are used so that the rate of evaporation can be controlled. Using different solvents also allows for different components of the coating to dissolve [51].

Solvent evaporation changes during the formation of the polymer network. Before

this network formation, evaporation depends on vapour pressure. Afterwards, solvent is retained in the network and evaporation depends on a much slower diffusion process. The rate of evaporation in this diffusion process does not depend on the initial evaporation rate, or upon its molar volume. Up to 20% of solvent may be retained in the network due to this change in the evaporation rate [53]. Similarly to conversion, solvent evaporation results in shrinkage of an epoxy-amine network. Again, this can lead to delamination and cracking one of the network if evaporation occurs in a vitrified network [5]. This is generally reduced if the solvent evaporates more slowly, although in crosslinked systems the opposite may be the case. For a mixture of solvents, the magnitude of the stress induced from evaporation is determined by the less volatile solvent [54]. Again similarly to conversion, upon vitrification, solvent evaporation is massively reduced. It is possible that during the formation of tensile stresses after vitrification, solvent is retained in the network so as to minimise stress. Retained solvent has negative impacts on the network properties, reducing hardness and increasing water sensitivity [5]. On the other hand insufficient solvent can lead to de-wetting of the coating, resulting in unprotected areas of substrate [51]. Solvent can also be distributed inhomogeneously throughout the network, leading to further negative effects [5].

Curing with solvent has been shown to lower the maximum conversion of epoxy and reduce crosslink density in the polymer network, slightly reducing the T_g of the final network [55] [56]. Curing with solvents affects the epoxy-amine's reaction kinetics by changing the local temperature as the solvent evaporates. The effect of this evaporation is similar to lowering the cure temperature by 10°C. This reduces the rate of conversion. The greater the boiling point of the solvent, the more the reaction rate is reduced, as there is more solvent to affect the cure [56]. The evaporation of solvent is believed to create small 'voids,' throughout the material, aiding the mobility of polymer chains, reducing tensile strength whilst in turn raising flexibility [55]. The reduction in epoxy conversion, as well as solvent having an 'interference effect' reduces the number of hydrogen bonds present in the network. This reduces the adhesion of the coating to metal by reducing its ability to form hydrogen bonds with the metal oxide surface layer[57].

2.5.1 Solubility of Molecules in Solvents

The ability of molecules to dissolve in a liquid is governed by the intramolecular forces between the molecule and the liquid. For a polar molecule, these would be hydrogen bonds or dipole-dipole interactions. For non-polar molecules, these would arise from Van der Waals forces. Liquids with similar solubility parameters, δ, are expected to be miscible:

$$\delta = \sqrt{\frac{\Delta E_v}{V_m}} \tag{2.36}$$

where ΔE_v is the energy of vaporization and V_m is the molar volume. Solvents can be split into three groups: weakly hydrogen-bonded, moderately hydrogen-bonded and strongly hydrogen-bonded. For a mixture of solvents, the δ value can be determined

from the average of the constituent solvents, taking their ratios into account. The δ values of polymers can be determined by seeing how well they dissolve in the different solvents. This solubility parameter can be expressed through the solubility parameters based on hydrogen bonding, δ_h; dipole-dipole (polar) interactions, δ_p and Van-der-Waals forces (dispersion), δ_d to give an overall solubility for the solvent, δ_s:

$$\delta_s{}^2 = \delta_d{}^2 + \delta_p{}^2 + \delta_h{}^2 \tag{2.37}$$

This value of δ_s can effectively be plotted as a three-dimensional coordinate (with the value of δ_d being doubled). For a polymer, the solubility parameter can be represented as a sphere in this three-dimensional system, the 'sphere of solubility,' defined by its centre position and radius, R_p. This radius is determined by seeing which solvents the polymer dissolves in: if it dissolves in the solvent, the R_p is set so that the polymer's sphere of solubility encompasses the 3-D coordinate of the solvent, set by the solvent's three solubility parameters. For a solvent that has yet to be tested, if the distance between the coordinates of δ_s and the centre of the sphere of solubility, R_s, is less than the radius of the sphere of solubility, R_p i.e. the position of the solvent in this 3-D space lies with thin the sphere of the polymer, then the polymer would be soluble in the solvent [53].

2.6 Performance of Coatings

Epoxy resins see use as protective coatings due to high water, chemical and heat resistance, display excellent mechanical strength and toughness as well as good adhesion to metals [58]. The chemical resistance is believed to come from the backbone of epoxy molecules containing stable carbon-carbon and ether bonds. Unreacted epoxy resins of low molecular weight have a higher functional group density than those of high molecular weight, resulting in higher crosslink density polymers. This leads to increased solvent resistance as mobility is reduced meaning that it is more difficult for molecules to penetrate the network. Chemical resistance and hardness also increase with increased crosslink density, whereas impact resistance decreases [51]. Crosslink density, and thus the beneficial and negative properties associated with it, are maximized when conversion is at its maximum. Maximum crosslink density is therefore found in epoxy-amine resins of stoichiometric ratio [59]. Excess epoxy has been found to reduce crosslink density at a greater rate than equivalent excess amine [59].

Adhesion to a metal substrate can be improved by increasing the polarity of the coating. This can be done by upping the density of OH bonds. However, increased OH bonds results in an increase in crosslink density. An increased crosslink density increases stress during film formation, due to reduced mobility in the film. Therefore an increase in the polarity of the coating actually reduces the overall stress required to remove the coating from the substrate. These stresses can be reduced by incorporating a softer network into the coating [46].

References

[1] G. Strobl. *The Physics of Polymers*. 2nd ed. Springer, 1997.

[2] J. M. G. Cowie and V Arrighi. *Polymers : Chemistry and Physics of Modern Materials*. 3rd ed. Taylor and Francis Group, 2007.

[3] John D. McCoy et al. "Cure mechanisms of diglycidyl ether of bisphenol A (DGEBA) epoxy with diethanolamine". In: *Polymer* 105 (2016), 243–254. DOI: 10.1016/j.polymer.2016.10.028.

[4] R. A. L. Jones. *Soft Condensed Matter*. Oxford University Press, 2014. Chap. Phae Transitions.

[5] A. R. Marrion. *The Chemistry and Physics of Coatings*. 2nd ed. The Royal Society of Chemistry, 2004.

[6] K. P. Pang and J. K. Gillham. "Competition between cure and thermal degradation in a high Tg epoxy system: Effect of time and temperature of isothermal cure on the glass transition temperature". In: *Journal of Apllied Polymer Science* 39.4 (1990), pp. 909–933. DOI: 10.1002/app.1990.070390411.

[7] K. C. Cole, J. J. Hechler, and D. Noel. "A New Approach to Modeling the Cure Kinetics of Epoxy Amine Thermosetting Resins. 2. Application to a Typical System Based on Bis [4-(diglycidylamino)phenyl]methane and Bis(4aminophenyl)Sulfone". In: *Macromolecules* 24.11 (1991), pp. 3098–3110. DOI: 10.1021/ma00011a012.

[8] G. Adam and J. Gibbs. "On the Temperature Dependence of Cooperative Relaxation Properties in Glass-Forming Liquids". In: *The Journal of Chemical Physics* 43.1 (1965), pp. 139–146. DOI: 10.1063/1.1696442.

[9] L. H. Sperling. *Introduction to Physical Polymer Science*. 2nd ed. John Wiley and Sons, Inc., 1992.

[10] S. P. Andersson and O. Andersson. "Relaxation Studies of Poly(propylene glycol) under High Pressure". In: *Macromolecules* 21.9 (1998), pp. 2707–3162. DOI: 10.1021/ma971282z.

[11] C. M. Roland et al. "Supercooled dynamics of glass-forming liquids and polymers under hydrostatic pressure". In: *Reports on Progress in Physics* 68.6 (2005), pp. 1405–1478. DOI: 10.1088/0034-4885/68/6/R03.

[12] R. P. White and J. E. G Lipson. "Polymer Free Volume and Its Connection to the Glass Transition". In: *Macromolecules* 49.11 (2016), 3987–4007. DOI: 10.1021/acs.macromol.6b00215.

[13] A. Sorrentino and R Pantani. "Pressure-dependent viscosity and free volume of atactic and syndiotactic polystyrene". In: *Rheologica Acta* 48 (2009), 467–478. DOI: 10.1007/s00397-009-0348-x.

[14] R. Simha and T. Somcynsky. "On the statistical thermodynamics of spherical and chain molecule fluids". In: *Macromolecules* (1969), pp. 342–350.

[15] T. Pakula. "Collective dynamics in simple supercooled and polymer liquids". In: *Journal of Molecular Liquids* 86.1-3 (2000), pp. 109–121. DOI: 10.1016/S0167-7322(99)00132-4.

[16] G. S. Grest and M. H. Cohen. "Liquid-glass transition: Dependence of the glass transition on heating and cooling rates". In: *Physical Review B* 21.9 (1980), pp. 4113–4117. DOI: 10.1103/PhysRevB.21.4113.

[17] E. A. DiMarzio. "On the Second-Order Transition of a Rubber". In: *JOURNAL OF RESEARCH of the National Bureau of Standards* 68A.6 (1964), pp. 611–617. DOI: 10.6028/jres.068A.059.

[18] I Avramov. "Pressure dependence of viscosity of glassforming melts". In: *Journal of Non-Crystalline Solids* 262.1-3 (2000), pp. 258–263. DOI: 10.1016/S0022-3093(99)00712-7.

[19] M. Paluch and C. Roland. "The Avramov model of structural relaxation". In: *Journal of Non-Crystalline Solids* 316.2-3 (2003), pp. 413–417. DOI: 10.1016/S0022-3093(02)01963-4.

[20] M. Urbaniak and K Grudzinski. "Time-temperature-transformation (TTT) cure diagram for EPY® epoxy system". In: *Polimery* 52.2 (2007), pp. 117–126. DOI: 10.14314/polimery.2007.117.

[21] S. T. Cholake et al. "Quantitative analysis of curing mechanisms of epoxy resin by mid- and Near- Fourier transform Infra Red Spectroscopy". In: *Defence Science Journal* 64.3 (2014), pp. 314–321. DOI: 10.14429/dsj.64.7326.

[22] N. Sbirrazzuoli et al. "Isoconversional kinetic analysis of stoichiometric and off-stoichiometric epoxy-amine cures". In: *Thermochimica Acta* 447.2 (2006), pp. 167–177. DOI: h10.1016/j.tca.2006.06.005.

[23] J. Mijovic and J Wijaya. "Reaction Kinetics of Epoxy/Amine Model Systems. The Effect of Electrophilicity of Amine Molecule". In: *Macromolecules* 27 (1994), pp. 7589–7600.

[24] L. Xu and J. R. Schlup. "Etherification versus amine addition during epoxy resin/amine cure: An in situ study using near-infrared spectroscopy". In: *Applied Polymer* 67.5 (1998), pp. 769–959. DOI: 10.1002/(SICI)1097-4628(19980131)67:5<895::AID-APP15>3.0.CO;2-N.

[25] N. Sbirrazzuoli et al. "A Study of Epoxy-Amine Cure Kinetics by Combining Isoconversional Analysis with Temperature Modulated DSC and Dynamic Rheometry". In: *Macromolecular Chemistry and Physics* 204.15 (2003), pp. 1815–1821. DOI: 10.1002/macp.200350051.

[26] B. E. F. Ekbrant, A. L. Skox, and A. E. Daugaard. "Epoxy-Rich Systems with Preference for Etherification over Amine-Epoxy Reactions for Tertiary Amine Accelerators". In: *Macromolecules* 54.9 (2021), pp. 3907–4454. DOI: 10.1021/acs.macromol.0c02630.

[27] C. M. Sahagun and S. E. Morgan. "Thermal Control of Nanostructure and Molecular Network Development in Epoxy-Amine Thermosets". In: *Applied Materials and Interfaces* 4.2 (2012), pp. 564–572. DOI: 10.1021/am201515y.

[28] I. E. Dell'Erba and R. J. J Williams. "Homopolymerization of epoxy monomers initiated by 4-(dimethylamino)pyridine". In: *Polymer Engineering Science* 46.3 (2006), pp. 351–359. DOI: 10.1002/pen.20468.

[29] A. Vasquez et al. "Polymerization of epoxides in the presence of tertiary amino alcohols". In: *Journal of Polymer Science Part A: Polymer Chemistry* 28.9 (1990), pp. 2305–2319. DOI: /10.1002/pola.1990.080280907.

[30] J. Ehlers et al. "Theoretical Study of the Epoxy-Amine Curing Reaction". In: *Macromolecules* 40.12 (2007), pp. 4370–4377. DOI: 10.1021/ma070423m.

[31] M. Hesabi, A. Salimi, and M. H. Beheshty. "Effect of tertiary amine accelerators with different substituents on curing kinetics and reactivity of epoxy/dicyandiamide system". In: *Polymer Testing* 59 (2017), pp. 344–354. DOI: 10.1016/j.polymertesting.2017.02.023.

[32] T. Dinnissen. "Amine blushing and blooming of epoxy binder systems in protective coatings". In: *Paint and Coatings Industry* 22.2 (2006), pp. 66–68, 70.

[33] A. S. D. Shackleford. "Using Positron Annihilation as a Method to Characterise Epoxy Networks with Regards to Chemical Resistance". PhD thesis. The University of Sheffield, Faculty of Engineering, Department of Mechanical Engineering, 2019.

[34] C. Bannister et al. "The influence of ambient cure chemistry and stoichiometry on epoxy coating surfaces". In: *RSC Advances* 12 (2022), pp. 28746–28754. DOI: 10.1039/d2ra05067f.

[35] K. Horie et al. "Calorimetric investigation of polymerization reactions. III. Curing reaction of epoxides with amines". In: *Journal of Polymer Science Part A-1: Polymer Chemistry* 8.6 (1970), pp. 1357–1372. DOI: 10.1002/pol.1970.150080605.

[36] X. Wang and J. K. Gillham. "Competitive Primary Amine/ Epoxy and Secondary Amine/Epoxy Reactions: Effect on the Isothermal Time-to-Vitrify". In: *Journal of Applied Polymer Science* 43.12 (1991), pp. 2267–2277. DOI: 10.1002/abio.370040210.

[37] S. Vyazovkin and N. Sbirrazzuoli. "Mechanism and Kinetics of EpoxyAmine Cure Studied by Differential Scanning Calorimetry". In: *Macromolecules* 29.6 (1996), pp. 1867–1873. DOI: 10.1021/ma951162w.

[38] M. R. Vanlandingham, R. F. Eduljee, and J. W. Gillespie Jr. "Moisture diffusion in epoxy systems". In: *Journal of Applied Polymer Science* 71.5 (1999), pp. 787–798. DOI: 10.1002/(SICI)1097-4628(19990131)71:5<787::AID-APP12>3.0.CO;2-A.

[39] O. Starkova et al. "Anomalous water diffusion in epoxy/carbon nanoparticle composites". In: *Polymer Degradation and Stability* 164 (2019), pp. 127–135. DOI: 10.1016/j.polymdegradstab.2019.04.010.

[40] J. Wang et al. “Effect of curing agent polarity on water absorption and free volume in epoxy resin studied by PALS”. In: *Nuclear Instruments and Methods in Physics Research B* 268.14 (2010), pp. 2355–2361. DOI: 10.1016/j.nimb.2010.04.010.

[41] C-H. Chen and G. S. Springer. “Moisture Absorption and Desorption of Composite Materials”. In: *Journal of Composite Materials* 10.1 (1976), pp. 2–20. DOI: 10.1177/002199837601000101.

[42] M. Lai et al. “An experimental–numerical study of moisture absorption in an epoxy”. In: *Composites Part A: Applied Science and Manufacturing* 43.7 (2012), pp. 1053–60. DOI: 10.1016/j.compositesa.2012.01.027.

[43] A. M. Atta et al. “Epoxy resins from rosin acids: synthesis and characterization”. In: *Polymers for Advanced Technologies* 15.9 (2004), pp. 514–522. DOI: 10.1002/pat.507.

[44] F. X. Perrin, M. H. Nguyen, and J. L. Vernet. “Water transport in epoxy–aliphatic amine networks – Influence of curing cycles”. In: *European Polymer Journal* 45.5 (2009), 1524–1534. DOI: j.eurpolymj.2009.01.023.

[45] J. Mijovic and H. Zhang. “Molecular Dynamics Simulation Study of Motions and Interactions of Water in a Polymer Network”. In: *The Journal of Physical Chemistry B* 108.8 (2004), pp. 2557–2563. DOI: 10.1021/jp036181j.

[46] M. Piens and H. De Deurwaerder. “Effect of coating stress on adherence and on corrosion prevention”. In: *Progress in Organic Coatings* 43.1-3 (2001), pp. 19–24. DOI: 10.1016/S0300-9440(01)00243-0.

[47] J. Zhou and J. Lucas. “Hygrothermal effects of epoxy resin. Part I: the nature of water in epoxy”. In: *Polymer* 40.20 (1999), pp. 5501–5512. DOI: 10.1016/S0032-3861(98)00790-3.

[48] J. Zhou and J. Lucas. “Hygrothermal effects of epoxy resin. Part II: variations of glass transition temperature”. In: *Polymer* 40.20 (1999), pp. 5513–5522. DOI: 10.1016/S0032-3861(98)00791-5.

[49] S. O. Han and L. T. Drzal. “Water absorption effects on hydrophilic polymer matrix of carboxyl functionalized glucose resin and epoxy resin”. In: *European Polymer Journal* 39.9 (2003), pp. 1791–1799. DOI: 10.1016/S0014-3057(03)00099-5.

[50] T. Wang et al. “Methanol degradation mechanisms and permeability phenomena in novolac epoxy and polyurethane coatings”. In: *Journal of Coatings Technology and Research* 18.3 (2021), 831–842. DOI: 10.1007/s11998-020-00446-w.

[51] P. A. Sørensen et al. “Anticorrosive coatings: a review”. In: *Journal of Coatings Technology and Research* 6.2 (2009), pp. 135–176. DOI: 10.1007/s11998-008-9144-2.

[52] M. Pramanik et al. “Amidoamine: Synthesis, disparity in cure with epoxy resins between bulk and solvent systems, and structure–property relationships of its epoxy-based coatings”. In: *Polymer Engineering and Science* 59.S1 (2019), E69–E81. DOI: 10.1002/pen.24858.

[53] R. Lambourne and T. A. Strivens, eds. *Paint and Surface Coatings: Theory and Practice*. 2nd ed. Woodhead Publishing Ltd, 1999. ISBN: 85573 348 X.

[54] D. Perera. “Stress phenomena in organic coatings. Paint and coating testing manual”. In: (1995), pp. 655–672.

[55] C. Yi et al. “Curing kinetics and mechanical properties of epoxy based coatings: The influence of added solvent”. In: *Progress in Organic Coatings* 124 (2018), pp. 165–174. DOI: 10.1016/j.porgcoat.2018.08.009.

[56] H. Shing-Gwo and W. Chung-Sheng. “DSC and FTIR analysis of the curing behaviors of epoxy/DICY/solvent open systems”. In: *Thermochimica Acta* 316.2 (1998), pp. 167–175. DOI: 10.1016/S0040-6031(98)00356-6.

[57] K. Miyauchi et al. “A study of adhesion on stainless steel in an epoxy/dicyandiamide coating system: Influence of glass transition temperature on wet adhesion”. In: *Progress in Organic Coatings* 99 (2016), pp. 302–307. DOI: 10.1016/j.porgcoat.2016.06.002.

[58] E. Duemichen et al. “Analyzing the network formation and curing kinetics of epoxy resins by in situ near-infrared measurements with variable heating rates”. In: *Thermochimica Acta* 616 (2015), 49–60. DOI: 10.1016/j.tca.2015.08.008.

[59] Fred Meyer et al. “The effect of stoichiometry and thermal history during cure on structure and properties of epoxy networks”. In: *Polymer* 36.7 (1995), 1407–1414. DOI: 10.1016/0032-3861(95)95918-q.

Chapter 3

Methods

3.1 Preparation of Cured Epoxy-Amine Networks

3.1.1 Sample Preparation

Samples of were prepared and cured with and without homopolymerizing agent and solvents. The epoxy used was initially DER331 and after that UC0003, (both supplied by Akzo-Nobel, Felling UK). The UC0003 supplied contained mainly DER331, but also contained Epicote 828 and Razeen LR 1150 both DGEBA based epoxies. DER331 is a Bisphenol A diglycidyl ether (DGEBA) epoxy. The epoxide equivalent weight (EEW) of the epoxy was determined via titration. MXDA (Sigma-Aldrich) was used as the amine crosslinking agent. It had an amine-hydrogen equivalent weight (AHEW) of 34gmol^{-1}. The required amine mass, m_A was determined using:

$$m_A = r \cdot m_E \frac{\text{AHEW}}{\text{EEW}} \tag{3.1}$$

Where r is the required stoichiometry (the ratio of amine functional groups to epoxy functional groups) of the sample and m_E is the mass of epoxy used. The homopolymerizing agent used was DMP-30 (Sigma-Aldrich), with a molar mass of 265.4gmol^{-1}. Moles of DMP-30 equivalent to 3% of the moles of the epoxy were used. A mixture of o-xylene (Sigma Aldrich) and butanol (Honeywell) of ratio 3:1 of xylene mass: butanol mass were used as the solvents. Solvent was added so that it comprised 40% of the overall mixture mass.

The initial preparation method was taken from Alec Shackleford's thesis [1]. Samples of epoxy-amines were prepared with the aim of having maximum conversion of epoxy and amine into a polymer network. This preparation could be split into two parts: the pre-cure mixing and the subsequent curing of samples. The pre-cure mixing needed to distribute the constituents of the mixture evenly. The thermal cure aimed to achieve maximum conversion of epoxy and amine. For both stages of preparation, adverse reactions such as carbamation and oxidation needed to be minimized. DSC measurements of T_g after cure, as shall be outlined in section 3.2, were used as a proxy for this conversion, with a maximum T_g indicating a maximum conversion.

The required mass of epoxy was weighed out into a glass beaker. In order to prevent carbamation, the beaker was covered with Parafilm, with a small puncture in it to allow the addition of the other mixture components. It could be observed by eye that without the Parafilm cover, a white layer would form on the surface of the epoxy-amine mixture, indicative of carbamation. The required masses of amine and DMP-30, followed by the solvents, were then added via pipette. A glass stirring rod was placed through the hole in the Parafilm before being covered again by additional layers of Parafilm to prevent carbamation or any contamination getting into the mixture during mixing.

The required pre-cure regime to adequately distribute the mixture was determined by comparing these different regimes to the T_g of the final cured samples. After the pre-cure regime, mixes were weighed out into DSC pans. They were placed in a freezer at -10°C in order to reduce curing, other reactions and solvent evaporation. All samples were then subsequently cured together.

Non-solvent mixtures were stirred for five minutes and left for fifteen minutes. Results for mixes of UC0003 and MXDA of stoichiometries r=1 and 0.57 are shown in table 3.1. There is little change in T_g for mixes of either stoichiometry from one stir to four stirs. Two mixtures stirred once had multiple samples made to check if their T_g was consistent. Their low error values, coming from the standard deviation of these results, shows that T_g is consistent, meaning that one stir is enough to produce a well-mixed mixture. Furthermore, additional stirring would increase epoxy-amine conversion, raising the mixture viscosity, making it difficult to pour into molds. This was especially the case for non-solvent mixtures using DMP-30, which had increased viscosities compared to their non-DMP-30 counterparts. This five minutes of stirring would introduce air bubbles into the mixture. Therefore, after stirring, the mixtures were left for fifteen minutes, during which time the majority of air bubbles would leave naturally. Sonication was not used to remove air bubbles as the induced vibrations would heat the mixture, again raising conversion in the mixture, making it more viscous and difficult to pour. As an alternative to hand-mixing, non-solvent mixtures were mixed used a DAC 150 FVZ-K Speed Mixer (Synergy Deviced Ltd UK) for five minutes at 2,000rpm. This mixing process did not create air bubbles in the mixture, and so did not need a fifteen minute wait period.

Pre-Cure Procedure	r=1 T_g (°C)	r=0.57 T_g (°C)
1 × stir + wait	114.9 ± 0.8	52.4 ± 0.2
1 × stir + wait	115.9 ± 0.4	50 ± 2
1 × stir + wait	115.47	
2 × stir + wait	117.66	
3 × stir + wait	118.95	
4 × stir + wait	117.77	48.87
4 × stir + wait + 2hr wait	120.80	47.38

Table 3.1: Post-cure T_g of mixes of UC0003 and MXDA of r=1 and 0.57, depending on their mixing procedure pre-cure. Stir + wait refers to a five minute stir followed by a fifteen minute wait procedure. Different results for the same pre-cure procedure come from different sample sets. The stated error comes from the standard deviation in results from mixtures in which multiple samples were taken.

Solvent mixtures required four five-minute stirs with fifteen minute wait periods followed by a 45 minute wait after the final stir in order to achieve a consistent T_g. Table 3.2 shows that this pre-cure procedure and more extensive ones, T_g remains consistently ∼82°C. Multiple samples from the same mix also show a relatively consistent T_g. This pre-cure procedure was therefore taken as the most efficient to adequately distribute the constituent ingredients in the mixture. Solvent mixtures also had to be hand-stirred as the Speed Mixer could not mix the solvent and epoxy-amine layers as well as manual stirring could.

Pre-Cure Procedure	T_g (°C)
4 × stir + wait	99 ± 7
4 × stir + wait + 45min wait	84 ± 1
4 × stir + wait + 45min wait	83.8 ± 0.9
4 × stir + wait + 45min wait	87 ± 3
4 × stir + wait + 45min wait	84 ± 4
4 × stir + wait + 3hour wait	82 ± 7

Table 3.2: Post-cure T_g of mixes of UC0003 and MXDA of r=1, cured with solvents, depending on their mixing procedure pre-cure. Stir + wait refers to a five minute stir followed by a fifteen minute wait time. Different results for the same pre-cure procedure come from different sample sets. The stated error comes from the standard deviation in results from mixtures in which multiple samples were taken.

Samples were transferred into molds to be cured. Non-solvent samples were cured in PTFE molds whilst solvent samples were cured in silicone molds. It was found for silicone molds that non-solvent samples ended up with bubbles. It was postulated that these bubbles came from moisture evaporating from the silicone during cure, although this was not investigated. Given the non-solvent samples viscosity, these bubbles could not leave the epoxy-amine before it cured. This did not appear to be the case for solvent samples, likely due to their reduced viscosity, allowing the bubbles to leave the samples. It was found that solvent samples cracked in PTFE molds. This was likely due to the larger volume changes these samples went through as solvent evaporated during cure. For DSC measurements, 5-10mg of sample was weighed out into DSC pans before curing.

The samples were cured for two hours at 60°C, one hour at 100°C and one hour at 160°C under ambient conditions in an oven (Binder Germany). It took ∼25 minutes for the oven to heat from 60°C to 100°C, and ∼25 minutes to heat from 100°C to 160°C. Due to curing under ambient conditions, there was the risk of carbamation occurring. The T_g of samples cured in ambient condition was compared to the T_g of those cured under a nitrogen environment (Heraues T6060 oven, Thermo Scientific). The difference in T_g between samples cured in the two ovens was negligible. Given the ease of using the ambient conditions oven, it was used in preference to the nitrogen oven. As stated in chapter 2, section 2.3.6, the reactivity rate of secondary amines in comparison to primary amines increases with temperature. The 60°C cure therefore allowed for primary amine reactions with fewer secondary amine reactions. The 160°C cure then allowed for the secondary amine reactions to take place. Xylene has a boiling point of 143-145°C [2] and butanol 119°C [3]. The 100°C cure therefore allowed for solvents to evaporate without boiling. This cure was enough to reach a maximum T_g in non-solvent samples. Solvent samples required an additional cure up to ∼195°C in order to reach maximum conversion. The change in T_g for solvent samples cured with and without this additional 200°C cure is shown in figure 3.1. Upon the completion of this cure, samples were removed from their molds and placed in a vacuum desiccator.

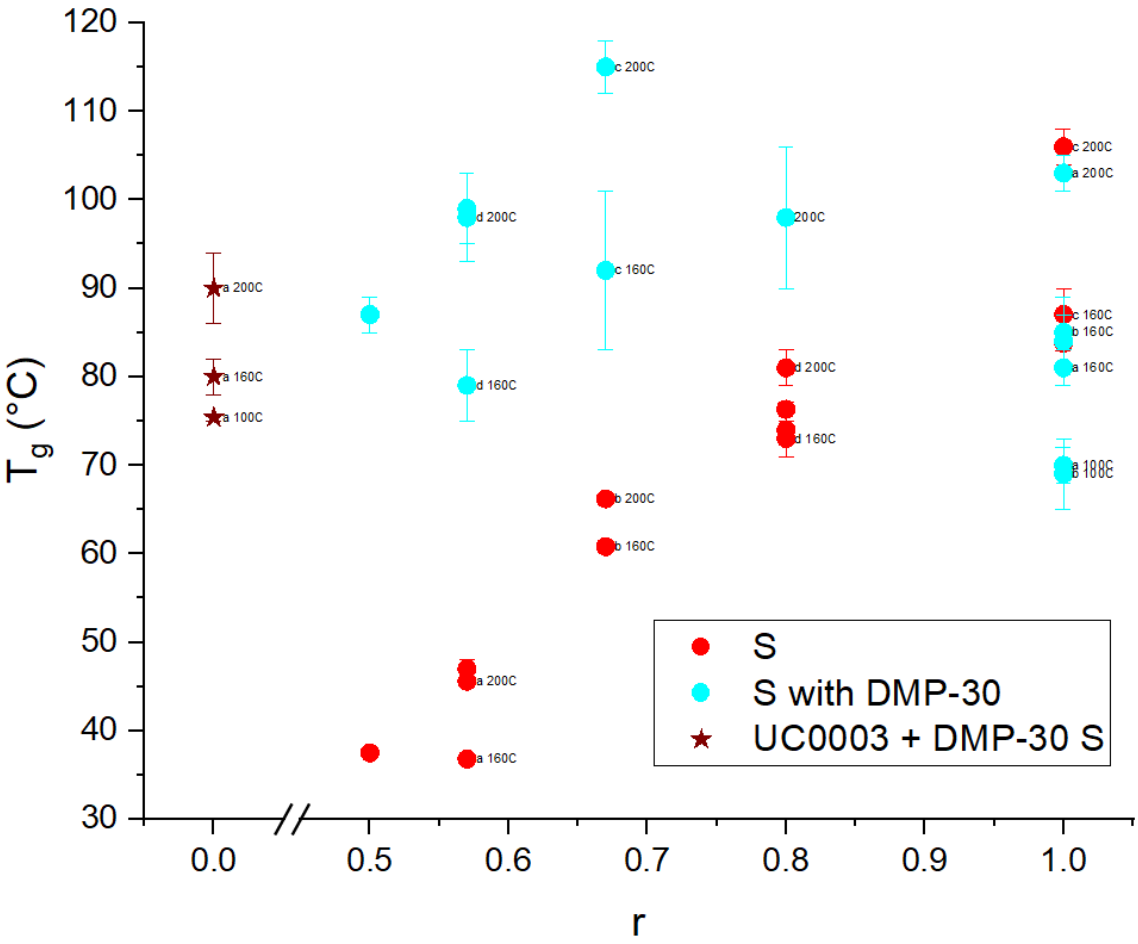

Figure 3.1: T_g results of formulations cured with solvents, with and without DMP-30, for different oven cures. Those labeled as '100°C' had a cure of two hours at 60°C and one hour at 100°C. Those labeled as '160°C' had a cure of two hours at 60°C, one hour at 100°C and one hour at 160°C. Those labeled as '200°C' had a cure of two hours at 60°C, one hour at 100°C, one hour at 160°C before being heated up to 200°C. Samples labeled with the same letter came from the same epoxy-amine mix. Those unlabeled had a 160 cure. Error bars arise from the standard deviation of results taken from the same mixture and cure.

3.1.2 Sample Naming Convention and Formulations used

As there were many different formulations used in this investigation, a shortening of the names of samples of different adopted. The stoichiometry is stated as a number at the start of the sample name. 'NS' and 'S' refers to samples cured without solvents and with solvents (xylene:butanol, in a 3:1 ratio by mass), respectively. If a sample was cured with DMP-30, it is stated as 'with DMP-30.' As purely homopolymerized networks do not have any MXDA, and so differ from all other samples, instead of being stated as '0 NS with DMP-30' they are stated as 'UC0003 + DMP-30' or 'UC0003 +

DMP-30 S' if cured with solvents.

The list of formulations created are as follows:

1. Non-solvent (NS): UC0003, MXDA
2. Non-solvent with DMP-30 (NS with DMP-30): UC0003, MXDA, DMP-30
3. Non-solvent with DMP-30, without MXDA (UC0003 + DMP-30): UC0003, DMP-30
4. Solvent (S): UC0003, MXDA, Xylene, Butanol
5. Solvent with DMP-30 (S with DMP-30): UC0003, MXDA, DMP-30, Xylene, Butanol
6. Solvent with DMP-30, without MXDA (UC0003 + DMP-30 S): UC0003, DMP-30, Xylene, Butanol

For formulations cured with MXDA, samples were made such that stoichiometry varied from r=1 to r=0.57.

3.2 Differential scanning calorimetry (DSC)

Differential scanning calorimetry (DSC) is a technique used to measure the heat flow into a sample as it undergoes a reaction or phase transition, to an accuracy of less than ±1% [4]. For the investigations described in this thesis, DSC was used to determine the epoxy conversion and glass transition temperature, T_g of different formulations of epoxy resins. DSC was used in the investigations discussed in chapters 4 and 6. This is done by measuring the difference in energy input between the sample and a reference, as a function of temperature. The sample and reference are placed in metal pans. Heat is provided by thermoelectric discs placed underneath these pans. Temperature sensors, placed externally to the samples, are used to measure temperature differences between the sample and reference in order to determine heat flow [4].

Epoxy conversion was determined from the heat flow in a system during a reaction. Heat flow, ΔH is defined as:

$$\Delta H = \Delta T C_p \tag{3.2}$$

Where ΔT is the change in temperature and C_p is the heat capacity of the system at constant pressure. Due to DSC working with small temperature changes, C_p can be treated as a constant [4]. The heat capacity for the opening of an epoxide ring is 94.5kJmol^{-1} [5]. With a known mass of epoxy in the sample, the expected heat flow for all the epoxy ring-openings, or 100% conversion of epoxy, can be determined. This can be compared to the heat flow, as measured via DSC, in order to determine % conversion of epoxy.

The glass transition temperature, T_g can also be determined via DSC by changes in

heat flow. As an object undergoes a phase transition, its heat capacity changes. The heat capacity is dependent on the change in entropy, δS, over a temperature range, δT:

$$c_p = T\Big(\frac{\delta S}{\delta T}\Big)_p \tag{3.3}$$

Where c_p is the specific heat capacity at constant pressure, p. At T_g, there is a discontinuity in the relationship $(\delta S)/(\delta t)$. There is therefore a decrease in the heat capacity at this transition and a decrease in the heat flow [6]. In the investigations detailed in this thesis, a DSC 25 (TA Instruments) was used to measure the enthalpy of cure and T_g of epoxy-amines. Uncured, or partially cured, samples were heated from an initial temperature of -80°C to 200°C. Cured samples were heated from 5°C. Samples were then cooled to their initial temperature before being heated back up to 200°C. The initial T_g and enthalpy of reaction of uncured and partially cured samples were measured in the initial heating cycle. The heating and cooling rates were both $10°\text{Cmin}^{-1}$. The T_g of cured samples, and of those cured in by the initial heating cycle, was measured in the second heating cycle. An example of DSC heat cycles and the features produced is shown in figure 3.2.

3.3 Thermogravimetric Analysis (TGA)

Thermogravimetric analysis is a technique in which the mass of a substance is measured as a function of temperature or time (over a controlled temperature). It is effectively used to measure a mass change, and rate of mass change, in a sample as it is heated or cooled [7]. This can be done under different environmental atmospheres to determine how reactions with gases in the environment affect samples (in this case during cure) [8]. The sample is placed in a pan on a balance and heated in a furnace. From these, the sample mass can be precisely measured and the temperature controlled [7]. Although results from TGA are not shown, the technique was used to determine that there was little evaporation when samples where cured without solvents, and that when using solvents during curing, at what temperatures these solvents evaporated.

3.4 Small-Angle Neutron Scattering (SANS)

Small-angle neutron scattering (SANS) is a technique for measuring structural properties of a material by measuring how a beam of neutrons scatter off the material. Scattering techniques such as SANS can give information on structures from a range of lengthscales, from the micron to Angstrom scale [9]. In terms of of crosslinked polymer networks, this has allowed information such as network size [10], the distance between polymer chains [10] and the length of monomer units to be investigated [11].Chapter 5 discusses the changes in network structure of epoxy-amine resins, as measured by SANS.

3.4.1 The Scattered Beam

Scattering methods probe the structure of matter by measuring how particle beams scatter off them. How these particles scatter depends on the forces that arise between them and the target. Neutrons interact with the nuclei of atoms via the strong nuclear

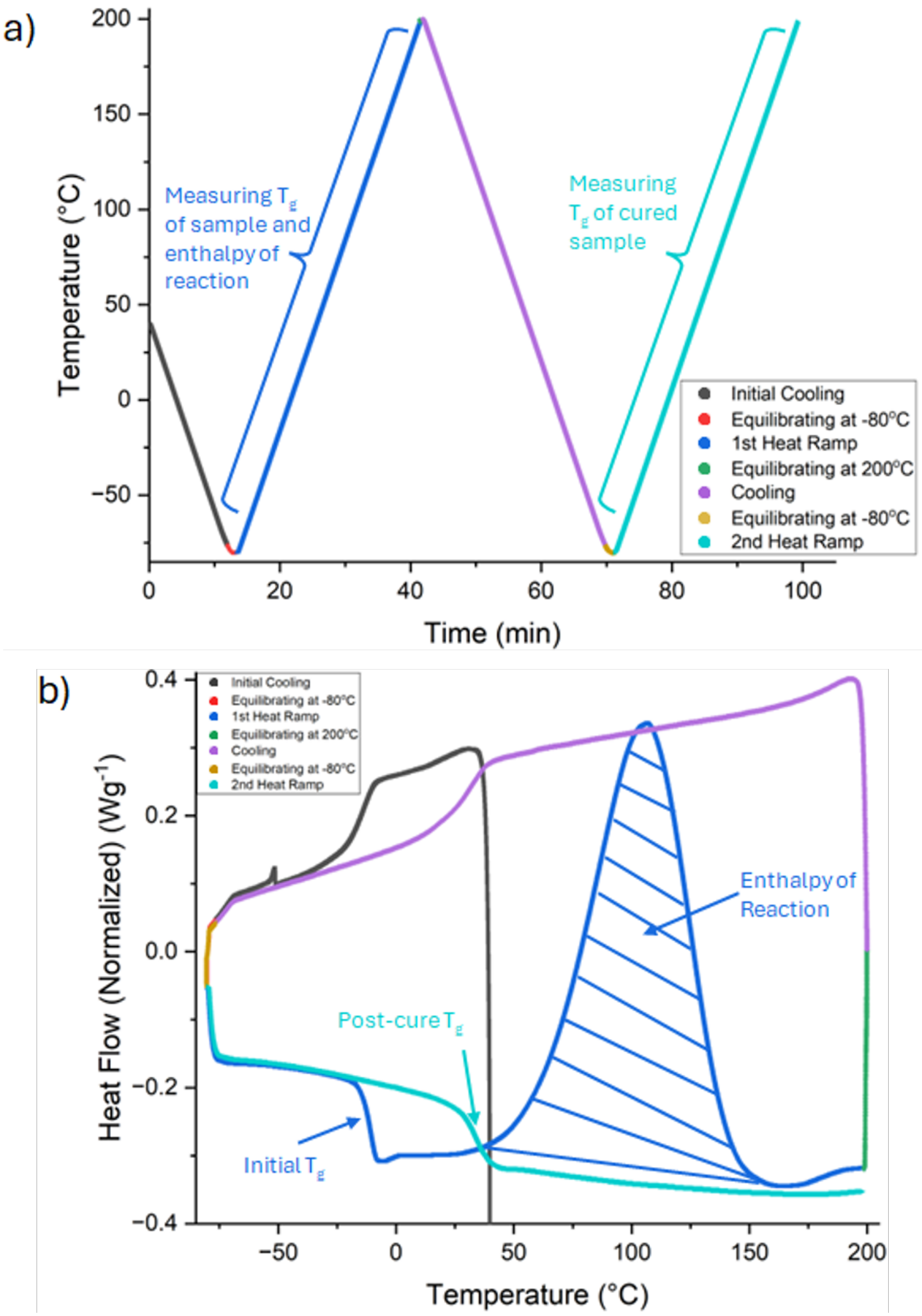

Figure 3.2: DSC results for an uncured epoxy-amine (epoxy: DER331, amine: MXDA) of excess epoxy. a) shows the different heating regimes and what is measured for each. b) shows the T_g's and the enthalpy of the curing reaction produced during the heating cycles.

force. The scattering of the incident particle is shown in figure 3.3. It can be characterized by its change in momentum and energy following interaction with the target: the momentum transfer, $\boldsymbol{P}$ and energy transfer, $\boldsymbol{E}$:

$$\boldsymbol{P} = \hbar\boldsymbol{k_i} - \hbar\boldsymbol{k_f} = \hbar\boldsymbol{Q} \tag{3.4}$$

$$\boldsymbol{E} = \hbar\boldsymbol{\omega_i} - \hbar\boldsymbol{\omega_f} = \hbar\boldsymbol{\omega} \tag{3.5}$$

Where $\hbar$ is the reduced Planck constant ($\hbar = \frac{h}{2\pi}$), $\boldsymbol{k_i}$ and $\boldsymbol{k_f}$ are the initial and final wavevectors of the particle and $\boldsymbol{Q}$ is the wavevector transfer. $\boldsymbol{\omega_i}$ and $\boldsymbol{\omega_f}$ are the initial and final frequencies of the particle.

For the simplest case of elastic scattering, there is no loss of energy in the interaction. This scattering can therefore be considered as a function of momentum, or wavevector. For a neutron, the energy transfer is given by its change in kinetic energy:

$$E = \frac{|\hbar\boldsymbol{k_i}|^2}{2m_n} - \frac{|\hbar\boldsymbol{k_f}|^2}{2m_n} \tag{3.6}$$

Where m_n is the mass of the neutron. For $E = 0$, the wavevector must remain unchanged. Therefore, the wavelength, λ also remains unchanged:

$$|\boldsymbol{k_i}| = |\boldsymbol{k_f}| = \frac{2\pi}{\lambda} \tag{3.7}$$

As shown in figure 3.3, the scattered particle is deflected by angle 2θ.

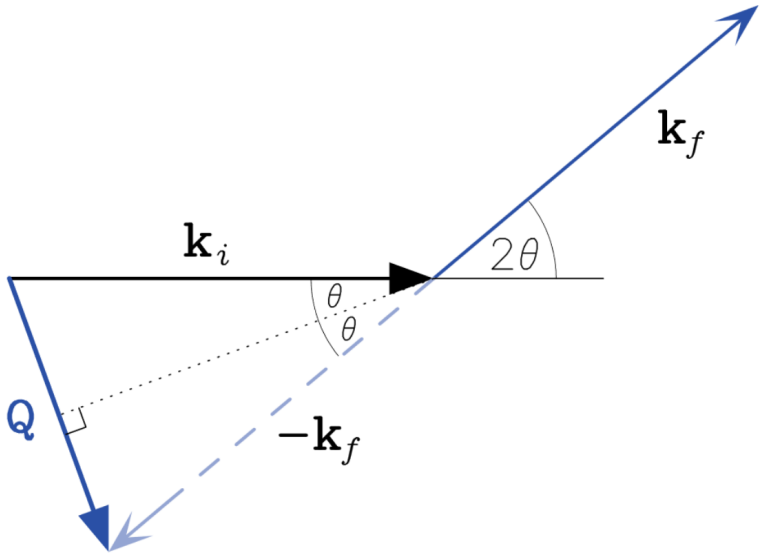

Figure 3.3: The vector diagram for elastic scattering, deflected at angle 2θ.

$\boldsymbol{Q}$ forms two right-angled triangles with $\boldsymbol{k_i}$ and $\boldsymbol{k_f}$. From equation 3.7, the hypotenuse of these triangles is $\frac{2\pi}{\lambda}$. The magnitude of $\boldsymbol{Q}$ is therefore:

$$Q = 2 \times \frac{2\pi}{\lambda}\sin\theta = \frac{4\pi}{\lambda}\sin\theta \tag{3.8}$$

For the direction of $\boldsymbol{Q}$, the z-axis is taken as the direction in which the incident beam

travels:

$$\boldsymbol{k_i} = \left(0, 0, \frac{2\pi}{\lambda}\right) \tag{3.9}$$

The direction of the outgoing beam is taken using angles 2θ and ϕ:

$$\boldsymbol{k_f} = (\sin 2\theta \cos\phi,\ \sin 2\theta \sin\phi,\ \cos 2\phi) \tag{3.10}$$

The wavevector transfer, $\boldsymbol{Q} = \boldsymbol{k_i} - \boldsymbol{k_f}$ can therefore be given as:

$$\boldsymbol{Q} = \frac{4\pi}{\lambda}\sin\theta(-\cos\theta\cos\phi,\ -\cos\theta\sin\phi,\ \sin\phi) \tag{3.11}$$

The incident particle, travelling as part of a beam in the z direction, has the wavefunction:

$$\psi_i = \psi_0 e^{ikz} \tag{3.12}$$

$$\text{where } \psi_0 = |\psi_0| e^{i(\phi_0 - \omega t)} \tag{3.13}$$

Where the incident flux, $\boldsymbol{\Phi} = |\psi_0|^2$ and $k = \frac{2\pi}{\lambda}$. As the scattered particles are no longer part of a beam, their density drops off as distance, r increases. Their wavefunction is given as:

$$\psi_f = \psi_0 \mathrm{f}(\lambda, \theta)\frac{e^{ikr}}{r} \tag{3.14}$$

The function $\mathrm{f}(\lambda, \theta)$ states the chance that a particle of a certain wavelength is deflected in a certain direction. For the case of neutrons scattering off atomic nuclei, $\mathrm{f}(\lambda, \theta)$ tends to be invariant in relation to the wavelength and scattering angle:

$$\mathrm{f}(\lambda, \theta) = -b \tag{3.15}$$

The term b is known as the 'scattering length.' The negative sign is used by convention. The scattering is invariant due to the short range of the strong force ($\sim 10^{-14}$m) in comparison to the wavelength of thermal neutrons ($\sim 10^{-10}$m). b depends on the make-up of the target nucleus and the orientation of its spin relative to that of the neutron. Due to having quantum mechanical spin, neutrons possess a magnetic dipole moment. They can therefore be deflected by magnetic interactions with target nuclei. Due to this, as the scattering angle, and therefore the wavevector transfer, Q, increases, the form factor, $\mathrm{f}(\lambda, \theta)$, decreases [12].

3.4.2 The SANS Signal

In a SANS measurement, the detector measures the number of neutrons of a specific wavelength, scattered through a range of angles. The signal or flux is the number of neutrons that arrive over an area per unit time. This flux is given as $I(Q)$:

$$I(Q) = I_0(\lambda)\Delta\Omega\eta(\lambda)T(\lambda)V_s\frac{\delta\Sigma}{\delta\Omega}(Q) \tag{3.16}$$

Where I_0 is the incident flux, $\Delta\Omega$ is the solid angle defined by the size of a detector pixel, η is the detector efficiency, T is the neutron transmission of the sample and V_s is the volume of the sample illuminated by the neutron beam. I_0, $\Delta\Omega$ and η are all detector-dependent. T, V_s and $\frac{\delta\Sigma}{\delta\Omega}$ are sample dependent. $\frac{\delta\Sigma}{\delta\Omega}$ is the differential scanning cross-sectional area and is the dependent variable in scattering measurements. It is

related to the size, shape and interactions between scattering centres in the sample:

$$\frac{\delta\Sigma}{\delta\Omega}(Q) = NV^2(\Delta\rho)^2P(Q)S(Q) + B \tag{3.17}$$

Where N is the number concentration of scattering centres, V is the volume of a single scattering centre, $\Delta\rho$ is the contrast in scattering length, P is the form factor and S is the structure factor (discussed in section 3.4.3) [13].

Differences in neutron scattering length density, $\Delta\rho$, produce a differential scattering cross-section and therefore the SANS signal. ρ is determined using the equation:

$$\rho = N \cdot \sum_i b_i = \sum_i \frac{\delta N_A}{M} \cdot b_i \tag{3.18}$$

Where b_i is the coherent neutron scattering length of a nucleus, i. The magnitude b_i is determined by the neutron-nucleus interaction. δ is the bulk density of the molecule, N_A is Avogadro's constant and M is the molecule's molecular weight. The scattering lengths and cross-sections of relevant nuclei are shown in table 3.3. Scattering length densities of materials relevant to the investigations detailed in this thesis are shown in table 3.4. A negative scattering length means that the phase of the scattered neutrons has been shifted by 180°. σ_{coh} is the coherent cross-section. σ_{inc} and σ_{abs} are the incoherent and absorption cross-sections, respectively. These terms reduce the neutron sample transmission. σ_{inc} also raises the background signal [13].

Nucleus	b (10^{-15}m)	σ_{coh} (10^{-28}m^2)	σ_{inc} (10^{-28}m^2)	σ_{abs} (10^{-28}m^2)
^{1}H	-3.7423	1.7583	80.27	0.3326
^{2}D	6.674	5.592	2.05	0.000519
^{12}C	6.6535	5.559	0	0.00353
^{7}N	9.37	11.03	0.5	1.91
^{6}O	5.805	4.232	0	0.00019

Table 3.3: Relevant nuclei and their coherent scattering lengths, b and cross-sections, σ. σ_{coh} refers to the coherent cross-section, σ_{inc} refers to the incoherent cross-section and σ_{abs} refers to the absorption cross-section. [14]

Solvent	Scattering Length Density (10^{-6}Å^{-2})
Cured DGEBA:MXDA	1.30
Cured Deuterated DGEBA:MXDA	3.31
DER331	3.30
H_2O	-0.56
CH_3OH	-0.37
D_2O	6.37
CD_3OD	5.80

Table 3.4: Table showing scattering length densities for the cured epoxy-amines, the epoxy and hydrogenous and deuterated water and methanol. Values determined for neutron wavelengths from 0.9-13Å[15].

$\Delta\rho$, and therefore the intensity of the SANS signal is dependent upon changes in the density, molecular weight and scattering length of the sample. As can be seen in table 3.3, there is a great difference in the scattering lengths of hydrogen and deuterium due to the sign difference. SANS signals can therefore be altered by building molecules with deuterium rather than hydrogen [13].

3.4.3 Form Factor and Structure Factor

The form factor, $P(Q)$, and structure factor, $S(Q)$ are dimensionless functions that describe how $\frac{d\Sigma}{d\Omega}(Q)$ is affected by interference effects in neutron scattering. $P(Q)$ describes the effect of the interference when neutrons scatter off different parts of the same scattering centre. These interference effects are dependent on the size and shape of the scattering centre. For a homogeneous sphere of radius R, $P(R)$ is given as:

$$P(Q) = \Big[\frac{3(\sin(QR) - QR\cos(QR))}{(QR)^3}\Big]^2 \tag{3.19}$$

For a Gaussian distribution of segment density about a centre of mass:

$$P(Q) = \frac{2[\exp(-Q^2R_g^2) + Q^2R_g^2 - 1]}{(Q^2R_g^2)^2} \tag{3.20}$$

Where R_g is the radius of gyration. Meanwhile, $S(Q)$ describes the effect of interference from neutrons scattering off different scattering centres.It is dependent on the degree of local order in the sample and interactions between different scattering centres. It is given as:

$$S(Q) = 1 + \frac{4\pi N}{QV_s}\int_0^\infty [g(r) - 1]r\sin(Qr)\mathrm{d}r \tag{3.21}$$

Where $g(r)$ is a density distribution function. It is generally a damped oscillatory function with a maxima corresponding to the distance of each nearest neighbour, r. $S(Q)$ tends to 1 at high-Q as the concentration of scattering centres dilutes [13].

3.4.4 Scattering Regimes and Their Information

The intensity of the SANS signal over the measured Q-range is generally displayed as a log-log plot. This allows for clarity in the different Q-ranges, which give information from different length-scales in the target sample. This information is shown in table

3.5

	Scattering Regime (for $0 < c < c^*$)		
	Low-Q ($Q < R_g^{-1}$)	Intermediate-Q ($\pi R_g^{-1} < Q < l^{-1}$)	High-Q ($l^{-1} < Q$)
Information Gained	Overall dimensions Molecular Weight	Overall dimensions Molecular Weight Excluded volume component	Cylindrical Structure Chain Flexibility
Relevant fits	Guiner (Equation 3.22)		Porod (Equation 3.24)

	Scattering Regime (for $c^* < c$)	
	$Q < \xi^{-1}$	$Q > \xi^{-1}$
Information Gained	Correlation length	Correlation length
Relevant fits	Debye-Beuche (Equation 3.28)	Modified Zimm (Equation 3.29)

Table 3.5: Information gained from SANS measurements from different Q-regimes, for different polymer concentrations, c, less than and greater than the overlap concentration, c^*. c^* denotes the upper limit of a 'dilute solution,' when the total volume occupied by polymer chains is equal to that of the solution it is in and begin to interact with each other [16]. R_g is the radius of gyration and l refers to the persistence length [13].

Guinier and the Radius of Gyration

Near $Q = 0$, the differential cross-section is found to be:

$$\frac{\delta\Sigma}{d\Omega}(Q) \approx NV^2(\Delta\rho)^2 \exp\Big(-\frac{(QR_g)^2}{3}\Big) \tag{3.22}$$

R_g is the radius of gyration, the radial distance that a point mass would have to be at in order to have the same moment of inertia as the given body. R_g depends on the size of the overall object and is independent of the scattering properties of the individual monomers [17]. It can thus be used to determine the size of a polymer chain. For a particle made up of N identical elements, the square of the radius of gyration is:

$$\bar{R^2} = \frac{1}{N}\sum_{i=1}^{N}\langle r_i^2\rangle \tag{3.23}$$

Where r_i is the distance from the ith bead to the centre of mass [18]. The radius of gyration measurement is dominated by the largest lengthscale. It therefore cannot be measured if $R_g > Q_{min}^{-1}$ [12].

Porod

For higher Q values ($Q >> R^{-1}$), the differential cross-section in a two-phase system drops off with Q^{-4}. For spherical particles:

$$\left(\frac{d\sigma}{d\Omega}\right)_{el} \approx \left(\frac{N}{V}\right)\frac{16\pi^2 R^2}{Q^4}\cos^2(QR) \tag{3.24}$$

Most objects can be treated as spherical due to orientational averaging, if they have a smooth interface with a sharp SLD contrast and do not smooth out to nothingness in any direction. Instrumental resolution at high Q means that the cosine-squared function can be averaged to $\frac{1}{2}$. As $Q \to \infty$, the differential cross-section becomes described by Porod's Law:

$$\left(\frac{d\sigma}{d\Omega}\right)_{el} \to \left(\frac{N}{V}\right)\frac{2\pi S_p}{Q^4} \tag{3.25}$$

Where S_p is the surface area of the target particle [12]. As the differential cross-section now depends on the surface area of the target, information on the shape of the target can be ascertained from the scattering signal at these higher Q values. It can also give information into how well mixed a polymer is, and if it exists as one phase or two [17]. The scattering signal, featuring the Guinier and Porod regimes, for a sphere is shown in figure 3.4.

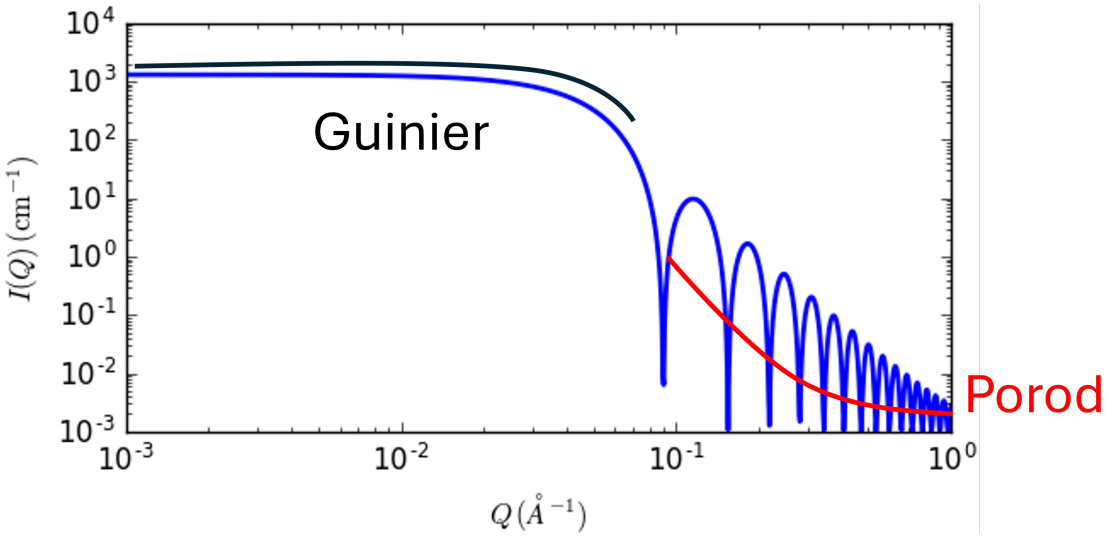

Figure 3.4: Scattering intensities and Q ranges for a sphere. The Guinier law is labeled with a black line and the Porod with a red line [19].

Correlation Length

The Guinier and Porod fits are used at high-Q, for polymer concentrations greater than the 'overlap concentration,' c^*. For solutions of concentrations greater than c^* polymer concentrations are similar to the concentrations of individual polymer coils. Scattering intensity at this length scale is therefore dependent on the average mesh

size of the polymer network the correlation length, ξ. Scaling theories predict ξ to be:

$$\xi = R_g\Big(\frac{c}{c^*}\Big)^{\nu/(1-3\nu)} \tag{3.26}$$

$$\text{where } c^* = \frac{M}{N_A R_g^3} \tag{3.27}$$

Where ν is the volume of a segment. For $Q > \xi^{-1}$,the scattering intensity can be given using a 'modified Zimm approximation.' For $Q < \xi^{-1}$, the Debye-Beuche function can be used:

$$\text{for } Q > \xi^{-1}\text{: } \frac{\delta\Sigma}{\delta\Omega}(\Delta\rho)^2\frac{\xi^3}{1+Q^2\xi^2} \tag{3.28}$$

$$\text{for } Q < \xi^{-1}\text{: } \frac{\delta\Sigma}{\delta\Omega}(Q) = 8\pi\phi(1-\phi)(\Delta\rho)^2\frac{\xi^3}{1+Q^2\xi^2} \tag{3.29}$$

3.4.5 Scattering in Amorphous Materials

Although amorphous materials do not have a uniform structure like crystals, at smaller scales there is some ordering as molecules align themselves with each other. The autocorrelation function (ACF), of the SLD function, $\beta(\boldsymbol{r})$ is a combination of two terms:

$$\text{ACF}[\beta(\boldsymbol{r})] = g_1(\boldsymbol{r}) + g_2(\boldsymbol{r}) \tag{3.30}$$

$$\text{where } g_1(\boldsymbol{r}) = \sum_{j=1}^{N}\int\int\int_V \beta_j(\boldsymbol{r'}-\boldsymbol{r_j}) * \beta_j(\boldsymbol{r'}-\boldsymbol{r_j}+\boldsymbol{r})d^3\boldsymbol{r'} \tag{3.31}$$

$$\text{and } g_2(\boldsymbol{r}) = \sum_{j\neq k}\int\int\int_V \beta_j(\boldsymbol{r'}-\boldsymbol{r_j}) * \beta_k(\boldsymbol{r'}-\boldsymbol{r_k}+\boldsymbol{r})d^3\boldsymbol{r'} \tag{3.32}$$

The ACF gives information on the distance distribution of structures in the function. $\beta_j(\boldsymbol{r})$ is the SLD function of atom j, centred at origin ($\boldsymbol{r_j} = 0$). The first term, $g_1(\boldsymbol{r})$ gives information on the correlation of each atom with itself. It has a maximum at the origin and decreases as $\boldsymbol{r}$ increases. For neutron scattering, this drop-off is determined by the thermal motion of the target atoms. The second term, $g_2(\boldsymbol{r})$ depends on the spatial distribution of atoms, and the type of these atoms. $g_2(\boldsymbol{r})$ gives information on the sample structure. $g_2(\boldsymbol{r})$ produces a strong signal at interatomic distances. For example, in water this would be the covalent bonds O-H (r = 1.0Å), the hydrogen bond O|||H (r ≈1.9Å) and the VdW bond H$\cdots$H (r = 1.6Å) [12]. The differential cross-section is proportional to the ACF:

$$\left(\frac{d\sigma}{d\Omega}\right)_{el} \approx \int\int\int_V \text{ACF}[\beta(\boldsymbol{r})]e^{i\boldsymbol{Q}\cdot\boldsymbol{r}}d^3\boldsymbol{r} \tag{3.33}$$

The differential cross-section can also be stated in relation to a structure factor, $S(Q)$. For $Q \neq 0$:

$$\left(\frac{d\sigma}{d\Omega}\right)_{el} = \left\langle |f(Q)|^2 \right\rangle S(Q) \tag{3.34}$$

$$\text{where } S(Q) = 1 + \frac{4\pi\alpha(Q)}{Q}\int_0^\infty r[g(r)-1]\sin(Qr)dr \tag{3.35}$$

$g(r)$ is the normalized version of g_2. Using the average value of the SLD, $\left\langle \beta \right\rangle$, equation 3.32 becomes:

$$g_2(r) \to \left\langle \beta \right\rangle^2 V \tag{3.36}$$

$$\text{therefore } g(r) = \frac{g_2(r)}{\left\langle \beta \right\rangle^2 V} \tag{3.37}$$

$\alpha(Q)$ is also given as:

$$\alpha(Q) = \frac{\left\langle \beta \right\rangle^2 V}{\left\langle |f(Q)|^2 \right\rangle} N \tag{3.38}$$

$$\tag{3.39}$$

Where n is the atomic number density. For neutron scattering, $f_j(Q)$ is equal to the coherent scattering length in the j$^{\text{th}}$ nucleus, $\left\langle b_j \right\rangle$ and is therefore independent of Q. The SLD average is $\left\langle \beta \right\rangle = n\left\langle b \right\rangle$. Therefore, for neutron scattering, $\alpha(Q) = n$ [12].

References

[1] A. S. D. Shackleford. "Using Positron Annihilation as a Method to Characterise Epoxy Networks with Regards to Chemical Resistance". PhD thesis. The University of Sheffield, Faculty of Engineering, Department of Mechanical Engineering, 2019.

[2] Merck KgaA. *o-Xylene*. `https://shorturl.at/uxISQ` [Accessed: (28/09/23)]. 2023.

[3] Honeywell International Inc. *1-Butanol*. `https://lab.honeywell.com/shop/1-butanol-537993` [Accessed: (28/09/23)]. 2023.

[4] TA Instruments. *THE CASE FOR A GENERIC DEFINITION OF DIFFERENTIAL SCANNING CALORIMETRY*. `https://www.tainstruments.com/pdf/literature/TA081.pdf` [Accessed: (27/09/24)].

[5] S. Mortimer, A. J. Ryan, and J. L. Stanford. "Rheological behavior and gel-point determination for a model lewis acid-initiated chain growth epoxy resin". In: *Macromolecules* 34.9 (2001), 2973–2980. DOI: 10.1021/ma001835x.

[6] *Soft Condensed Matter*. 1st ed. Oxford University Press, 2002. ISBN: 978-0-19-850589-1.

[7] PerkinElmer. *FREQUENTLY ASKED QUESTIONS Thermogravimetric Analysis (TGA)*. `https://resources.perkinelmer.com/lab-solutions/resources/docs/faq_beginners-guide-to-thermogravimetric-analysis_009380c_01.pdf` [Accessed: (27/09/24)].

[8] A. Coats and J. Redfern. "Thermogravimetric Analysis. A Review". In: *Analyst* 88 (1053 1963), pp. 906–924. DOI: 10.1039/AN9638800906.

[9] C. M. Jeffries et al. "Small-angle X-ray and neutron scattering". In: *Nature Reviews Methods Primers* 70.1 (2021). DOI: https://doi.org/10.1038/s43586-021-00064-9.

[10] J. Witte et al. "A comparison of the network structure and inner dynamics of homogeneously and heterogeneously crosslinked PNIPAM microgels with high crosslinker content". In: *Soft Matter* 15 (2000), 792–802. DOI: 10.1039/c8sm02141d.

[11] R. Lovell and A. H. Windle. "WAXS investigation of local structure in epoxy networks". In: *Polymer* 31.4 (1990), pp. 593–601. DOI: 10.1016/0032-3861(90)90274-3.

[12] *Elementary Scattering Theory*. 1st ed. Oxford University Press, 2011. ISBN: 978-0-19-922868-3.

[13] R. A. Pethrick and J. V. Dawkins, eds. *Modern Techniques For Polymer Characterisation*. John Wiley and Sons, 1999. Chap. 7: Small Angle Neutron Scattering. ISBN: 0-471-96097-7.

[14] A-J. Dianoux and G. Lander, eds. *Neutron Data Booklet*. 2nd ed. OCP Science, 2003. Chap. 1.1: Neutron Scattering Lengths. ISBN: 0-9704143-7-4.

[15] *Scattering Length Density Calculator*. http://www.refcalc.appspot.com/sld [Accessed: (02/08/24)].

[16] T. Rodrigues, F. J. Galindo-Rosales, and L. Campo-Deaño. "Critical overlap concentration and intrinsic viscosity data of xanthan gum aqueous solutions in dimethyl sulfoxide". In: *Data in Brief* 33 (2020), pp. 1–5. DOI: 10.1016/j.dib.2020.106431.

[17] J. S. Higgins and H. C. Benoit. *Polymers and Neutron Scattering*. 1st ed. Oxford Science Publications, 2002. ISBN: 0-19850063-7.

[18] M. Fixman. "Radius of Gyration of Polymer Chains". In: *The Journal of Chemical Physics* 36 (1962), pp. 306–310. DOI: 10.1063/1.1732501.

[19] The SasView Project. *sphere*. https://www.sasview.org/docs/user/models/gaussian_peak.html [Accessed: (29/04/26)]. 2023.

Chapter 4

Reaction Kinetics and Final Glass Transition Temperature of Epoxy-Amines Cured with a Tertiary Amine Homopolymerizing Agent

Abstract

Epoxy-amine coatings are used as protective coatings on ships, aircraft, trains, wind turbines and other civil infrastructure in order to prevent corrosion. These coatings have not only excellent chemical, moisture and corrosion resistance but also good mechanical strength, toughness and adhesion to surfaces. To achieve these beneficial properties polymer networks of high crosslink densities are required. This requires high degrees of conversion of epoxy and amine, which necessitates care in preparing exact stoichiometric ratios. To overcome this requirement, tertiary amine catalysts can be used to homopolymerize excess epoxy in epoxy rich, formulations. In this investigation, the conversion of epoxy-amine resins of different stoichiometries, with and without homopolymerizing agent, were measured in a system comprising of Bisphenol A based epoxy, DER331, m-Xylylenediamine (MXDA), and a homopolymerizer, 2,4,6-tris(dimethylaminomethyl)phenol (DMP-30). Differential scanning calorimetry (DSC) was used to measure the enthalpy throughout cure and the final glass transition temperature, T_g, of the crosslinked networks. In-situ near-infrared (N-IR) spectroscopy was employed to measure conversion throughout curing, in comparison with DSC. Formulations without DMP-30 show a decrease in T_g as excess epoxy is increased. With DMP-30, T_g remained constant and similar to that of a stoichiometric ratio of epoxy-amine without DMP-30, regardless of the excess epoxy. The presence of DMP-30 hompolymerizes all excess epoxy, resulting in a maximum conversion of epoxy. The final T_g of a purely homopolymerized sample (no MXDA) was greater than those

cured with MXDA or a mixture of MXDA and DMP-30. Conversion measured via DSC showed increased conversion for formulations of excess epoxy when DMP-30 was added. Marked differences were observed between conversion estimated from DSC and NIR.

4.1 Introduction

Epoxy resins display excellent mechanical strength and toughness; they possess excellent chemical, moisture and corrosion resistance; as well as good electrical insulation, thermal and adhesive properties. Therefore they are popular choices as adhesives and protective barrier coatings [1]. The conversion of epoxy, or the degree of cure, of an epoxy resin impacts its crosslink density and thus both its physical and chemical properties. When using inflexible crosslinking agents such as MXDA, epoxy-amine resins of equal number of epoxy and amine functional groups (stoichiometric ratio) display the highest glass transition temperature (T_g), as they possess maximal cross-linking density [2]. It is therefore important to achieve the maximum degree of cure to produce high cross-linked networks that have the smallest diffusion coefficients to permeants. An alternative approach (to using a two part epoxy and difunctional crosslinker at stochiometric formulation to achieve a high degree of cure) is to include a tertiary amine accelerator, such as 2,4,6-tris(dimethylaminomethyl)phenol (DMP-30). DMP-30 can act as both a catalyst for epoxy-amine polymerization [3, 4, 5] and also as a catalyst for the homopolymerization of epoxy [6]. DMP-30's role as a catalyst for homopolymerization is discussed in chapter 2, section 2.3.3. The homopolymerization reaction occurs via an etherification reaction, involving both a tertiary amine and a hydroxyl group, both groups are present on DMP-30. Tertiary amines thus allow for higher degrees of curing of epoxy-rich formulations.

One common method to measure the properties of epoxy resins and their reactions during cure has been differential scanning calorimetry (DSC) [7, 8, 9]. Within a given resin system, T_g is a useful proxy for the degree of cure. The T_g of epoxy-amine resins of differing ratios, with and without a tertiary amine (BDMA) has been measured precisely [10]. Quantitatively DSC can measure the enthalpy of reaction during the curing reaction. This allows the degree of cure from the reaction to be determined. Using DSC in this way, the different reactions rates and the onset of the reaction of primary and tertiary amines with epoxide groups has also been measured [10, 11].

Near-Infrared (NIR) spectroscopy has also been previously been used to measure the degree of cure. Changes in the relative absorption intensities of epoxide, amine and hydroxide functional groups can be used to measure the level of curing. This allows for the kinetics of epoxy/amine reactions and the degree of cure to be studied directly throughout the curing process [1, 12, 13].

Although there has been previous work studying the different reactions that occur between amine curing agents and tertiary amine accelerators with epoxies [14], little work appears to have been done to study their impact when the stoichiometry, the

ratio of functional groups of crosslinking agent (the amine) to monomer (the epoxy), of the epoxy-amine is changed. In this investigation, DSC was used to measure the change in T_g of epoxy amines, both before and after curing at elevated temperature to reach maximum cure conversion. This was done at stoichiometric ratio and with an excess of epoxy, as well as with and without the tertiary amine DMP-30, in order to measure the effect of DMP-30 before and after curing. NIR spectroscopy was used to quantify the changes and conversion of epoxide throughout cure and also to measure the effect of DMP-30 on the cure reaction through a typical thermal cure reaction.

4.2 Experimental Section

4.2.1 Materials

The epoxy used was UC0003 (supplied by Akzo-Nobel, Felling UK), this is a Bisphenol A diglycidyl ether (DGEBA) epoxy. The UC0003 supplied contained mainly DER331, but also contained Epicote 828 and Razeen LR 1150 both DGEBA based expoxies. Two batches of UC0003 were used, one with an epoxide equivalent weight of 173gmol^{-1}, and another of 172gmol^{-1}. The amine, m-Xylylenediamine (MXDA) and the accelerator, 2,4,6-Tris(dimethylaminomethyl)phenol (DMP-30) were purchased from Sigma Aldrich and used as received.

4.2.2 Titration to Determine Epoxide Equivalent Weight of Epoxy

Tetraethylammonium bromide (Sigma Aldrich) (25g) was dried at 100°C for one hour. Tetraethylammonium bromide solution was produced by dissolving 25g in 100ml of glacial acetic acid (Sigma Aldrich, molarity: 17.4M, reagent grade). Crystal violet indicator was prepared by dissolving 20mg of crystal violet (Sigma Aldrich) in 20ml of glacial acetic acid. A mass of 0.1092 - 0.1683g of UC0003 was dissolved in 10ml of chloroform and solubilised using a vortex mixer. The epoxy solution was pippetted into a conical flask. Subsequently 20ml of glacial acetic acid and 10ml of tetraethylammonium bromide solution were added to the flask, which was manually swirled before 4-6 drops of crystal violet indicator were added. Perchloric acid (Sigma Aldrich, 0.1M, reagent grade) was then titrated against this solution until the solution turned a clear yellow colour. The epoxide equivalent weight (EEW) was then determined via the following equation 6.2:

$$EEW(\text{gmol}^{-1}) = \frac{\text{sample mass(g)}}{\text{titre (dm}^3\text{)} \times \text{perchloric acid concentration (mol dm}^{-3}\text{)}} \quad (4.1)$$

This procedure was repeated twice and an average used to determine UC0003's EEW.

4.2.3 Cross-linked Network Preparation

We define r as the ratio of amine hydrogens to epoxide groups. Samples with UC0003 epoxy and MXDA diamine crosslinker, have stochiometries, r, from $r = 0.5$ to $r = 1$, i.e. a 50% excess of epoxy to no excess. Samples were made with and without DMP-30. UC0003 was weighed out into a container using a precision balance (A&D FZ-3000iWP, Abingdon, United Kingdom). This mass was subsequently used to determine the required mass of DMP-30 and MXDA. For samples with DMP-30, moles of DMP-30 equivalent to 3% of the EEW of UC0003 (for an EEW of 172gmol^{-1}, 0.0463g of

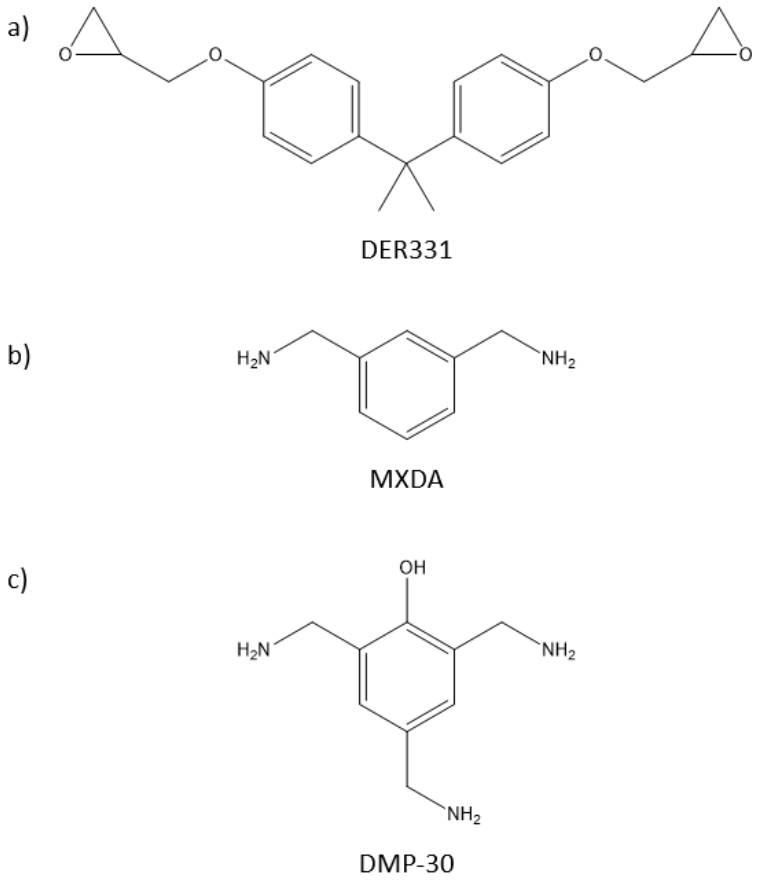

Figure 4.1: Materials used to make the polymerized networks. a) DER331, b) m-Xylylenediamine (MXDA) and c) 2,4,6-Tris(dimethylaminomethyl)phenol (DMP-30).

DMP-30 was added for each gram of epoxy). DMP-30 was added before MXDA was added. The mixture was then stirred either by hand using a glass rod, or in a DAC 150 FVZ-K Speed Mixer (Synergy Deviced Ltd UK) at 2000rpm. Samples stirred by hand were covered in Parafilm to prevent oxidation or carbamation of the MXDA. All samples were mixed for 5 minutes. As mentioned in chapter 3 section 3.1.1, it was determined that this mixing regime mixed the components well enough to produce a polymer of maximum T_g once cured. There was negligible difference in the final T_g of samples mixed via hand compared to using a roatating high speed mixer (Speed Mixer Synergy UK). For DSC use, 5-10mg samples were then weighed out into T-Zero DSC pans using the end of a glass pipette. Oven-cured samples were cured in an oven (Binder Germany) under ambient atmosphere at 60°C to for two hours, followed by one hour at 100°C then one hour at 160°C. It took around 25 minutes to heat the oven from 60°C to 100°C and around 45 minutes to heat from 100°C to 160°C. Curing was also carried out in an oven under a nitrogen atmosphere, but there was little difference in the measured T_g of samples cured in these two environments.

4.2.4 Differential Scanning Calorimetry

Differential scanning calorimetry (DSC) was performed using a DSC 25 (TA Instruments). Samples were made using 5-10mg of epoxy amine mix, placed in aluminium pans. The final T_g of these samples was measured via DSC using the oven-cured samples. Uncured samples were also heated to cure in the DSC. This allowed measurement of the T_g of uncured samples and the enthalpy of the curing reaction. In addition, the T_g and residual enthalpy of samples that underwent curing at ambient temperature were also measured. Samples were cooled down to -80°C before being heated up to 200°C. They were then cooled down to -80°C and heated to 200°C again. The temperature ramp throughout was 10°Cmin^{-1}.

As cure would proceed at room temperature it is important to quantify this curing. The time at room temperature is termed the pot life. This pot life was taken as the time between the start of the mixing and the start of the measurement cycle. DSC measurements were made to compare differences in T_g's and enthalpies of samples as their time at ambient temperature (potlife) increased. The first sample's potlife was treated as the time the mixing process started up to the time the DSC measurements commenced. Subsequent samples were treated as having 120 minutes extra pot life, as that was how long each DSC cycle took.

The T_g, the temperature range of T_g, and enthalpy peak areas were measured using the software package TRIOS (TA Instruments). T_g was determined from the second heat ramp. Using the measured mass and the enthalpy of reaction, the extent of reaction, p can be determined by comparing it to the theoretical enthalpy of reaction for 100% conversion:

$$p = \frac{\Delta H_0}{\Delta H_{epoxy}} \tag{4.2}$$

Where ΔH_0 is the measured enthalpy of an uncured sample and ΔH_{epoxy} is the enthalpy of opening the epoxide ring of the epoxide groups (for one mole of epoxy, ΔH_{epoxy} =-94.5kJmol^{-1} [15]). Samples measured for their conversion were those with the shortest potlife, so as to reduce curing before the DSC scans. Pot lives ranged from 25 to 50 minutes. Conversion after 45 minutes at ambient temperature was measured to be 1.0% that of the final conversion after curing via heating. It was therefore assumed that conversion over these 25 to 50 minutes was small enough for these samples to be treated as being fully uncured. DSC scans were also used to measure conversion after different sections of the oven cure. This was done by removing samples cured in DSC pans from the oven before the cure was finished. The extent of reaction after a certain section of the cure, p_1 was determined using a modified version of equation 4.3:

$$p_1 = C_{end}\frac{\Delta H_{epoxy} - \Delta H_1}{\Delta H_{epoxy}} \tag{4.3}$$

Where C_{end} is the theoretical maximum conversion of epoxy and ΔH_1 is the enthalpy after partial curing. For formulations of epoxy-amine of stoichiomtric ratio or excess epoxy, C_{end} is equivalent to the formulation's stoichometry.

4.2.5 Near-Infrared (NIR) Spectroscopy

NIR spectroscopy was carried out with an NIRQuest 2500 (Ocean Optics). The measurement integration time was varied and set to maximise the absorption reading without the detector being saturated. To improve the counting 25 scans were averaged and a boxcar width of 5 nm was used. Sample mixtures were placed in a gasket of 1.8mm thickness, sandwiched between two glass slides. Absorption intensities through the glass slides, without the sample mixture, were taken with and without the light source on so as to remove background measurements from ambient light and from the glass slides from the actual absorption results. Samples were placed on a THMS600 heating stage (Linkam Scientific UK) at 60°C to carry out the curing regime of 2hrs at 60°C, 1hr at 100°C and 1hr at 160°C, with a heat ramp of 10°Cmin^{-1} between each temperature. Absorption spectra were taken every minute. Absorption spectra at the start of each cure temperature, and then at 30 minute intervals were plotted. The steps for determining conversion from these spectra is shown in figure 4.2. The initia spectra are shown in figure 4.2a). A minimum intensity was observed at 7500-8000cm^{-1}. The minimum at higher wavenumbers was not used as it was not a clear, flat minimum, but would continuously drop off, making it difficult to determine a true minimum in this region. This minimum was set to 0 so that subsequent scaling of results could be carried out without an offset. The spectra with this offset are shown in figure 4.2b). The results were then normalized to the peak at 4632cm^{-1}. The spectra in the wavenumber range 3900-4700cm^{-1} before normalization are shown in figure 4.2c) and after in figure 4.2d). This peak at 4632cm^{-1} is the absorption peak from phenol groups which do not change in concentration during the cure, and therefore should not change in absorption intensity. This has previously been used as a reference peak for epoxy content measurements [12]. The area of the peak associated with epoxide content, at ∼4529cm^{-1} was determined via integration, using the range from which the peak at the start of cure appeared to start and end (from 4467cm^{-1} - 4564cm^{-1}). This range is shown as

the range inbetween the red lines shown in figure 4.2d). An initial conversion % was then calculated by treating the conversion at the start of curing as 0, then dividing the area of the epoxide peak at each section of cure by its area at the start of cure. This conversion was then scaled to the 'true conversion' using the T_g and conversion results from DSC measurements. For instance, if DSC measurements showed a formulation to have a conversion of 0.8, the NIR conversion results were scaled by 0.8.

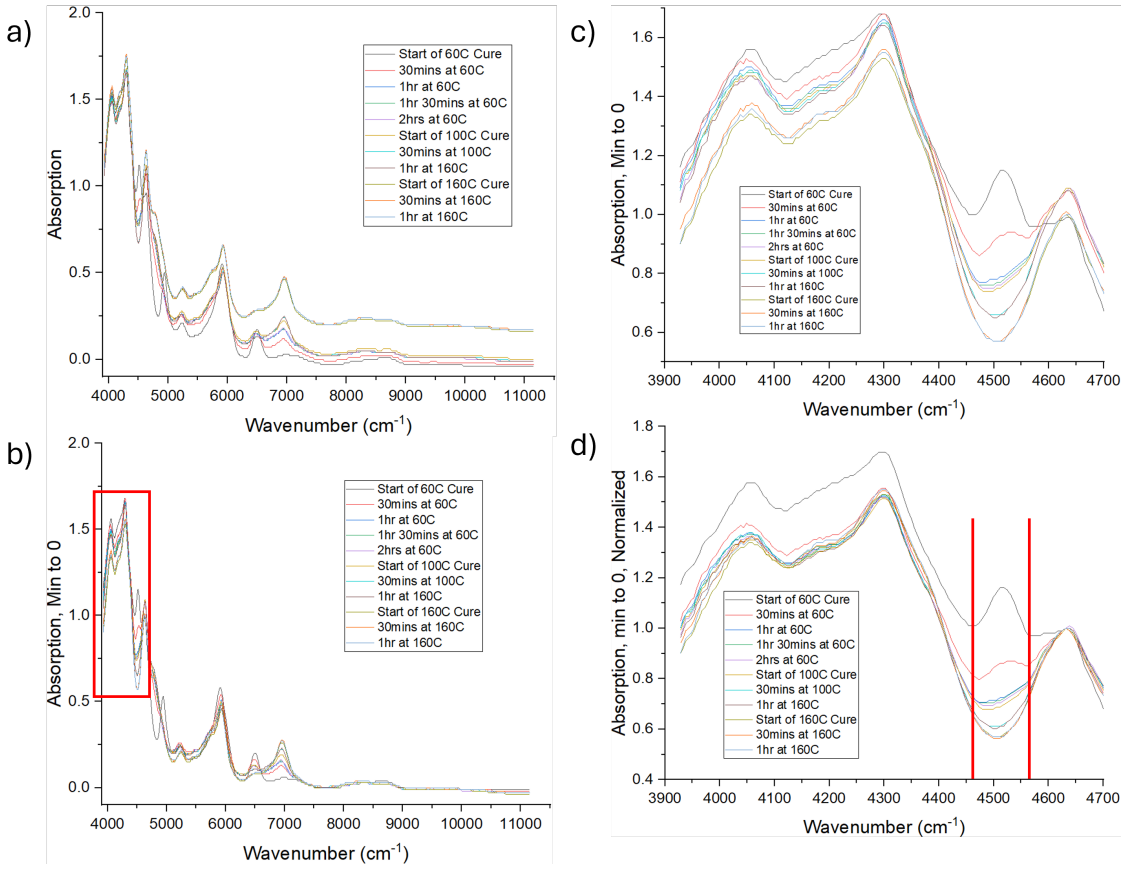

Figure 4.2: The absoprtion spectra of a sample of initially uncured mix of UC0003 and MXDA of stoichiometric ratio, as it is cured. Each line indicates a different point in the cure regime. a) shows the intial absorption spectra. b) shows the spectra with the minimum between 7500-8000cm^{-1} set to 0. The red square indicates the absorption spectra in the region of 3900-4700cm^{-1}, as shown in c). d) shows the absorption spectra in the range 3900-4700cm^{-1}, normalized to the peak at 4632cm^{-1}, associated with the phenol group. The red lines indicate the region of the absorption peak associated with the epoxy group. An integration of this region was taken to determine relative conversion of epoxy during cure.

4.3 Nuclear Magnetic Resonance Spectroscopy (NMR)

Solid state ^{13}C cross-polar magic-angle-spinning (CP/MAS) NMR spectra in the solid state were obtained using a 500MHz Bruker Advance III HD spectrometer at 125.13MHz using a zirconia rotor of 4mm diameter. Conventional single contact $^{1}H \rightarrow ^{13}C$ cross polarization with high proton decoupling during the signal acquisition was performed. A pulse duration of 3.5μs, contact time of 2ms, repetition time of 6s, spectral width of 36kHz and spinning speed of 12kHz were used. Chemical shifts δ[PPM] were referenced to the adamantane signal at 38.48PPM.

Samples were polished into a fine powder to enable the NMR spectra to be measured. Samples were held in place with a vacuum before being machine-cut with a 30mm high speed steel slot drill.

DER331, MXDA and their reaction products, as shown in figure 2.6 are shown in figure 4.3. Each carbon is numbered, with each number referring to a different δ value from $^{1}3C$ NMR, as predicted by [16]. These δ values are shown in table 4.1.

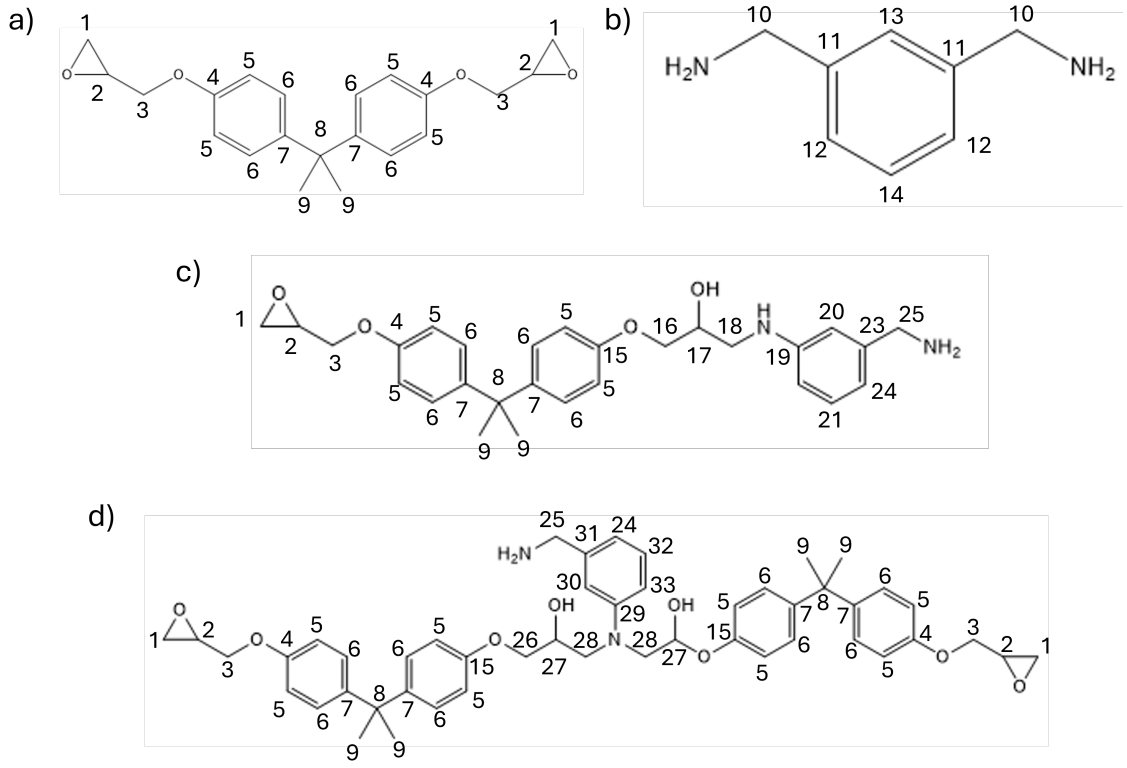

Figure 4.3: The molecules present during the reactions of DER331 and MXDA. Each carbon is labelled with a number that refers to a different δ value predicted by [16] for ^{1}3C NMR. δ values are shown in table 4.1. a) shows DER331, b) shows MXDA. c) shows the product of the initial, primary amine - epoxy reaction between DER331 and MXDA. d) shows the product of another DER331 molecule interacting with the secondary amine molecule shown in c).

Reference Number	δ (ppm)
1	44.64
2	50.1033
3	69
4	156.44
5	114.44
6	127.9
7	147.81
8	41.17
9	30.715
10	46.4
11	143.6
12	125.3
13	125.7
14	128.5
15	157.27
16	70.81
17	68.35
18	46.04
19	148.54
20	116
21	129.4
22	109.94
23	143.95
24	125.1
25	46.125
26	70.5
27	65.3
28	56.75
29	151.7
30	123.8
31	143.95
32	129.65
33	110.4

Table 4.1: Carbons, as numbered in figure 4.3 and their theoretical δ values for ^{1}3C NMR, as determined by [16].

4.4 Results

4.4.1 Final T_g of Samples Cured With and Without DMP-30 for Varying Levels of Excess Epoxy

Figure 4.4 presents the T_g for a series of samples of UC0003 comprising various ratios of MXDA and DMP-30 and cured in an oven, for 2 hrs at 60 °C, 1 hr at 100 °C and

1 hr at 160 °C.

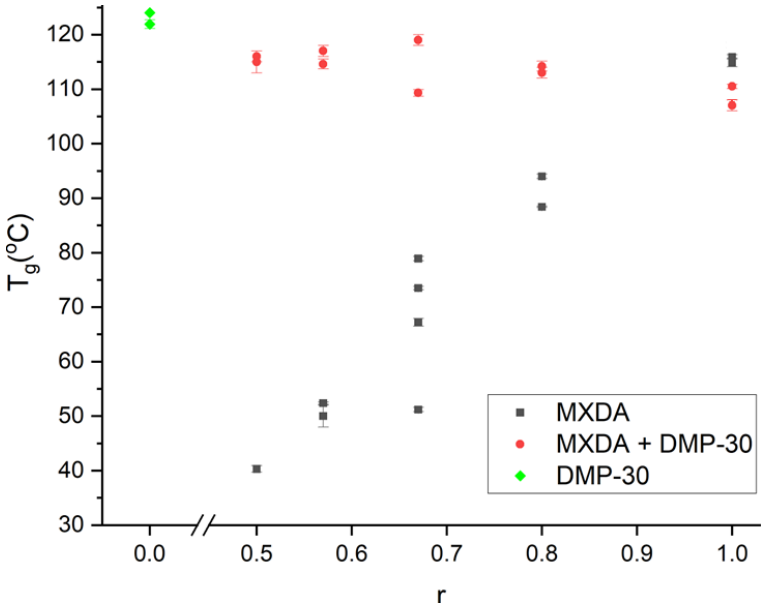

Figure 4.4: Plot of the change in glass transition temperature for oven-cured samples of UC0003 mixed with MXDA and DMP-30. For samples with MXDA, samples were made with r values between 0.5 and 1. Samples made with only DMP-30 as the curing agent are shown as having $r = 0$. T_g was determined via DSC, from the temperature range at which heat flow changed. Error bars originate from the averaging of multiple samples taken from the same mixture i.e. repeats.

For samples without DMP-30, as the level of amine decreases, the T_g decreases from ∼115°C at the stoichiometric ratio, $r = 1.0$, to ∼40°C for $r = 0.5$. This is due to the increasing amount of epoxy that does not cure as the amount of MXDA decreases. A reduced conversion of monomer is known to reduce T_g by reducing the crosslink density of the polymer [17]. One of the results for $r = 0.67$ has a T_g of 51.2 ± 0.4°C. This appears to be an anomalous result, but it is unclear how this arose, the other three samples follow linear trend with r. With the inclusion of DMP-30 into the mixture, the T_g's are higher than without DMP-30 for all stoichiometries, aside from $r = 1$. They are slightly lower for the stoichiometric ratio at ∼106-115°C before increasing to a constant ∼112-118°C for $r \leq 0.8$. The constant T_g as amine levels decrease is due to the DMP-30 allowing the excess epoxy to homopolymerize, increasing the overall conversion of epoxy to that similar to the stoichiometric mix without DMP-30, even though there is less MXDA. It was initially believed that the stoichiometric formulation with DMP-30 has a lower T_g due to unreacted amine. This would have a plasticizing effect on the final polymer network, raising the mobility of polymer chains, thus lowering the polymer's T_g [17]. Some of the epoxy that would normally react with MXDA instead homopolymerizes due to the presence of DMP-30, thus leaving behind excess MXDA. However, as shall be discussed in section 4.4.3, it appears as though this is

not the case. Rather, there appears to be a reaction involving MXDA, DMP-30 and the polymer network that lowers the formulation's T_g, that occurs at $\sim$150°C.

It appears as though the samples cured with DMP-30 do not form separate networks of homopolymerized polymer and amine-cured polymer. This is validated by the singular T_g values measured via DSC. This would also explain the difference in the sample that is cured without MXDA - it is a different network to those with a mix of homopolymized and amine-cured polymer. T_g would be higher in the solely homopolymerized sample due to the reduced flexibility of the phenol groups in the epoxy, compared to those in MXDA which contain additional methylene bridges. It has been previously reported that epoxy-amines with different curing agents produce singular glass transition temperatures, providing evidence that the different networks are effectively homogeneous and that they are effectively forming a single network [18]. Alternatively, the higher T_g may be due to the homopolymerized network having no residual unreacted epoxy or diamine in these systems which could potentially act as a plasticiser.

It could be the case that that due to the similar T_g's of the polymerized $r = 1$ and purely homopolymerized networks, as shown in figure 4.4, that there could be two similar T_g's in the hybrid networks that appear as one. If this were the case, the range of T_g's of these hybrid networks should be greater than the purely polymerized or homopolymerized formulations. The temperature range of these glass transitions is shown in figure 4.5. Samples cured with both MXDA and DMP-30 show T_g ranges similar to that of $r = 1$ without DMP-30, and lower than their counterparts without DMP-30. This provides further evidence that there is only one glass transition, and therefore only one network in samples both partially polymerized by MXDA and homopolymerized by DMP-30. The T_g range increase for formulations without DMP-30 as excess epoxy increases. This comes from a reduction in conversion, resulting in more dangling chain ends in the network, and a range of networks of different sizes. These different-sized networks will have different T_g's, causing this resultant range.

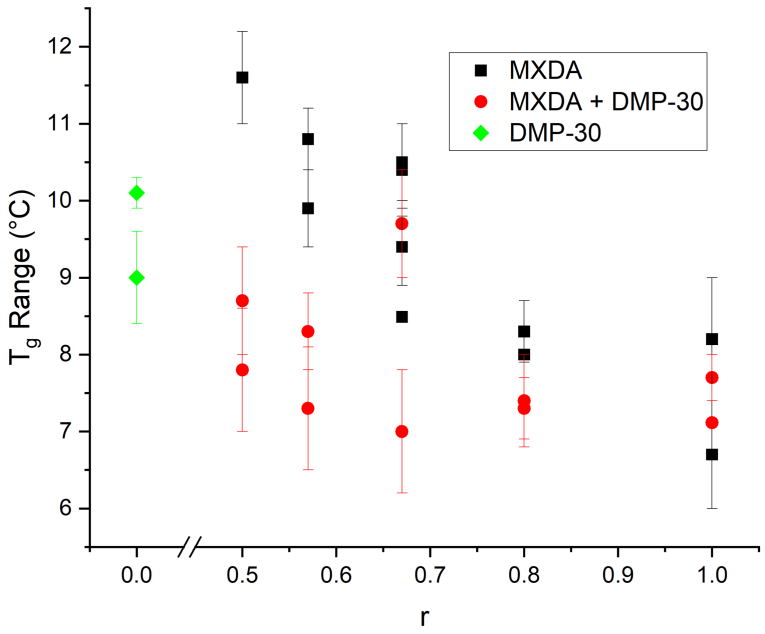

Figure 4.5: Plot of temperature range of the glass transition of samples of UC0003 cured with MXDA of $0.5 \leq r \leq 1$, cured with and without DMP-30. A stoichiometry of 0 corresponds to a purely homopolymerized sample. Error bars originate from the averaging of results from multiple samples made from the same mixture.

4.4.2 Conversion at Ambient Temperature

In order to measure the curing rates at ambient temperature of samples cured with MXDA, DMP-30 or both, samples were left at ambient temperature before having their T_g's measured via DSC. figure 4.6a) shows the changes in T_g over the course of one day. Other sets of samples were left for one day, six days and 28 days. These results are shown in 4.6b).

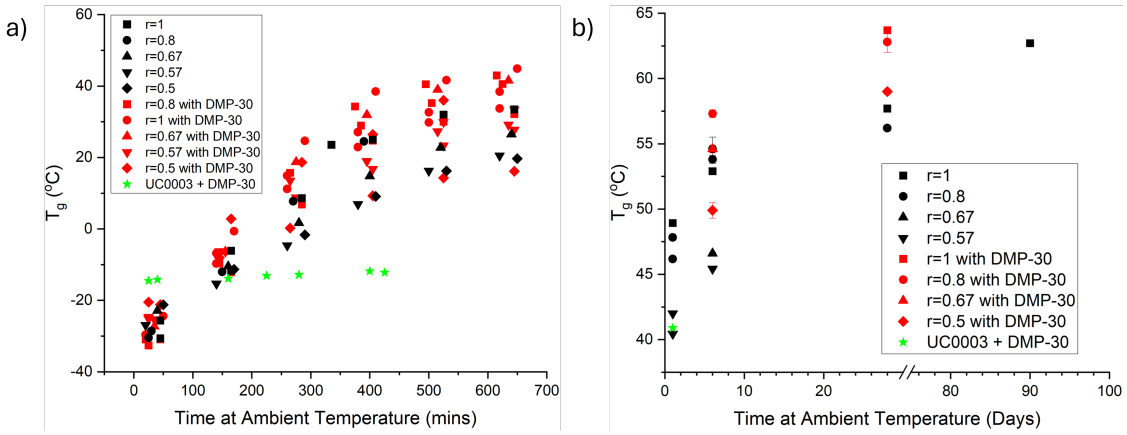

Figure 4.6: Graph showing the change in T_g of formulations of epoxy-amine resins with and without DMP-30 with increasing time left at ambient temperature. a) shows the change in T_g over the course of one day. b) shows the change in T_g over 1, 8, 27 and 90 days. It should be noted that the samples used for the results shown in a) are not from the same batch as those used for the results shown in b). UC0003 + DMP-30 refers to a purely hopolymerized sample (no MXDA). Results show the average of 3 samples from the same batch. Error bars show the standard deviation of these results.

It can be assumed that any change in T_g for $r = 1$ and UC0003 + DMP-30 can be taken as an increase in conversion, due to epoxy-amine and homopolymerization reactions, respectively. From figure 4.6, it can be seen that all formulations that included MXDA saw an increase in T_g over time. This shows that the epoxy-amine reaction is occurring at ambient temperature.

Figure 4.6a) shows that there was little change in T_g for UC0003 + DMP-30, the formulations cured only via homopolymerization, over the course of the initial 450 minutes. Although this may appear to show that the homopolymerization reaction does not occur at ambient temperature, the initial T_g of this formulation, -14.5°C, is greater than that of all other samples, with the rest having T_g's < -20°C. For this formulation, curing occurred during the initial stirring step. Due to the lack of MXDA to reduce viscosity, the mixture became very viscous. This occurred to an extent that the mixture became difficult to stir with a glass rod. Curing therefore slowed down to an extent that there was no clear change in T_g over the next 450 minutes. It does not however seem possible that the trend in T_g for UC0003 + DMP-30 shown in figure 4.6 would result in a T_g of 40.9°C after one day of curing at ambient temperature, as shown in figure 4.6b). A raised ambient temperature should not be the case, as the the UC0003 + DMP-30 results taken in 4.6b) were taken in April, whereas the data in 4.6a) was from July and August, when ambient temperatures should have been higher. All the other results from figure 4.6a) seem to agree with those from figure 4.6b).

By comparison to figure 4.4, it can be seen that the T_g for r=0.5 cured with DMP-

30 produced a greater T_g after 9 days at ambient temperature than r=0.5 (without DMP-30) when cured at elevated temperatures in the oven. As this oven-cure should produce the maximum T_g, this must mean that this increased T_g in r=0.5 when cured with DMP-30 must be due to homopolymerization, which must occur at ambient temperature. The difference with this formulation as compared to UC0003 + DMP-30 is that MXDA was present to act as a plasticizer, increasing mobility of reactants, thus increasing reaction rate.

From figure 4.6b) it can be seen that T_g increased as excess epoxy was reduced (stoichiometry increased to 1). This was due to the increased chance of epoxy-amine reactions occuring due to there being more equal amounts of epoxy and amine. It would also be the case that due to increased amine levels, more overall reactions could occur, so higher T_g's could be reached. Furthermore, with the inclusion of DMP-30, the T_g was raised. This is to some extent due to homopolymerization. It is however unclear how much of this increase in T_g was due to DMP-30 acting as a catalyst for the epoxy-amine reaction, and how much was due to homopolymerization.

Figure 4.6 shows an increased T_g for all formulations as time progresses. It can therefore be concluded that epoxy-amine polymerization and homopolymerization via DMP-30 occur at ambient temperature. Over the course of 9 and 28 days, samples with DMP-30 have a higher T_g than their counterparts without DMP-30. This shows that the addition of DMP-30 raises the conversion rate of epoxy; either by the additional mechanism of homopolymerization, accelerating the homopolymerization reaction, or both. By comparison to figure 4.4, it can be seen that the T_g for r=0.5 with DMP-30, when left at ambient temperature for 9 days, is greater than that of the oven-cured r=0.5 (without DMP-30). Given that this oven-curing is believed to produce the maximum T_g, homopolymerization must occur at ambient temperature to obtain this greater T_g value. The formulation without MXDA, UC0003 + DMP-30, in which polymerization can only occur via homopolymerization, showed a lower T_g over its six days of curing compared to those with MXDA and MXDA and DMP-30. This appears to show that the homopolymerization reaction is slower than the the epoxy-amine reaction. This could be due to differences between the homopolymerized epoxy and epoxy-amine networks. A less-flexible network would reduce conversion rate when polymerization is limited by diffusion rate at greater conversions [8]. The greater abundance of MXDA as compared to DMP-30 in the initial mixture could be an additional reason as to why conversion appears to be greater in the MXDA-only formulations compared to the DMP-30-only formulation. Given that the homopolymerization reaction occurs slower than the epoxy-amine polymerization reaction, it appears that the increase in T_g when curing with both MXDA and DMP-30 as opposed to just DMP-30 would come from the DMP-30 catalyzing the epoxy-amine reaction as opposed to homopolymerization.

4.4.3 Enthalpy of Cure and the Enthalpy Peak

The epoxy conversion for samples with MXDA, both with and without DMP-30, is shown in figure 4.7. The extent of cure for samples without DMP-30 follows the same

trend as seen for the oven-cured T_g results in that the epoxy conversion decreases with r. Samples with DMP-30 have a higher conversion than their counterparts without DMP-30, but they do not go to full conversion as might have been expected. This is believed to be due to the DMP-30 induced homopolymerization reaction occurring more slowly than the step polymerization reaction. As r decreases in formulations cured with DMP-30, more homopolymerization is required. Conversion therefore decreases as this homopolymerization cannot fully occur within the time of the DSC heat cycle. Given that there was no exotherm for DSC measurements of oven-cured formulations using DMP-30, it was taken that this curing procedure allowed for a completion of all reactions, both epoxy-amine and homopolymerization. As stated in section 4.2.3, the oven cure spent over four hours above 60°C. In comparison, each 10°C DSC heat cycle spent 14 minutes above this temperature, a much-reduced time.

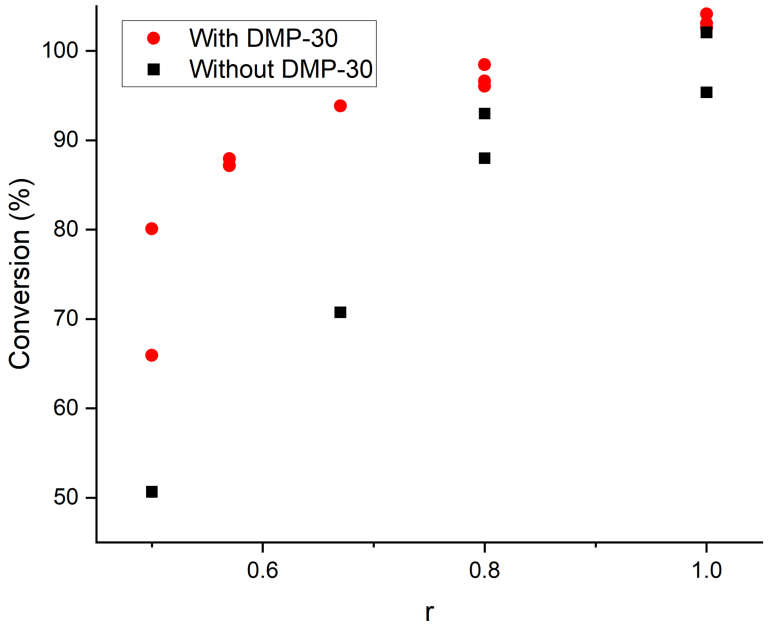

Figure 4.7: Graph of the extent of reaction for samples of UC0003 and MXDA, both with and without DMP-30, and varying levels of MXDA. Measured via DSC measurements of exotherms of uncured sample mixtures. Conversion was taken as the difference between the enthalpy of reaction of an uncured sample as it cured compared with the expected enthalpy for 100% conversion.

The shape of the enthalpys peak of reaction for samples without DMP-30, for potlifes of <1 hour and >10 hours, are shown in figure 4.8. Heat flows were normalized to their maximum peak heights so as to enable better comparison of the peak shapes between the different stoichiometric ratio formulations. The size of the enthalpy peak did decrease as potlife increased, agreeing with the results from section 4.4.2 that polymerization reactions occur at ambient temperature.

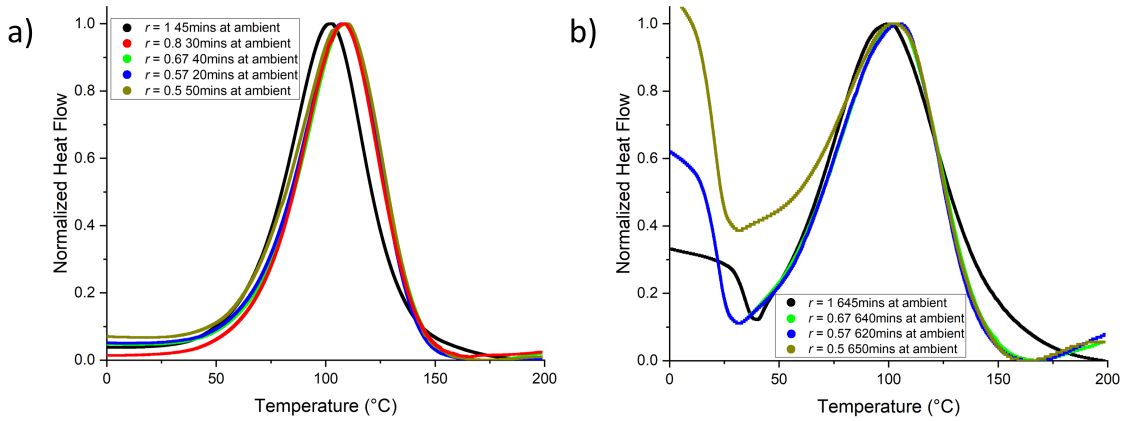

Figure 4.8: Enthalpy peaks of samples without DMP-30, directly cured in the DSC. The peaks have been normalized to the maximum peak height, to enable better comparison of peak shape. a) is for samples with the shortest potlife. b) is for samples of the longest potlife tested, ∼10-11 hours.

As seen in figure 4.8, there is very little difference in the shape of the enthalpy peaks for samples without DMP-30 as the MXDA content changes. These epoxy-amine samples also show very little change in the enthalpy peak shape as their potlife increases. Samples of stoichiometric mix had a lower peak enthalpy temperature than samples of excess epoxy. As time at ambient temperature increased, the peak temperature of the enthalpy curve decreased. Over the course of ∼600minutes, for samples of r=1, this was a decrease from $\sim$ 103°C to $\sim$ 100°C. For samples of < 1, from $\sim$ 109°C to $\sim$ 103°C.

By comparing the difficulty in stirring the mixture, samples containing DMP-30 showed greater viscosity than their counterparts without. This viscosity increased as stoichiometry decreased, or as the level of homopolymerization increased i.e. as the amount of MXDA decreased. The enthalpy peak of reaction for samples with DMP-30 is shown in figure 4.9. The figure shows the enthalpy for samples of shorter potlife (∼40minutes) and the enthalpy for samples with a longer potlife (∼400minutes). Again, there was a decrease in enthalpy peaks as potlife increased, showing that both polymerization and homopolymerization reactions occur at ambient temperature.

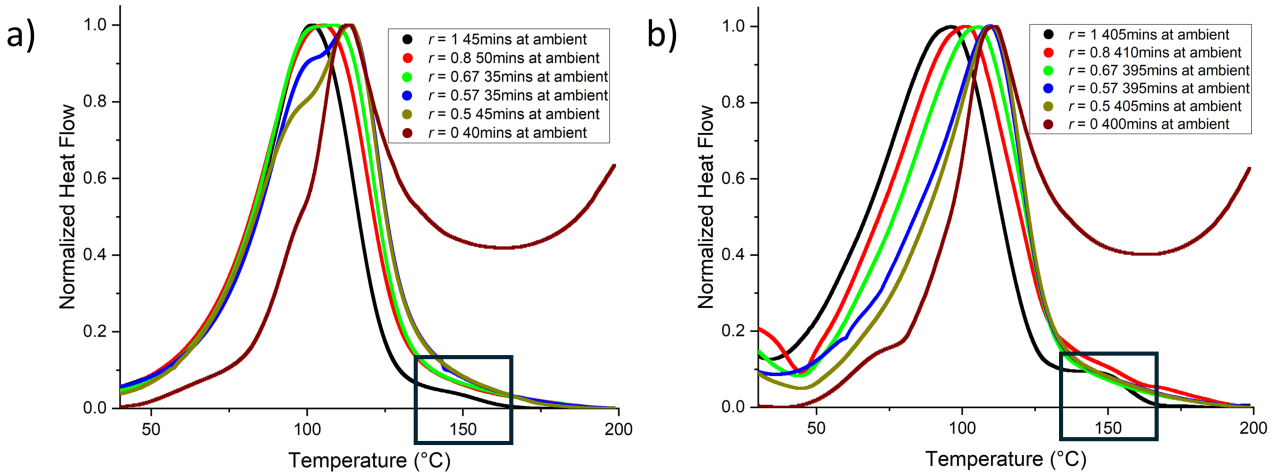

Figure 4.9: Enthalpy peaks of samples with DMP-30, cured in DSC. Peaks normalized to maximum peak height to allow for better comparison of peak shape. a) shows samples of the shortest potlife. b) shows samples of longest potlife, ∼400minutes. The black squares highlights the additonal enthalpy peak at 150°C of r=1 for both the short and long potlife results. r=0 indicates a fully homopolymerized network.

There are clear changes in the shape of the enthalpy curves for samples cured with DMP-30, as the amount of MXDA changes and as the potlife is altered. For samples having the shortest potlife (figure 4.9a)), the sample of stoichiometric ratio has a single enthalpy peak at $\sim$ 100°C. As r decreases to 0.5 and then to zero MXDA content, two peaks form with a lower peak still at $\sim$ 100°C and a higher temperature peak at $\sim$ 115°C. After a potlife of ∼400 minutes, all samples with MXDA display one enthalpy peak that shifts linearly in temperature from a peak of $\sim$ 95°C at $r = 1$ to $\sim$ 110°C at $r = 0.5$. Unlike the amine reaction, the DMP-30 catalysed homopolymerization reaction appears to occur in two separate distinct stages. This can be seen in the UC0003 + DMP-30 results in figure 4.9. The first stage occurs at $\sim$ 100°C, the same temperature at which the epoxy-amine reaction exhibits a peak. For samples of shorter potlife, a distinct second peak can be seen, occurring at $\sim$ 112°C, which we assign to DMP-30. As the amount of MXDA is reduced, the homopolymerization reaction becomes more evident, resulting in enhancement of this peak. The UC0003 with MXDA reaction dominates at ambient temperature, after more than ten hours of potlife, there are no amine-epoxy reactions occurring during the heating cycle in the DSC, only the reaction of the epoxy with DMP-30. As the UC0003 and DMP-30 reaction occurs much more slowly at room temperature, after ten hours there is still some ring-opening left in the UC0003 + DMP-30 sample, resulting in two peaks being present. The first peak however is now at a considerably lower temperature, ∼70°C.

The change in temperature of the peak enthalpy with time, for formulations cured both without and with DMP-30, is shown in figure 4.10.

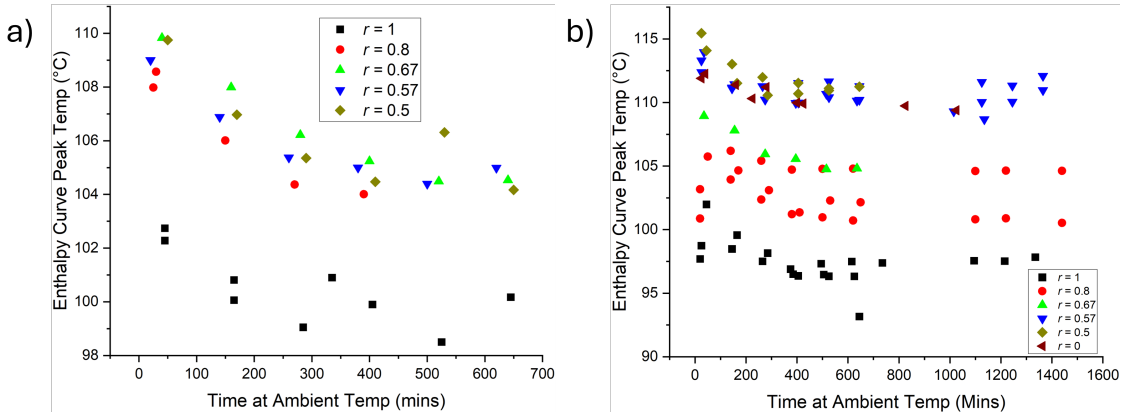

Figure 4.10: Dynamic DSC data showing the change in peak enthalpy temperature with time for samples a) without DMP-30, and b) with DMP-30. r=0 refers to a purely homopolymerized network

In formulations with DMP-30, the peak enthalpy temperature for the initial peak increases as amine levels decrease. This may be due to the increased prominence of the second peak, as shown in figure 4.9. For formulations without DMP-30, the temperature of peak enthalpy remains constant for samples of different levels of excess epoxy. There is however clearly a different temperature of maximum enthalpy for the stoichiometric formulation. We are currently unsure as to why this difference arises. For all formulations, the temperature of maximum enthalpy decreases with time. It is unclear as to why exactly the temperature of the enthalpy curve decreases as time at ambient temperature increases, but it is believed to be connected to the fact that curing takes place at ambient temperature. It may possibly be due to the initial enthalpy curve being a combination of separate mechanisms in the epoxide ring opening, each mechanism providing its own enthalpy contribution. As some reaction mechanisms take place at ambient temperature, their contributions to the enthalpy peak drop off. In this case, it would be expected that the enthalpy peak would shift to higher temperatures, as the lower contribuition is reduced. However, the opposite happens, with the temperature of peak enthalpy reaction reducing as time at ambient temperature increases. It is unclear why this is the case.

As can be seen in both figures 4.9a and b, there is a further peak at $\sim$ 150°C for the sample at stoichiometric ratio. It may also be present on the sample of $r = 0.8$, but it is less clear. It does not appear to be present for the samples with $r < 0.8$. The size of this peak remains constant as potlife increases. Looking at figure 4.8, this peak is also not present in samples without DMP-30. Due to the consistent intensity of this peak, it is believed to occur only at these elevated temperatures, on the crosslinked polymer network. This peak was measured by curing samples for two hours at 60°C and then 100°C before measuring the final enthalpy via DSC. The enthalpy of this peak and subsequent changes in T_g were measured. Formulations of r=1, 1.25 and 0.8 with DMP-30 were analysed in order to determine how excess amine and epoxy affected this

peak. r=1.25 without DMP-30 was also analysed as a comparison for a formulation with excess amine but without DMP-30. Three samples for each formulation were analysed. The results are stated in table 4.2.

Formulation	T_g Before 150°C Reaction	T_g After 150°C Reaction	Change in T_g After Reaction
r=1.25 with DMP-30	92±4	89±1	-4±3
r=1.25 without DMP-30	83.47±0.01	82.80±0.03	-0.68±0.03
r=1 with DMP-30	118.8±0.1	104.93±0.01	-13.9±0.1
r=0.8 with DMP-30	118.7±0.9	117.3±0.5	-1.4±0.1

Table 4.2: Table showing the T_g for formulations before and after a possible reaction at 150°C. Error is the standard deviation of the average of multiple results

There is a clear, measurable drop in T_g for both r=1 and 1.25 with DMP-30. In comparison, the three samples of r=0.8 showed a drop of only 1.4±0.4°C. There is a peak at 150°C, but it appears that this is at least in-part due to the epoxy conversion reactions that are still ongoing. This makes it difficult to determine if there is a separate non-conversion reaction at 150°C that is clearly present for r=1 with DMP-30. The samples of r=1.25 without DMP-30 did not show an enthalpy peak at ∼150°C and only displayed a T_g drop of 0.68±0.03°C. From these results, it can be concluded that a reaction occurs at ∼150°C between DMP-30 and MXDA that reduces the T_g of the epoxy-amine network. It is therefore only present in formulations of excess amine with DMP-30 (r=1 is treated as having excess amine due to some epoxy being homopolymerized, this may also be true to a lesser extent for r=0.8). We are currently unsure as to what this reaction is. In the samples of r=1.25, there is a slight dip in the first heat cycle before the glass transition. We are also unsure what this is, but it again should have something to do with excess amine.

Figure 4.11 shows NMR results for samples of $r = 1$, cured with and without DMP-30. These samples underwent cure cycles of two hours at 60°C, two hours at 60°C and 1 hour at 100°C, and of full cure. There are five peaks that appear both with and without DMP-30. The peaks at ∼31PPM and ∼42PPM correspond to the two end carbons inbetween the two benzene rings in MXDA. They do not change during cure as these carbons do not react. The peaks at ∼50PPM and ∼58PPM correspond to carbons in the epoxy ring. As the epoxy ring is opened during reactions, the intensity of these peaks changes as the reaction progresses. The peak at ∼70PPM corresponds to carbons bonded to oxygen atoms, not in the epoxy ring. This includes carbon atoms connected to hydroxyl groups and so exhibits a change in intensity as hydroxyl concentration increases during the reaction. There is a peak on r=1 with DMP-30 that only exists after the 160°C cure, at ∼48PPM. It is unclear what carbon this corresponds

to, but it provides further evidence of a reaction that only occurs in the presence of DMP-30 that results in a change in the overall network structure.

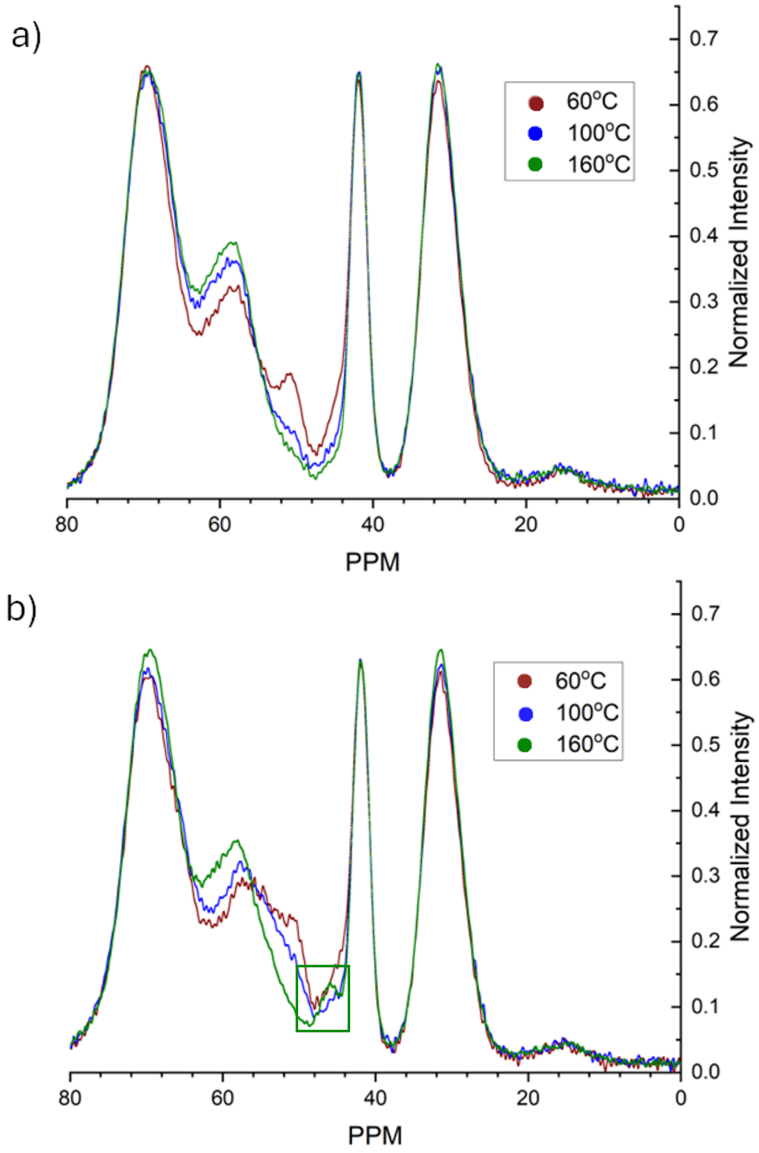

Figure 4.11: Solid state NMR results for samples of a) r=1 and b) $r = 1$ cured with DMP-30. Results are shown for cures of two hours at 60°C, two hours at 60°C and one hour at 100°C, and two hours at 60°C, one hour at 100°C and one hour at 160°C. The peak at ∼48PPM for the 160°C cure of r=1 with DMP-30 is shown in the square. Changed figure to portrait.

4.4.4 Conversion During Cure

Samples had their conversions measured at different stages of curing via DSC as well as during cure via NIR spectroscopy. Conversions of formulations measured both by DSC and NIR are shown in figure 4.12. DSC and NIR measurements of the same formulation were nominally the same, but of different batch mixtures.

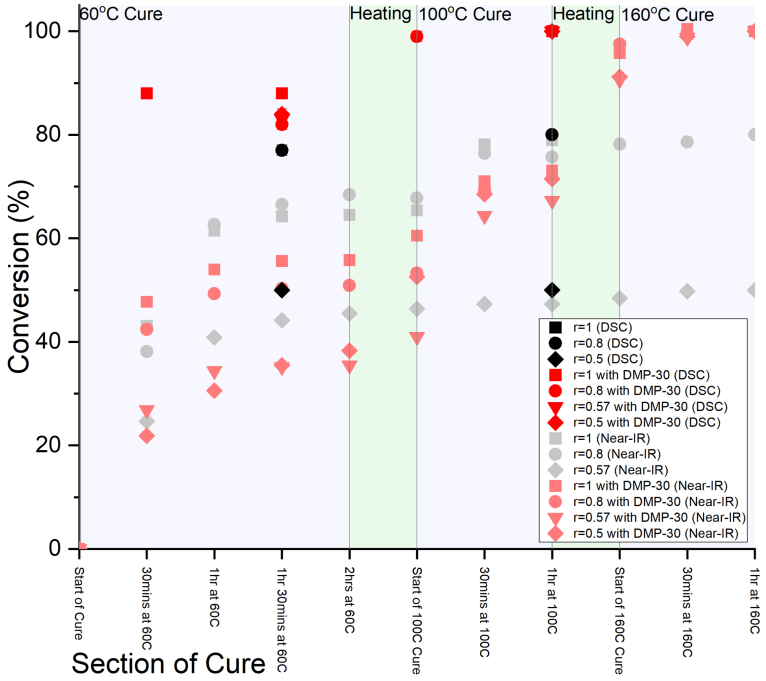

Figure 4.12: Graph showing the conversion of epoxy-amine resins, as determined by DSC and near-infrared measurements. Formulations without DMP-30 are shown in black. Those cured with DMP-30 are shown in red. Conversions measured by DSC are shown in opaque colours. Conversions measured by NIR are shown in semi-transparent colours. There is a DSC conversion measurement of r=1 for 30 minutes at 60°C, giving a conversion of 88%. This cannot be seen as it is covered by the r=1 with DMP-30 measurement.

Results from DSC analysis show a greater conversion than the NIR results before heating up to 160°C, for formulations both with and without DMP-30. These DSC results indicate that homopolymerization is occurring due to DMP-30, as formulations of r=0.8, 0.57 and 0.5 all have conversions greater than 80%. This agrees with the results for samples cured at ambient temperature, from figure 4.6.

Given the simplicity of the DSC method over the NIR method in obtaining conversion, its results are taken as more reliable than the NIR results. For NIR measurements, the change in area across the peak associated with the epoxide absorption at 4529cm^{-1} It has been shown that there is an amine absorption peak at ∼4529cm^{-1}, and that the

phenol peak at ∼4632cm^{-1} changes with temperature [19]. This amine peak has not been seen when measuring the absorption spectrum of pure MXDA. This is also the case for DMP-30. Before normalization of the phenol peak, it was measured that there were changes in the absorption intensity of this peak, with an absorption intensity of 1.29 being measured at the start of cure, and 1.21 at 160°C. This difference does not account for the difference between the DSC and NIR conversion results. It has also been shown that the peak at ∼4300cm^{-1} increases after ∼55% conversion [12]. This increase could reduce the decrease in the epoxide peak and explain why the supposed conversion is lower than expected. It is apparent that the fitting of separate peaks would be more suitable. However, it has been found to be very difficult to fit peaks that successfully align with the different peaks in the region of the epoxide absorption peak. Due to this, little confidence could be sought in these fits, as they appeared to either be incorrectly fitted, approximate or could be fit in multiple different ways to render what appeared to be a suitable fit. There therefore appears to be no correct approach to determine epoxy conversion accurately from NIR spectroscopy. The full set of conversions as measured by NIR spectroscopy can be found in appendix A.1.

4.5 Conclusions

The effects of adding the homopolymerizing agent DMP-30 on the glass transition temperature and the conversion of epoxy-amine resins were determined. The crosslinking of the networks was performed at ambient temperatures as well as using a conventional optimised high temperature curing protocol. Via differential scanning calorimetry (DSC), it was determined that the addition of a homopolymerizing agent, DMP-30, to epoxy-amine samples allowed for full epoxy conversion, regardless of the amine fraction. Without DMP-30, conversion of epoxide groups is reduced as the level of excess epoxy increases. As conversion decreased, so too did T_g, in line with previous investigations [2]. The addition of DMP-30 consistently increases T_g in formulations with excess epoxy. Furthermore formulations of both epoxy-amine and homopolymerized networks showed low T_g ranges, indicating that these two networks form part of the same network, rather than two distict networks. DMP-30 is therefore highly beneficial to coating performance, as it will reduce the amount of non-crosslinked amine that can act as a plasticizing agent whilst still creating a homogeneous network. These will reduce permeant uptake and transport through the coating.

DSC measurements of samples cured at ambient temperature show that DMP-30 causes homopolymerization at low temperatures. It was also shown that conversion is greater in formulations having both MXDA and DMP-30 than just MXDA. This is most likely be due to DMP-30 catalyzing the epoxy-amine reaction. Formulations of only epoxy and DMP-30 showed a far lower degree of conversion at ambient temperature. This may be due to network differences reducing diffusion rate and thus the conversion rate.

DSC measurements of samples cured for two hours at 60°C followed by one hour at 100°C showed that for samples of $r \geq 1$ (i.e excess diamine) with DMP-30, there is a reaction at ∼150°C that reduces the T_g of the sample. This is not seen in formulations

of r <1 with DMP-30, or for formulations without DMP-30. Therefore for this to happen requires excess amine and the presence of DMP-30, but it is not clear what this reaction is, or why it reduces a sample's T_g. The assumption is that the network must become degraded (the molecular weight) between crosslinks must increase in order for T_g to be reduced.

The level of conversion at different stages of cure was measured via DSC and near-infrared (near-IR) spectroscopy. The DSC results again showed that homopolymerization occurred via DMP-30 at elevated temperatures. This contradicted the NIR results which indicated that homopolymerization did not occur until samples were heated from 60°C to 100°C. Currently, the DSC results are believed to be correct, due to the more direct approach of measuring the enthalpy to determine conversion. With NIR conversion measurements, changes in the epoxide absorption peak are obscured by neighbouring absorption peaks. It is therefore difficult to accurately quantify changes in the epoxide peak and ascertain if this is due purely to conversion of epoxide groups.

Bibliography

[1] E. Duemichen et al. "Analyzing the network formation and curing kinetics of epoxy resins by in situ near-infrared measurements with variable heating rates". In: *Thermochimica Acta* 616 (2015), 49–60. DOI: 10.1016/j.tca.2015.08.008.

[2] Fred Meyer et al. "The effect of stoichiometry and thermal history during cure on structure and properties of epoxy networks". In: *Polymer* 36.7 (1995), 1407–1414. DOI: 10.1016/0032-3861(95)95918-q.

[3] J. Ehlers et al. "Theoretical Study of the Epoxy-Amine Curing Reaction". In: *Macromolecules* 40.12 (2007), pp. 4370–4377. DOI: 10.1021/ma070423m.

[4] K. C. Cole, J. J. Heckler, and D. Noel. "A New Approach to Modeling the Cure Kinetics of Epoxy Amine Thermosetting Resins. 2. Application to a Typical System Based on Bis[4- (diglycidylamino)phenyl]methane and Bis(4-aminophenyl) Sulfone". In: *Macromolecules* 24.11 (1990), pp. 3098–3110. DOI: 10.1021/ma00011a012.

[5] V. L. Zvetkov. "A Modified Kinetic Model of the Epoxy-Amine Reaction". In: *Macromolecular Chemistry and Physics* 203.3 (2002), pp. 467–476. DOI: 10.1002/1521-3935(20020201)203:3<467::AID-MACP467>3.0.CO;2-Q.

[6] John D. McCoy et al. "Cure mechanisms of diglycidyl ether of bisphenol A (DGEBA) epoxy with diethanolamine". In: *Polymer* 105 (2016), 243–254. DOI: 10.1016/j.polymer.2016.10.028.

[7] C. Yi et al. "Curing kinetics and mechanical properties of epoxy based coatings: The influence of added solvent". In: *Progress in Organic Coatings* 124 (2018), pp. 165–174. DOI: 10.1016/j.porgcoat.2018.08.009.

[8] N. Sbirrazzuoli et al. "A Study of Epoxy-Amine Cure Kinetics by Combining Isoconversional Analysis with Temperature Modulated DSC and Dynamic Rheometry". In: *Macromolecular Chemistry and Physics* 204.15 (2003), pp. 1815–1821. DOI: 10.1002/macp.200350051.

[9] H. Shing-Gwo and W. Chung-Sheng. "DSC and FTIR analysis of the curing behaviors of epoxy/DICY/solvent open systems". In: *Thermochimica Acta* 316.2 (1998), pp. 167–175. DOI: 10.1016/S0040-6031(98)00356-6.

[10] Jocelyne Galy, Abed Sabra, and Jean-Pieirre Pascault. "Characterization of epoxy thermosetting systems by differential scanning calorimetry". In: *Polymer Engineering and Science* 26.21 (1986), 1514–1523. DOI: 10.1002/pen.760262108.

[11] Björn Erik Ekbrant, Anne Ladegaard Skov, and Anders E. Daugaard. "Epoxy-rich systems with preference for etherification over amine-epoxy reactions for tertiary amine accelerators". In: *Macromolecules* 54.9 (2021), 4280–4287. DOI: 10.1021/acs.macromol.0c02630.

[12] Jovan Mijovic and Sasa Andjelic. "A study of reaction kinetics by near-infrared spectroscopy. 1. comprehensive analysis of a model epoxy/amine system". In: *Macromolecules* 28.8 (1995), 2787–2796. DOI: 10.1021/ma00112a026.

[13] Gilbert Lachenal, Alain Pierre, and Nicolas Poisson. "FT-nir spectroscopy: Trends and application to the kinetic study of epoxy/triamine system (comparison with DSC and SEC results)". In: *Micron* 27.5 (1996), 329–334. DOI: 10.1016/s0968-4328(96)00022-4.

[14] M. Hesabi, A. Salimi, and M. H. Beheshty. "Effect of tertiary amine accelerators with different substituents on curing kinetics and reactivity of epoxy/dicyandiamide system". In: *Polymer Testing* 59 (2017), pp. 344–354. DOI: 10.1016/j.polymertesting.2017.02.023.

[15] S. Mortimer, A. J. Ryan, and J. L. Stanford. "Rheological behavior and gel-point determination for a model lewis acid-initiated chain growth epoxy resin". In: *Macromolecules* 34.9 (2001), 2973–2980. DOI: 10.1021/ma001835x.

[16] D. Banfi and L. Patiny. "www.nmrdb.org:ResurrectingandProcessingNMRSpectraOnline". In: *CHIMIA* 62.4 (2008), pp. 280–281. DOI: 10.2533/chimia.2008.280.

[17] J. M. G. Cowie and V Arrighi. *Polymers : Chemistry and Physics of Modern Materials*. 3rd ed. Taylor and Francis Group, 2007.

[18] N.C. Beck Tan et al. "Network structure of bimodal epoxies — a small angle X-ray scattering study". In: *Polymer* 40 (1999), pp. 4603–4614. DOI: 10.1016/S0032-3861(99)00096-8.

[19] A. Janisse. "Effect of Cure Protocol on Network Formation and Properties of Epoxy-Diamine Thermosets". PhD thesis. University of Southern Mississippi, 2019.

Chapter 5

Network Structure of Hydrogenous and Deuterated Epoxy-Amine Polymer Networks as Measured by Small-Angle Neutron Scattering

Abstract

Epoxy-amine resins are a popular choice as protective coatings to resist corrosion. As well as good corrosion resistance, they have good chemical and moisture resistance, are mechanically strong and tough, and adhere to surfaces. However, they ultimately fail to prevent corrosion. One hypothesis is that 'voids,' regions of low crosslink density, exist in the coating, into which water can enter. Water swells these voids, eventually forming pathways across the entire network. In this investigation, small-angle neutron scattering (SANS) was used to probe the network structure of samples of epoxy-amine resins cured with and without solvent. Samples were submerged in water and methanol to understand how swelling affected their network structure. Samples cured without solvent showed a lower Porod scale and a higher Porod exponent than their counterparts cured with solvent. It is believed that this was due to voids appearing in the solvent-cured formulations, most likely formed due to solvent and epoxy-amine phase separation during cure. Subsequent solvent evaporation would then leave voids in the final coating. Upon immersion in deuterated water and methanol, the Porod exponent and scale changed in solvent-cured samples to be more similar to the non-solvent samples. In this case, we believe that water and methanol entered the voids, swelling them until they became too large to be seen in our SANS measurements. Thus, contrast between void and network could not be seen and the samples appeared smooth. At the mid-Q range, there was increased scattering intensity in solvent-cured samples after immersion in water and then methanol. Again, this is believed to be due to these

solvents entering voids in the network, leading to increased scattering contrast as they replace the air. This change in intensity was not seen in formulations cured without solvent, due to the lack of voids for water or methanol to enter. Formulations were also made with deuterated epoxy. For these samples, a peak was seen at $\sim 0.4 \text{Å}^{-1}$. This was taken to be the deuterated phenol rings in the epoxy. This peak shifts to lower Q for solvent-cured samples immersed in methanol, indicating that methanol is also increasing the spacing between network chains.

5.1 Introduction

Epoxy-amine resins display excellent mechanical strength and toughness; they have good chemical, moisture and corrosion resistance; as well as good electrical, thermal and adhesive properties. Coupled with relatively low cost, these resins are therefore seen as a popular industrial choice as adhesives and barrier coatings [1]. However in operation nearly all organic coatings will eventually fail as barriers that inhibit corrosion, even whilst on the face of it remaining largely intact. The current theory is that over time degradation of the coating results in the formation of a network of pathways throughout the layer, ultimately resulting in the initiation of corrosion at the metal coating interface [2]. One possible way in which the process of corrosion may be accelerated could be via formation of a heterogeneous network in the crosslinked resin. This would occur at the point of formation and would result in regions of high crosslink density and areas of low-crosslink density, the latter having a much greater free volume[3]. Upon exposure to water, there would be diffusion of water to occupy the lower crosslink regions, which being intrinsically lower in crosslink density would automatically have a lower glass transition temperature, T_g and as such considerably more mobile polymer chains. As motion and rearrangement of the polymer chains takes place, this water would also move as well, hydrogen bonding to the chains. Movement of the water would be via hopping to other free volume regions and essentially creating water pathways throughout the entire network. Thus, a conduction pathway would form that allows migration of solvated ions through the entire thickness of the coating [4].

Industrially formulated epoxy-amine coatings are made more processable via the use of solvent diluents, such as xylene and butanol. This has the added complexity that network formation occurs simultaneously with crosslinking and solvent evaporation/removal. The addition of solvent improves the ease of application by lowering the viscosity of the mixture [5] and also prolonging the potlife and working time, during which the coating can be applied. Solvents can also affect the curing reactions kinetics, for example hydroxyl groups can also catalyse epoxy-amine reactions [6]. However, it has been shown that formulations incorporating solvent possess lower degrees of conversion, lower tensile strength and lower elastic moduli [7]. There is also the issue of phase separation during curing [8], the questions being does this takes place and (if so) how important is it in terms of affecting overall performance. Furthermore, the volatility of solvents used poses safety and regulatory issues: exposure to vapours can affect the operators central nervous system, and can pose fire and explosion risks [9].

Scattering techniques, such as small and wide-angle x-ray scattering (SAXS and WAXS) and small-angle neutron scattering (SANS) can be used to measure the variation in length scale and composition/density of crosslinked epoxy coatings on the micron to Angstrom scale [10]. Scattering techniques have been used to investigate the overall network size [11], the distance between polymer chains [11] and length of monomer units [12, 13] in crosslinked polymer networks. Given that SANS measures changes in the scattering length density, which is closely linked to molecular composition and density, deuterated epoxies have been used to provide contrast for SANS measurements of epoxy-amine networks. Through this, it has been shown that epoxy-amines cure to form both a homogeneous network [14] [15] and a heterogenous network [16]. All of the SANS experiments to date [14, 15, 16] that studied phase separation in epoxy networks used Jeffamine crosslinker molecules. These are relatively large oligomers based on a backbone of poly(ethylene glycol) with diamine functionality at the chain ends, and have an intrinsic radius of gyration. Other scattering studies [17] have shown heterogeneities to exist in epoxy novolac phenolic resins during cure, with areas of high crosslink density and low crosslink density. It was also shown that a reduction in curing agent resulted in a reduction in areas of high crosslink density [17]. Studies have also examined polymer networks that have been immersed in solvents such as acetone [15] [16], methanol [17] and THF [18]. Solvent enters the free volume, thus providing greater scattering contrast (deuterated solvents can also be used) between regions of different composition and cross link density in the polymer network, enhancing the measured SANS signal. Solvents can also be used to swell the network, providing further information on network structure and if the material is in the rubber regime, enabling the effective distance between crosslinks to be measured.

5.2 Experimental Section

5.2.1 Materials

The hydrogenous epoxy used was UC0003 (Supplied by Akzo-Nobel, Felling UK), this is a type F/A Bisphenol a diglycidyl ether (DGEBA) epoxy. The UC0003 supplied contained mainly DER331, but also contained Epikote 828 and Razeen LR 1150, all epoxies based on DGEBA. Two batches of UC0003 were used, one with an epoxide equivalent weight (EEW) of 173gmol^{-1}, and another of 172gmol^{-1}. The deuterated epoxy used was D16 bisphenol A diglycidyl ether (Farapack Polymers Ltd, Sheffield UK). The deuterated version of DGEBA has deuterons in place of the hydrogens in the phenol groups, in the central CH_3 groups. It was measured to have an EEW of 196gmol^{-1}. The amine, m-Xylylenediamine (MXDA) and the accelerator, 2,4,6-Tris(dimethylaminomethyl)phenol (DMP-30) were purchased from Sigma Aldrich (Gillingham UK) and used as received. Solvents used were o-xylene (Sigma Aldrich) and 1-butanol (Honeywell).

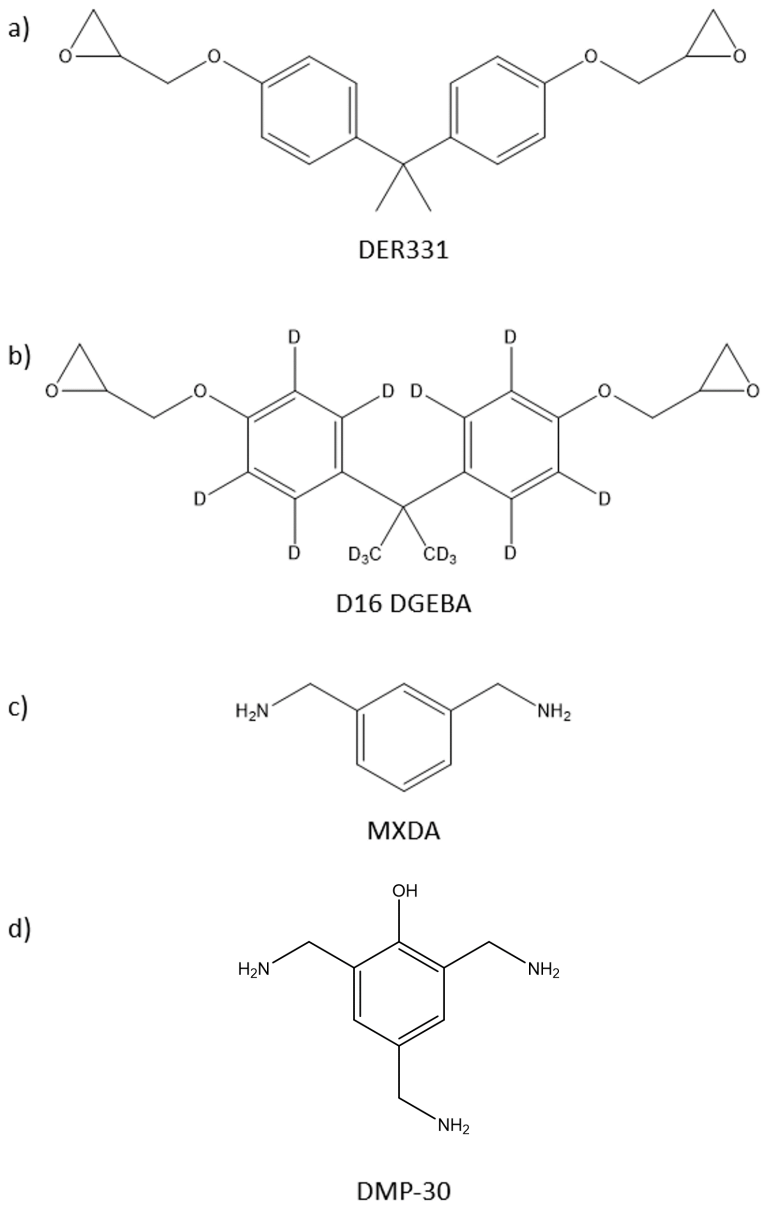

Figure 5.1: Materials used to make the crosslinked epoxy networks. a) shows the hydrogenous epoxy, DER331. b) shows the deuterated epoxy, D16 DGEBA. c) and d) show the amine curing agent, m-Xylylenediamine (MXDA) and the homopolymerizing agent, DMP-30, respectively.

5.2.2 Synthesis of Deuterated Epoxy

Deuterium labelled (D16) bisphenol-A diglycidyl ether DGEBA was synthesised based on a procedure from Wu and Bauer, using deuterated phenol rings and deuterated toluene [19]. This was performed by Dr Andrew Pryke of Farapack Polymers. The synthesis was done in two steps. Step one produced D16 labelled bisphenol A from

deuterated phenol. Step two in turn used this product to produce D16 bisphenol-A diglycidyl ether (D16 DGEBA).

9.67g of D6 Phenol was dissolved in 20ml of D6 toluene. 9.38g of deuterated sulphuric acid, 3.08g of D_2O and 0.034g of thyoglycolic acid were added to the mixture. The mixture was then stirred at 35°C. 42.8g of D6 acetone was dissolved in 5ml of D6 toluene. This solution was added to the initial mixture via a dropping funnel. During stirring, a solid formed. The mixture was heated to 50°C to keep it mobile and to maintain homogeneity and stoichiometry. The mixture was stirred for another 4 hours at 35°C. After leaving overnight, the contents were poured into a beaker containing 50ml of D_2O. 5ml of D6 toluene was used to wash the reactor previously containing the mixture. This was also added to the D_2O. Solid sodium bicarbonate ($NaHCO_3$) was added via spatula to the new mixture to neutralize the mixture's pH. The temperature of the mixture was again elevated to maintain solubility. The mixture produced an aqueous phase which was removed via a 10ml Gilson pipette. A further 10ml of D6 toluene was added and stirred into the mixture. The mixture was once again left to stand before more aqueous phase was removed. The remaining organic toluene phase was heated to 80°C to ensure complete dissolution before being transferred to a stoppered conical flask. This was warmed to give a clear solution before being lagged with foil and left to cool slowly before being placed in a fridge overnight to fully crystallise. This solid phase was separated via filtration (no. 2 grade sinter in a conical Buchner funnel) before being redissolved in 20ml of D6 toluene and cooled again. The solid was again separated by filtration before being dried under high vacuum at ambient temperature. ^{1}H NMR was taken of the solid and compared to the spectrum of its hydrogenous equivalent Bisphenol-A synthesis. The yield of D16 bisphenol-A was 7.72g or 64% (based on half of the initial phenol moles).

6g of the D16 bisphenol-A was added to 50ml (59g) of epichlorohyrdrin and 0.13ml of D_2O. This mixture was stirred and heated at 95°C. 2.05g of NaOH pellets were added over the course of 10-15 minutes. The stirring speed of the mixture had to be raised to stop the NaOH from sticking to the sides of the reactor vessel. After one hour at 95°C, the mixture was cooled to 30°C. Excess epichlorohyrdrin was removed via distillation. The mixture temperature was subsequently raised back to 95°C until no further distillation was observed. By this point, the mixture was semi-solid. ∼40ml of $CDCl_3$ was added to the mixture, making it into a slurry. The slurry was passed through a filter (consisting of a hyflo supercel bed (∼0.5cm) over a no. 3 sinter) to remove any salt formed in the reaction. The solution formed was cloudy. It was made clear by polishing it in a centrifuge at 2500rpm for 15 minutes. The $CDCl_3$ was removed from the product by rotary evaporation at a water bath temperature of 35°C under bench vacuum. The product was taken to high vacuum overnight to fully dry it. The final product of deuterated D16 DGEBA was 9.79g, ∼90% of the expected yield for this second stage. The overall yield over the two steps was 57.6% based on the amount of d16 phenol used.

5.2.3 Titration to Determine Epoxide Equivalent Weight (EEW) of Epoxy

Tetraethylammonium bromide (Sigma Aldrich) (25g) was dried at 100°C for one hour. Tetraethylammonium bromide solution was produced by dissolving 25g in 100ml of glacial acetic acid (Sigma Aldrich, molarity: 17.4M, reagent grade). Crystal violet indicator was prepared by dissolving 20mg of crystal violet (Sigma Aldrich) in 20ml of glacial acetic acid. A mass of 0.1092 - 0.1683g of UC0003 was dissolved in 10ml of chloroform and solubilised using a vortex mixer. The epoxy solution was pippetted into a conical flask. Subsequently 20ml of glacial acetic acid and 10ml of tetraethylammonium bromide solution were added to the flask, which was manually swirled before 4-6 drops of crystal violet indicator were added. Perchloric acid (Sigma Aldrich, 0.1M, reagent grade) was then titrated against this solution until the solution turned a clear yellow colour. The EEW was determined using the equation:

$$EEW(\text{gmol}^{-1}) = \frac{\text{sample mass(g)}}{\text{titre } (\text{dm}^3) \times \text{perchloric acid concentration (mol dm}^{-3})} \tag{5.1}$$

This procedure was repeated twice and an average was obtained in order to determine the UC0003's EEW.

5.2.4 Cross-linked Network Preparation

All samples were made with either hydrogenous (UC0003) or deuterated epoxy, and MXDA diamine crosslinker. Samples of stoichiometries of r=1 and 0.5 were made. Due to a miscalculation and the availability of deuterated epoxy not enabling for further sample production, deuterated epoxy samples made with solvent had slightly different stoichiometries of 1.11 and 0.54. Hydrogenous samples were made with and without DMP-30. Samples cured with solvent were made for both hydrogenous and deuterated epoxies. These comprised of 60% epoxy-amine, 30% xylene and 10% butanol, by mass.

To make the samples, epoxy was first weighed into a container using a balance (AD FZ-3000iWP). This mass was subsequently used to determine the required mass of DMP-30 and MXDA. For samples with DMP-30, DMP-30 equivalent to 3% of the moles of epoxy groups of UC0003 was added via glass pipette (SLS Nottingham UK). MXDA was also added via pipette. For samples cured with solvent, the required masses for xylene and butanol was then determined before xylene and then butanol were added, both via pipette. For samples without solvent, the mixture was then stirred either by hand using a glass rod, or in a DAC 150 FVZ-K Speed Mixer (Synergy Deviced Ltd UK) at 2000rpm. Samples stirred by hand had the container opening covered in Parafilm to prevent oxidation or carbamation of the MXDA. Samples prepared without solvent were mixed for five minutes, as it was determined that this suitably mixed the constituent parts of the mix well enough to reach a maximum T_g after curing, confirmed via differential scanning calorimetry (DSC) measurements. There was negligible difference in the final T_g of non-solvent samples mixed via hand compared to those made using the Speed Mixer. Samples with solvent were mixed via hand as it was determined that the Speed Mixer did not mix the solvent, epoxy and amine adequately. Furthermore, four five-minute stirs, with fifteen-minute wait periods inbetween each

stir, followed by a final 45-minute wait were required to fully mix the epoxy, amine and solvent mixture. DSC measurements of solvent samples after cure showed that this four-stir regime with a further wait period was the minimum pre-cure stirring regime that gave consistent final T_g values, and presumeably similar degrees of cure.

Non-solvent samples were cured in PTFE moulds with an area of 24×25mm. They were poured in so that they formed a full layer on the bottom of the mould. Acetate sheets were placed on the bottom of the moulds so that the samples could easily be removed from the moulds once fully cured. Solvent samples were found to crack in these PTFE moulds and so were cured in more flexible 26×48mm silicone moulds. Samples were cured in an oven (Binder) under an ambient atmosphere at 60°C for two hours, then one hour at 100°C and finally one hour at 160°C. This initial 60°C cure would give time for the primary amines to react with the epoxy. The 160°C cure would then allow the secondary amines to react. However, if the cure went straight from 60°C to 160°C, there would be the risk of the solvents boiling off rapidly, xylene having a boiling point of 143-145°C [20] and butanol 119°C [21]. The 100°C cure therefore allowed the solvents to evaporate before the cure temperature was elevated further. It took around 25 minutes to heat from 60°C to 100°C and around 45 minutes to heat from 100°C to 160°C. Curing was also carried out in an oven under a nitrogen atmosphere, but there was little difference in the samples cured in these two environments, with negligible difference in the final T_g.

All samples were then mechanically polished down to 1mm, the required thickness for the SANS experiments. Samples were held in place with a vacuum before being machine-cut down to 1mm with a 30mm high speed steel slot drill. The tops and bottoms of samples were cut so that both sides became flat.

5.2.5 Positron Annihilation Light Spectroscopy (PALS)

The PALS measurements were carried out at the University of Sheffield using a home-built PALS instrument, this uses a 50ns fast coincidence circuit [22]. Identical samples of 1mm thickness were taped together, either side of a ^{22}Na positron source, between a pair of fast plastic scintillators and photomultiplier tubes to obtain lifetime spectra. Each lifetime spectra was collected for a minimum of one million counts, with a time resolution of 470ps.

The lifetime, T_{oPs} of the longest-living positron annihilation pathway, ortho-Positronium (oPs) is used to determine free volume void radius using the Tao-Eldrup Model:

$$\frac{1}{T_{oPs}} = 2\left[1 - \frac{R}{R+1.66} + 2\pi\sin\left(\frac{2\pi R}{R+1.66}\right)\right] \tag{5.2}$$

Where R is the void radius. From this, the free volume, FV and fractional free volume, FFV can be determined:

$$FV = \frac{4}{3}\pi R^3 \tag{5.3}$$

$$FFV = I_3 \times FV \tag{5.4}$$

Where I_3 is the relative intensity of the oPs annihilation lifetime. The PALS output data is given as a histogram of positron lifetimes. A Python code was used determine the average oPs lifetime and therefore average void size from this data [23].

5.2.6 SANS Measurements

SANS measurements were perfomed using the LARMOR beamline at the ISIS second target station (Rutherford Appleton Laboratory, Oxfordshire, UK). The incident wavelengths used spanned the range 0.5-12.5Å and gave a momentum transfer (Q range) from 0.003-0.7Å^{-1}, giving information on lengthscales of 9Å-2000Å. A narrow polydispersity hydrogenous/deuterated polymer blend sample was used as a standard to provide accurate Q calibration and allow the data to be put on an absolute scale. Samples were loaded into the automated samples positioning stage with temperature control. Two measurements were taken for each sample: one of the SANS scattering and one to measure the transmission.

Samples were immersed in the water or methanol (Sigma Aldrich Co Ltd (Dorset, UK)). before SANS measurements were taken. In order to provide maximum scattering contrast between solvent and sample, hydrogenous samples were immersed in deuterated water or methanol, and deuterated samples were immersed in the hydrogenous equivalent. Immersion was carried out at 60°C to accelerate uptake, given that SANS measurements only took place over three days. Sample masses were taken before and after immersion to determine % solvent uptake. Samples were weighed in the morning, afternoon and evening of each day until there was no further mass increase, indicating that the solvent uptake had saturated. The sample surfaces were mopped dry with precision wipes to remove excess surface solvent droplets. For SANS measurements, the samples were then wrapped in aluminium foil to reduce solvent loss. Samples were then remounted, and again the SANS and the transmission were measured for each sample. In some instances both water and methanol were measured for the same sample, if this was the case the measurements were performed first using water then methanol, as methanol is a much better solvent for our networks than water. Samples were then dried at 50°C before being immersed in water.

A background measurement was taken using an empty beam with just aluminium foil. The results were plotted with the background subtracted from each measurement as the SANS intensity versus momentum transfer. All the samples were of similar thickness (∼1mm), however the actual measured thickness was determined for each individual sample using a micrometer and inputted into the data processing pipeline.

Examining the SANS data we first began by splitting the Q range into three sections. The low-Q range gave information on the Porod regime, which we ascribe to the presence of large length scales most likely due to the presence of what has previously been termed clustering phenomena [24]. The middle-Q range gives information on the 'correlation length' or 'mesh size,' ξ, the average distance between neighbouring chains in a polymer [25]. It is the radius of a volume below which, intramolecular forces

dominate and above which, intermolecular forces dominate [26]. For a crosslinked network specifically, it is the spacing between crosslinks [27]. This gives information on the crosslinked polymer network. The high-Q range probes length scales smaller than polymer chains and we ascribe this to the repeat distance linking the epoxy and amine network subunits, giving information on the monomers in the polymer network.

5.3 Results

Examples of SANS data for the four formulations (hydrogenous epoxy cured with and without solvent, and deuterated epoxy cured with and without solvent) are shown on figure 5.2. Results are shown for dry samples and after immersion in water and methanol, except for deuterated epoxy cured without solvent which had no samples immersed in methanol. The three different Q ranges examined can be seen in these results, marked out by the vertical lines: low-Q, which showed the increase in intensity, the Q range before the lines labelled with the subscript 1; mid-Q, which showed differences for samples when dry and immersed in water and methanol, the Q range inbetween the lines labelled with the subscripts 1 and 2; and high-Q, which featured a peak in deuterated epoxy samples, the Q range after the lines labeled with the subscript 2. d, w and m refer to dry, immersed in water and immersed in methanol data sets, respectively.

Figure 5.2 shows that there was a change in the scattering patterns after immersion in solvents only for samples cured with processing solvent. It is believed that phase separation occurs for epoxy-amines cured with solvent, with separate domains forming of epoxy-amine and of the solvents. During the curing process, the solvents evaporated, leaving behind empty voids into which the solvents could enter, and in the case of methanol, swell the network. Furthermore, for the deuterated sample cured in solvent, there was a clear difference in the scattering patterns for immersion in water and methanol. For water, there was only a change at the lower Q range, whereas for methanol, there was an intensity change across the entire Q range. This was due to methanol being able to swell the network, allowing it to access all length scales in our measured Q range. Water is a weaker swelling agent than methanol and so could not swell the network, meaning it could not access the smaller free volumes that methanol can. Thus, water only changed scattering intensity over a restricted Q range, predominantly the lower Q range.

For deuterated epoxy samples cured with solvent, there was an increase in intensity when immersed in hydrogenous solvents. For hydrogenous epoxy samples cured with solvent, immersion in deuterated solvents had the opposite effect, lowering the intensity. This was due to the difference in the scattering length densities (SLD) of deuterated and hydrogenous solvents. Calculated SLD values are shown in table 5.1.

Solvent	Scattering Length Density (10^{-6}Å^{-2})
Cured DGEBA:MXDA	1.30
Cured Deuterated DGEBA:MXDA	3.31
DER331	3.30
H_2O	-0.56
CH_3OH	-0.37
D_2O	6.37
CD_3OD	5.80

Table 5.1: Table showing scattering length densities for the cured epoxy-amines, the epoxy and hydrogenous and deuterated water and methanol. Values determined for neutron wavelengths from 0.9-13Å[28].

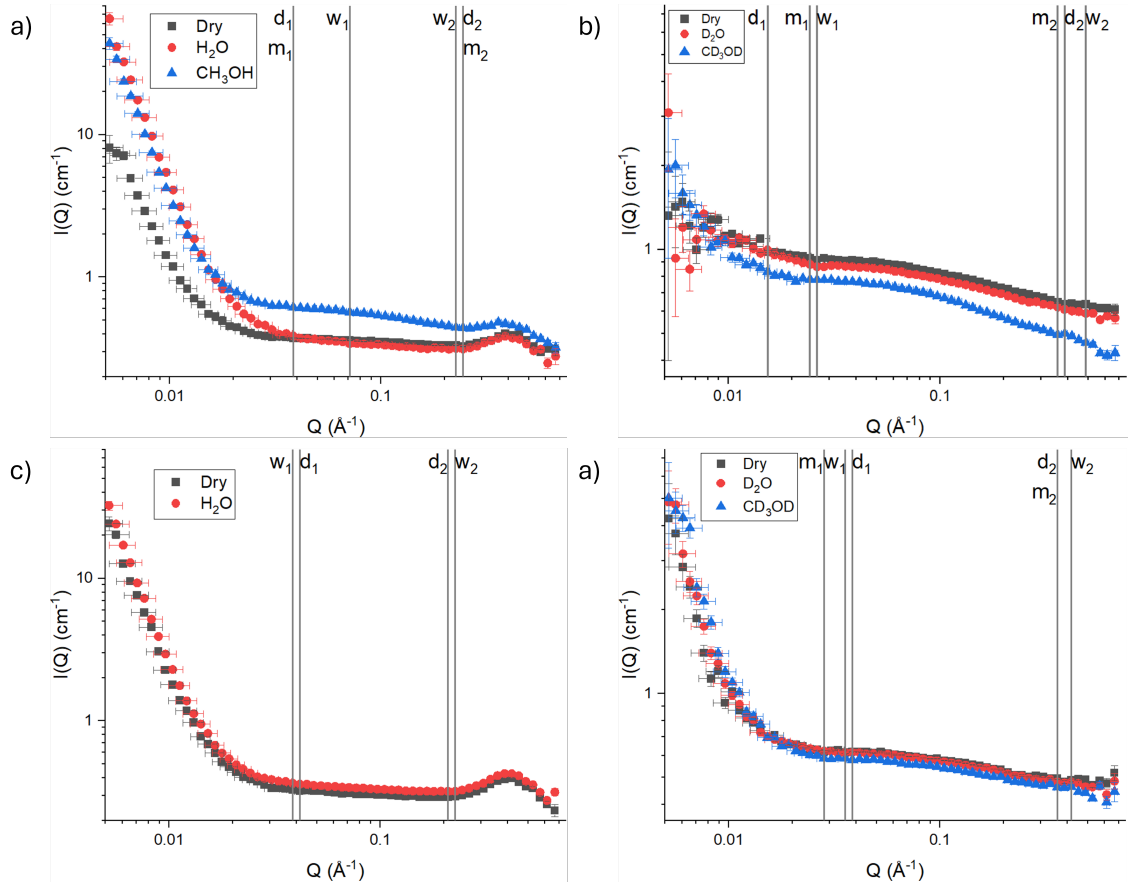

Figure 5.2: SANS results for epoxy-amines before and after immersion in solvent. a) shows r=1.11, cured with deuterated epoxy and solvents. b) shows r=1, cured with hydrogenous epoxy and solvent. c) shows r=1, cured with deuterated epoxy and no solvent. d) shows r=1 cured with hydrogenous epoxy and no solvent. Scattering patterns are shown for the dry sample (black squares), after immersion in water (red circles) and after immersion in methanol (blue triangles). Note the scale of the y-axes is different for the deuterated samples, a) and c) compared to the hydrogenous samples, b) and d). The vertical lines indicate the separate Q ranges, used for different fits. d, w and m refer to the data sets for dry samples, those immersed in water and those immersed in methanol, repectively. The subscript 1 indicates the end of the low-Q range and the start of the mid-Q range. The subscript 2 indicates the end of the mid-Q range and the start of the high-Q range. Error in Q arises from uncertainty in distance between sample and detector. Error in intensity arises from counting statistics.

5.3.1 Low-Q fitting

The SANS results at low-Q were fitted using using a correlation length model. This gives the intensity of the resultant SANS signal as:

$$I(Q) = \frac{A}{Q^n} + \frac{C}{1 + (Q\xi)^m} + \text{background} \tag{5.5}$$

The first part of the equation describes the Porod scattering from clusters and larger network heterogeneities. n is the Porod exponent, describing the overall network homogeneity, and A is its scaling factor. The second term is a Lorentzian function that describes scattering from the polymer mesh. m is the Lorentzian exponent, detailing polymer-solvent interactions, ξ is the correlation length, and C is its associated scaling factor [24]. Fittings were carried out using the fitting software SasView. Example fits are shown for a deuterated and hydrogenous dry samples of r=1, cured with solvents, in figure 5.3. Note on figure 5.3a) that the fit does not cover the low-Q peak, as this affected the quality of the fit and is does not cover the area of interest for the fit. For hydrogenous samples, fits were generally good. Reduced χ^2 values ranged between 0.7 and 2.4. For deuterated samples, 13 of the 17 fits had reduced χ^2 values between 0.7 and 1.8. r=0.54 S, dry and immersed in methanol displayed reduced χ^2 values of 4.1744 and 10.543, respectively. r=0.54 S and r=0.5 NS, both immersed in water, displayed reduced χ^2 values of 40.899 and 43.971, respectively.

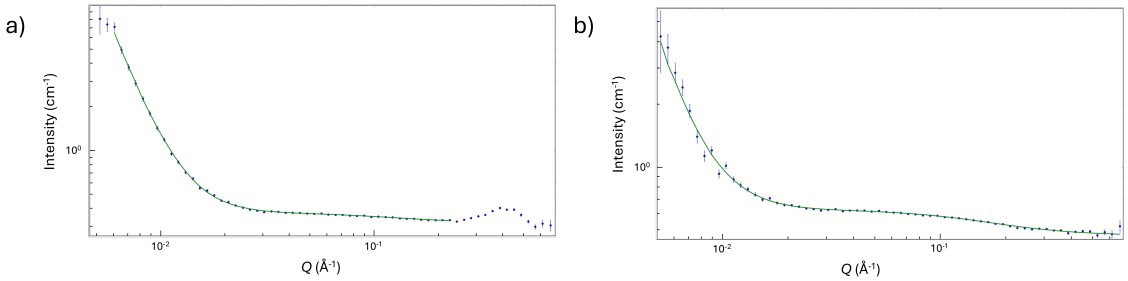

Figure 5.3: Low-Q fits used to determine the Porod exponent and scale, and the correlation length of dry samples of r=1, cured with solvents, using the fitting software SasView. a) shows the results and fit for a sample with deuterated epoxy. b) shows the results and fit for a sample with hydrogenous epoxy.

Using equation 5.5, the Porod exponent and Porod scales of the samples were determined. The Porod exponent results are shown in figures 5.4 and 5.5 for hydrogenous and deuterated samples, respectively. Porod scale results are shown in figures 5.6 and 5.7. As there were a greater range of formulations made with hydrogenous epoxy samples, these results are shown split three graphs: dry, after immersion in water and after immersion in methanol. The greater number of samples using hydrogenous epoxy meant it was clearer to determine any trends from the hydrogenous results rather than the deuterated. The Porod exponent for the dry samples, shown in figure 5.4a) was measured to be between 3 and 4, indicating a more solid, smooth structure. Non-solvent samples are composed purely of epoxy-amine chains, homogeneous throughout

on this lengthscale. The Porod scale of these dry non-solvent samples was also low. It is believed that due to the homogeneous nature of these samples their characteristic length scale would cover the entire sample, too large to appear on these SANS measurements. They therefore had a minimum Porod scale, and a Porod exponent that showed them to be completely smooth. The solvent samples had a lower Porod exponent, between 2 and 3. This points towards a less solid, coiled structure. This is believed to come from the separation of solvent and epoxy-amine during cure, forming separate areas of high concentration of solvent and epoxy-amine. The solvent evaporates during cure, leaving behind 'voids,' creating an inhomogeneous network of polymer chains and voids. The solvent samples thus had a less-solid structure than their counterparts cured without solvents. The size of these voids is shown by the Porod scale, being between 10^{-5} and 10^{-7}.

There was little change in Porod exponent and scale in non-solvent samples when immersed in water or methanol, as shown in figures 5.4b) and c), 5.5, 5.6 b) and c), and 5.7. These homogeneous samples take up little solvent, and thus there was little change in their SANS signals in this Q range. Solvent samples did show a change in their Porod exponent and scale, with the Porod exponent increasing after immersion in water and then increasing further after immersion in methanol to have a similar value to that of the non-solvent samples. The Porod scale showed a similar trend, decreasing for solvent samples upon immersion in water and then further again after immersion in methanol, to be similar to that of non-solvent samples. In solvent samples, water and methanol can enter the empty voids and swell them. These voids therefore increase in size, reducing the Porod scale. Due to being able to form non-polar bonds with the network as well as hydrogen bonds, methanol is a much better solvent for the network than water. Methanol can therefore swell the network when it enters voids, increasing the size of these voids, so much so that these voids were too large to be measured by this SANS setup. These samples therefore appeared completely homogeneous, and so had a similar Porod exponent and scale to that of the homogeneous non-solvent samples. Water swelled the voids in solvent samples to a size that could still be measured. This increase in void size is shown by a decrease in the Porod scale. The increase in the Porod exponent upon immersion in water is unexpected. This increase indicates a clearer divide between network and void. It was expected that this divide should be made less-clear, as chain ends should be attracted to the water in the voids, forming hydrogen bonds with it, and so extend into the voids. At the moment we are unsure of why the Porod exponent in solvent samples increased upon immersion in water.

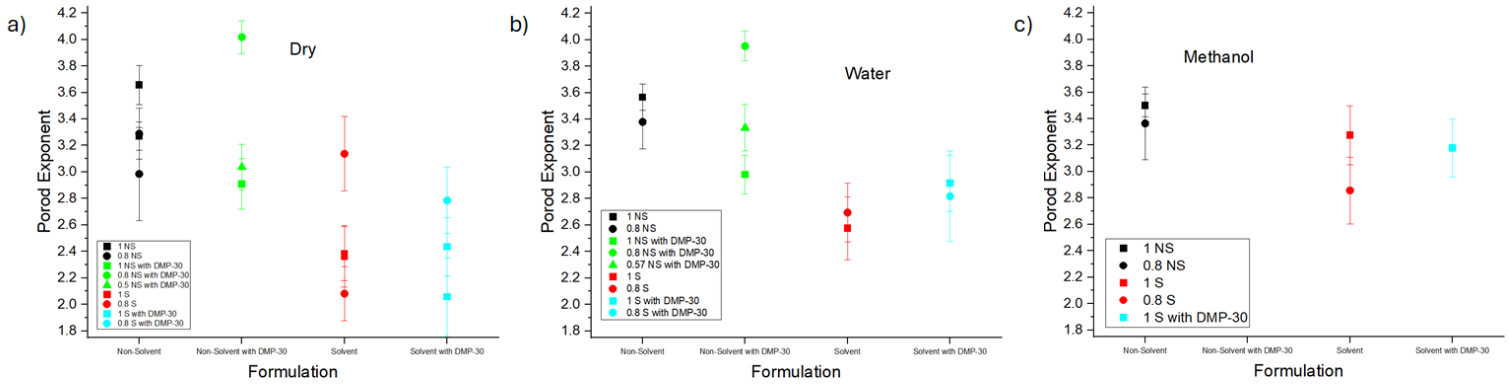

Figure 5.4: Porod exponent values of epoxy-amines using hydrogenous epoxy for a) dry samples, b) those immersed in water and c) those immersed in methanol. Error arises from fitting errors.

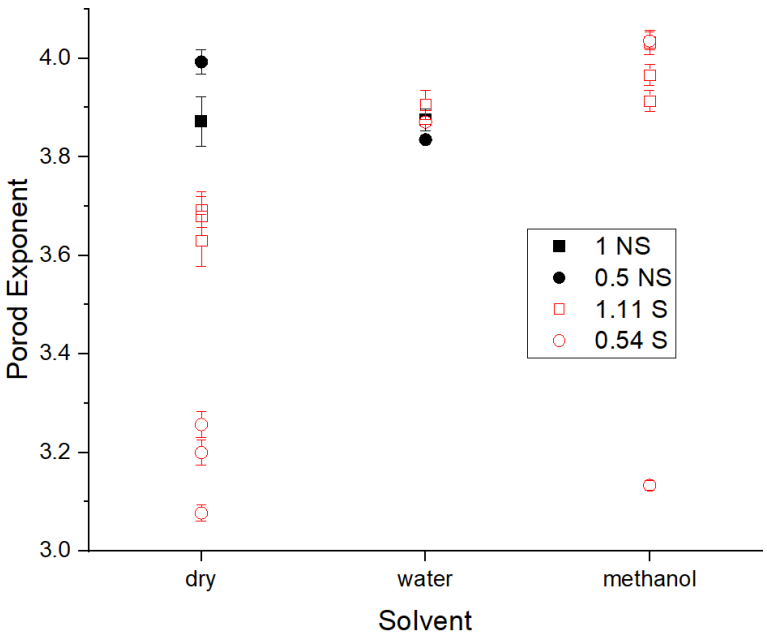

Figure 5.5: Porod exponent values of epoxy-amines using deuterated epoxy. Error arises from fitting errors.

It was more difficult to determine whether stoichiometry had an impact on the Porod scale. Looking at the deuterated results in figure 5.7, it would appear that a drop in stoichiometry from 1 resulted in a greater Porod scale, with stoichiometry having a greater impact than whether the sample was cured with solvents or not. However, given that there are far fewer results than the hydrogenous set, and that there appeared to be a few outliers that go against this trend, this conclusion cannot be stated with confidence.

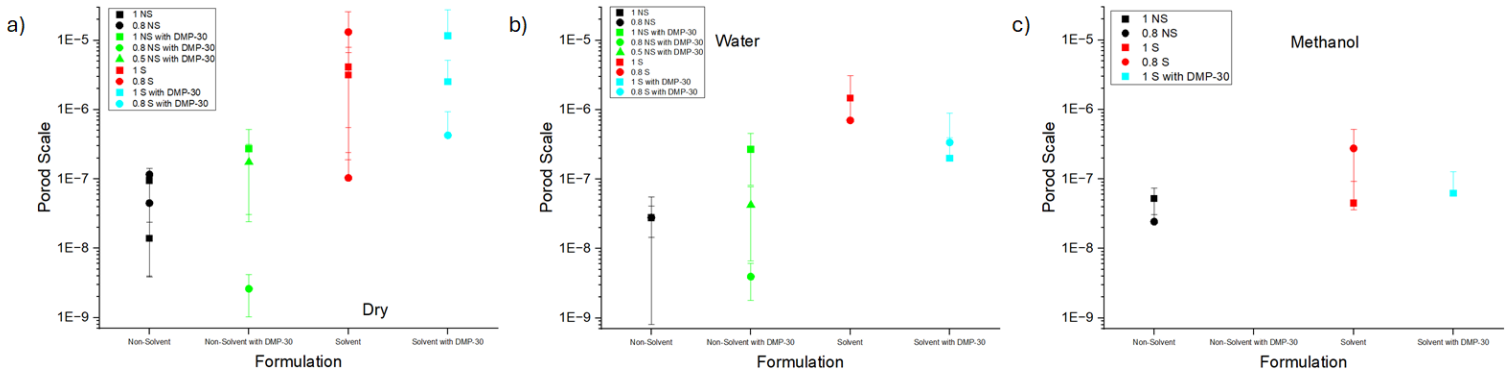

Figure 5.6: The Porod scales of epoxy-amines using hydrogenous epoxy. a) shows Porod scales for dry samples, b) from samples immersed in water and c) from those immersed in methanol. Errors arise from fitting errors.

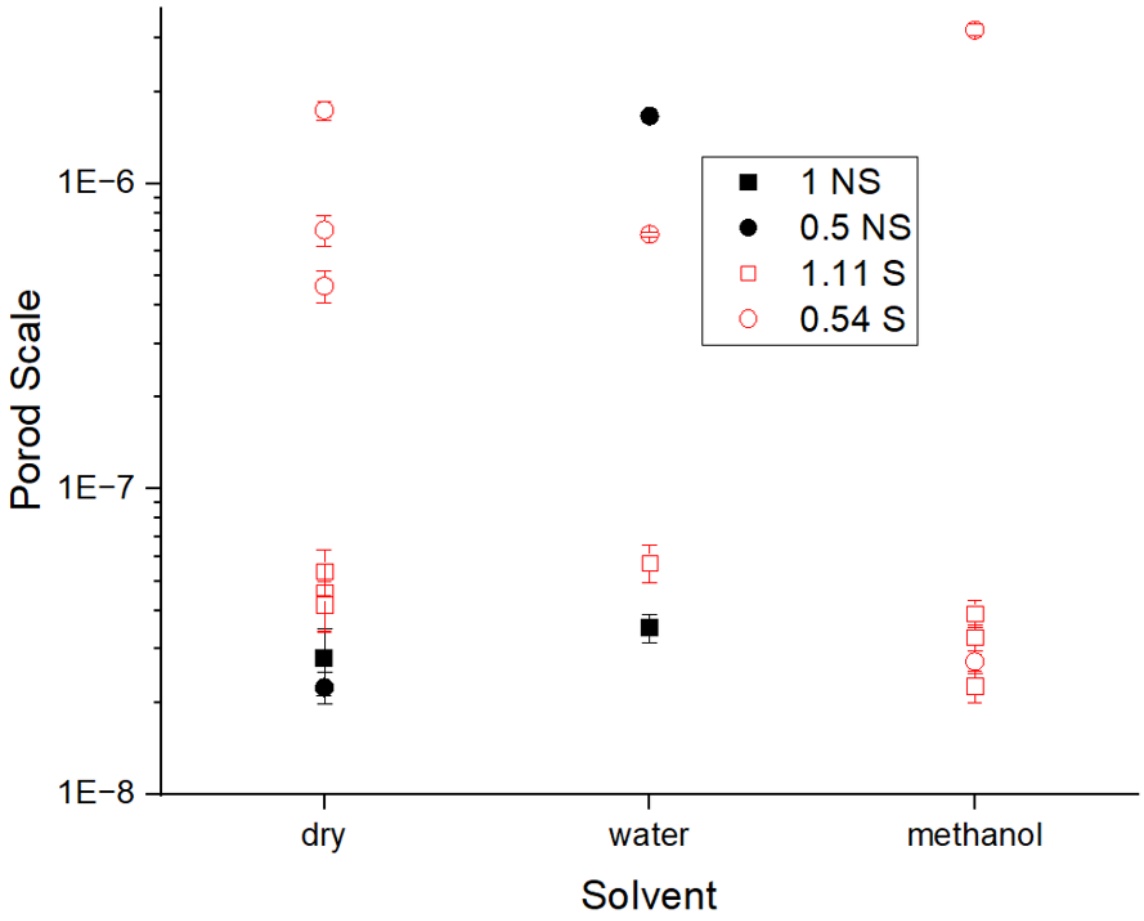

Figure 5.7: The Porod scales of epoxy-amines using deuterated epoxy. Error arises from fitting errors.

5.3.2 Correlation Length

The correlation length, ξ, was determined for both the deuterated and hydrogeneous epoxy samples using equation 5.5. The fitted correlation lengths for hydrogenous and deuterated samples are shown in figures 5.8 and 5.9.

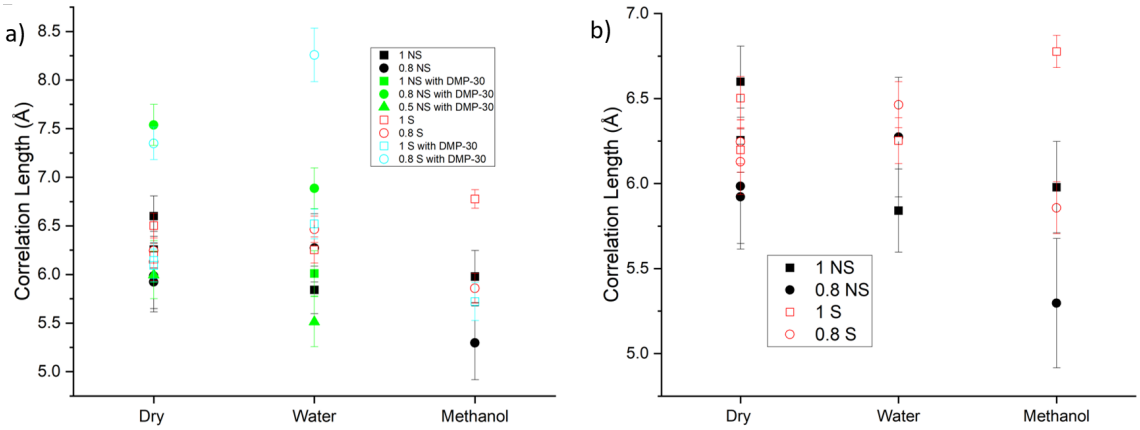

Figure 5.8: Graph showing correlation length results for a) all hydrogenous samples and b) hydrogenous samples without DMP-30. Samples cured without solvents are shown in black when cured without DMP-30, and green when with. Samples cured with solvents are shown in hollow shapes of red when cured without DMP-30 and of blue when with. Stoichiometries of 1 are displayed with squares, of 0.8 with circles and of 0.5 with triangles. Error arises from fitting errors.

There appeared to be little difference in correlation length with changing stoichiometry or when curing with solvents. These formulations all exhibited a correlation length between 4.9 and 6.9 Å. It is unclear whether the addition of DMP-30 affected the correlation length. It is understandable that stoichiometry and processing solvents would not have an impact on correlation length: these should only have had an impact on the overall size of the network, not on the actual distance between polymer chains. There were a couple of results from samples cured with DMP-30 with a correlation length above 7Å. These appear to have been anomalous, given other results for samples with DMP-30, of varying stoichiometry with and without solvent, that showed similar correlation lengths to those without DMP-30. With these anomalous values removed, there appeared to be little difference in correlation length with the addition of DMP-30. This makes sense: the homopolymerized network should be of a similar structure to the polymerized epoxy-amine network.

There appeared to be little change in the correlation length upon immersion in water or methanol, with all results lying within a similar range for all formulations. This appeared to be the case for samples immersed in water, but for samples with methanol it was harder to ascertain given the range of values from fewer results. There was however a large error in the correlation length results. This made it difficult to properly compare how solvent uptake affected the correlation length for our coatings of different formulations.

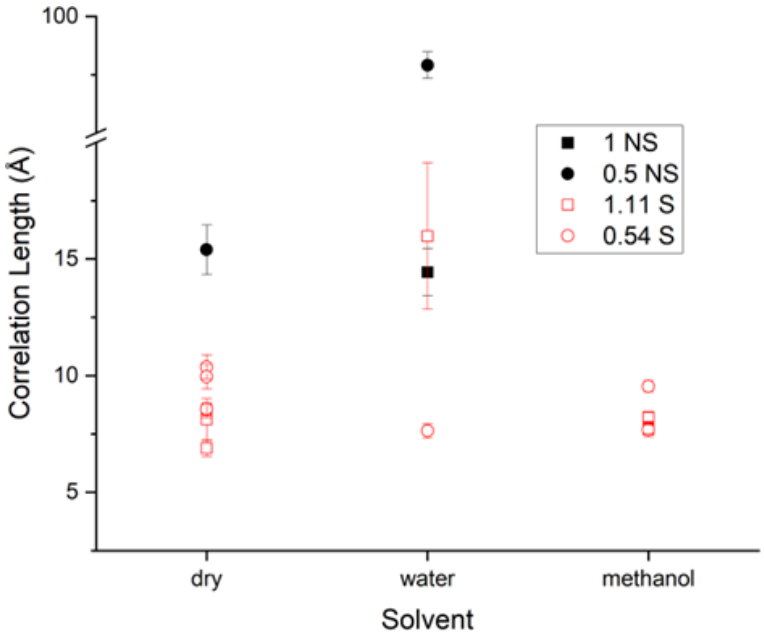

Figure 5.9: Graph showing correlation length results for deuterated samples. Samples cured without solvents are represented by black symbols and those cured with solvents as red symbols. Stoichiometries of 1 (non-solvent) and 1.11 (solvent) are represented by squares. Stoichiometries of 0.5 (non-solvent) and 1.11 (solvent) are represented by circles.

Deuterated samples showed a larger correlation length than the hydrogenous samples, with dry samples having correlation lengths ranging from 6.5 to 18.1Å. They also showed greater variation. It is difficult to compare changes in correlation length with stoichiometry or when curing with solvents due to the lack of results with deuterated samples. This increase in variation may have arisen from the peak in deuterated samples at q ~0.4Å^{-1} making fitting more difficult as it approaches lower Q. The majority of results have correlation lengths between 6 and 11 Å, similar to that of the hydrogenous samples. It could be the case then that deuterated samples were of of similar correlation length to the hydrogenous samples. Overall, it still appeared that there was little change in correlation length upon swelling deuterated samples in water and methanol.

5.3.3 Mid-Q Intensity

The average mid-Q regime scattering intensity of each sample was measured. The results are shown in figure 5.10. The low-Q limit of this regime was determined as when the intensity clearly started to increase. The high-Q limit was determined by when the intensity started to flatten off. Both of these limits were determined by eye.

These two boundaries are shown as the Q-range between the lines with subscripts 1 and 2, as shown in figure 5.2.

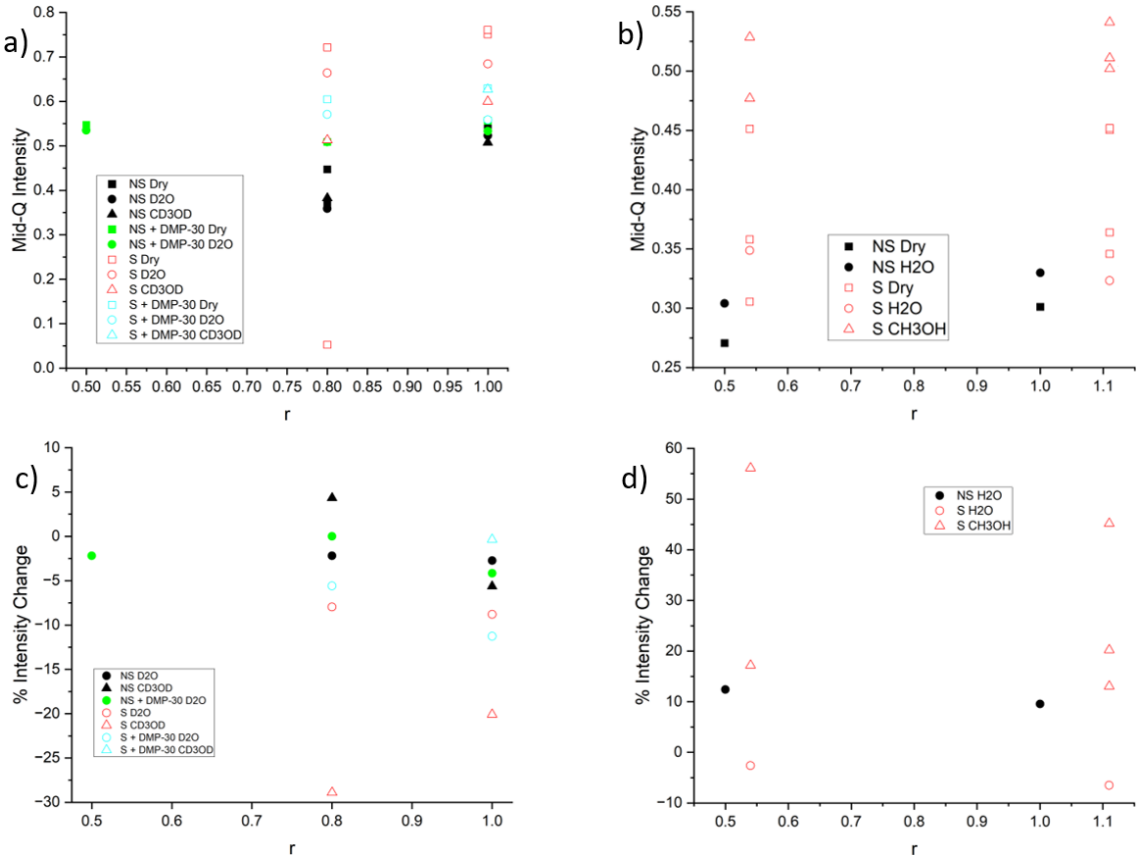

Figure 5.10: Results showing the mid-Q intensities of a) hydrogenous epoxy samples and b) deuterated epoxy samples. The change in intensity upon immersion in solvent is shown in c) for hydrogenous samples and d) for deuterated samples. For samples without DMP-30, non-solvent samples are shown in black and solvent samples are shown in red. With DMP-30, non-solvent samples are shown in green and solvent samples are shown in light blue. Dry samples are shown as squares, those immersed in water as circles and those in methanol as triangles.

As seen on figures 5.10 a) and b), there was a greater intensity for formulations cured with solvents compared to their counterparts cured without solvents. As stated before, it is believed that this increased intensity came from the contrast between high and low crosslink density regions that form when cured with solvents. From these mid-Q intensity results, it appears that these domains are of a size that they scatter neutrons in this mid-Q range. Without solvents present during curing, these domains do not form. There was therefore little scattering in the mid-Q range for the more homogeneous non-solvent samples.

As seen in figures 5.2 and 5.10 c) and d), there was little change in scattering intensity in samples without solvent when immersed in solvent. In samples cured with solvent there was little change with the addition of water, although there is a clear change with the addition of methanol. This further supports the idea of separate domains of solvent and epoxy-amine in formulations cured with solvent. Methanol could get into these now-vacant solvent domains and swell them, increasing the scattering intensity in this mid-Q regime. There was little swelling in non-solvent samples as these separate domains do not exist for methanol to fill. When deuterated methanol was added to hydrogenous epoxy samples with solvent, it lowered the intensity. This was the opposite case for when hydrogenous methanol was added to deuterated epoxy samples with solvent. This was due to the difference in scattering length density in deuterated methanol compared to that of hydrogenous methanol, as shown in table 5.1.
Figure 5.10a) shows that for non-solvent samples without DMP-30, there was a clear drop in intensity with lowered stoichiometry. This relationship could also be seen for the solvent samples in figure 5.10a) and the deuterated non-solvent samples in figure 5.10b). It was less clear in the deuterated solvent samples in figure 5.10b). As stoichiometry is reduced from r=1, there is less amine, resulting in greater levels of unreacted epoxy after curing. This epoxy effectively acts as noise in the SANS signal, thus reducing the signal intensity . When DMP-30 was added, this drop in intensity when r drops below 1 was not seen. This was due to the excess epoxy homopolymerizing in the presence of DMP-30, thus reducing noise from excess epoxy.

Samples cured with solvents showed a reduction in intensity in the mid-Q regime when cured with DMP-30. This may have been due to DMP-30 acting as a catalyst for the epoxy-amine reaction [29] [30] [31], thus allowing for greater conversion before the solvents and epoxy-amines split into separate domains. There could therefore possibly be a reduction in the number of domains of the size that increases scattering in this regime. This is however hard to state with confidence as there are too-few results comparing formulations with and without DMP-30 to make these arguments concrete.

5.3.4 Network Spacing: Peak at $\sim 0.4\text{Å}^{-1}$

The scattering patterns of the deuterated samples, shown in in figures 5.2a) and c), showed a peak at $\sim$0.4Å^{-1}. This peak was in a similar Q position for formulations cured with and without solvent. A peak at this position had been observed before in x-ray scattering results of epoxy-amines by Lovell and Windle [12]. Here, they surmised that this peak arose due to the spacing between epoxy molecules, separated by the amine they are bonded to. This would agree with the fact that we are only seeing this with deuterated epoxy samples. With deuterated epoxy and hydrogenous amine, there is sufficient enough neutron scattering length density contrast between the two for there to be a measurable signal in our results. With hydrogenous epoxy, there is very little neutron scattering length density contrast between the epoxy and the amine, and therefore no peak is seen. Using the scattering fitting software, SasView, a Gaussian curve was fitted to each scattering result for deuterated epoxy samples, using

the model:

$$I(Q) = (\text{scale}) \cdot \exp\left[-\frac{(Q-Q_0)^2}{2\sigma^2}\right] + \text{background} \tag{5.6}$$

Where $I(Q)$ refers to the intensity of the signal, Q_0 is the Q value on which the peak is centered and σ is the standard deviation [32]. 18 measurements, 13 produced reduced χ^2 values between 0.5 and 1.5. The 3 dry r=0.54 S samples produced reduced χ^2 values of 0.26793, 0.37549 and 0.46486. The r=0.54 S sample, immersed in water, produced a reduced χ^2 value of 0.32787. One of the r=1.11 S samples immersed in methanol produced a reduced χ^2 value of 2.6343.

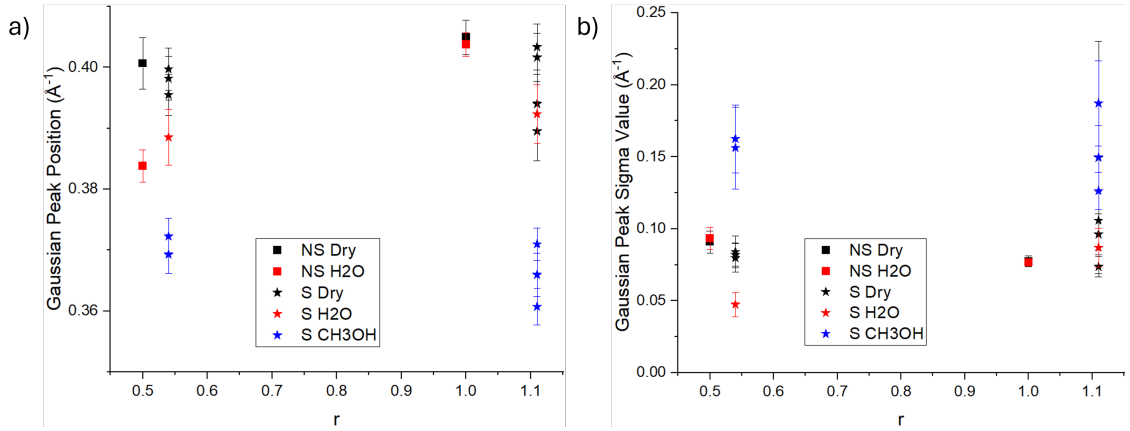

Figure 5.11: Gaussian curve peak position for the peak measured at Q ~0.4Å^{-1} for deuterated epoxy samples. The position of the curve's peak is shown in a) and the width of the peak is shown in b). Samples cured without solvent are shown as squares, samples cured with solvents are shown as stars. Dry samples are black, samples immersed in water are red and samples immersed in methanol are blue. As these samples used deuterated epoxy, the solvents used were hydrogenous.

Figure 5.11 shows similar peak positions and widths for both dry samples and those immersed in water. This was true for samples cured with and without solvents. However, when methanol was added to solvent samples, there was a clear shift in the peak position to a lower Q value. There appeared also to be an increase in the width of these peaks. These results are comparable to those seen in figure 5.2. Methanol swelled the samples cured with solvents, increasing the distance between epoxy molecules, thus reducing the Q value of this high-Q peak. Here, it would be swelling of the actual epoxy-amine domains. Although there were no results for deuterated epoxy samples cured without solvent and then immersed in methanol, it can be expected that there would be little change, as there would be little swelling in these samples. It would be expected that if the spacing between epoxy monomers increases, then so too should the mesh size of the network. However, as previously discussed, there was no change in correlation length in solvent samples after immersion in methanol, shown in figure 5.9. It is believed that there was a change in correlation length, but it was too small to notice, given the size of error in these results. This is compounded by the large

error values given for the correlation length. Of note also is that Lovell and Windle measured a change in the Q value of this peak with the formulation's stoichiometry. Between r=1 and 0.5, a change in Q of 0.1 was seen for samples cured without solvents. This was not clear on our results. Our results however do agree with our model of the epoxy-amine network. There should be little change in network structure between non-solvent samples of different r and so little change in this low-Q peak.

It is of some interest that the spacing between the epoxy groups of the deuterated samples is greater than their correlation lengths. Figure 5.9 gives the majority of correlation lengths as being between 6.5 and 11Å. Correlation length in a crosslinked polymer is conventionally defined as the spacing between crosslinks. It therefore is unclear why the correlation length is less than the value of this high-Q peak, which should be the spacing betwen monomers, which should also be the spacing between crosslinks.

5.3.5 PALS

PALS experiments were carried out on samples cured with and without solvent, both with and without DMP-30 as well as samples made up using UC0003 and DMP-30, without MXDA. The results, as shown in figure 5.12, give information on how well-packed the epoxy-amine network is. Three measurements were taken per sample. These PALS measurements produced free volume measurements in the range of 60-120Å^3, or diameters of ∼5-6Å, smaller length scales than the SANS setup could measure (a minimum of ∼ 9Å).

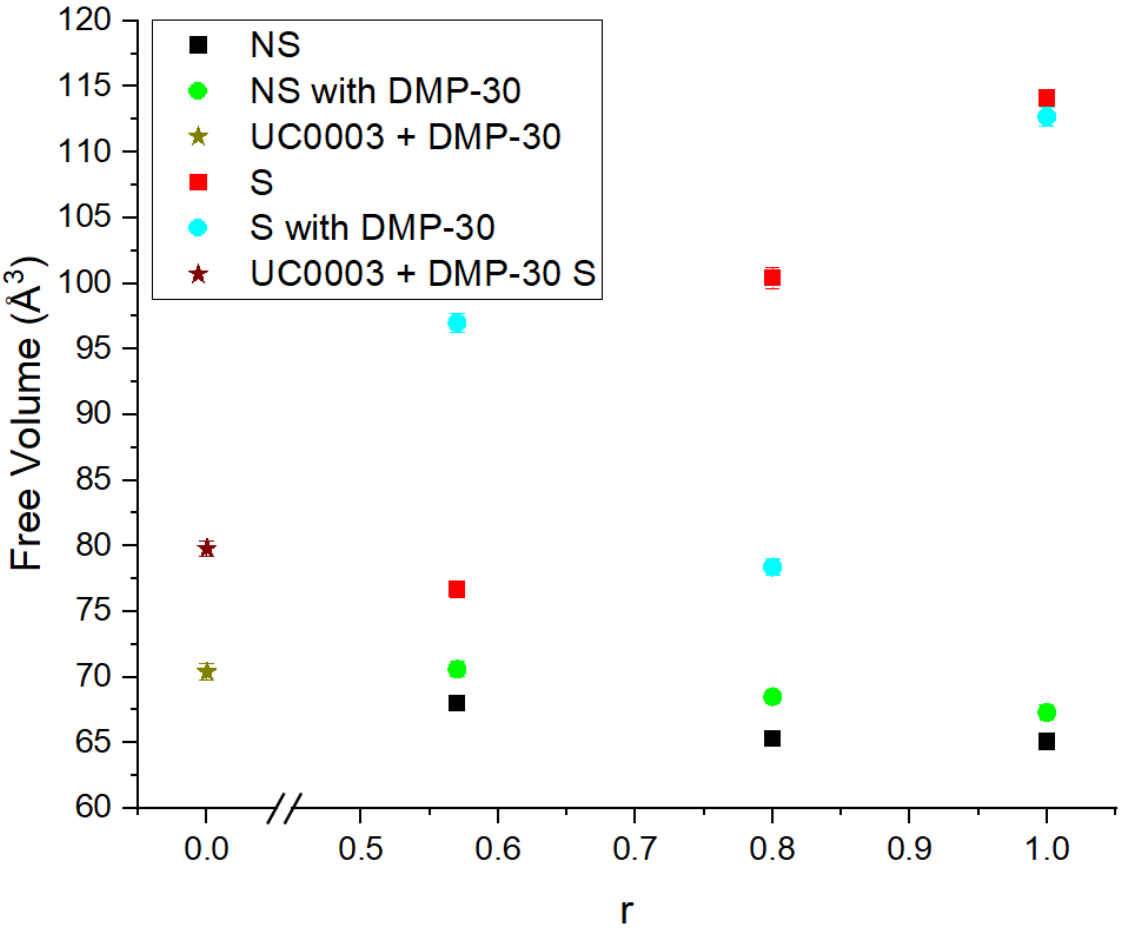

Figure 5.12: PALS measurements of epoxy amines cured with and without solvents, both with and without DMP-30 as well as just epoxy and DMP-30.

Formulations cured with solvent had greater free volume sizes than those cured without. Non-solvent samples displayed free volume sizes of 65-71Å^3 (radii of 2.5-2.6Å). For comparison, water has a radius of ∼1.35Å[33] and methanol ∼1.8Å[34]. Non-solvent samples cured with DMP-30 displayed slightly greater free volume sizes than their counterparts cured without. The free volumes in solvent samples decrease from 114Å^3 (radius of 3.0Å) for r=1 to 77Å^3 (radius of 2.6Å) for r=0.57. It appears therefore that heterogeneities in solvent samples exist on Angstrom lengthscale. It would appear also that these heterogeneities decrease in size as stoichiometry decreases in solvent samples.

5.4 Conclusions

The network structure of crosslinked epoxy-amine resins cured with and without solvent was studied via small-angle neutron scattering (SANS). This was done for samples made with deuterated epoxy to provide contrast between the epoxy and amine. Samples were also made with hydrogenous epoxy. Samples had their scattering profiles

measured when dry and after immersion in water and subsequently methanol, in order to measure their network nanostructures and the effect of solvent swelling upon it. We postulate that samples cured with a processing solvent contain 'voids' that are formed during the curing process via phase separation of solvent and epoxy-amine. Voids subsequently appear as the solvent evaporates. Solvent molecules such as water and methanol can enter these voids, potentially swelling the network. Changes to the measured scattering patterns arose in the solvent-cured samples after immersion in water and methanol. There was little to no change in the measured SANS scattering in samples cured without solvents after their immersion in solvent, further supporting this hypothesis of void formation when curing with solvents.

To enable simplification of the conclusions the SANS data for the measured Q range was broken into three regions: low-Q, the region featuring the Porod slope and relating to large-scale network feautures; high-Q, featuring the peak seen in samples with deuterated epoxy and relating to spacing between monomers; and middle-Q, the region in-between concerning correlation length, the average spacing of polymer chains.

At low-Q, the non-solvent samples all displayed Porod exponents close to 4. This would indicate that any features on this lengthscale are perfectly smooth. This supports the assertion that non-solvent epoxy-amines are homogeneous. This is supported by the low Porod-scales: the actual length-scales of the networks were too big to be measured with our SANS Q range. This caused the SANS results that would make the features in this lengthscale appear smooth. In the solvent-cured samples, the interface between void and network was not perfectly smooth, producing a Porod exponent of ($\sim$2-3), below that of the non-solvent samples. The reduced value of the Porod exponent in solvent samples was attributed to the rough boundary between polymer network and void. It would not be a clean, immediate transition between the two but rather a gradual drop-off in the density of polymer chains. The size of these voids can be seen by the Porod scale, of 10^{-7} to 10^{-5}. Immersion in water increased the Porod exponent and decreased the Porod scale. The Porod exponent was believed to decrease due to water entering the voids, swelling them. The increase in Porod exponent was unexpected: we would expect the interface between the void and network to become less clear, resulting in a lower Porod exponent, due to hydrogen bonds forming between chain ends and water. Swelling solvent samples in methanol reduced the Porod scale and raised the Porod exponent further, so that solvent and non-solvent samples had the same Porod exponent results and scale results. As methanol is a better solvent and therefore swelling agent than water, it is believed that the voids present in solvent samples had swollen completely beyond the range of our SANS measurements. Solvent samples therefore appear as smooth and homogeneous as the non-solvent samples. Little difference was seen between formulation of different stoichiometry or those cured with or without DMP-30.

For the mid-Q region, correlation length was found to be $\sim$7Å for all formulations, regardless of their stoichiometry, whether they were cured with solvents or not, or

whether they were dry, or had been immersed in water or methanol. This showed that the mesh size of the epoxy-amine network remained similar for all coatings used, regardless of these factors. The SANS scattering signal intensity of solvent samples was measured to be greater than their non-solvent counterparts. We attribute this again to voids, this time of smaller size. Upon immersion in solvent, there was little change in this mid-Q intensity in non-solvent samples. Furthermore, methanol produces a change in the mid-Q intensity in solvent-cured samples but water did not. Methanol is a better solvent than water for the crosslinked network and so swelled the network, and as such could enter these smaller domains, changing the contrast in domains as they go from air-network to methanol-network. Intensity was seen to decrease for hydrogenous non-solvent and solvent samples when cured with excess epoxy. This was most likely due to the excess epoxy remaining uncured and effectively acting as 'noise' in the scattering results. Curing with the catalyst DMP-30 results in similar intensities regardless of stoichiometric ratio as the excess epoxy is instead homopolymerized.

At high-Q, there was an obvious peak at $Q \sim 0.4\text{Å}^{-1}$ for samples made with deuterated epoxy. This has been seen before [12], and was due to scattering between the deuterated phenol peak on the epoxy and the hydrogenous amine, effectively showing the distance between neighbouring epoxy molecules. This peak was not seen when using hydrogenous epoxy as there would have been little effective neutron scattering contrast between epoxy and amine. The position and width of this peak was similar for dry non-solvent and solvent-cured samples, again showing that the appearance of any voids did not actually affect the epoxy-amine network structure spacing. The height of the peak did differ (qualitatively). We presume this is correlated to the number density of neighbouring epoxy-amine units, with the non-solvent being greater in magnitude. The peak position decreased in Q for solvent-cured samples when they were immersed in methanol, indicating that the spacing between epoxy molecules increased. Methanol therefore swells the actual building blocks of the epoxy-amine network. This swelling may not be seen in the correlation length results due to those measurements being less precise, as there is possibly a distribution of mesh sizes, making it harder to see clear trends. This change in peak position and width was not seen for samples immersed in water. This was attributed to water being a weaker swelling agent for epoxy-amines than methanol. Water was unable to swell the network meaning it could not access free volumes in between polymer chains. It is unclear why the spacing of epoxy monomers is of greater size than the correlation length, for the same epoxy-amine formulation.

Our conclusions are affected by the Q-range of the SANS measurements. It is difficult to state that apparent voids in solvent-cured samples swell to greater length scales when immersed in methanol without being able to go to lower Q values to confirm this. A great range of results with high error values meant that more subtle differences due to formulation changes may have been missed. This is especially true for the results for samples made with deuterated epoxy, which featured fewer measurements.

Bibliography

[1] E. Duemichen et al. "Analyzing the network formation and curing kinetics of epoxy resins by in situ near-infrared measurements with variable heating rates". In: *Thermochimica Acta* 616 (2015), 49–60. DOI: 10.1016/j.tca.2015.08.008.

[2] T. Nguyen, J. B. Hubbard, and J. M. Pommersheim. "Unified model for the degradation of organic coatings on steel in a neutral electrolyte". In: *JCT, Journal of Coatings Technology* 68.855 (1996), 45–56.

[3] C. M. Sahagun and S. E. Morgan. "Thermal Control of Nanostructure and Molecular Network Development in Epoxy-Amine Thermosets". In: *ACS Applied Materials and Interfaces* 4.2 (2000), pp. 564–572. DOI: 10.1021/am201515y.

[4] S. Morsch et al. "Mapping water uptake in organic coatings using AFM-IR". In: *Faraday Discussions* 180 (2015), pp. 527–542.

[5] G. Zhang et al. "Permeable epoxy coating with reactive solvent for anticorrosion of concrete". In: *Progress in Organic Coatings* 117 (2018), pp. 29–34. DOI: 10.1016/j.porgcoat.2017.12.018.

[6] J.-E. Ehlers et al. "Theoretical Study on Mechanisms of the Epoxy-Amine Curing Reaction". In: *Macromolecules* 40.12 (2007), pp. 4370–4377. DOI: 10.1021/ma070423m.

[7] C. Yi et al. "Curing kinetics and mechanical properties of epoxy based coatings: The influence of added solvent". In: *Progress in Organic Coatings* 124 (2018), pp. 4165–174. DOI: 10.1016/j.porgcoat.2018.08.009.

[8] M. Dušková-Smrčková, K. Dušek, and P. Vlasák. "Solvent activity changes and phase separation during crosslinking of coating films". In: *Macromolecular Symposia* 198.1 (2003), pp. 259–270. DOI: 10.1002/masy.200350822.

[9] P. A. Sorensen et al. "Anticorrosive coatings: a review". In: *Journal of Coatings Technology and Research* 6.2 (2009), pp. 135–176. DOI: 10.1007/s11998-008-9144-2.

[10] C. M. Jeffries et al. "Small-angle X-ray and neutron scattering". In: *Nature Reviews Methods Primers* 70.1 (2021). DOI: https://doi.org/10.1038/s43586-021-00064-9.

[11] J. Witte et al. "A comparison of the network structure and inner dynamics of homogeneously and heterogeneously crosslinked PNIPAM microgels with high crosslinker content". In: *Soft Matter* 15 (2000), 792–802. DOI: 10.1039/c8sm02141d.

[12] R. Lovell and A. H. Windle. "WAXS investigation of local structure in epoxy networks". In: *Polymer* 31.4 (1990), pp. 593–601. DOI: 10.1016/0032-3861(90)90274-3.

[13] S. Yamamoto et al. "Off-stoichiometry effect on the physical properties of epoxy resins". In: *Polymer Journal* 57 (2024), 357–366. DOI: 10.1038/s41428-024-00983-w.

[14] S. J. Bai. "Crosslink distribution of epoxy networks studied by small-angle neutron scattering". In: *Polymer* 26.7 (1985), pp. 1053–1057. DOI: 10.1016/0032-3861(85)90228-9.

[15] W.L. Wu et al. "Epoxy Network Structure. 4. A Neutron Scattering Study of Epoxies Swollen in a Deuteriated Solvent". In: *Macromolecules* 21.3 (1988), 756–764.

[16] W.L. Wu and B. J. Bauer. "Network structure of epoxies - a neutron scattering study: 2". In: *Polymer* 27.2 (1986), pp. 169–180. DOI: 10.1016/0032-3861(86)90322-8.

[17] A. Izumi et al. "Cross-link inhomogeneity in phenolic resins at the initial stage of curing studied by 1 H-pulse NMR spectroscopy and complementary SAXS/WAXS and SANS/WANS with a solvent-swelling technique". In: *Polymer* 103 (2016), 152–162. DOI: 10.1016/j.polymer.2016.09.067.

[18] M. Aoki et al. "Mesoscopic Heterogeneity in the Curing Process of an EpoxyAmine System". In: *Macromolecules* 52.5 (2019), pp. 2075–2082. DOI: 10.1021/acs.macromol.8b02416.

[19] W. L. Wu and B. J. Bauer. "Network structure of exposies. I: A neutron scattering study". In: *Polymer Communications (Guildford)* 26.2 (1985), pp. 39–42.

[20] Merck KgaA. *o-Xylene*. https://shorturl.at/uxISQ [Accessed: (28/09/23)]. 2023.

[21] Honeywell International Inc. *1-Butanol*. https://lab.honeywell.com/shop/1-butanol-537993 [Accessed: (28/09/23)]. 2023.

[22] A. S. D Shackleford. "Using Positron Annihilation as a Method to Characterise Epoxy Networks with Regards to Chemical Resistance". PhD thesis. The University of Sheffield, Faculty of Engineering, Department of Mechanical Engineering, 2019.

[23] Joseph Orgill. *JoeOrgill/PALS*. https://github.com/JoeOrgill/PALS/blob/main/PALS_refined.py [Accessed: (17/09/24)]. 2022.

[24] B. Hammouda, D. L. Ho, and S. Kline. "Insight into Clustering in Poly(ethylene oxide) Solutions". In: *Macromolecules* 37.18 (2004), pp. 6932–6937. DOI: 10.1021/ma049623d.

[25] P.-G de Gennes. *Scaling Concepts in Polymer Physics*. Ithaca, New York: Cornell University Press, 1979.

[26] N. S. Davidson, R. W. Richards, and A. Macconachie. "Determination of Correlation Lengths in Swollen Polymer Networks by Small-Angle Neutron Scattering". In: *Macromolecules* 19.2 (1986), pp. 434–441. DOI: 10.1021/ma00156a034.

[27] T. Kopač, A. Ručigaj, and M. Krajnc. "The mutual effect of the crosslinker and biopolymer concentration on the desired hydrogel properties". In: *International Journal of Biological Macromolecules* 159 (2020), pp. 557–569. DOI: 10.1016/j.ijbiomac.2020.05.088.

[28] *Scattering Length Density Calculator*. http://www.refcalc.appspot.com/sld [Accessed: (02/08/24)].

[29] J. Ehlers et al. "Theoretical Study of the Epoxy-Amine Curing Reaction". In: *Macromolecules* 40.12 (2007), pp. 4370–4377. DOI: 10.1021/ma070423m.

[30] K. C. Cole, J. J. Heckler, and D. Noel. "A New Approach to Modeling the Cure Kinetics of Epoxy Amine Thermosetting Resins. 2. Application to a Typical System Based on Bis[4- (diglycidylamino)phenyl]methane and Bis(4-aminophenyl) Sulfone". In: *Macromolecules* 24.11 (1990), pp. 3098–3110. DOI: 10.1021/ma00011a012.

[31] V. L. Zvetkov. "A Modified Kinetic Model of the Epoxy-Amine Reaction". In: *Macromolecular Chemistry and Physics* 203.3 (2002), pp. 467–476. DOI: 1022-1352/2002/03020467$17.50+.50/0.

[32] The SasView Project. *gaussian peak*. https://www.sasview.org/docs/user/models/gaussian_peak.html [Accessed: (24/07/24)]. 2023.

[33] P. Schatzberg. "Molecular diameter of water from solubility and diffusion measurements". In: *The Journal of Physical Chemistry* 71.13 (1967), pp. 4569–70.

[34] Y. Tang, D. Dubbeldam, and S. Tanase. "WaterEthanol and MethanolEthanol Separations Using in Situ Confined Polymer Chains in a MetalOrganic Framework". In: *ACS Applied Materials Interfaces* 11.44 (2019), 4138341393. DOI: 10.1021/acsami.9b14367.

Chapter 6

The Solvent Uptake Characteristics of Epoxy-Amine Polymer Networks

Abstract

Epoxy-amines see use in a wide-range of industries as protective coatings against corrosion. Epoxy amines used as coatings are cured with solvents in order to reduce their viscosity, making them easier to apply. These coatings eventually fail in this task. Pathways form in seemingly intact coatings, allowing solvents to penetrate them. These pathways eventually span the entire coating, allowing solvent to reach the previously protected surface, resulting in corrosion. It has been hypothesised that curing with solvents brings about this failure mechanism. Solvents separate from the epoxy-amine mixture during cure, resulting in a heterogeneous mixture of low crosslink density (voids) and high crosslink density regions. Solvent can enter these voids and swell them, resulting in the pathways that eventually lead to the failure of anti-corrosive coatings. This hypothesis was investigated by measuring the differences in uptake in methanol and water between samples of epoxy-amines cured with and without solvents. The epoxy used was a Bisphenol A based epoxy, DER331. The amine was m-Xylylenediamine (MXDA). The solvent was a 3:1 mixture of xylene and butanol, by mass. It comprised 60% of the total mixture, again by mass. Epoxy-amines were made of stoichiometric ratio and excess epoxy, and with the homopolymerizing agent, 2,4,6-tris(dimethylaminomethyl)phenol (DMP-30). The initial uptake rate was proportional to the square root of time spent immersed in the solvent, indicating Fickian diffusion. This initial uptake rate was greater in samples cured with solvents. This was believed to be due to the presence of voids when curing with solvents. Uptake in solvent samples increased with cure rate, which brought about larger voids in the final samples. At the point of evaporation of curing solvents, formulations with greater cure rates would be more viscous, meaning they cannot fill voids as well as those of lower cure rates. Void sizes therefore increase in solvent-cured formulations as curing rate increases. Solvent-cured samples also exhibited mass loss, which was also believed

to increase with increased void size due to increased cure rate. An increase in void sizes would lead to greater separation of polymer network. Sections of the network not covalently bonded to the rest of the network could therefore be leached out during solvent uptake. Uptake in non-solvent samples was dependent on crosslink density and the density of hydrogen bonding sites. This dependence on hydrogen bonding was more prominent in water uptake than in methanol.

6.1 Introduction

Epoxy-amine resins display excellent mechanical strength and toughness; chemical, water and corrosion resistance; and adhesive properties. Therefore they are a popular choice as anti-corrosion protective coatings [1]. It is beneficial for these coatings to have a high crosslink density, as this reduces mobility in the polymer network, reducing the ability for solvents to penetrate the polymer network. Other beneficial properties are also optimised by maximising crosslink density, such as chemical resistance and toughness, although hardness is reduced [2]. For less-flexible epoxies and amines, such as those used in anti-corrosive coatings, increased crosslink density, and the beneficial properties it brings, are achieved by maximizing the conversion of epoxy and amine into the polymer network. Conversion is optimal when the epoxy-amine is at 'stochiometric ratio,' when there are equal number of amine groups as epoxy groups [3, 4], meaning there is no excess of epoxy or amine to go unreacted. Crosslink density decreases with excess epoxy and amine, with excess epoxy being found to reduce crosslink density greater than excess amine [3]. An alternative method to using a stoichiometric ratio of epoxy and amine is to use an excess of epoxy and cure with a tertiary amine accelerator, such as 2,4,6-tris(dimethylaminomethyl)phenol (DMP-30). DMP-30 contains both a tertiary amine and a hydroxyl group. Through these two groups, DMP-30 can act as a catalyst for epoxy homopolymerization, thus raising conversion in an epoxy-amine mixture with excess epoxy [5]. The presence of a hydroxyl group in DMP-30 also catalyses the epoxy-amine reaction, raising the curing rate [6, 7, 8, 9].

Epoxy-amines used as coatings are mixed with solvents in order to reduce their viscosity, making it possible to apply them to surfaces via spraying [2, 10]. This raised mobility in the polymer network due to the presence of solvents also suppresses its glass transition temperature, T_g. This effectively raises conversion and T_g once the solvent evaporates when curing at lower temperatures [11]. Mixes of multiple solvents, such as xylene and butanol, are used in order to control the volatility and polarity of the solvent mixture. Controlling the volatility of the solvent allows for the evaporation rate, and therefore the suppression of the T_g of the coating, to be controlled [11]. Controlling the volatility allows for different components to dissolve in the solvent [2]. Curing with solvents is not without its drawbacks. Solvent evaporation can lead to cracking. Retained solvent in the network reduces hardness, raises its sensitivity to water and reduces adhesion [11, 12]. Evaporating solvents also pose health risks. Solvent vapours can affect a person's central nervous system, and are a fire and explosion risk [2]. There is also the possibility of phase separation between solvent and polymer network, resulting in the presence of 'voids' in the coating once solvent evaporation

has occurred [12, 13].

Anti-corrosive coatings eventually fail, even those with little apparent or obvious defects. Local water uptake eventually results in pathways throughout the network, allowing for corrosion to occur [14]. This is thought to come about from heterogeneities, resulting in areas of low crosslink density through which permeants can more easily pass [15]. Homogeneous networks also exhibit uptake, controlled by the intrinsic free volume naturally present in a polymer network [16]. This occurs via two processes. First, a quick (Fickian) diffusion into free spaces. During this stage, the solvent enters free volumes in the network and forms hydrogen bonds at available sites in the polymer network. Initially, for short time periods, this uptake is proportional to the square root of immersion time:

$$M_t = \frac{4M_m}{2L}\sqrt{\frac{tD}{\pi}} \tag{6.1}$$

Where M_t is the % uptake, M_m is the maximum % uptake, L is the samples thickness, doubled as it is assumed two sides are exposed, t is the time of immersion and D is the diffusion coefficient [17]. Equation 6.1 assumes that $\frac{M_t}{M_m} < 0.5$. This is followed by a slower uptake mechanism in which the polymer network relaxes, opening up more hydrogen bonding sites [18]. Beyond the failure of their primary task, uptake in protective coatings has been shown to reduce the T_g of the network and reduce its other beneficial properties such as its toughness [19, 20, 21, 22], and accelerating ageing (the long-term relaxation of chains)[23].

The uptake of water in polymer networks, and specifically epoxy and epoxy-amine networks, has been well-studied. Moisture uptake is dependent on the free-volume of the polymer network [12, 16, 17, 19], the polymer's affinity for water [19, 22] and ageing effects [24]. The presence of the free volumes is dependent on the crosslink density and therefore stoichiometry, of the polymer, its chain stiffness and its 'cohesive energy density.' With low enough conversion, negative uptake has been observed, possibly due to the leaching of excess epoxy [25]. The affinity for water is dependent on the number of hydrogen-bonding sites in the polymer. In epoxies, these are plentiful due to flexible hydroxyl groups that form due to epoxy ring opening [19], resulting in water uptake of 1-7% [25]. Diffusion into regions of low-crosslink density, formed by a heterogeneous network due to conversions below 100%, dominates the uptake. However, this 'unbound' water does not disrupt the polymer network. It is the 'bound' water, which forms hydrogen bonds with the network, breaking hydrogen bonds between different parts of the network, that swells and plasticizes the network [19, 21]. This bound water can be defined as type one or type two. Type one forms one hydrogen bond with the polymer network. Type two forms two hydrogen bonds. In this way, type two forms pseudo-crosslinks with the network, actually increasing the network's crosslink density, raising its T_g [26, 27, 28]. The initial Fickian diffusion is based upon the uptake of this bound water into the free volume. Subsequent non-Fickian diffusion from network relaxation possibly occurs due to uptake of this bound water [29].

Besides water uptake, there have been some uptake investigations involving other solvents, such as methanol [16, 26, 30]. Due to it being able to form both hydrogen bonds and non-polar bonds with the epoxy-amine network, methanol has been shown to have higher affinity for organic coatings than water, resulting in greater uptake and degradation than when immersed in water, as well as leaching of constituents of the polymer network. There are few investigations into uptake in organic coatings via solvents other than water, or comparison between solvents. This untapped area of investigation could offer more information into the chemical influences of uptake mechanisms. Furthermore, despite other investigations into the nature of coatings cured with solvents, there appears to be little in the way of uptake in these systems, despite the relevance to their real-world applications. In this investigation, the uptake of epoxy-amine coatings immersed in water and methanol was measured. Epoxy-amines of stoichiometric ratio and excess epoxy were used, for those cured with and without solvents as well as with and without DMP-30.

6.2 Experimental Section

6.2.1 Materials

The epoxy used was UC0003 (Supplied by Akzo-Nobel, Felling UK), this is a Bisphenol A diglycidyl ether (DGEBA) epoxy. The UC0003 supplied contained mainly DER331, but also contained Epicote 828 and Razeen LR 1150 both DGEBA based expoxies. The epoxide equivalent weight (EEW) was determined to be $187\pm8 \mathrm{gmol}^{-1}$. The amine, m-Xylylenediamine (MXDA) and the accelerator, 2,4,6-Tris(dimethylaminomethyl)phenol (DMP-30) were purchased from Sigma Aldrich and used as received. Solvents used were o-xylene (Sigma Aldrich) and 1-butanol (Honeywell).

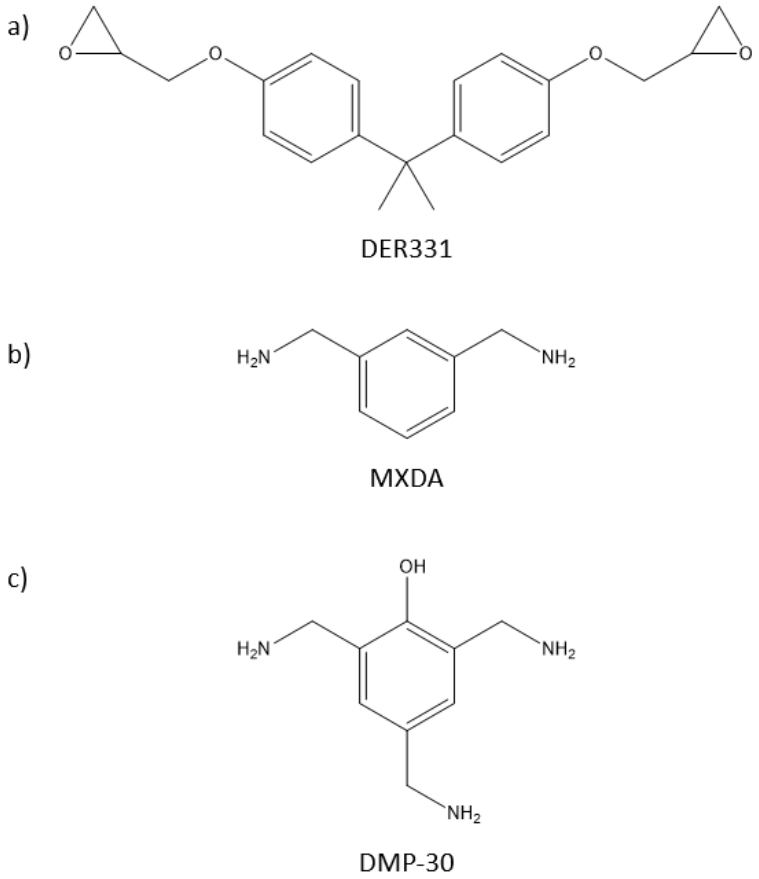

Figure 6.1: Materials used to make the crosslinked epoxy networks. a) shows the epoxy DER331, b) shows the amine curing agent m-Xylyenediamine and c) shows the homopolymerizing agent DMP-30.

6.2.2 Titration to Determine Epoxide Equivalent Weight (EEW) of Epoxy

Tetraethylammonium bromide (Sigma Aldrich) (25g) was dried at 100°C for one hour. Tetraethylammonium bromide solution was produced by dissolving 25g in 100ml of glacial acetic acid (Sigma Aldrich, molarity: 17.4M, reagent grade). Crystal violet indicator was prepared by dissolving 20mg of crystal violet (Sigma Aldrich) in 20ml of glacial acetic acid. A mass of 0.1092 - 0.1683g of UC0003 was dissolved in 10ml of chloroform and solubilised using a vortex mixer (make). The epoxy solution was pippetted into a conical flask. Subsequently 20ml of glacial acetic acid and 10ml of tetraethylammonium bromide solution were added to the flask, which was manually swirled before 4-6 drops of crystal violet indicator were added. Perchloric acid (Sigma Aldrich, 0.1M, reagent grade) was then titrated against this solution until the solution

turned a clear yellow colour. The EEW was then determined via equation 6.2:

$$EEW(\text{gmol}^{-1}) = \frac{\text{sample mass(g)}}{\text{titre (dm}^3) \times \text{perchloric acid concentration (mol dm}^{-3})} \quad (6.2)$$

This procedure was repeated twice and an average was obtained in order to determine UC0003's EEW.

6.2.3 Cross-linked Network Preparation

We define r as the ratio of amine hydrogens to epoxide groups. Samples with UC0003 epoxy and MXDA diamine crosslinker, have stochiometries, r, from $r = 0.5$ to $r = 1$, i.e. a 50% excess of epoxy to no excess. Samples were made with and without DMP-30, and with and without processing solvents. These solvent samples comprised of 60% epoxy-amine, 30% xylene and 10% butanol, by mass. To make the samples, epoxy was first weighed into a container using a balance (AD FZ-3000iWP). This mass was subsequently used to determine the required mass of DMP-30 and MXDA. For samples with DMP-30, DMP-30 equivalent to 3% of the EEW of UC0003 was added via glass pipette (SLS Nottingham UK), MXDA was also added via pipette, prior to adding DMP-30. For samples cured with solvent, the required masses for xylene and butanol were determined before xylene and then butanol were added, both via pipette.

For samples without solvent, the mixture was then stirred either by hand using a glass rod, or in a DAC 150 FVZ-K Speed Mixer (Synergy Deviced Ltd UK) at 2000rpm. Samples stirred by hand had the container opening covered in Parafilm to prevent oxidation or carbamation of the MXDA. Samples prepared without solvent were mixed for 5 minutes, as it was determined that this suitably mixed the constituent parts of the mix well enough to reach a maximum T_g after curing, measured via differential scanning calorimetry (DSC) measurements. There was negligible difference in the final T_g of non-solvent samples mixed via hand compared to using the Speed Mixer. Samples with solvent were mixed via hand as it was determined that the Speed Mixer did not mix the solvent, epoxy and amine together well. Furthermore, four five-minute stirs, with fifteen-minute wait periods in between each stir, were required to fully mix the epoxy, amine and solvent mixture. DSC measurements of solvent samples after cure showed that this four-stir regime was the minimum number of stirs that gave a consistent final T_g value.

Non-solvent samples were cured in PTFE moulds with an area of 24×25mm. Acetate sheets were placed onto the bottom of the moulds so that samples could be more easily removed once fully cured. Sample mixtures were poured in so that they formed a full layer on the bottom of the mould. Solvent samples were found to crack in these PTFE moulds and so were cured in more flexible 26×48mm silicone moulds. For differential scanning calorimetry (DSC) measurements, samples were cured in an oven (Binder) under an ambient atmosphere at 60°C for two hours, then one hour at 100°C and finally one hour at 160°C. This initial 60°C cure would give time for the primary amines to react with the epoxy. The 160°C cure would then allow the secondary amines to react. Later solvent samples were heated up to ∼195°C after the

160°C cure in order to fully cure them. However, if the cure went straight from 60°C to 160°C, there would be the risk of the solvents boiling off rapidly, xylene having a boiling point of 143-145°C [31] and butanol 119°C [32]. The 100°C cure therefore allowed the solvents to evaporate before the cure temperature was elevated further. It took around 25 minutes to heat from 60°C to 100°C and around 45 minutes to heat from 100°C to 160°C. Curing was also carried out in an oven under a nitrogen atmosphere, but there was little difference in the samples cured in these two environments, with negligible difference in final T_g. It has been observed that formulations of $r \geq 1$ with DMP-30 experience a drop in T_g when an unknown reaction occurs at ∼150°C. This drop in T_g was clearest for $r = 1$. In order to investigate how this drop in T_g affects the solvent uptake, a set of samples of r=1 with DMP-30, cured with and without solvents was made without the final 160°C cure (removed after one hour at 100°C).

Samples used for the swelling experiments were mechanically polished down to a uniform thickness of either 1mm or 1.5mm. Samples were held in place with a vacuum before being machine-cut down to 1mm with a 30mm high speed steel slot drill. The tops and bottoms of samples were cut so that both sides became flat.

6.2.4 Swelling

Sets of samples of 1mm and 1.5mm thick were slotted into grooves in PTFE moulds. These moulds were placed in glass containers which were subsequently filled with solvent, either deionized water or methanol. The grooves of the moulds were 3mm deep. They were 1.1mm thick for the 1mm thick samples, and 1.6mm thick for the 1.5mm thick samples. Moulds with wider grooves were substituted as required for when the samples swelled beyond the thickness of their grooves. The moulds and containers were 86mm long and 70mm wide. Solvent was added so that all the samples were clearly submerged. Containers were refilled with solvent when levels were low enough that the tops of samples were no longer fully immersed. Samples were left to swell either at room temperature or at 30°C. For those at room temperature, samples in water were left in the lab. Samples in methanol were left in a fume cupboard. Samples swollen at 30°C were placed in a polyethylene container in a water bath set to 30°C. Overall, there were eight sets of samples: sets of 1mm and 1.5mm thick samples, submerged in methanol or water, at 30°C or room temperature.

Individual samples were weighed using a set of scales (Sartorius). They were first weighed before immersion, then subsequently every hour for water samples or every 30 minutes for methanol samples on the first day. Over the next four days, three measurements were taken daily. After that, one measurement was taken each day and then once a week. Samples were removed from grooves using a set of tweezers and dried before weighing. Methanol samples were dried using lens cleaning tissues (Thorlabs). Water samples were dried using delicate task wipers (KIMTECH) and brushed down with lens cleaning tissues to remove fibres from these wipers. Samples were resubmerged immediately following weighing. Lids were placed back on the container once all the samples in the container were weighed. Once all the day's measurements

were taken for a container, it was sealed using Parafilm to seal the container, reducing solvent loss via evaporation.

After solvent uptake reached an apparent equilibrium, with samples not gaining or losing any mass, the sets of samples were dried. The samples surfaces were dried using again lens cleaning tissues or task wipers. Moulds and containers were dried using task wipers. The grooves of the moulds were dried with a nitrogen gun. Initial sample mass was taken and then subsequent mass measurements taken every hour on the first day of drying, three times for the next four days and then once a day after that. Samples were kept in the same moulds and in the same containers, and left to dry at ambient temperature. Containers were left uncovered throughout the day until the last measurement, when lids were put on the containers and sealed with Parafilm.

6.2.5 Density Measurements

Simple density measurements were taken by weighing dry samples using on a set of scales (Sartorius). Samples were cuboid in shape, with known width and length from their moulds and thickness through polishing. Density was therefore determined by dividing their mass by their geometric volume. Samples that were damaged, i.e. had chipped edges or corners, were not considered for density measurements.

Density was also determined via helium pycnometry. A Micrometrics AccuPyc^{TM} II 1345 gas pycnometer using helium, in a 0.72cm^3 cup with a 1cm^3 AccuPyc^{TM} ball calibration standard. For helium pycnometry measurements, in order to fit in the pycnometer's measurement chamber, samples were cured in cylindrical moulds of 10mm diameter and ∼1mm deep.

6.2.6 Positron Annihilation Light Spectroscopy (PALS)

PALS measurements were carried out by placing the source of positrons, a radioactive Na22 source between a pair of identical samples before placing this "sandwich" between the 2 detectors of the Sheffield PALS instrument. The samples were taped together on one edge to keep the sample contained. Data was recorded using the QtPALS software [33]. The instrument was allowed to count until 1 million annihilations were measured. This took around 6 hours. Each measurement was repeated twice for each sample pair.

Data from the QtPALS software was presented in the form of a histogram of the ortho-positronium (oPs) lifetimes. Once 1 million lifetimes were measured the data was analysed using custom-written Python code. The data was fitted to a convolution of a Gaussian and 3 exponential decays. Each lifetime represents an annihilation process. The Tao-Eldrup model [34] [35] was then used to convert the decay rate of the oPs into an average free volume pore size. Fractional free volume, the total free volume of the sample measured as a percentage of the total volume, was calculated by multiplying the free volume by intensity:

$$FFV = I_3 \times FV \tag{6.3}$$

Intensity was calculated by the ratio of the exponential heights, where I_3 is the intensity of the oPs exponent calculated by:

$$\frac{I_3}{(I_1 + I_2 + I_3)} \tag{6.4}$$

Where I_1 and I_2 are the intensities of the free positron decay and para-positronium decay, respectively.

6.2.7 Differential scanning calorimetry (DSC)

DSC was performed using a DSC 25 (TA Instruments). Samples were made using 5-10mg of epoxy amine mix, placed in aluminium pans via pipette, before curing using the regime described in section 6.2.3. The final glass transition temperature, T_g of these samples was measured via DSC using the oven-cured samples. Samples were cooled down to 5°C before being heated up to 200°C. They were then cooled down to 5°C and heated to 200°C again. The temperature ramp throughout was 10°Cmin^{-1}. The T_g and enthalpy peak areas were measured using the software package TRIOS (TA Instruments). The T_g was determined from the second heat ramp.

6.3 Results

6.3.1 Density, Free Volume and Network Properties

Density measurements, as measured by dividing their mass by their geometric volume, are shown in figure 6.2. Although there was a large variation in density results, non-solvent results appeared to have a greater density than solvent results, with solvent samples generally having a density in the range of 0.75-1.03gcm^{-3} and non-solvent samples in the range of 1.03-1.20gcm^{-3}. The spread of results may have arisen from samples not being perfectly cuboid. Minor damage to the sample surface by polishing or other means would affect this final density measurement. There appeared to be little difference in density for variations between non-solvent samples of different stoichiometries, or when DMP-30 was introduced. For solvent-cured samples, a lower stoichiometry seemed to produce higher densities, such that those of r=0.57 had similar densities to non-solvent samples. For both non-solvent and solvent samples, trends in stoichiometry may be obscured by the range of density results. Samples of a purely homopolymerized network, those cured with DMP-30 and without MXDA, showed densities similar to that of other non-solvent samples.

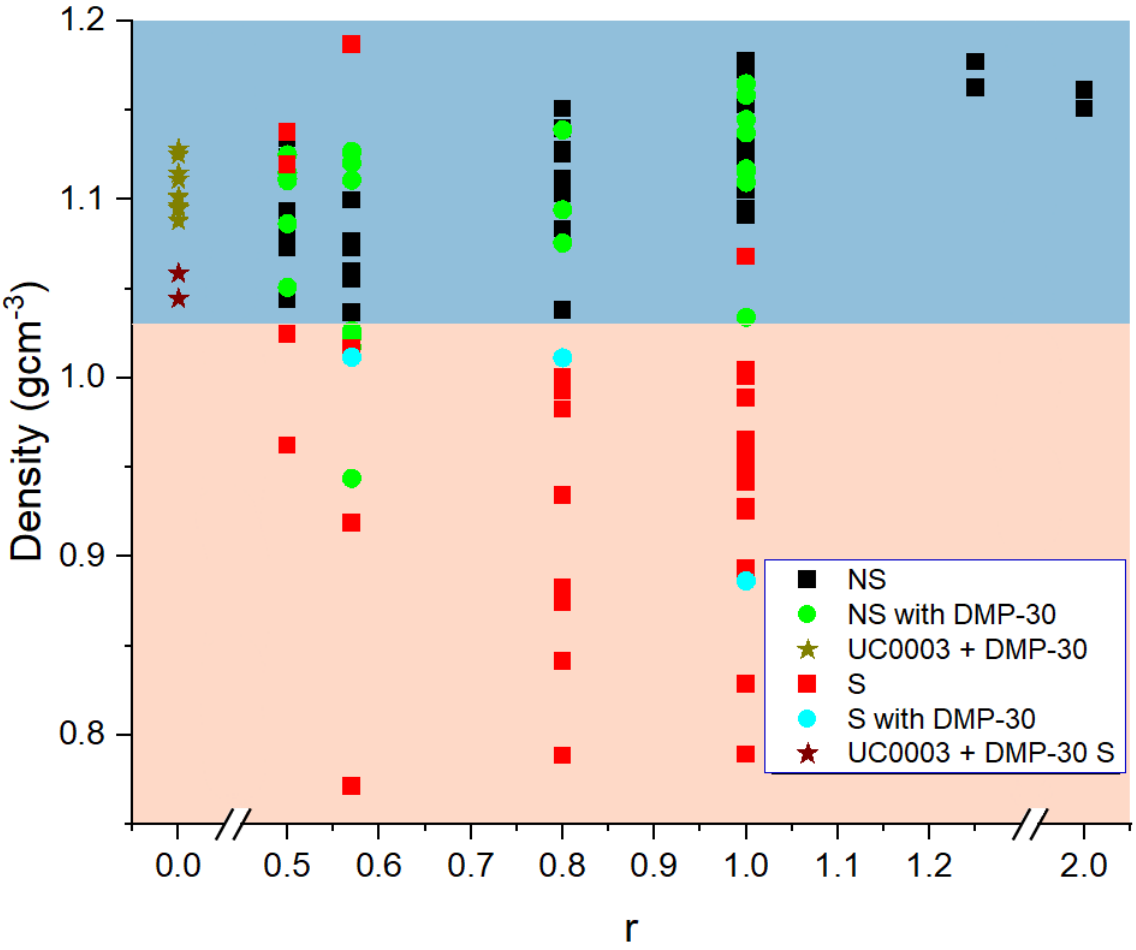

Figure 6.2: Density measurements of samples of epoxy-amine resin, cured with and without solvents and with and without DMP-30. Density was calculated from the sample mass and its cuboid volume. The higher-density region, predominantly occupied by non-solvent samples is shown in blue. The lower-density region, predominantly occupied by solvent samples is shown in light red.

The fractional free volume (FFV) of samples and the average size of these free volumes, as measured by PALS, are shown in figure 6.3. Non-solvent formulations had smaller free volume and lower FFV than solvent formulations of less excess epoxy ($r \geq 0.8$). The trend mirrors the density results shown in figure 6.2. It was concluded that the density of solvent samples is lower due to the lower free volume. Solvent samples showed a clear decrease in both FFV and free volume as excess epoxy decreased such that samples of r=0.57 showed similar FFVs and free volumes whether they were cured with or without solvents. Again, this similarity between non-solvent and solvent samples of r=0.57 is seen in the density measurements. As seen in figure 6.2, solvent samples with r=0.5 showed greater densities than solvent samples having lower excess epoxy, so that their densities were similar to non-solvent samples. This is however less

obvious than in the free volume results. As it was believed that the increase in free volume from solvent samples was due to the presence of voids, it is also believed that the FFV (and size of free volumes) decreased due to some reduction in these voids. It is difficult to determine the influence of curing with DMP-30 on the free volumes in solvent samples with the FFV and free volume for r=0.57, r=0.8 and r=1 S with DMP-30 not following a clear trend. However, if the results for $r = 0.57$ and r=0.8 of these solvent-cured with DMP-30 samples were swapped, there would be a clear trend in this set of formulations, showing free volume decreasing with stoichiometry. This would agree with those of the solvent-cured samples. Despite this, there does not seem to be a clear reason to switch these two results around. The free volumes of non-solvent samples appear to have been little affected by changes in stoichiometry. Non-solvent samples show a reduction in FFV when cured with DMP-30, but an increase in average free-volume size. An increase in free volume size as FFV decreases has been observed previously in samples that underwent a post-cure. This was explained by stating that as crosslink density increased, the FFV decreased, merging free volumes together so that they combined, increasing their average size [36]. Something similar could be happening here.

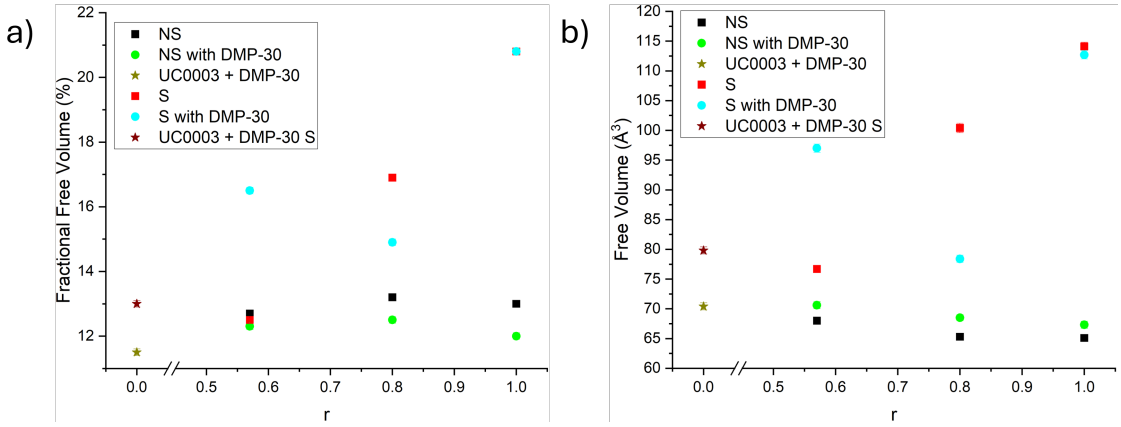

Figure 6.3: Free volume measured in PALS for epoxy-amine resins, cured with and without solvent and DMP-30. a) shows the % of free volume in each sample. b) shows the average size of these free volumes.

Helium pycnometry measurements are shown in table 6.1. Density measurements are also shown if the sample batch was used for both swelling and helium pycnometry. Non-solvent samples showed similar densities regardless of stoichiometry. Given the accuracy of helium pycnometry, this reinforces the idea that density does not vary with stoichiometry. The single measurement of a non-solvent sample with DMP-30 did show a greater density than the other non-solvent samples, but more results would be needed before firm conclusions can be made. Density, as measured by helium pycnometry, was similar for both solvent and non-solvent samples. As helium pycnometry determines the volume of a sample by how much helium it can take up, it is believed that the helium entered the free volumes of the solvent samples and so only measured the volume of the

epoxy-amine network. Network structure is believed to be very similar for samples of the same stoichiometry, cured with and without solvent. This is further supported by the T_g results, shown in figure 6.4. For samples of the same formulation, those cured in solvent showed a similar T_g. It has been reported before that curing epoxy-amines in solvent results in a slightly lower T_g [12]. As T_g is dependent on conversion and network structure, solvent processing therefore does not affect the sample's network structure.

Formulation	Helium Pycnometry Density (10^{-4}gmm^{-3})	Mass/Volume Density (10^{-4}gmm^{-3})
1 NS	11.947±0.003	-
1 NS	11.940±0.002	11
0.57 NS	11.973±0.001	-
1 S	11.792±0.008	8.3
0.57 S	11.966±0.004	-
0.57 S	11.980±0.003	-
0.57 NS with DMP-30	12.163±0.001	11

Table 6.1: Density of epoxy-amine resins, cured with and without solvent and DMP-30, as measured via helium pycnometry. The number in the formulation refers to the stoichiometry of the sample. NS and S refers to whether the sample was cured without solvent (non-solvent), or with. Density measurements from cuboid volume for samples from the same sample set as those used in pycnometry measurements are shown if measured.

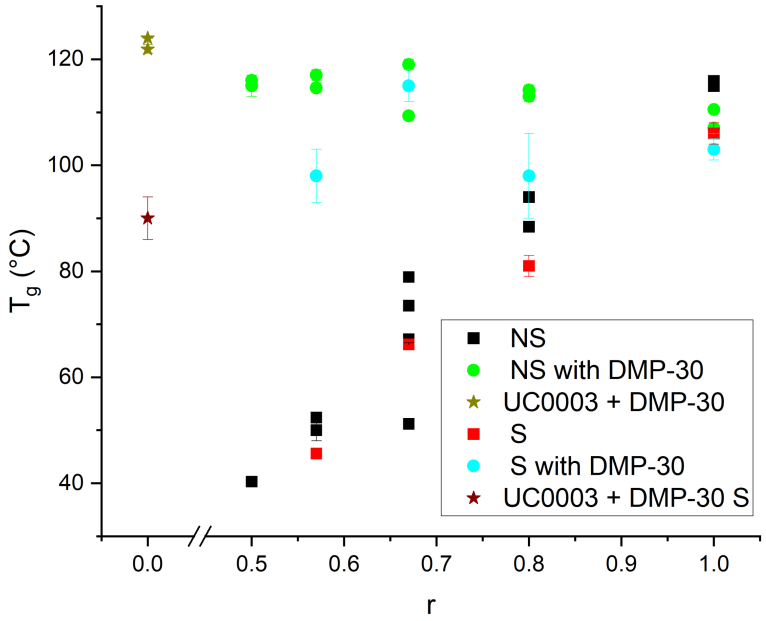

Figure 6.4: Glass transition temperatures of samples cured with and without solvent, both with and without DMP-30, as measured via DSC. Error arises from the averaging of multiple samples taken from the same epoxy-amine mixture.

6.3.2 Uptake

Solvent uptake was measured as mass uptake, normalized against sample surface area so that samples could be reliably compared. This was plotted versus the square root of time, as from equation 6.1, the initial uptake should be proportional to the square root of time. An example set of results for 1mm samples immersed in 30°C water is shown in figure 6.5. Figure 6.5a) shows the uptake over 500 hours. Figure 6.5 b) shows the uptake over the first week for non-solvent samples, cured without DMP-30. Fitting lines for the rate of uptake over the course of the first day and the rest of the first week are shown in red. Uptake measurements for all the sample sets can be found in the appendix.

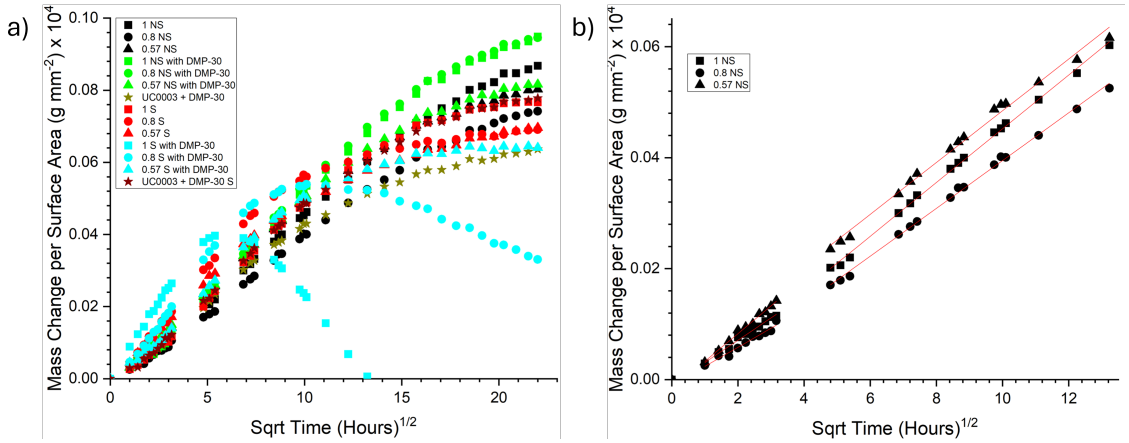

Figure 6.5: Mass uptake of samples of 1mm thick fully-cured epoxy-amine samples, immersed in water at 30°C, normalized to the individual sample's surface area. a) shows the uptakes over 500 hours. b) shows the uptakes of non-solvent samples over the first week of immersion. The red lines indicate the fits used to obtain rate of uptake over the course of the first day and for the rest of the first week. Updated graph to include clear fits

It can be seen that there is an initial linear regime before the rate of uptake decreases. For samples cured with solvent, and those without solvent but having high levels of excess epoxy, there is then a decrease in uptake. Although not shown in this set of measurements, some of these samples end up with a negative uptake. For solvent samples, this mass loss is believed to come about due to the presence of voids. The polymer network is more loosely connected than in a homogeneous network. Domains of this network can thus break-off and leave when immersed in solvents. For non-solvent samples of lower $r < 0.7$, it is believed that excess epoxy is being removed when immersed in the solvent. This can occur as for our samples, a conversion of 0.7 is required for gelation [11].

Uptake over the course of the first week is shown in figure **??**b). The initial linear relationship can be seen on all samples, at least for the first few measurements. Due to the difficulties in comparing the end uptake of samples, with there being mass loss and other changes in uptake, sample uptake was compared by comparing their uptakes from this initial linear regime. This was done by performing a linear fit on these initial results using OriginPro 2024. Uptake rates were measured to be generally lower for day one compared to the rest of week one. Fits were therefore taken separately for day one and the rest of week one. The simplest answer for this difference is that the increased number of measurements taken for day one resulted in the samples being out of their solvent for longer, and so lost more mass. However, this seems somewhat unlikely, as at most they would be out for a minute every thirty minutes, a time period that does not seem long enough to have an impact on uptake. Regardless of the cause, uptake rates for day one and the rest of week one were plotted separately. The week

one results were preferred as they had lower error. If it was not possible to obtain week one results, due to samples losing the linear relationship between uptake and $t^{1/2}$ before day one ended, the day one results were compared.

Uptake results for samples of epoxy-amine resins of different stoichiometries, immersed in methanol are shown in figure 6.6. There is little error in either the day one or week one results for the samples submerged in methanol.

Samples cured with solvent generally showed higher uptake than those cured without solvent. Again, this is explained by the formation of voids in solvent samples. Methanol can easily get into these empty spaces, resulting in greater uptake. There is also greater uptake for solvent samples as r increased to one. This may be somewhat unexpected. As r increases to one there is a more equal amount of epoxy and amine, and so a greater chance of reaction. Reaction rate thus increases as r increases to r=1. This would mean that at the stage of cure in which voids are being created (when the solvent is evaporating), a greater proportion of epoxy-amine reactions would have occurred, raising viscosity of the epoxy-amine mixture. The mixture therefore would not be able to fill the voids as much, resulting in final voids sizes greater than those networks with more excess epoxy. This would also explain why the solvent samples cured with DMP-30 have higher uptake than their counterparts of the same stoichiometry cured without DMP-30: the DMP-30 catalyses the epoxy-amine reaction, raising cure rate further. It should be noted that these results bear resemblence to the free volume results shown in figure 6.3. These voids therefore at least in part exist on the scale of 60-120Å^3. It should also be noted that the samples used in the results shown in 6.6c) were from the same set as those used for PALS measurements (figure 6.3). It therefore seems that the lower-than-expected initial uptake rate and free volume for the solvent sample cured with DMP-30 of r=0.8 were due to deficiencies in this sample rather than anything else.

Samples cured without solvent and without DMP-30 show an increase in uptake as stoichiometry decreases, so that uptake of r=0.57 NS has higher uptake than r=0.57 S. There is also a decrease in uptake in non-solvent samples of $r < 1$ when curing with DMP-30. These trends in non-solvent samples are believed to come about due to the presence of excess epoxy affecting the crosslink density of the network. As excess epoxy increases, the crosslink density of the network decreases. The network thus becomes more flexible. DMP-30 allows this excess epoxy to homopolymerize, raising the crosslink density and reducing uptake so that it is similar to $r = 1$ NS without DMP-30. These trends in non-solvent samples are similar to their T_g trends, as shown in figure 6.4. This would make sense: T_g is dependent on crosslink density. It is believed that the homopolymerized network is of a slightly higher crosslink density than the epoxy-amine network, producing a slightly higher T_g. This would also explain why the uptake in non-solvent samples with DMP-30 decreases as stoichiometry decreases: there is a greater proportion of homopolymerized network. There is also greater uptake for $r = 1$ when curing with DMP-30 compared to curing without. This difference is also seen on the T_g results. This difference in T_g has been noted before and has

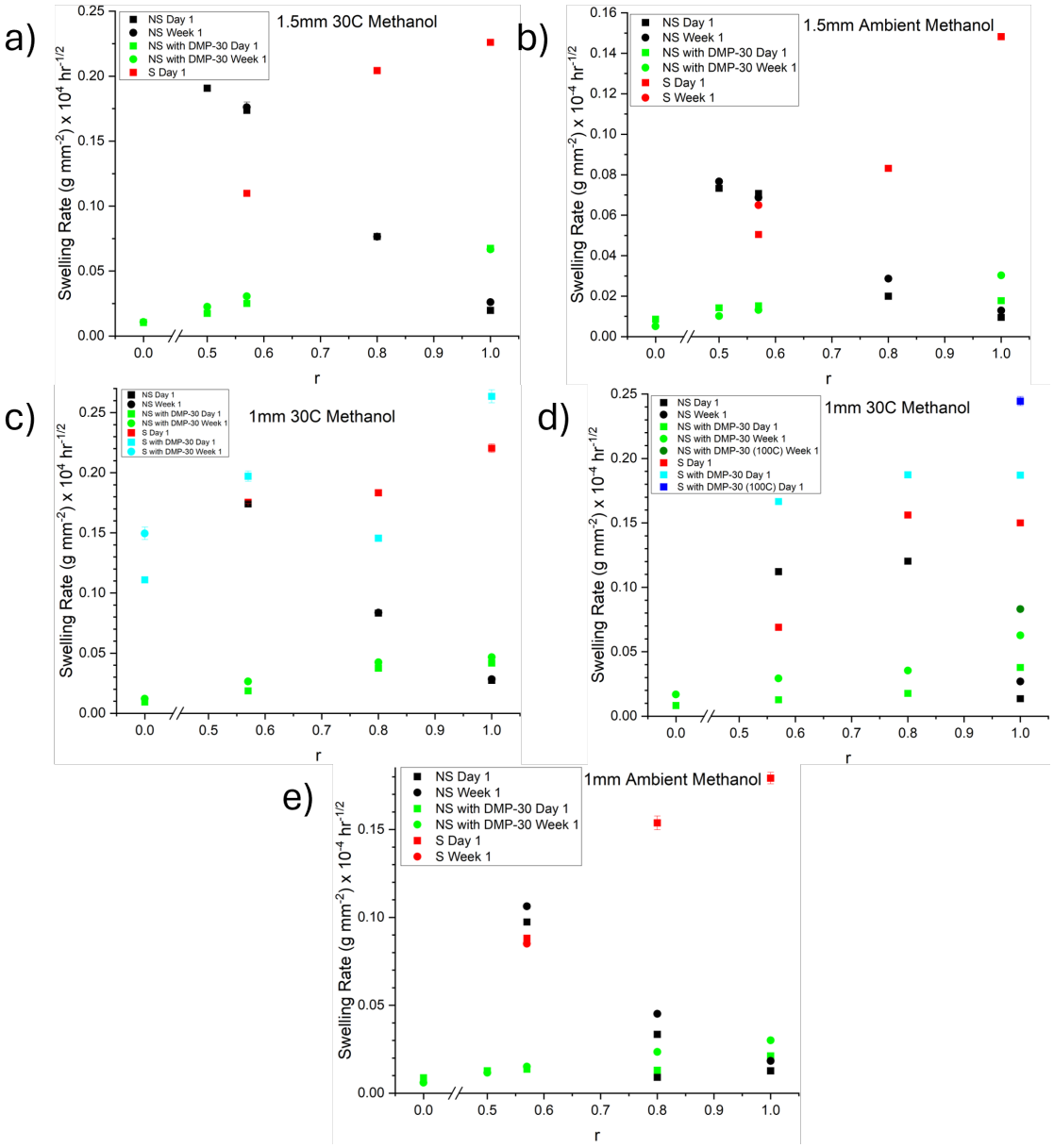

Figure 6.6: Mass uptake rate, normalized to sample surface area, of samples submerged in methanol. Results shown for both the first day and the subsequent week where possible. a) shows uptake rate for 1.5mm samples at 30°C. b) shows uptake rate for 1.5mm samples immersed at ambient temperature. c) and d) shows uptake rate for 1mm samples immersed at 30°C and e) shows it for 1mm samples immersed at ambient temperature. Error bars come from error in the fits.

not been completely explained. Part of the increase in uptake however could be due to excess amine present in the network due to epoxy being polymerized. This excess amine would reduce crosslink density in the same way in which excess epoxy would, thus raising uptake. However, this does not explain why r=1 NS with DMP-30 has greater uptake without the 160°C cure (shown in figure 6.6d) in dark green). Without the 160°C cure, this formulation had a higher T_g, so it was expected to have lower uptake. It is unclear why this is not the case.

Uptake in water for non-solvent samples, cured with and without DMP-30, is shown in figure 6.7 and for solvent samples in figure 6.8. Due to water being a poorer solvent for the network than methanol, there was far lower uptake in samples immersed in water than in methanol. This resulted in a higher proportional uncertainty in the water results. Given this error, the non-solvent and solvent results are shown separately so that comparisons between different stoichiometries of samples with and without solvent can be made more easily. Figure 6.7 only shows week one results as all the non-solvent samples were still in the linear regime for week one, and the day one results had much larger error. Figure 6.8 shows uptake for both day one and week one as some of the solvent samples become non-linear before the end of week one and so needed to be compared to other day one results.

There were clear differences not just in the amount of uptake when immersed in methanol or water, but in the differences in uptake between the different formulations. These differences may to come from the chemical differences between water and methanol. Given that all the atoms in water can form hydrogen bonds, which is not the case in methanol, water can more easily form hydrogen-bonds than methanol. Figure 6.7 shows that for non-solvent samples immersed, samples of r=1 have a greater uptake than those of r=0.8. This uptake then increased as the stoichiometry decreased to r=0.57. There is still the effect of reduced crosslink density as stoichiometry moves away from r=1, raising uptake. However, it is expected that for r=1, there is not 100% uptake, and so there is a small amount of excess amine. This amine can form hydrogen bonds with the water, raising uptake rate. Water is significantly more attracted to these hydrogen bonds than methanol. This uptake from excess amine thus outweighs the reduction of uptake due to increased crosslink density for r=1 NS when immersed in water, but not in methanol. This difference is shown in the uptake plots for 1mm non-solvent samples of $0.5 \leq r \leq 2$ immersed in 30°C water and methanol, shown in figure 6.9. It can be seen that the minimum uptake for samples immersed in methanol was for $r = 1$, but for water it was $r = 0.8$, highlighting the increase for samples immersed in water due to excess amine. For both water and methanol, there was increased uptake due to both excess epoxy, at $r = 0.5$ but a greater uptake due excess amine. The uptake in both came from a reduced crosslink density and hydrogen bonds forming with the oxygens in the epoxide ring. The uptake for $r > 1$ shows the increased uptake due to the amine groups being able to more easily form hydrogen bonds, both with water and methanol.

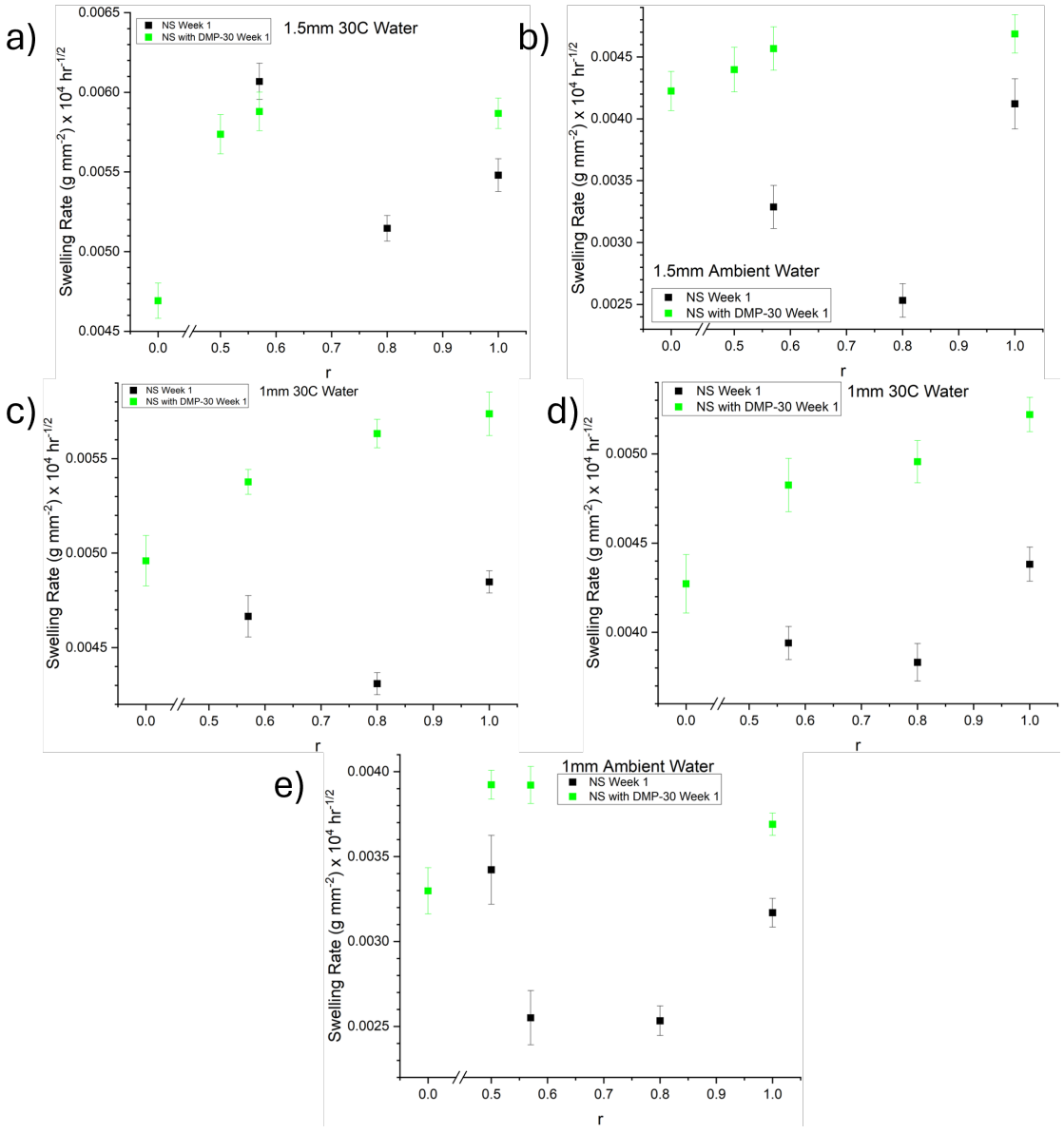

Figure 6.7: Mass uptake rate of water, of samples cured without solvents, normalized to their surface area, when submerged in water. Mass uptake taken for the first week, without the first day of results. a) shows uptake rate for 1.5mm samples at 30°C. b) shows uptake rate for 1.5mm samples immersed at ambient temperature. c) and d) shows uptake rate for 1mm samples immersed at 30°C and e) shows it for 1mm samples immersed at ambient temperature. Error bars come from error in the fits.

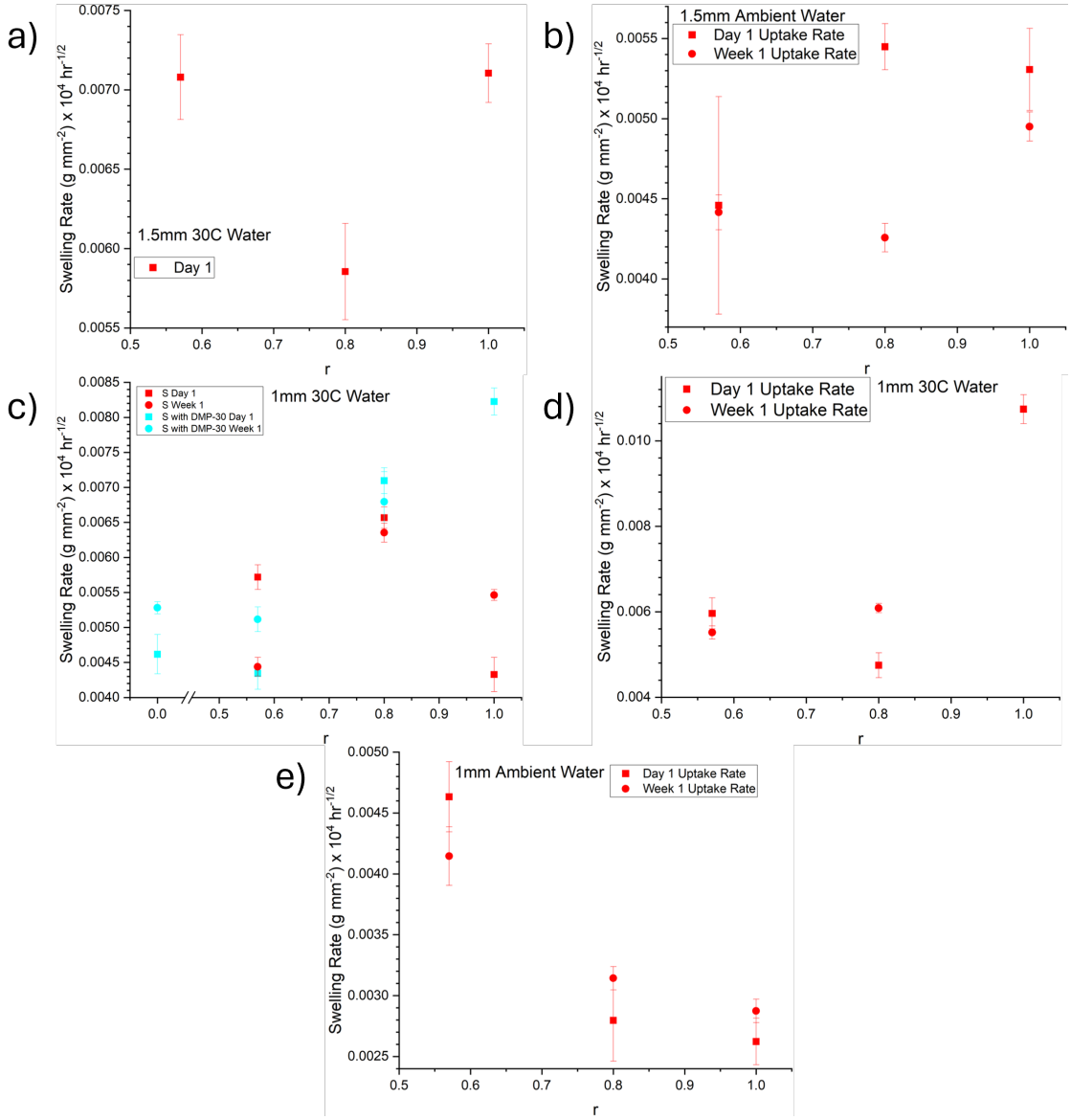

Figure 6.8: Solvent mass uptake rate for samples cured with solvent, normalized to their surface area, when immersed in water. Mass uptake rate taken for the first day and the subsequent first week, when possible. a) shows uptake rate for 1.5mm samples at 30°C. b) shows uptake rate for 1.5mm samples immersed at ambient temperature. c) and d) shows uptake rate for 1mm samples immersed at 30°C and e) shows it for 1mm samples immersed at ambient temperature. Error bars come from error in the fits.

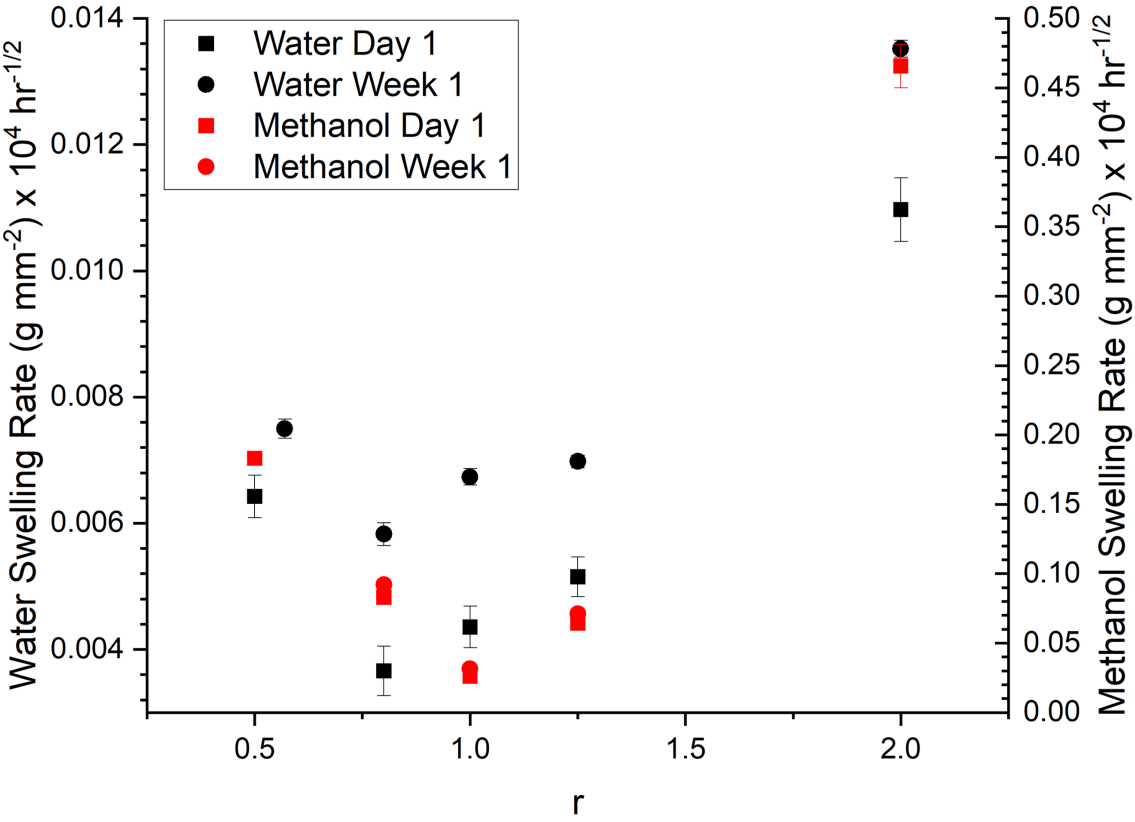

Figure 6.9: Rate of uptake for 1mm-thick non-solvent samples of $0.5 \leq r \leq 2$ immersed in 30°C water and methanol. Results are shown for the rate of uptake over the first day of immersion in solvent and over the course of the rest of the first week. Error bars show error in fitting.

Figure 6.7 shows also that non-solvent samples cured with DMP-30 had a higher uptake than those cured without. It is not completely clear why this was the case. There still could be the effect of homopolymerization resulting in more excess amine for those formulations with less excess amine. However, this does not explain why $r = 0.57$ NS with DMP-30 had higher uptakes than $r = 1$ NS. It should have no excess amine whereas we believe that $r = 1$ NS does. The homopolymerized network should also have a higher crosslink density than the polymerized epoxy-amine network. These two factors should both result in a higher uptake in $r = 1$ NS than $r = 0.57$ NS with DMP-30. We currently have two theories that attempt to explain this increased uptake in water for non-solvent samples when cured with DMP-30. Firstly it could be due to the increased crosslink density raising the average size of free volumes in the network despite lowering the FFV, as shown in figure 6.3. Water would enter these larger voids, but would not swell them enough to gain access to other voids, leading to greater uptake in samples of greater free volume sizes as opposed to greater FFV. Methanol on the other hand did swell these voids to a great enough degree that it could enter voids, resulting in greater uptake for samples with larger FFV. The alternative hypothesis

comes from the ability of water to form hydrogen bonds with the two networks. Both contain groups that can form hydrogen bonds, the homopolymerized network containing ether groups and the epoxy-amine network containing hydroxyl groups, but it has been postulated that the differences in density of these groups in the two networks allows for more water to form hydrogen bonds with the homopolymerized network. However, both these hypotheses do not explain why uptake decreases in non-solvent samples cured with DMP-30 as stoichiometry decreases. The increased proportion of homopolymerization should raise uptake, as crosslink density increases and ether group density becomes more suitable for hydrogen-bonding with water.

Solvent samples generally showed greater uptake than non-solvent samples when immersed in water. The difference was less than when immersed in methanol, with a number of solvent samples having similar or less uptake than non-solvent samples cured with DMP-30. Again this change is explained by water being more able to easily form hydrogen bonds than methanol. The epoxy-amine network contains hydroxyl groups with which water can form hydrogen bonds. This would reduce the difference in uptake between entering the polymer network and the empty space present in solvent samples. However, this free space available in the solvent samples still has an influence on uptake. Due to the error in uptake in solvent samples when immersed in water, it is difficult to determine whether there was a difference in uptake between solvent samples of different stoichiometry and when cured with DMP-30.

Samples cured with solvents routinely showed a drop in uptake after a period of uptake. The time at which the rate of mass loss exceeded that of uptake is shown in figure 6.10 for solvent samples immersed in methanol and in figure 6.11 for those immersed in water. This point was determined by fitting a Bigaussian fit in OriginPro to determine the point of peak uptake [37]. Although uptake and mass loss are both expected to be a diffusion process, this fit did provide a good estimate for this peak uptake point. Samples that did not show this peak i.e. did not reach a point in which the rate of mass loss was greater than uptake, did not have their results shown. If a good fit could not be reached, such as in the case peak uptake occurred between the first and second day when there was a clear gap in results, the peak time was estimated from the last point of positive uptake and the first point of negative uptake. These results are shown in figures 6.10 and 6.11.

For samples immersed in methanol, the only exceptions were in the 1mm 30°C results in figure 6.10 c), in which r=0.57 with DMP-30 had a lower peak time than expected and in figure 6.10 d), in which the solvent samples cured with DMP-30 had near-identical peak times. For water samples, the exceptions were in 1mm samples immersed in 30°C water and ambient water (figures 6.11 c) and e), respectively) where there were greater peak times in the solvent samples of r=1 than r=0.8.

The reduced time at which point the rate of mass loss exceeds that of uptake is concluded to come from increased void size in samples with faster cure rates. These larger voids would constitute a more heterogeneous network. There would be a greater num-

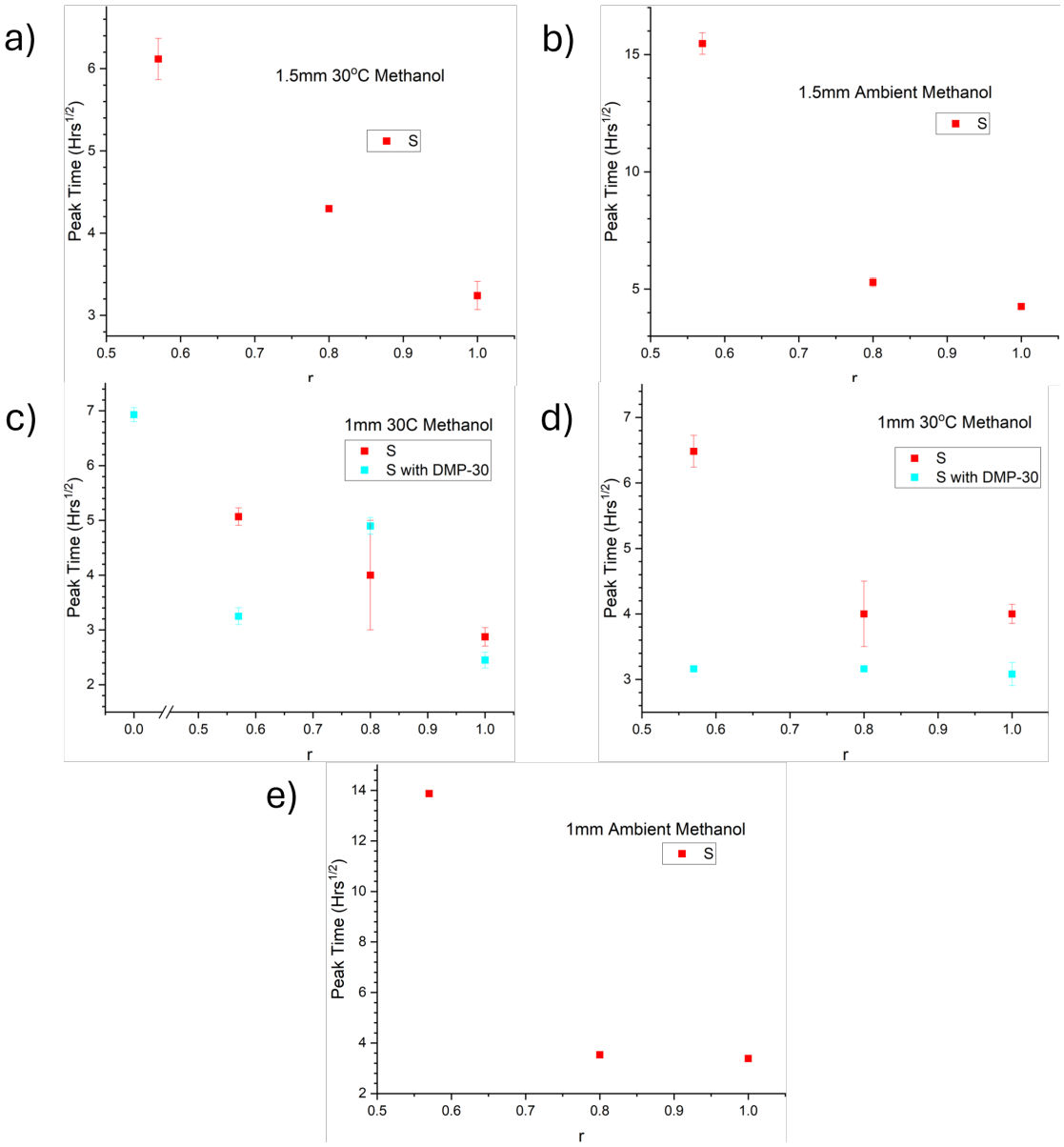

Figure 6.10: Times at which the rate of mass loss exceeds that of uptake in epoxy-amines cured with solvents, for samples immersed in methanol. a) shows that of 1.5mm thick samples immersed in methanol at 30°C. b) shows that of 1.5mm thick samples immersed in methanol at ambient temperature. c) and d) shows that of 1mm thick samples immersed in methanol at 30°C. e) shows that of 1mm thick samples immersed in methanol at ambient temperature. Error comes from error in the fit used to determine this peak uptake, or from estimating the point of maximum uptake.

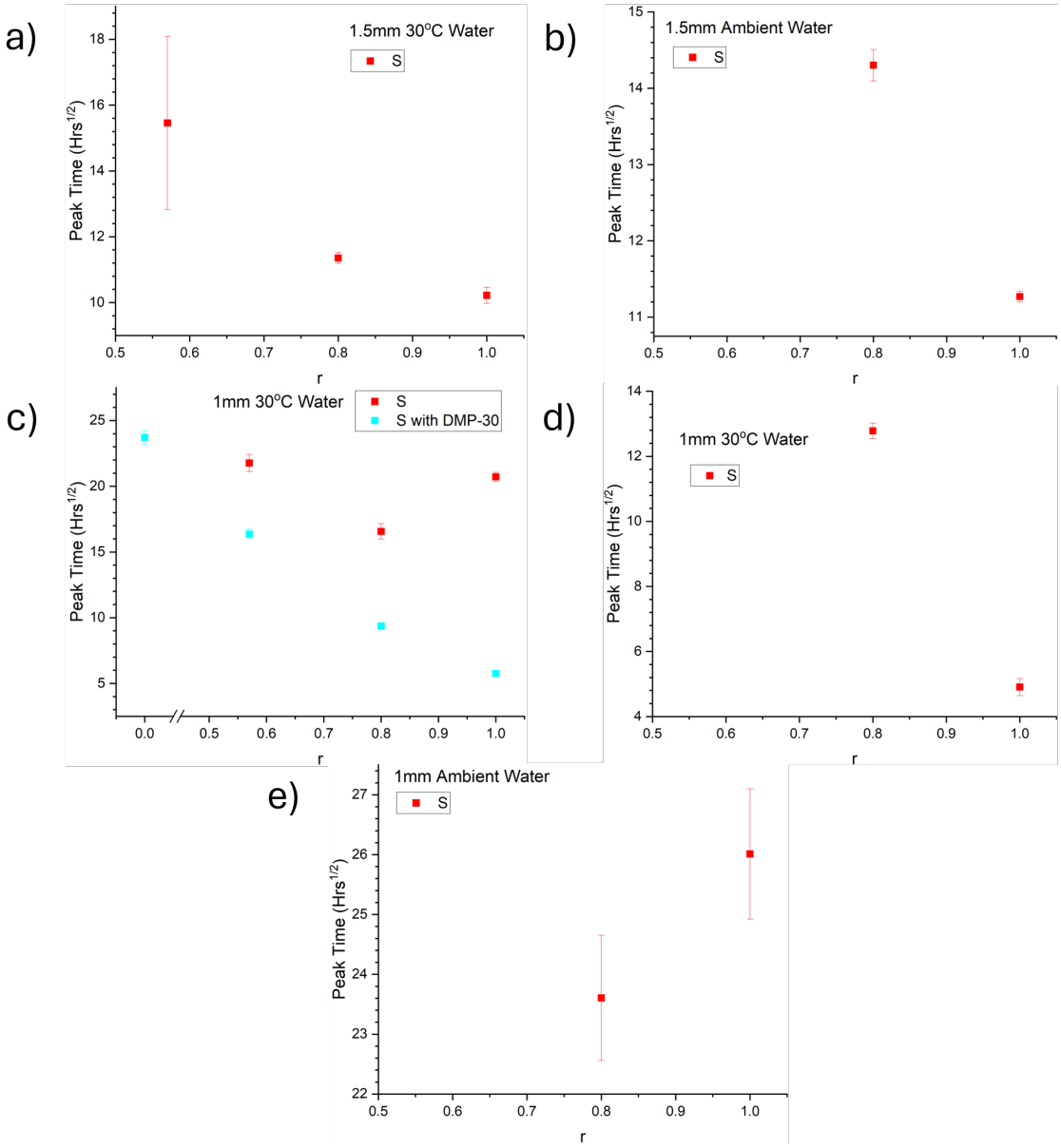

Figure 6.11: Times at which the rate of mass loss exceeds that of uptake in epoxy-amines cured with solvents, immersed in water. a) shows that of 1.5mm thick samples immersed in water at 30°C. b) shows that of 1.5mm thick samples immersed in water at ambient temperature. c) and d) shows that of 1mm thick samples immersed in water at 30°C. e) shows that of 1mm thick samples immersed in water at ambient temperature. Error comes from error in the fit used to determine this peak uptake, or from estimating the point of maximum uptake.

ber of smaller, separate parts of epoxy-amine in these networks, parts that are not covalently bonded to other parts of the network. These parts, held to the rest of the network by weaker intermolecular forces, could break off more easily when immersed in solvent, resulting in greater mass loss in these more heterogeneous networks. In these cases, there is a time of initial uptake into voids in the samples. Once these voids have been filled, uptake decreases. More isolated parts of the network, with fewer crosslinks would be less strongly bound. They would therefore be more susceptible to breaking off into the solvent and being leached out into the solvent over time. In this way, mass loss increases after initial uptake. From figures 6.10 and 6.11, the time of peak uptake decreased to shorter times with the inclusion of DMP-30, indicating that this change lead to an increased mass loss. As previously stated, DMP-30 should raise the rate of conversion, and so produce larger voids and a more heterogeneous network than when curing without. It is this increase in heterogeneity that lead to an increased mass loss. Three sets of samples immersed in water, 1.5mm samples at ambient temperature and 1mm samples cured at 30°C and ambient temperature (figures 6.11 b), d) and e), respectively) show no peak for solvent samples of r=0.57. These samples should have smaller voids than those of r=0.8 and 1, leading to there being no point at which the rate of mass loss exceeds uptake. For epoxy-amines, methanol is a stronger swelling agent than water. It can therefore probe the smaller voids in r=0.57 and leach out more epoxy-amine. There is therefore always a point at which mass-loss exceeds uptake in these formulations when immersed in methanol, but not in water.

The methanol results from figure 6.10 mirrored the methanol uptake measurements from figure 6.6, supporting the hypthesis of uptake mechanisms in solvent samples depending on cure rate. The water results in figure 6.11 showed these trends despite them not being evident in the water uptake results from figure 6.8. The mass loss rate results show that mechanisms for solvent samples also depend on cure rate when immersed in water. Due to the reduced uptake when immersed in water, the mass loss could have a greater influence on overall uptake in those immersed in methanol, where uptake is much higher. This mass loss therefore could have obscured or distorted the difference in uptake in solvent samples as stoichiometry was changed.

6.3.3 Drying

The initial rate of drying was measured for 1.5mm and 1mm samples previously immersed in 30°C methanol, 1.5mm samples immersed in water at ambient temperature and 1mm samples immersed in 30°C water. The results are shown in figure 6.12.

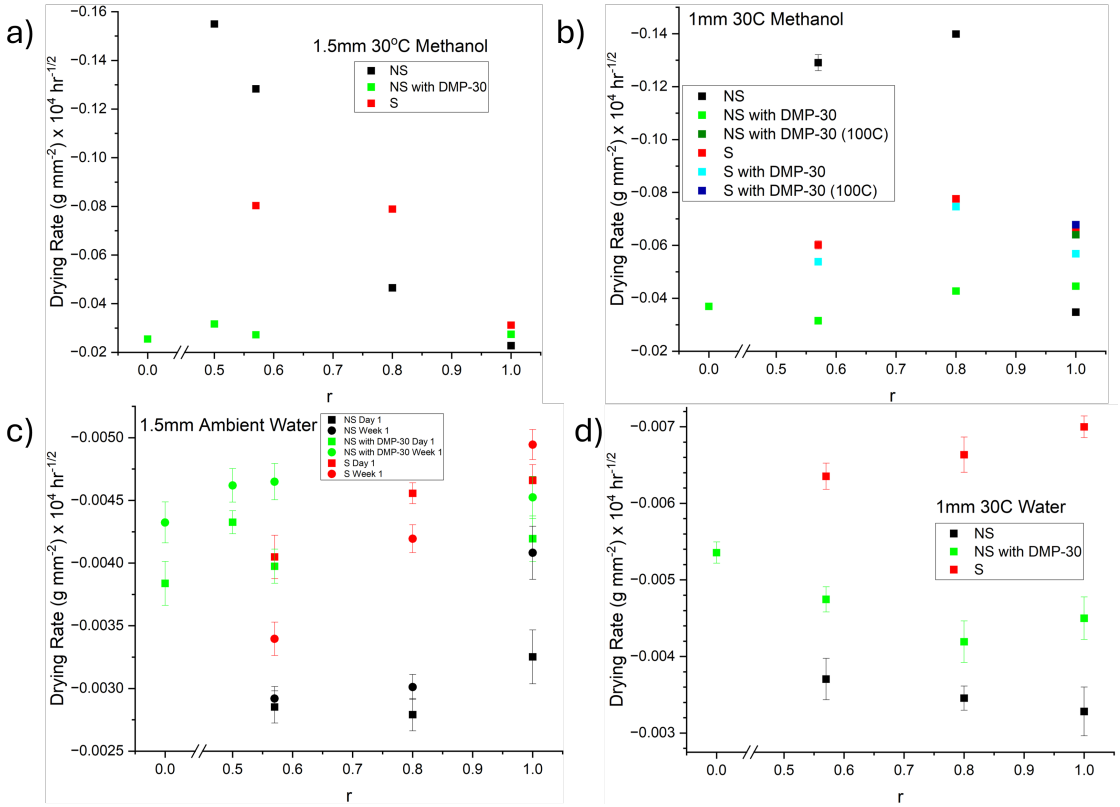

Figure 6.12: Drying rate measurements of epoxy-amine samples after reaching apparent equilibrium during uptake. a) shows 1.5mm samples immersed in 30°C methanol, its corresponding uptake shown in figure 6.6 a). b) shows 1mm samples immersed in 30°C methanol, its corresponding uptake shown in figure 6.6 c). c) shows 1.5mm samples immersed in water at ambient temperature, its corresponding uptake shown in figures 6.7 b) and 6.8 b). d) shows 1mm samples immersed in 30°C water, its corresponding uptake shown in figure 6.7 d) and 6.8 d). All results are for the first day of drying, aside from c), which shows results for both the initial day of drying and for the subsequent week.

Similarly to the uptake results, the drying rate is greater for samples immersed in methanol, and for those at elevated temperatures. For samples immersed in methanol, the drying rate is similar for non-solvent samples compared to their uptake, shown in figure 6.6. The solvent samples however show reduced uptake. This may be due to the difference in bonds between the solvent and non-solvent samples. In non-solvent samples, the methanol would mainly form bonds with the polymer network, via hydrogen bonding and dipole-dipole bonding. In solvent samples, methanol would mainly enter voids, bonding with other methanol molecules. These methanol-methanol bonds would be stronger than the methanol-network bonds. There would therefore be proportionally less evaporation of methanol from voids in solvent samples than from the network in non-solvent samples. The drying rate of samples previously immersed in water is

similar in magnitude to their uptakes, shown in figures 6.7 and 6.8. The differences in drying between the different formulations also follows the same trends. Water can only form hydrogen-bonds. It is therefore bonded in this way throughout the samples, both when it is bonded to itself in voids, or when it is bonded to the polymer network. Evaporation of water therefore only depends on the volume it has taken up, resulting in drying rate being similar to uptake rate.

6.4 Conclusions

The solvent uptake over time of cured epoxy-amines was measured in order to determine how changes in formulation affects solvent ingress. Cured samples were made of stoichiometric ratio and excess epoxy, with and without curing solvents (xylene and butanol) and with and without the homopolymerizing agent DMP-30. Samples were immersed in water or methanol and weighed periodically to determine uptake over time. In all samples, solvent uptake was shown to be Fickian in nature. Greater uptake of methanol than water meant that uptake trends were clearer for samples immersed in methanol than in water.

The magnitude and initial rate of uptake was greater for samples cured with solvents. The current hypothesis is that solvents separate from the epoxy-amine mixture during curing, before they evaporate. This leaves 'voids,' areas of low crosslink density. Increased uptake of solvent comes from these solvents being able to enter the voids. Uptake increased in solvent samples in formulations as stoichiometry approached one, and DMP-30 was used. These both raise cure rate, meaning that as solvents evaporate, the epoxy-amine network is more fully-formed, therefore more viscous and so cannot enter the voids as much, leading to overall increased void sizes. Almost all solvent samples showed mass loss after a period of uptake. Similarly to the trends in uptake, this mass loss occurred in solvent samples as stoichiometry approached one, and when DMP-30 was used. Again, an increased rate of cure leads to more voids and a more heterogeneous polymer network. There will therefore be greater amounts of the network not bonded to other parts by covalent bonds, meaning they can be leached from the network during immersion in solvent. Upon drying solvent samples immersed in methanol, there was less mass loss than expected in comparison to non-solvent samples. In non-solvent samples, where there are no voids, methanol enters the network. Methanol in non-solvent samples is more likely to form intermolecular bonds with the polymer network, whereas in solvent samples, methanol in voids are more likely to form intermolecular bonds with other methanol molecules. These methanol-methanol bonds are stronger than the methanol-network bonds. Methanol in voids present in solvent samples therefore require more energy to evaporate, resulting in reduced mass loss during drying.

Uptake in non-solvent samples, which do not contain voids, was dependent on the crosslink density and the presence of hydrogen-bonding sites in the network, agreeing with previous uptake measurements into polymer networks [12, 16, 17, 19, 22]. This dependence on h-bonding sites was more critical for water uptake than methanol. For

methanol, there was a minimum uptake at r=1, with formulations of excess amine having greater uptake due to the greater density of h-bonding sites in MXDA than in UC0003. Formulations utilizing DMP-30 exhibited methanol uptakes similar to that of r=1, due to increased crosslink density from excess epoxy being homopolymerized. Uptake decreased as the proportion of the network being homopolymerized increased, due to this network having a higher crosslink density than the epoxy-amine network. These results agreed with PALS result, which showed a reduced fraction of free volume in non-solvent samples as stoichiometry approached one and when DMP-30 was used. Water uptake displayed a minimum in non-solvent samples at r=0.8. At lower stoichiometries, excess epoxy lowers crosslink density, raising uptake. Above this, there is excess amine, increasing h-bonding density. Although conversion is greater in r=1 than r=0.8, there would be some excess amine due to incomplete cure, raising water uptake. There was some confusion in the uptake of non-solvent samples cured with DMP-30 when immersed in water. Uptake was greater than equivalent formulations cured without DMP-30, indicating that the presence of the homopolymerized network leads to greater uptake. Two possibilities were raised. Firstly, the h-bonding site density is greater in the homopolymerized network than the epoxy-amine network, outweighing the raised crosslink density when immersed in water. Alternatively, PALS results show an increased size of free volumes in non-solvent samples as fractional free volume increased. Water, which is not as good a swelling agent of the epoxy-amine network as methanol, would be able to enter the larger free volumes initially available, but not the overall larger amount of free volume in the entirety of the polymer network. Uptake would therefore increase as crosslink density increased. However, neither of these hypotheses can explain why uptake subsequently decreased as the proportion of homopolymerized network increased. It is likely that there is another cause for this oddity in water uptake. Non-solvent samples of stoichiometries $r < 0.7$ showed mass loss after initial uptake. These formulations do not reach gel point. Subsequently, uncured epoxy leaches from the network during immersion.

The results show clear trends in uptake of epoxy-amines. In non-solvent samples, uptake decreased with crosslink density, as expected, and with h-bonding site density. Solvent samples showed increased uptake. This gave support to the hypothesis that curing samples cause voids to appear in the resultant sample. Formulations of solvent samples with increased cure rate displayed greater uptake, likely due to this producing voids of greater sizes. Differences in uptake trends when immersing samples in water and methanol allowed information to be obtained on both the physical and chemical nature of the epoxy-amine networks, highlighting the benefit of using different solvents. Due to mass loss, difficulties in fully drying samples, and sample damaged throughout measurements, final solvents were not measured. It would be beneficial to determine this final uptake to ascertain more information on the structure of these epoxy-amines and to properly determine diffusion constants. To reduce error and uncertainty, samples of one thickness should be used; and higher, more controlled temperatures to reach this final uptake faster. Furthermore, samples of more different stoichiometries could be used to investigate how this affects uptake. Specifically, stoichiometries around

r=1, to determine how excess amine and epoxy affect uptake, and stoichiometries of $r < 0.5$ with DMP-30, to investigate majority homopolymerized networks.

Bibliography

[1] E. Duemichen et al. "Analyzing the network formation and curing kinetics of epoxy resins by in situ near-infrared measurements with variable heating rates". In: *Thermochimica Acta* 616 (2015), 49–60. DOI: 10.1016/j.tca.2015.08.008.

[2] P. A. Sørensen et al. "Anticorrosive coatings: a review". In: *Journal of Coatings Technology and Research* 6.2 (2009), pp. 135–176. DOI: 10.1007/s11998-008-9144-2.

[3] Fred Meyer et al. "The effect of stoichiometry and thermal history during cure on structure and properties of epoxy networks". In: *Polymer* 36.7 (1995), 1407–1414. DOI: 10.1016/0032-3861(95)95918-q.

[4] E. B. Caldona, D. O. Wipf, and D. W. Smith. "Characterization of a tetrafunctional epoxy-amine coating for corrosion protection of mild steel". In: *Progress in Organic Coatings* 151 (2021). DOI: 10.1016/j.porgcoat.2020.106045.

[5] John D. McCoy et al. "Cure mechanisms of diglycidyl ether of bisphenol A (DGEBA) epoxy with diethanolamine". In: *Polymer* 105 (2016), 243–254. DOI: 10.1016/j.polymer.2016.10.028.

[6] M. Hesabi, A. Salimi, and M. H. Beheshty. "Effect of tertiary amine accelerators with different substituents on curing kinetics and reactivity of epoxy/dicyandiamide system". In: *Polymer Testing* 59 (2017), pp. 344–354. DOI: doi.org/10.1016/j.polymertesting.2017.02.023.

[7] J. Ehlers et al. "Theoretical Study of the Epoxy-Amine Curing Reaction". In: *Macromolecules* 40.12 (2007), pp. 4370–4377. DOI: 10.1021/ma070423m.

[8] K. C. Cole, J. J. Heckler, and D. Noel. "A New Approach to Modeling the Cure Kinetics of Epoxy Amine Thermosetting Resins. 2. Application to a Typical System Based on Bis[4- (diglycidylamino)phenyl]methane and Bis(4-aminophenyl) Sulfone". In: *Macromolecules* 24.11 (1990), pp. 3098–3110. DOI: 10.1021/ma00011a012.

[9] V. L. Zvetkov. "A Modified Kinetic Model of the Epoxy-Amine Reaction". In: *Macromolecular Chemistry and Physics* 203.3 (2002), pp. 467–476. DOI: 10.1002/1521-3935(20020201)203:3<467::AID-MACP467>3.0.CO;2-Q.

[10] G. Zhang et al. "Permeable epoxy coating with reactive solvent for anticorrosion of concrete". In: *Progress in Organic Coatings* 117 (2018), pp. 29–34. DOI: 10.1016/j.porgcoat.2017.12.018.

[11] A. R. Marrion. *The Chemistry and Physics of Coatings*. 2nd ed. The Royal Society of Chemistry, 2004.

[12] C. Yi et al. "Curing kinetics and mechanical properties of epoxy based coatings: The influence of added solvent". In: *Progress in Organic Coatings* 124 (2018), pp. 165–174. DOI: 10.1016/j.porgcoat.2018.08.009.

[13] M. Dušková-Smrčková, K. Dušek, and P. Vlasák. "Solvent activity changes and phase separation during crosslinking of coating films". In: *Macromolecular Symposia* 198.1 (2003), pp. 259–270. DOI: 10.1002/masy.200350822.

[14] T. Nguyen, J. B. Hubbard, and J. M. Pommersheim. "Unified model for the degradation of organic coatings on steel in a neutral electrolyte". In: *JCT, Journal of Coatings Technology* 68.855 (1996), 45–56.

[15] C. M. Sahagun and S. E. Morgan. "Thermal Control of Nanostructure and Molecular Network Development in Epoxy-Amine Thermosets". In: *ACS Applied Materials and Interfaces* 4.2 (2000), pp. 564–572. DOI: 10.1021/am201515y.

[16] M. Jackson et al. "Effect of free volume hole-size on fluid ingress of glassy epoxy networks". In: *Polymer* 52.20 (2011), pp. 4528–4535. DOI: 10.1016/j.polymer.2011.07.042.

[17] J. Wang et al. "Effect of curing agent polarity on water absorption and free volume in epoxy resin studied by PALS". In: *Nuclear Instruments and Methods in Physics Research Section B: Beam Interactions with Materials and Atoms* 268.14 (2010), pp. 2355–2361. DOI: 10.1016/j.nimb.2010.04.010.

[18] S. Morsch et al. "Mapping water uptake in organic coatings using AFM-IR". In: *Faraday Discussions* 180 (2015), pp. 527–542. DOI: 10.1039/c4fd00229f.

[19] M. R. VanLandingham, R. F. Eduljee, and J. W. Gillespie. "Moisture diffusion in epoxy systems". In: *Applied Polymer Science* 71.5 (1999), pp. 787–798. DOI: 10.1002/(SICI)1097-4628(19990131)71:5<787::AID-APP12>3.0.CO;2-A.

[20] M. Lai et al. "An experimental–numerical study of moisture absorption in an epoxy". In: *Composites Part A: Applied Science and Manufacturing* 43.7 (2012), pp. 1053–1060. DOI: 10.1016/j.compositesa.2012.01.027.

[21] J. Mijović and H. Zhang. "Molecular Dynamics Simulation Study of Motions and Interactions of Water in a Polymer Network". In: *The Journal of Physical Chemistry B* 108.8 (2003), 2557–2563. DOI: 10.1021/jp036181j.

[22] L. C. Soles et al. "Contributions of the nanovoid structure to the kinetics of moisture transport in epoxy resins". In: *Journal of Polymer Science Part B: Polymer Physics* 38.5 (2000), pp. 776–791. DOI: 10.1002/(SICI)1099-0488(20000301)38:5<776::AID-POLB15>3.0.CO;2-A.

[23] C. Bockenheimer, Fata. D., and W. Possart. "New aspects of aging in epoxy networks. II. Hydrothermal aging". In: *Journal of Applied Polymer Science* 91.1 (2003), pp. 369–377. DOI: 10.1002/app.13093.

[24] G. Pitarresi et al. “Absorption kinetics and swelling stresses in hydrothermally aged epoxies investigated by photoelastic image analysis”. In: *Polymer Degradation and Stability* 111 (2015), pp. 55–63. DOI: 10.1016/j.polymdegradstab.2014.10.019.

[25] L. C. Soles et al. “Contributions of the nanovoid structure to the moisture absorption properties of epoxy resins”. In: *Journal of Polymer Science Part B: Polymer Physics* 36.17 (1998), pp. 3007–3154. DOI: 10.1002/(SICI)1099-0488(199812)36:17<3035::AID-POLB4>3.0.CO;2-Y.

[26] T. Wang et al. “Methanol degradation mechanisms and permeability phenomena in novolac epoxy and polyurethane coatings”. In: *Journal of Coatings Technology and Research* 18 (2021), 831–842. DOI: 10.1007/s11998-020-00446-w.

[27] S. O. Han and L. T. Drzal. “Water absorption effects on hydrophilic polymer matrix of carboxyl functionalized glucose resin and epoxy resin”. In: *European Polymer Journal* 39.9 (2003), pp. 1791–1799. DOI: 10.1016/S0014-3057(03)00099-5.

[28] J. Zhou and J. P. Lucas. “Hygrothermal effects of epoxy resin. Part I: the nature of water in epoxy”. In: *Polymer* 40.20 (1999), pp. 5505–5512. DOI: 10.1016/S0032-3861(98)00790-3.

[29] O. Starkova et al. “Anomalous water diffusion in epoxy/carbon nanoparticle composites”. In: *Polymer Degradation and Stability* 164 (2019), pp. 127–135. DOI: 10.1016/j.polymdegradstab.2019.04.010.

[30] F. Korkees, R. Swart, and I. Barsoum. “Diffusion mechanism and properties of chemical liquids and their mixtures in 977-2 epoxy resin”. In: *Polymer Engineering and Science* 62.5 (2022), pp. 1582–1592. DOI: 10.1002/pen.25946.

[31] Merck KgaA. *o-Xylene*. https://shorturl.at/uxISQ [Accessed: (28/09/23)]. 2023.

[32] Honeywell International Inc. *1-Butanol*. https://lab.honeywell.com/shop/1-butanol-537993 [Accessed: (28/09/23)]. 2023.

[33] Martin Petriska, Stanislav Sojak, and Vladimir Slugen. “Positron lifetime setup based on DRS4 evaluation board”. In: *Journal of Physics: Conference Series* 505 (Apr. 2014), p. 012044. DOI: 10.1088/1742-6596/505/1/012044.

[34] Morten Eldrup, D Lightbody, and John Neil Sherwood. “The temperature dependence of positron lifetimes in solid pivalic acid”. In: *Chemical Physics* 63.1-2 (1981), pp. 51–58.

[35] SJ Tao. “Positronium annihilation in molecular substances”. In: *The Journal of Chemical Physics* 56.11 (1972), pp. 5499–5510.

[36] S. Alessi et al. “Study of the Curing Process of DGEBA Epoxy Resin Through Structural Investigation”. In: *Macromolecular Chemistry and Physics* 216.5 (2015), pp. 538–546. DOI: 10.1002/macp.201400510.

[37] OriginLab Corporation. *30.4.1 Bigaussian*. https://www.originlab.com/doc/en/Origin-Help/Bigaussian-PAFunc [Accessed: (04/09/24)].

Chapter 7

Conclusions

7.1 Overview of Aims

The investigations in this PhD aimed to determine many important aspects of crosslinked epoxy-amine networks and their related properties. This was carried out in relation to their use as anti-corrosive coatings, specifically in their eventual failure to prevent corrosion. Network properties were measured for changes in stoichiometry, the use of a tertiary amine homopolymerizing agent, and when curing with solvents.

Samples of epoxy-amines were cured with and without solvent, both with and without a homopolymerizing agent. The epoxy used was DER331, a bisphenol A based epoxy. The amine used was m-Xylyenediamine (MXDA). Stoichiometric ratio and excess formulations were used. The amount of DMP-30 and solvents used, when they were used, was always kept constant. The homopolymerizing agent was 2,3,6-tris(dimethylaminomethyl)phenol (DMP-30). A quantity of DMP-30 equivalent to 3% of the moles of epoxy groups used. The solvents used were xylene and butanol, in a ratio of 3:1 xylene:butanol by mass. It was mixed with the epoxy and amine so that the solvents made up a total of 40% of the total mixture mass.

Three separate investigations were carried out over the course of this PhD investigating the network structures of epoxy-amine networks, as well as initially investigating an optimal cure procedure for these epoxy-amines:
1) Determining curing procedure for the epoxy-amines investigated that produced a consistent, optimal glass transition temperatures (T_g). This involved a pre-cure stage that aimed to mix the constituent components of the polymer together to obtain a consistent final T_g, and a curing regime that aimed to produce a maximum T_g. This was done for epoxy-amines cured with and without solvents, with and without DMP-30 and of stoichiometric ratio and excess epoxy.
2) Investigating the ability of the homopolymerizing agent, DMP-30, in homopolymerized all excess epoxy in epoxy-amines, and to form a homogenous epoxy-amine polymer network. Epoxy conversion and the final, fully cured, T_g of non-solvent samples of stoichiometric ratio and excess epoxy, cured with and without DMP-30, were investigated.

The final glass transition temperatures of formulations were measured via differential scanning calorimetry (DSC). Conversions during cure were also measured via DSC and near-infrared spectroscopy for non-solvent samples.
3) Investigating the internal structures of epoxy-amines, and how they are affected when solvents are used in the curing process. Network structures at multiple length scales were measured using small-angle neutron scattering (SANS). Epoxy-amines were made with deuterated epoxy in order to provide a contrast between this epoxy and the hydrogenous amine. Measurements were taken for dry samples as well as those immersed in water and methanol, in order to determine how uptake affected these network structures. Epoxy-amines of stoichiometric ratio and excess epoxy, and with and without DMP-30 also had network structures probed by SANS
4) Investigating the solvent uptake characteristics of epoxy-amines in order to understand uptake mechanisms and further understand network properties of epoxy-amines cured with and without solvents. Samples were immersed in water and methanol over a period of months, giving information on the physical and chemical nature of the epoxy-amine networks. Samples cured with and without solvent, with and without DMP-30, and of stoichiometric ratio and excess amine, were utilized in this investigation.

7.2 Experimental Conclusions

7.2.1 Sample Preparation

Samples creation can be split into two parts: pre-cure and cure. Optimization of the overall preparation procedure was determined by T_g measurements. For pre-cure, this would be a consistent T_g, showing the mixture had been optimally distributed. For the cure, this was a maximum T_g, showing that all the epoxy conversion reactions had occured. The curing regime is shown in table 7.1. All samples ended up displaying a consistent T_g that was considered to be a maximum, apart from solvent samples cured with DMP-30, which were not consistent between individual samples. It may be the case that more time is needed to distribute DMP-30 amongst epoxy when also mixing solvents. Work would need to be done in the future to determine the pre-cure regime required to optimise the solvent samples cured with DMP-30.

Pre-cure involved mixing the constituent parts of the formulations so that they were optimally distributed before curing. For non-solvent samples, a five-minute stir using a glass rod provided adequate mixing of the components. A high-speed rotating speed mixer was also found to distribute the mix sufficiently. For solvent samples, a pre-cure regime of four five-minute stirs with 15-minute wait periods in between, followed by a final 45-minute wait period was required. These samples had to be stirred using a glass rod that would mix the solvents together with the epoxy-amine. The speed mixer would leave the solvent layer separate from the epoxy-amine layer.

Non-solvent samples were cured for two hours at 60°C, then one hour at 100°C and then one hour at 160°C. Solvent samples required this cure as well as an additional 200°C cure. All samples were cured in an air oven as it was found that any carbamation

or oxidation that occured did not affect the final T_g. Non-solvent samples were cured in PTFE moulds. Solvent samples were cured in silicone moulds. The non-solvent samples could not be cured in the silicone moulds as it was found that the final samples contained bubbles. This is most likely due to the silicone mould absorbing moisture which evaporated during cure. Solvent samples did not contain any bubbles. This is believed to be due to the solvent samples being less viscous, allowing the evaporating bubbles to leave. Solvent samples could not be cured in the PTFE moulds as they were found to crack, most likely due to the less-flexible PTFE not accommodating changes in size in the solvent samples as solvent evaporated.

	Non-Solvent	Solvent
Pre-cure	Glass rod or speed mixer 1 × 5 minute stir	Glass rod 4 × 5 minute stir + 15 minute wait + additional 45 minute wait
Cure	PTFE Moulds 1 hour at 60°C + 1 hour at 100°C + 1 hour at 160°C	Silicone Moulds 1 hour at 60°C + 1 hour at 100°C + 1 hour at 160°C + 1 hour at 200°C

Table 7.1: Pre-cure and curing regimes for epoxy-amine samples cured with and without solvent.

7.2.2 Polymer Network Structures and the Kinetics of Cure

The final conversions of epoxy-amines cured with and without DMP-30 was as expected. For those without DMP-30, the conversion decreased as the level of excess amine decreased. With the addition of DMP-30, the final conversion appeared to be around 100%, regardless of the level of excess epoxy. This is due to the presence of DMP-30 allowing the excess epoxy to homopolymerize. Furthermore, the T_g of solvent samples were slightly less ($\sim$ 10°C) than their counterparts of equal stoichiometry cured without solvent. This drop has been reported before. The similarity between solvent and non-solvent samples indicates that the epoxy-amine network is unaffected by the presence of solvent.

The T_g of the fully homopolymerized network was only slightly greater than that of the fully polymerized network. This similarity is expected: DER331 and MXDA have similar structures, with both containing phenol groups. The increased T_g comes from an increased crosslink density or otherwise reduced flexibility in the homopolymerized network. Formulations cured with both MXDA and DMP-30, with excess epoxy, show similar T_g's to that of a sample of stoichiometric ratio, cured only with MXDA. Furthermore, these formulations display only one T_g, with a range lower than those of the same stoichiometry cured only with MXDA. These facts give evidence that the homopolymerized and polymerized bonds are all part of the same network.

The addition of DMP-30 has been shown to raise the rate of conversion in epoxy-amines, both at abient and elevated temperatures. This increased rate is at least partially due to additional conversion from homopolymerization. It is however unclear how much of this increase in conversion is due to DMP-30 also accelerating the epoxy-amine reaction. The homopolymerization reaction is slower than the epoxy-amine reaction with MXDA. For samples cured at ambient temperature, the T_g of epoxy amines increases for each stoichiometry when DMP-30 is included. However, the T_g still decreases in samples with DMP-30 as the level of excess epoxy is increased. The conversion also decreases in these samples as the level of excess epoxy is increased when sent through a curing regime of -80°C to 200°C at 10°Cmin^{-1}. The level of excess epoxy increases requires increased homopolymerization and reduced epoxy-amine polymerization. The subsequent reduction in T_g and conversion shows homopolymerization is slower than epoxy-amine polymerization (when using 3% DMP-30).

Enthalpy of reaction results showed that the kinetics of the homopolymerization reaction differed from the epoxy-amine polymerization reaction. For a pure epoxy-amine reaction, the enthalpy of reaction showed one peak. With the inclusion of DMP-30, a second peak formed at a higher temperature as the level of excess epoxy, and therefore the level of homopolymerization, increased. As time at ambient temperature increased, the enthalpy of this initial peak decreased so that only the higher temperature peak remained. This appeared to show that the homopolymerization reaction includes a step that occurs less at lower temperatures than the epoxy-amine reaction and the initial homopolymerization reaction. There was one oddity in the samples without DMP-30 in that all formulations had the same peak enthalpy temperature aside from the stoichiometric formulation. This displayed a lower peak enthalpy temperature. We are unsure why this is the case.

The T_g of the stoichiometric ratio formulation with DMP-30 has a lower T_g than stoichiometric ratio without DMP-30 and all the other stoichiometries with DMP-30. This is unexpected. This appears to be due to a reaction that occurs at ∼150°C. This is believed to be occur on the polymer network as it is believed that for a stoichiometric non-solvent formulation, most of the polymerization has occurred by the end of the 100°C section of the cure. Solid-state NMR results show a peak appearing at ∼48 PPM after this reaction has occurred. This peak does not appear in any formulations without DMP-30, or with excess epoxy. This reaction requires the polymer network, amine and DMP-30. Once it occurs it does not occur again. It is possible that this is due to the DMP-30 and/or excess amine being consumed in the reaction.

Near-infrared spectroscopy was used to measure conversion during cure by measuring the change in a peak associated with the epoxy ring. These results were found to conflict with conversion as measured by enthalpy of reaction via DSC. The DSC results were simpler and therefore more trusted. Determining the area of the epoxy ring peak via fitting of peaks also did not work. The number of neighbouring peaks made this method more time-consuming and ultimately more prone to error.

7.2.3 Network Structures From SANS

SANS measurements can be split into three different regimes: low, mid and high-Q. These regimes describe the structures of network heterogeneities, the structure of the polymer network and the spacing between individual monomers, respectively.

Low-Q measurements indicated that non-solvent samples were homogeneous. The Porod exponent was between 3 and 4, pointing towards a smooth structure. They also had a minimal Porod scale result, implying that this Q-range could not measure any heterogeneities. The scattering at low-Q did not change for non-solvent samples when immersed in water or methanol, as there were no heterogeneities for these solvents to enter. Solvent samples displayed a Porod scale between 10^{-5} and 10^{-7}, indicating the presence of heterogeneities in this Q-range. They also had Porod exponent results between 2 and 3, showing that the interfaces between these heterogeneities were not smooth. It is believed that there is phase separation between solvents and the epoxy-amine network during curing. As the solvent evaporates, it leaves behinds voids. These voids are the heterogeneities in solvent samples. Upon immersion in water, the Porod exponent decreased. This was taken to mean to the water was entering voids and swelling them to greater size. The Porod exponent decreased. This meant the heterogeneities were getting smoother, which was unexpected. It was thought that they would get rougher as loose polymer chains formed h-bonds with the water, splitting up the network around the heterogeneities. Upon immersion in methanol, the Porod exponent and scale for the solvent samples looked the same as those of the non-solvent samples. It is thought that the methanol swelled the heterogeneities in the solvent samples to a size too large to be detected from this SANS setup. They therefore appeared homogeneous, like the non-solvent samples.

From the mid-Q measurements, it was determined that correlation lengths were similar for both samples of all formulations. This shows that despite the heterogeneities at larger length scales, the actual polymer structure is similar for all samples, whether cured with DMP-30 or solvents. This agrees with the T_g results discussed in section 7.2.2. The correlation lengths also remain unchanged when immersed in water and methanol. These solvents can enter the heterogeneities, but they do not affect the polymer network, at least not enough to be measured from our results. Intensity measurements in this mid-Q regime show a greater intensity for solvent samples. This is believed to come from heterogeneities of smaller length scale. There was little change in intensity in solvent samples when immersed in water, but there was a clear change when immersed in methanol. This is because water cannot enter these smaller heterogeneities, but methanol can, being a better swelling agent. For non-solvent samples, there was a drop in intensity when stoichiometry decreased. This was due to excess epoxy reducing contrast in the SANS signal. This drop in intensity was not seen when cured with DMP-30, showing that DMP-30 homopolymerized the excess epoxy as expected. This is in agreement with conclusions on curing with DMP-30 as stated in section 7.2.2.

For epoxy-amines with deuterated samples, there was a peak seen at $\sim 0.4\text{Å}^{-1}$. This has been seen before and was taken to be the spacing between monomers in the network [1]. This peak position and width was similar for both non-solvent and solvent samples, again showing that curing with solvent does not greatly affect the actual polymer network structure of the resins. For solvent samples, the characteristics of this peak did not change when immersed in water, agreeing with the middle-Q regime results that water does not enter smaller heterogeneities. Methanol shifted the peak to lower Q values, showing that it can affect the network structure. This does disagree with the mid-Q correlation length results. It is believed that these low-Q results are more precise, and so we can see the effect of methanol on the network structure here. For the correlation length results, this change is lost in its range of results and large error values.

7.2.4 Uptake

The initial uptake rate of water and methanol non-solvent samples has been shown to be dependent on their crosslink density. This has been seen before. In water, initial uptake is also dependent on the presence of hydrogen bonds. In methanol, uptake increased in non-solvent samples as the level of excess epoxy increased. This uptake decreased as excess epoxy samples were cured with DMP-30. When curing with DMP-30, uptake is similar to r=1 without DMP-30, showing that the epoxy-amine and homopolymerized networks are functionally very similar, agreeing with T_g results as discussed in section 7.2.2. Also agreeing with conclusions drawn in section 7.2.2, uptake is reduced as the level of homopolymerization increases, showing that the homopolymerized network has greater crosslink density than the epoxy-amine network. For water uptake, non-solvent samples of r=1 displayed greater uptake than r=0.8. This is most likely due to come from uncured amine in r=1 forming hydrogen bonds with water, increasing uptake. Excess amine has higher uptake than excess epoxy for immersion in both water and methanol. This is believe to be due to hydrogen bonding. The formulation of r=1 with DMP-30 and its reaction at 150°C remains an oddity. With its reduced T_g after curing beyond that temperature, one would expect its uptake to increase. However, the opposite is the case. This is still unexplained.

In water, non-solvent samples cured with DMP-30 displayed greater uptake than those cured without. For less excess epoxy, this can be partially down to hydrogen bonds from excess amine due to some epoxy homopolymerizing, but this does not explain why partially-homopolymerized samples of lower stoichiometry have higher uptake. Two theories have been postulated. The first, that the ether groups in the homopolymerized network are of a density more beneficial for forming hydrogen-bonds with water than the density of hydroxyl groups in the epoxy-amine network. The second is that the increased crosslink density of the homopolymerized network results in free-volumes of greater average size. This is seen in our PALS results, and has been reported before. Water can enter more accessible free volumes, but cannot penetrate the network like methanol can and so cannot access all free volumes. This would agree with the SANS

results from section 7.2.3, which shows that methanol can penetrate smaller lengthscales than water. In this way, uptake of water would be more affected by free volume size, not by fractional free volume like methanol uptake is. However, neither of these theories explain why uptake decreases as the stoichometry decreases, and therefore the level of homopolymerization increases, in non-solvent samples cured with DMP-30.

At higher stoichiometries, solvent samples show greater uptake than non-solvent samples. This gives further evidence to the hypothesis that voids are created in these solvent samples, stated in section 7.2.3. Solvent can enter these voids, leading to greater uptake. This uptake is believed to increase as cure rate increases. This is shown by increased cure rate when stoichiometry increases, and when cured with DMP-30. Solvent samples also display mass loss. Again, it is believed that this mass loss is due to the presence of voids creating a more heterogeneous structure. This structure allows for more of the polymer network to be leached out during solvent uptake. The onset of the rate of mass loss exceeding that of uptake is earlier in solvent samples of faster cure rate, again due to the size of these heterogeneities. Uptake in water is more similar for solvent and non-solvent samples. This is believed to be due to the effect of increased uptake when forming hydrogen bonds with the network as opposed to filling voids.

Upon drying, samples previously immersed in water show mass loss rates similar to their uptake rates. Solvent samples show greater mass loss rates than non-solvent. This would be purely down to their being more water in the solvent samples than in the non-solvent, meaning more can leave. For the samples immersed in methanol, solvent samples showed a reduced mass loss. In solvent samples, the main uptake is into voids. In these, methanol would form more methanol-methanol bonds than methanol-network bonds. The opposite would be true in non-solvent samples, where uptake is mainly into free volumes in the network. These methanol-methanol bonds are stronger than methanol-network bonds, requiring more energy to break them. There is therefore reduced mass loss in solvent samples. This is not the case for water samples as water-water bonds and water-network bonds are the same (hydrogen bonds).

7.2.5 Other Investigations

PALS measurements show a greater size of free volumes, and a greater fractional free volume in solvent samples than in non-solvent samples. PALS measurements also show that the fractional free volume and size of these free volumes decreases in solvent samples as stoichiometry decreases, agreeing with results from 7.2.4 that void sizes decrease with stoichiometry. PALS measures free volumes on the Angstrom scale, showing that voids exist on lengthscales smaller than measured in the SANS measurements, discussed in 7.2.3. FFV decreased in non-solvent samples for homopolymerized networks, indicating a higher crosslink density for the homopolymerized network, agreeing with results from 7.2.2. They did show an increased average free volume size. It has been seen before that free volume sizes increases as FFV decreases [2].

Simple density measurements showed that solvent samples are less-dense than non-

solvent samples. Helium pycnometry results showed them to have similar densities. As helium pycnometry fills spaces in the sample to determine volume, it would fill the voids. The density measured is therefore only of the polymer network. These pycnometry results therefore agree with conclusions from sections 7.2.2 and 7.2.3 that besides the appearance of voids, the actual polymer network changes little when curing with solvents. The difference in the density results from these two methods also points to the presence of empty spaces (voids) in the solvent samples.

7.3 Conclusions and Possible Future Investigations

The polymer structure of epoxy-amines change little when cured with DMP-30 or solvents. The end conversion of epoxy groups due to amine polymerization and homopolymerization via DMP-30 both work as expected. The homopolymerized epoxy network is very similar to the epoxy-amine network, although the homopolymerized network has a slightly higher crosslink density. The presence of DMP-30 accelerates the epoxy-amine reaction. The homopolymerization reaction is slower than the epoxy-amine reaction. It has an initial stage of the reaction that has a similar activation energy to the epoxy-amine reaction, but then has a second stage that requires a higher activation energy. The epoxy-amine reaction in non-solvent samples of stoichiometric ratio have a lower enthalpy of reaction peak temperature than when excess amine is used. It is unclear why this is the case. There is a reaction at $\sim$150°C that appears to require excess amine, DMP-30 and acts on the polymer network, lowering its T_g. We are unsure as to the nature of this reaction and how it specifically affects the network. differential scanning calorimetry has been shown to be a useful tool in determining curing rates and T_g's for epoxy-amines. Difficulties were found using in-situ near-infrared spectroscopy in determining conversion of epoxy during cure.

Curing with solvents creates voids in the final network. It is hypothesized that phase separation between solvent and network occurs during cure. As the solvent evaporates, these voids are left in its place. A greater rate of cure results in greater void sizes, believed to be due to the more viscous epoxy-amine filling the voids less before fully curing. These voids range in size, with smaller networks being able to be probed by methanol, but not by water. Uptake of both water and methanol is controlled by the presence of voids and their apparent size. Non-solvent samples do not display these voids. Uptake of methanol in non-solvent samples is dominated by crosslink density. In water it is controlled by crosslink density density and the presence of hydrogen bonds, although there is some confusion with uptake in non-solvent samples cured with DMP-30. Methanol has been shown to have higher uptake and therefore reduced error, although water uptake is more pertinent to real-world applications. The use of both methanol and water has been shown to be beneficial in determining network structures in these epoxy amines.

The investigations carried out showed that the failure of epoxy-amines in their use as anti-corrosive coatings arises from the use of curing solvents. SANS measurements show inhomogeneities arising in epoxy-amines cured with solvents that are not present

in those cured without. Separation of solvent from epoxy-amine creates regions of low density of epoxy-amine. Subsequent evaporation of solvent creates voids, into which water can enter and reach the protected surface, resulting in corrosion. In this regard, it would be preferable to make epoxy-amine coatings without solvents, as they do not display these voids. For non-solvent samples, DSC measurements of final T_g values show the homopolymerizing agent DMP-30 is beneficial in reducing the required amount of amine whilst maintaining a 100% conversion of epoxy. Given that solvents reduce the viscosity of the epoxy-amine during curing, they may still be necessary to create coatings that can be practically applied to surfaces. In this case, formulations should be made that reduce the cure rate of the epoxy-amine. This can be done by not using DMP-30, which acts as an accelerant, and by reducing the stoichiometry of the mixture. A reduced cure-rate results in a less-viscous polymer at the point of solvent evaporation. The polymer can therefore fill the voids more, reducing their sizes.

The conclusions presented create a solid framework of the differences in epoxy-amine structures when curing with DMP-30 and solvents. However, there are unsolved questions. Work could be done to hopefully answer these questions, strengthen current conclusions and investigate the nature of curing with DMP-30 and solvents further. Firstly, changing the proportion of solvent in solvent formulations. It would help our understanding of the supposed appearance of voids in solvent samples. How would the size of voids, and the fraction of samples as voids change, and how would it affect uptake? This may help explain the chemical nature if void formation. Changes could also be made to the ratio of xylene and butanol. However, this would add further complexity and any changes in uptake due to these changes in the solvent mix used would need to be thought through carefully. Likewise, the amount of DMP-30 could be changed. This would help understand how homopolymerization rate changes with the amount of DMP-30. It may also show if there is a minimum level of DMP-30 to reach full conversion, and a maximum before which it affects network structure, in the same way excess epoxy and amine do. In order to determine why the reaction enthalpy peak temperature for r=1 non-solvent is lower than for excess epoxy, enthalpy measurements could be taken around r=1, and for excess amine. Similarly, enthalpy of reaction measurements could be taken for samples cured with solvents. This would be more difficult to measure conversion due to the evaporation of solvents, but it could give some useful information. All these solvent investigations could also be carried out with solvent samples cured with DMP-30. For this to be the case, the preparation of solvent samples cured with DMP-30 needs to be optimized. There is a lot that could be done with swelling measurements. The setup could first be simplified: one thickness, one controlled temperature. This would allow us to run tests on multiple samples and compare them. An elevated temperature, greater than 30°C would also allow us to reach equilibrium in our samples faster, allowing us to measure end uptake, where current results are lacking. There does appear to be little of interest in drying results, so samples should just be fully dried quickly at low pressure and high temperature to determine overall mass loss. With understanding of initial uptake rate, end uptake and mass loss, a more thorough analysis of the different mechanisms in the different formu-

lations could be carried out. Finally, more variations in stoichiometries could be carried out, especially in water and around the stoichiometric ratio. This would allow us better to understand differences in uptake due to changes in crosslink density and number of hydrogen bonding sites. For non-solvent samples with DMP-30, stoichiometries below 0.5 could be used to observe changes in mixed polymerized-homopolymerized network when the there is a greater level of homopolymerization than polymerization. To investigate the swelling in solvent samples, scattering measurements should be taken at lower Q values. This would help with the understanding of swelling of the largest voids when immersed in water and methanol. There is also the issue of the reaction in r=1 with DMP-30 at 150°C. This was the greatest confusion during this PhD. Potentially, infrared spectroscopy investigations, łalongside the NMR measurements, could be used to ascertain the chemical changes occurring during this reaction.

Bibliography

[1] R. Lovell and A. H. Windle. "WAXS investigation of local structure in epoxy networks". In: *Polymer* 31.4 (1990), pp. 593–601. DOI: 10.1016/0032-3861(90)90274-3.

[2] S. Alessi et al. "Study of the Curing Process of DGEBA Epoxy Resin Through Structural Investigation". In: *Macromolecular Chemistry and Physics* 216.5 (2015), pp. 538–546. DOI: doi.org/10.1002/macp.201400510.

Appendix A

Appendix

A.1 Conversions as Measured by Near-Infrared Spectroscopy

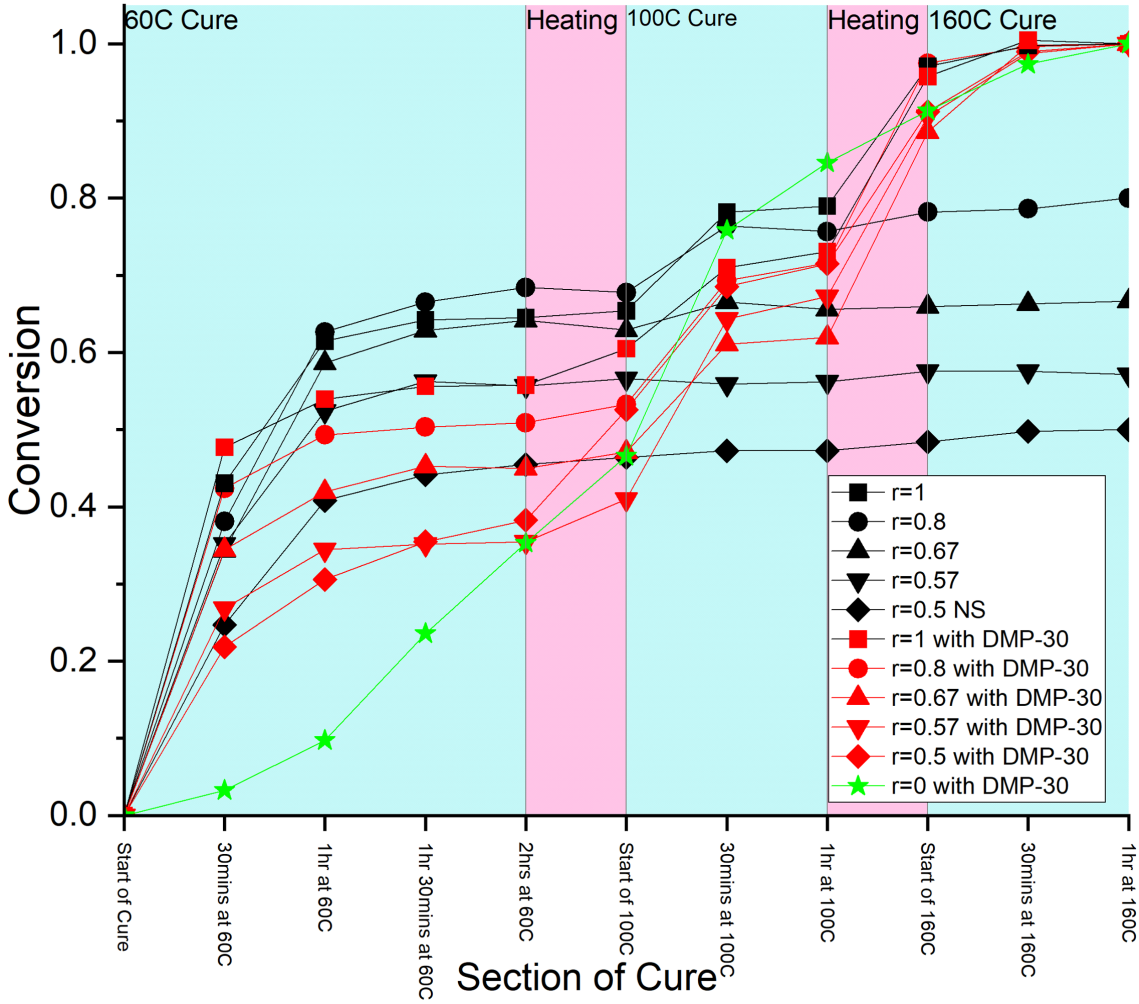

Figure A.1: Conversions of non-solvent epoxy-amines, cured with and without DMP-30, throughout the curing process, as measured by near-infrared spectroscopy.

A.2 Swelling

A.2.1 Full Uptake Over Time Results

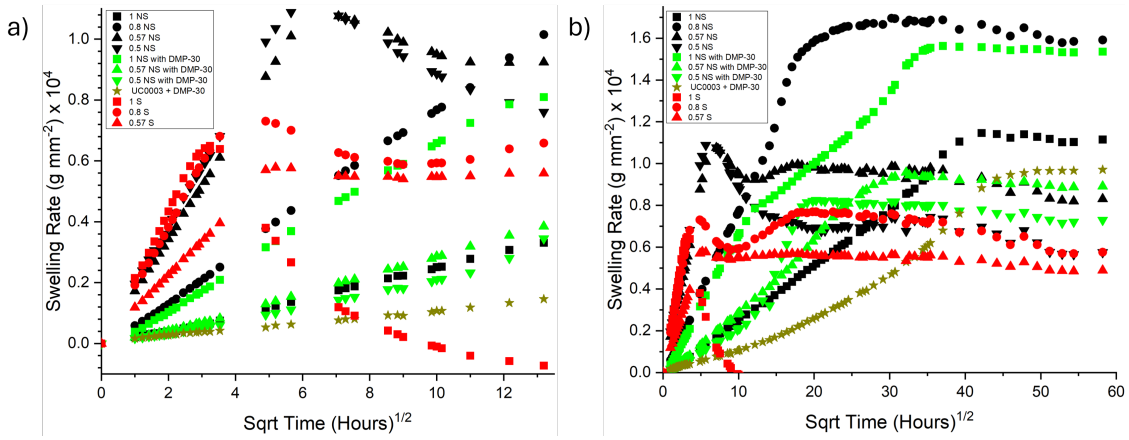

Figure A.2: Solvent uptake measurements for 1.5mm thick fully-cured epoxy-amine samples immersed in 30°C methanol. a) shows uptake for the first week and b) for the entire duration in which measurements were taken. The 1 S results, which showed an eventual negative mass uptake, are not shown fully on b). This was done to make the other results clearer.

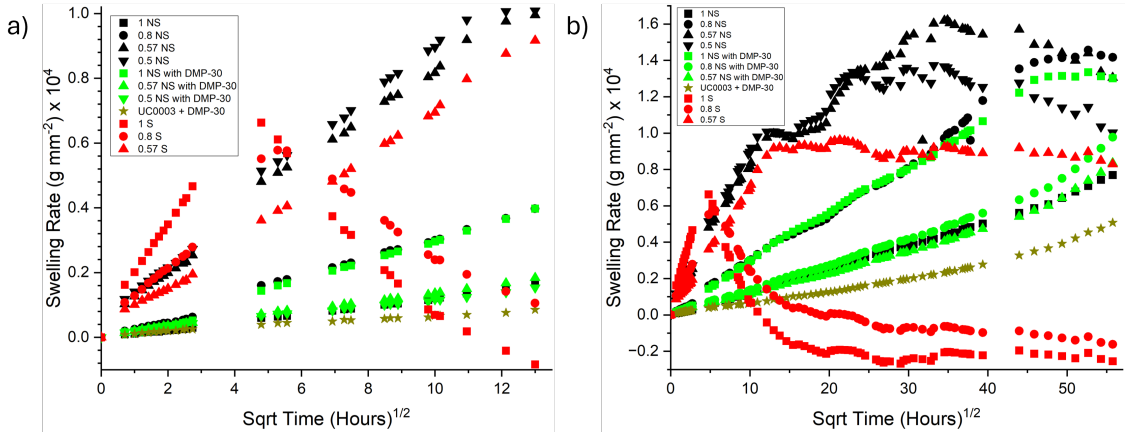

Figure A.3: Solvent uptake measurements for 1.5mm thick fully-cured epoxy-amine samples immersed in methanol at ambient temperature. a) shows uptake for the first week and b) for the entire duration in which measurements were taken.

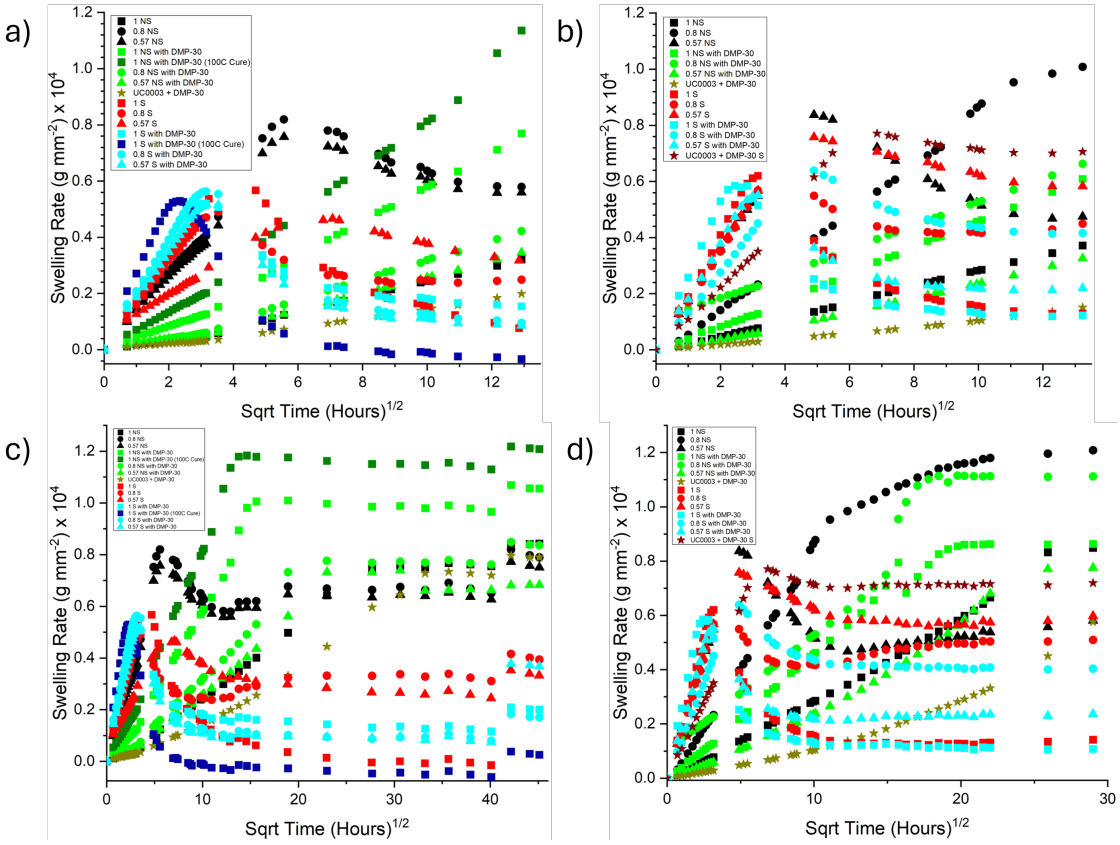

Figure A.4: Solvent uptake measurements for the two sets of 1mm thick fully-cured epoxy-amine samples immersed in 30°C methanol. a) and b) show uptake for the first week. c) and d) show uptake for the entire duration in which measurements were taken.

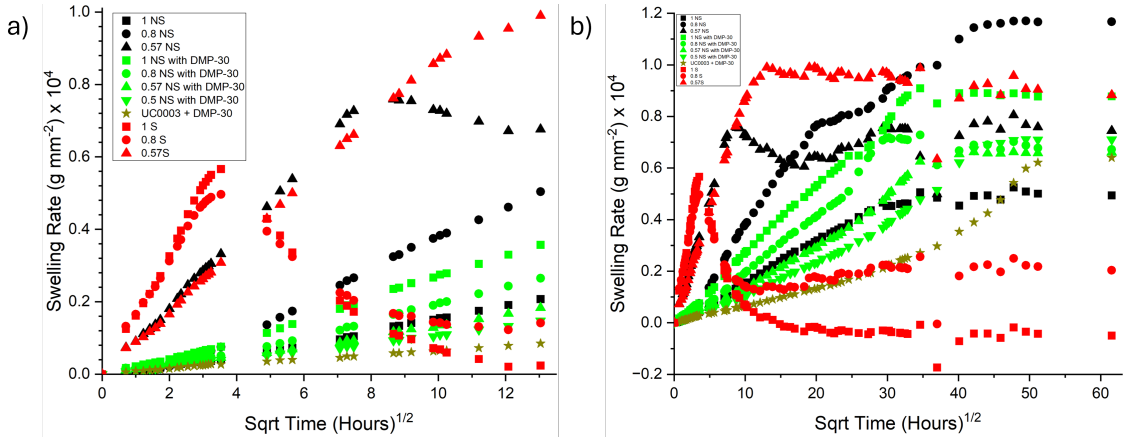

Figure A.5: Solvent uptake measurements for 1mm thick fully-cured epoxy-amine samples immersed in methanol at ambient temperature. a) shows uptake for the first week and b) for the entire duration in which measurements were taken.

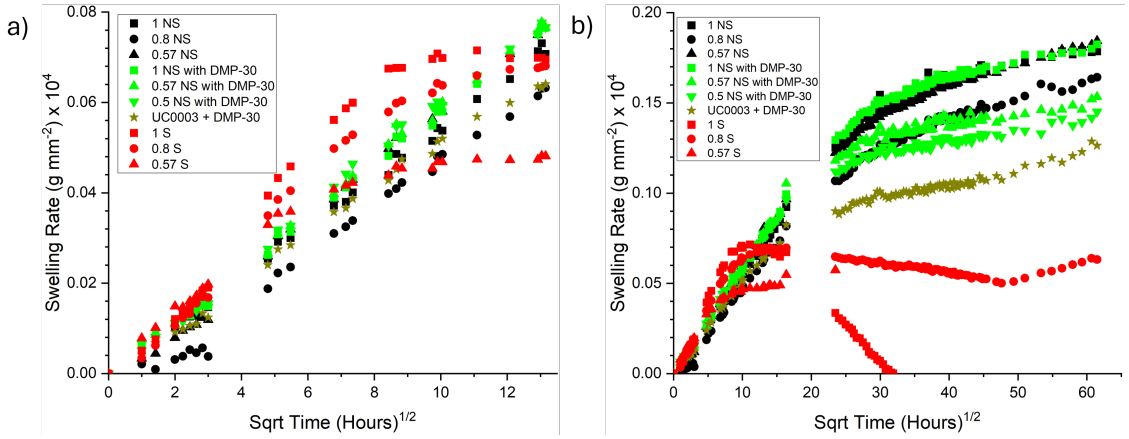

Figure A.6: Solvent uptake measurements for 1.5mm thick fully-cured epoxy-amine samples immersed in 30°C water. a) shows uptake for the first week and b) for the entire duration in which measurements were taken. The 1 S and 0.57 S results, which showed an eventual negative mass uptake, are not shown fully on b). This was done to make the other results clearerThe gap in results between 16.5 hours$^{1/2}$. and 23.4 hours$^{1/2}$. occurred due to the Christmas holiday. A corner broke off 0.57 S during the measurement taken at 14.1 hours$^{1/2}$. This corner was lost after the measurement at 23.5 hours$^{1/2}$.

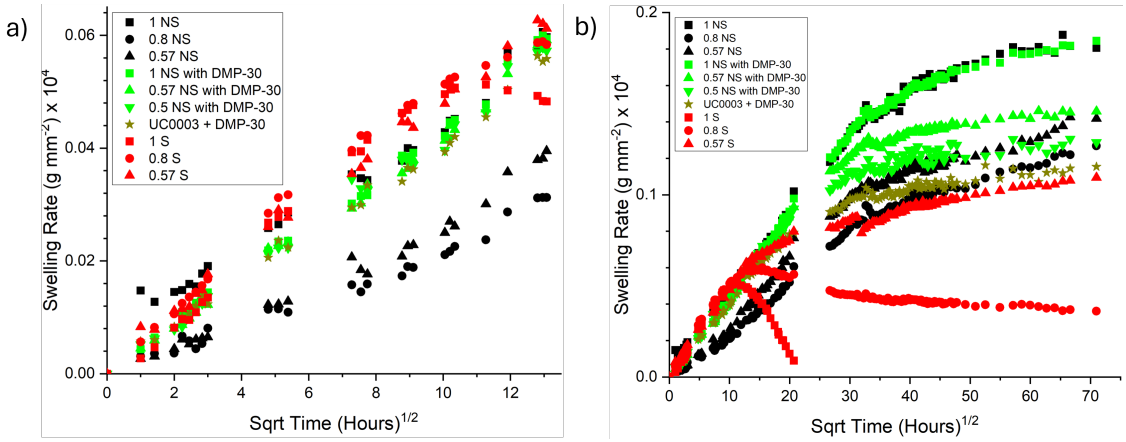

Figure A.7: Solvent uptake measurements for 1.5mm thick fully-cured epoxy-amine samples immersed in water at ambient temperature. a) shows uptake for the first week and b) for the entire duration in which measurements were taken. The 1 S results, which showed an eventual negative mass uptake, are not shown fully on b). This was done to make the other results clearer. The gap in results between 20.7 hours$^{1/2}$. and 26.7 hours$^{1/2}$. occurred due to the Christmas holiday.

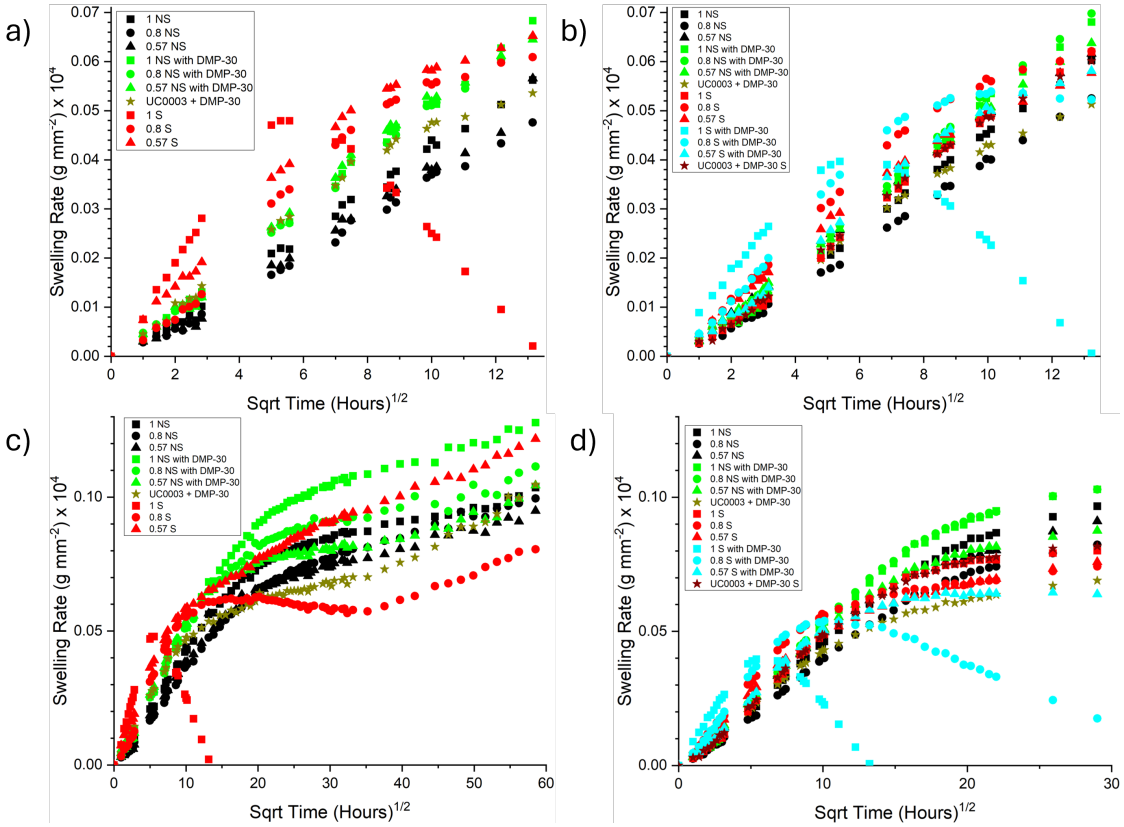

Figure A.8: Solvent uptake measurements for the two sets of 1mm thick fully-cured epoxy-amine samples immersed in 30°C methanol. a) and b) show uptake for the first week. c) and d) show uptake for the entire duration in which measurements were taken. The 1 S results in c) and the 0.57 S with DMP-30 results in d) are not fully shown. This is due to them displaying a negative uptake and to show this would obscure the other results.

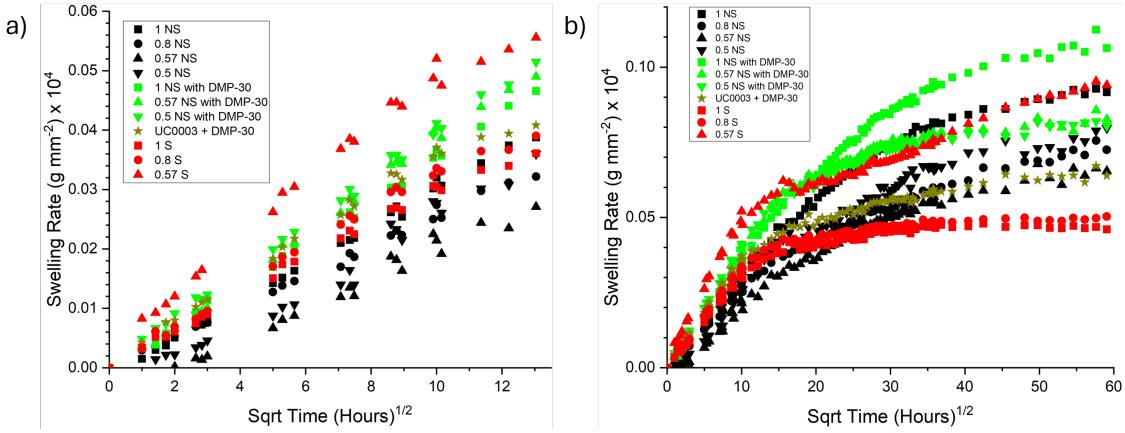

Figure A.9: Solvent uptake measurements for 1.5mm thick fully-cured epoxy-amine samples immersed in water at ambient temperature. a) shows uptake for the first week and b) for the entire duration in which measurements were taken.

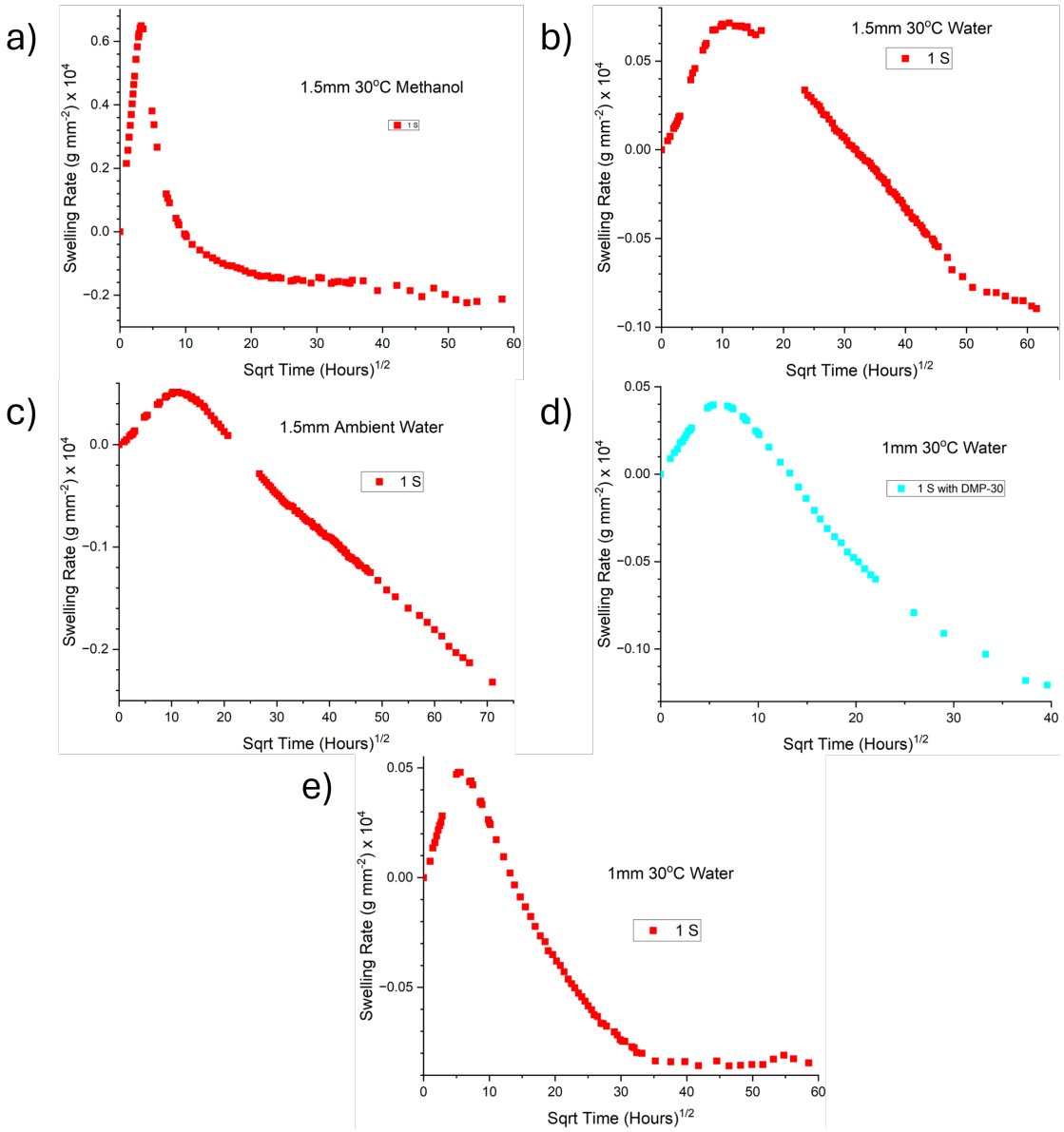

Figure A.10: Solvent uptake measurements, showing the mass loss for those samples that had large negative uptakes. a) shows results for 1.5mm 30°C methanol, b) for 1.5mm 30°C water, c) for 1.5mm ambient temperature water, and d) and e) for 1mm 30°C water.